SHEAR BEHAVIOR OF
SYNTHETIC FIBER REINFORCED CONCRETE BOX CULVERTS

By

MAHNAZ MOSTAFAZADEH

Presented to the Faculty of the Graduate School of
The University of Texas at Arlington in Partial Fulfillment
of the Requirements
for the Degree of

DOCTOR OF PHILOSOPHY

THE UNIVERSITY OF TEXAS AT ARLINGTON
October 2017

DEDICATION

To my Husband, Mehdi, and my daughter, Ariana

Acknowledgements

I would like to express my sincere appreciation and gratitude to my advisor, Professor Ali Abolmaali for his countless support and guidance without which completing this project was impossible. I would also like to thank my committee members, Dr. Shi-Ho Chao, Dr. Nur Yazdani and Dr. B.P. Wang for their time, guidance, and helpful suggestions.

Moreover, I would like to acknowledge the support of the Department of Civil Engineering at UTA. My sincere appreciation goes to all the staff, for their valuable assistance during this research.

I would also like to thank my colleagues and friends, a special thanks to Masoud Ghahremannejad who helped me during experimental tests on box culverts in CELB, the best of luck in his future work. In addition, I would like to acknowledge BASF for providing synthetic fibers and Forterra Pipe and Precast, and Northern Concrete Pipe for manufacturing box culverts for us to accomplish the experimental task of this research.

I am also very grateful to all my family members for their invaluable love, motivation, and encouragement. This journey would not have been possible without their contribution.

This acknowledgment would not be complete without declaring the utmost love, support, patience, and inspiration from my husband, Mehdi and my little daughter, Ariana to whom I am indebted forever.

October 25, 2017

Abstract

SHEAR BEHAVIOR OF
SYNTHETIC FIBER REINFORCED CONCRETE BOX CULVERTS

Mahnaz Mostafazadeh, PhD

The University of Texas at Arlington, 2017

Supervising Professor: Ali Abolmaali

This research pursues a comprehensive experimental study on the shear capacity of zero-slump, dry-cast Synthetic Fiber-Reinforced Concrete (SYN-FRC) with the aim of reducing or even eliminating stirrups in box culverts. Since using stirrups in structures such as box culverts need labor work and cause reinforcement congestion, eliminating or reducing stirrups in design, prevent poor-quality concrete, help better concrete compaction and could save manufacturer time and money over the years. This study first determined the shear capacity of synthetic fiber concrete matrix by varying fiber volume fraction. Then, FEA and full experimental tests have been conducted to evaluate the effect of using synthetic fiber in increasing the shear capacity of box culverts. Japan Society of Civil Engineers (JSCE) G-553 test method has been selected for evaluating the shear behavior of synthetic fiber reinforced concrete. In adjacent with shear test, flexural and compression behavior of concrete determined based on ASTM C1609 and ASTM C39, respectively. To investigate the effect of different concrete compressive strengths on material properties of synthetic fiber-reinforced concrete, two different concrete compressive strength values, 28 MPa (4,000 psi) and 34 MPa (5,000 psi) were selected. Two major phases were considered to

complete the study, which included: (1) Material test for two different concrete compressive strength values (4000 and 5000 psi) and developing shear strength for 7000 psi concrete compressive strength with different fiber volume fractions by using Finite Element Analysis (FEA); (2) Finite Element Modeling (FEM) on all of the ASTM C1577 box culverts equipped with different synthetic fibers dosage (260 cases) along with experimental tests on 5 full-scale box culverts in order to evaluate the FEM results.

The first phase is consist of three different material tests with more concentration on shear test. Since there is no standard shear test method documented in American Society for Testing and Materials (ASTM), therefore the Japan Society of Civil Engineering (JSCE) test method (with some alterations) was selected for extracting shear properties of SYN-FRC. The concrete used in this study was zero-slump, dry-cast one which is typically used for mass productions like concrete pipe, manhole and box culverts. The total number of 60 beams have been tested based on JSCE-G553 and ASTM C1609 for two different concrete compressive strength values. After finishing the material tests, Finite Element Analysis (FEA) has been conducted for developing the shear strength of 7000 psi concrete compressive strength with different fiber volume fractions and also to capture the tensile behavior of concrete equipped with different fiber volume fractions. In order to calibrate the material model defined in ABAQUS, the results of FEM were compared with experimental data.

After implementing phase I, phase II started which had more focus on the shear behavior of box culverts equipped with synthetic fiber along with conventional reinforcement. Different sizes of box culverts have been modeled in FEM by considering plain concrete and also synthetic fiber reinforced concrete. For evaluating the accuracy of FEM results, five full-scale tests have been conducted with optimum synthetic fiber volume fraction in concrete. The

test and FEM results demonstrated that the application of synthetic fibers in concrete yielded to significant improvements in material and structural behavior of concrete and these enhancements were greater at higher synthetic fiber dosage rates.

Table of Contents

List of Figures

List of Tables

CHAPTER 1

INTRODUCTION

1.1 Introduction

Precast concrete box culverts are one of the most multipurpose and cost effective pre-cast concrete products on the market today. The uses for pre-cast concrete box culverts are boundless. They can be used for underpasses, service tunnels, channels, outfalls, bridges, stream culverts, material handling, utility storage, chimneys, vertical storage, watertight holding tanks and more. Pre-cast concrete manufacturers offer a variety of standard box culverts as well as custom designs. ASTM Specification C1577, "Standard Specification for Precast Reinforced Concrete Monolithic Box Sections for Culverts, Storm Drains, and Sewers Designed According to AASHTO LRFD" specifies design and manufacturing requirements to promote quality and durability. Box Culverts and three-sided structures often require shear reinforcement on internal and external cages for the top, bottom and side walls when the height of fill above the top of the box section is more than the one tabulated in ASTM C1577, the live load exceeds HL-93 (the design truck or the design tandem) permitted by AASHTO, or the box dimensions are beyond the ones mentioned in ASTM C1577 Standards. However, using stirrups seems to be the most prevalent problem associated with box culverts design because of labor and material costs and the producers try to avoid using stirrups by increasing the concrete compressive strength and slab thickness. On the other hand, there would be some limitations in

increasing concrete compressive strength and also in changing the slab thickness because the manufacturer forms are typically fixed and are not adjustable. Therefore, using synthetic fibers in concrete (Syn-FRC) which shown in previous studies that have impressive effects in increasing tensile and shear strength of concrete can be a more desirable and economical alternative in designing underground structures like box culvert.

In regarding the shear performance of FRC, many studies have indicated that steel fibers can be used in lieu of stirrups in columns, beams and also as complementary shear reinforcement in precast, thin-webbed beams [1]. However, very limited research studies investigated the shear performance of synthetic fiber reinforced concrete (SYN-FRC). Therefore, commercial use of SYN-FRC is seriously hindered by the lack of field or experimental data of shear performance.

To doing the shear test, it is convenient first to consider three elementary fracture modes (Figure 1.1). It is worthy to mention that the general fracture is a linear combination of these three modes.

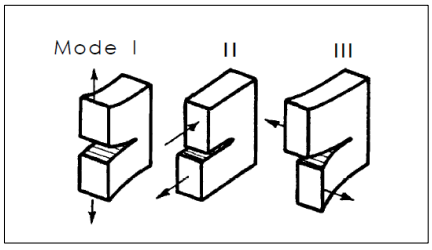

Figure 1.1- Modes I, II and III (Opening, Plane Shear, Anti-Plane Shear Fractures)

Mode I or opening mode: The crack surface displacements are normal to the crack plane

Mode II or edge sliding mode: the crack displacements are in the crack plane and normal to the crack border

Mode III or tearing mode: The crack surface displacements are in the crack plane and parallel to the crack edge.

Mode I fracture is considered as tensile fracture and mode II is considered as shear fracture [2].

1.2 Research need

This research pursues a comprehensive experimental study on the shear capacity of zero-slump, dry-cast synthetic fiber-reinforced concrete (SYN-FRC) with the aim of reducing or even eliminating stirrups in box culverts. Since using stirrups in structures such as box culverts need labor work and cause reinforcement congestion, eliminating or reducing stirrups in design, prevent poor-quality concrete, help better concrete compaction and could save manufacturer time and money over the years.

There has been no study to identify the shear capacity of synthetic fiber concrete composite. Thus, this study first determined the shear capacity of synthetic fiber concrete matrix by varying fiber volume fraction. Then, FEA and full experimental tests have been conducted to evaluate the effect of using synthetic fiber in increasing the shear capacity of box culverts. Japan Society of Civil Engineers (JSCE) G-553 test method has been selected for evaluating the shear behavior of synthetic fiber reinforced concrete. In adjacent with shear test, flexural and compression behavior

of concrete determined based on ASTM C1609 and ASTM C39, respectively. To investigate the effect of different concrete compressive strengths on material properties of synthetic fiber-reinforced concrete, two different concrete compressive strength values, 28 MPa (4,000 psi) and 34 MPa (5,000 psi) were selected. Two major phases were considered to complete the study, which included: (1) Material test for two different concrete compressive strength values (4000 and 5000 psi) and developing shear strength for 7000 psi concrete compressive strength with different fiber volume fractions by using Finite Element Analysis (FEA); (2) Finite Element Modeling (FEM) on all of the ASTM C1577 box culverts equipped with different synthetic fibers dosage (260 cases) along with experimental tests in order to evaluate the FEM results.

The first phase is consist of three different material tests with more concentration on shear test. Since there is no standard shear test method documented in American Society for Testing and Materials (ASTM), therefore the Japan Society of Civil Engineering (JSCE) test method (with some alterations) was selected for extracting shear properties of SYN-FRC. The concrete used in this study was zero-slump, dry-cast one which is typically used for mass productions like concrete pipe, manhole, and box culverts because the forms can be striped as soon as the concrete has been consolidated. The total number of 60 beams have been tested based on JSCE-G553 and ASTM C1609 for two different concrete compressive strength values. After finishing the material tests, Finite Element Analysis (FEA) has been conducted for developing the shear strength of 7000 psi concrete compressive strength with

different fiber volume fractions based on the shear test results for 28 MPa (4,000 psi) and 34 MPa (5,000 psi) concrete compressive strength values.

After implementing phase I, phase II started which had more focus on the shear behavior of box culverts equipped with synthetic fiber along with conventional reinforcement. Different sizes of box culverts have been modeled in FEM by considering plain concrete and also synthetic fiber reinforced concrete. For evaluating the accuracy of FEM results, full-scale tests have been conducted with optimum synthetic fiber volume fraction in concrete.

1.3 Literature review

The literature review for the current research can be separated into three different parts. The first part studies the different shear test methods used by researchers in order to obtain the shear capacity of concrete. Whereas in the second part of literature review the discussion will be concerned with mechanical properties and behavior of fiber reinforced concrete (FRC) mainly focused on the shear property of FRC and in the last part of literature review, the structural behavior of box culverts and the main reasons for using stirrups in box culverts have been investigated.

1.3.1 Shear test method

In the first category, the discussion will be on different shear test methods and why, in spite of many experimental works done over the years and continuing today, there is still no standard shear test method in American Society for Testing and Materials (ASTM) or Canadian Standards Association (CSA).

In 1967, Nicolae Iosipescu developed a test procedure that could predict failure of test specimens under pure shear load. A pure shear load is generated using a simple device that generates a shear force in a straight beam in the area of zero moment and results in failure of the specimen. Prior to this test, shear testing procedures existed, but not the failure of the material under pure shear stresses [3]. On the basis of principles of strength of materials and the theory of elasticity, Iosipescu established the pure shear testing method. He found that by creating angular notches on a specimen, the specimen will be weakened in desired failure point and maximum shear stresses remained constant through the cross section. As shown in Figure 1.2, Two 90° notches were cut to ¼ of the beam depth on both the top and bottom surfaces of the specimen.

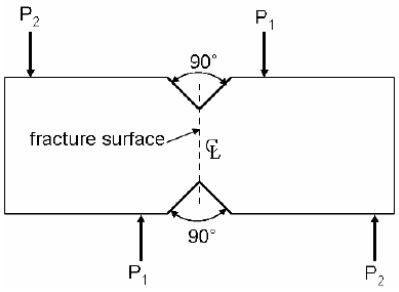

Figure 1.2 - Specimen geometry and loading for Iosipescu shear test [3]

The mode II fracture of concrete (shear fracture) was also investigated by Bazant and Pfeiffer [4]. Symmetrically notched beams were loaded in a manner that produced concentrated shear forces and failure zone. When loaded, cracks created between the two notch tips resulted in the failure of the specimen (Figure 1.3-(a)). The authors concluded that the mode II fracture of concrete (shear fracture) exists and they also

showed that mode II fracture like mode I. By narrowing the shear zone, the cracks propagated in the cross section plane rather than in an inclined direction.

The behavior described by Bazant and Pfeiffer conflicted with those observed in similar specimens tested by different researchers [2]. Ingraffea and panthaki [5] have discussed that there is tensile splitting stresses in the area between the notched tips and fracture originated from these stresses (Figure 1.3-(b)).

Bazant and Pfeiffer conducted some finite element analysis in support of the method they measured mode II fracture and the results displayed that the cracks initiated from the notch tips and propagated continuously toward the center, representing shear cracks. The results also confirmed the existence of tensile stresses between the crack tips but the inclined principal tensile stresses at the crack tips are much higher.

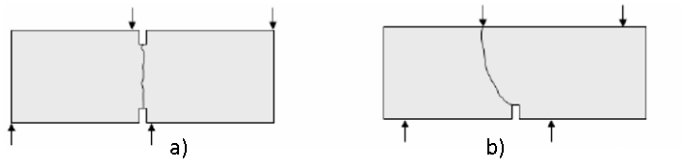

Figure 1.3 - Shear test methods used by different researchers (Guenther, 2007)

In 1987, Swartz and Taha [6] used similar test methods and based on obtained results, the principal fracture originated in the shear zone and not at the notch tips.

Based on all above discussion, no conclusion has been provided about any of the shear test methods used for obtaining the pure mode II fracture strength. Other stresses like tensile, bearing and web stresses at notch tips make the problem more complicated.

The shear capacity of fiber reinforced concrete has been investigated by many researchers by using different shear test methods such as Z-type push-off (double L-shape) test, Federation Intermationale de la Precontrainte (FIP) shear test and the Japanese Society of Civil Engineering (JSCE) shear test. The Z-type push-off test has been broadly used before but because it has reinforcement inside the specimen, it doesn't let the fibers distribute in specimen evenly and it is not also a standard test with specific specimen size and it's been used in different sizes. The FIP shear test method has been used by some researchers like Khanlou [7]. He used this method to investigate the shear capacity of steel fiber reinforced concrete and compared the results with analytical results. Based on his results, The FIP shear test could successfully predict the shear capacity of fiber reinforced concrete.

The direct shear behavior of steel fibers, one with flattened ends and a circular cross section and the other with a crimped geometry and a crescent cross section has been studied by Mirsayah and Bantia in 2002 by using JSCE-SF6 test method. The investigation showed that the JSCE-SF6 standard with some alterations can be used to acquire the shear capacity of fiber reinforced concrete [8]. In 2006, Majdzadeh studied the shear capacity of both steel and Synthetic fiber at different fiber volume fractions by using JSCE-SF6 method by considering some modifications [9]. The results showed that this method by applying some modifications can be used widely for obtaining the shear strength of fiber reinforced concrete.

Based on the above literature review on different shear test methods, the Japanese Society of Civil Engineering (JSCE) test method with some modifications (JSCE-

G553) has been used in this research for achieving the shear capacity of dry-cast concrete equipped with different fiber volume fractions [10].

1.3.2 Fiber reinforced concrete

Fiber reinforced concrete (FRC) is an innovative material which improves many engineering properties of concrete [11]. Previous studies have demonstrated the effectiveness of fibers in improving the different mechanical behavior of concrete. Songa et al. investigated the compressive and splitting tensile strengths and modulus of rupture for nylon and polypropylene fibers. Based on the results, the nylon fibers performed better than the polypropylene fibers, which reportedly reflected the higher tensile strength of the nylon fibers. When the polypropylene fiber was compared with plain concrete, it showed an improved compressive strength of 5.8% and a splitting tensile strength increase of 9.7%. Moreover, the impact resistance increased for the first crack and failure strengths by 11.9% and 17%, respectively [12]. Wilson and Abolmaali compared synthetic and steel fibers through ASTM C1609 flexural beam and ASTM C39 compressive cylinder testing. The results showed that the modulus of rupture and compressive strength of concrete with steel and synthetic fibers were improved [13]. Boulekbache et al. investigated the influence of the paste yield stress and compressive strength on the behavior of fiber-reinforced concrete (FRC) versus direct shear. The parameters considered were the steel fiber contents, the aspect ratio of fibers and the concrete strength. Three types of concretes with various compressive strength and yield stress were examined, an ordinary concrete (OC), a self-compacting concrete (SCC) and a high strength concrete (HSC). The results

showed that the fiber contents, fiber aspect ratio, and concrete strength influenced on the shear strength and ductility very considerably. According to the results, the yield stress of concrete has an important effect on the orientation and distribution of the fibers in the matrix. Moreover, the ductility in direct shear depends on the fiber orientation and is significantly improved when the fibers are perpendicular to the shear plane [14]. Wilson and Abolmaali evaluated the synthetic fibers as an alternative reinforcement in concrete pipes. The results demonstrated that synthetic fibers increase the impact resistance and toughness of concrete and reduce the crack width and plastic shrinkage seen in concrete pipes [15]. Peyvandi et al. undertook a comprehensive experimental research to evaluate the efficiency of different synthetic fibers (aramid, AR-glass, carbon, and polyvinyl alcohol) at various volume fractions in lean, zero-slump concrete materials used in the dry-cast method of concrete pipe production. Large-scale structural evaluation of concrete pipes indicated that 30% improvement in the load-carrying capacity of concrete pipes and reduction of welded wire fabric steel reinforcement layer in concrete pipes from two to one [16].

1.3.2.1 Effect of Fibers Reinforced Concrete (FRC) on shear reinforcement

It has been recognized that fiber reinforcement is an effective way to enhance the fracture toughness of concrete in all modes of failure. The effect of fiber reinforcement on shear strength of concrete is attributed to two main factors: 1) a direct factor imposed by the post cracking strength at the inclined shear crack (in a similar way to

stirrups), and 2) an indirect factor that increased the contribution of concrete to shear strength by improving aggregate interlock and dowel action of flexural reinforcement. Consequently, the shear strength of the concrete, ultimate shear capacity, and ductility of FRC beams are improved by using fibers in concrete. Several research studies that involved small and large-scale testing of FRC beams have confirmed this theory. Gustafsson (1999) investigated if steel fibers can replace stirrups as shear reinforcement in high strength concrete beams. Analysis of the results indicated that by adding steel fibers in relatively small concentrations, it is possible to reach shear capacities of the same order as in the case of conventional shear reinforcement [17]. Cho et al. (2009) had an investigation on the shear behavior of large-scale steel fiber reinforced prestressed concrete beam. Experimental results showed that the attained high shear strength suggests a minimum amount fiber volume less than 0.75% is probable for replacing conventional shear reinforcement in prestressed members [18]. Another experimental study on SFRC beams subjected to shear loading done by Minelli and Plizzari (2013). A total of 18 full-scale experiments without conventional shear reinforcement were carried out in order to investigate the effect of randomly distributed fibers on the shear behavior of concrete. Results showed that a relatively low amount of fibers (Vf <0.7%) can significantly increase the shear strength and ductility of the concrete beam without stirrups [19].

1.3.3 Experimental tests on box culverts

James [20] determined the safety of the precast concrete by conducting a study on box culverts under the service and design load without using the shear connectors.

This study used boxes by 152 cm (5 ft) and 213 cm (7 ft) clear span as per ASTM C850 and applied load on the culvert's span centerline at the supported male end, female end, and the unsupported edge in different tests. This study investigated steel stresses and deflections and compared them with analytically predicted steel stresses. Based on the test results, the box culvert design was conservative and the live load deflections and stresses caused by design service wheel loads are satisfactory without shear connectors.

A comprehensive field investigation of the behavior of a double-cell cast-in-place box culvert has been studied by Ahmad et al. [21]. The soil pressure, moment, and deflection of box culverts were measured during the test. The moment measurement was based on measuring strains in outer and inner steel rebars used inside the box culverts. The test results showed that the live-load effect beyond 8 ft of fill reduced significantly and the use of AASHTO's 1.75 distribution factor is effective regardless of the fill height.

Theoretical studies, field-testing, and also model testing have been accomplished by Frederick et al. [22]. The wheel load applied at the center of the 366 cm (12 ft) and 305 cm (10 ft) span boxes with and without shear connectors. The test results showed that the shear connectors and the edge beams were not required for the ASTM C850 box culverts.

Abolmaali and Garg [23] conducted a comprehensive study to evaluate the shear capacity of the precast reinforced concrete box culverts. The failure of twenty four full-scale box culverts has been studied by subjecting each box culvert to AASHTO HS-20 wheel load. In order to identify the critical shear location, the location of the

wheel load was varied from the tip of the haunch as a function of the top slab effective depth. Although the test specimens were loaded to present shear behavior, it was revealed that up to and beyond standard factored live load, all the test specimens behaved in the flexural mode. The shear cracks observed at loads equivalent to nearly twice of the aforementioned factored load. Based on this study, the shear behavior is not the prevailing behavioral mode for the concrete box culverts, and the live load distribution width equations in conjunction with the provisions for shear transfer devices reported in the current standard for box culverts need to be reconsidered.

An extensive study was conducted by Garg et al. [24] to obtain the location at which maximum shear stresses are induced. In this investigation, the center of the load plate (10 in.×20 in. ×1 in) was placed at three different locations, d, 1.5d and 2d (d is distance between the tip of the haunch to the edge of the load plate and is considered as effective depth of top slab) on 1.22 m× 1.22 m×1.22 m (4 ft×4 ft×4 ft) box culverts. The failure cracks were a combination of bond and shear cracks as a result of excessive shear stresses and arching action. In all the test specimens, initial flexural cracks forming at the top of the bottom slabs and bottom of the top slabs. For all the test specimens, hairline shear cracks initiated at the loads which were above the strength limit for live load used in design per AASHTO (2005). Therefore, the shear capacity of box culverts is adequate, and stirrups are not required.

1.4 Scopes and objectives

Related to this research, the objectives are to advance on the following forefronts:

1) To evaluate the shear capacity of synthetic fiber reinforced concrete
2) Use the above information to reduce or even eliminate stirrups in box culverts

To accomplish the above objectives, the following tests are proposed to be conducted:

1) Test method for shear strength of Synthetic fiber reinforced concrete (JSCE G-553)
2) Standard test method for flexural performance of Fiber-reinforced concrete (using beam with third-point loading, ASTM C1609) for using the data in FEA
3) Standard test method for compressive strength of cylindrical concrete specimens (ASTM C39)
4) Full-scale test on box culverts to evaluate the FEM results

CHAPTER 2

EXPERIMENTAL PROGRAM ON MECHANICAL PROPERTIES OF SYNTHETIC FIBER REINFORCED CONCRETE

2.1 Introduction

All the Material testing was conducted at the UTA Civil Engineering Laboratory. All the tests were on zero-slump concrete and the fibers were added manually to the mix design. It should be noted that all the tests were conducted at 7 days.

2.2 Properties of synthetic fibers

In this study, BASF Macro synthetic fibers have been used. The fibers are made from a blend of polypropylene resins and meet the necessities of ASTM C1116 [25]. The physical properties of fibers have been shown in Table 2.1 [26].

Typically, synthetic fibers have been used as another alternative for reinforcing concrete in order to control shrinkage, temperature and settlement cracking and provide an increase in flexural toughness and impact resistance, as well as to improve residual strength, durability and developed cohesion [26]. Figure 2.1 shows the type of fiber applied in this research.

Table 2.1 Physical properties of BASF Synthetic Fiber

Specific Gravity	0.91
Melting Point	320 ^{o} F (160 ^{0}C)
Ignition Point	1094 ^{0} F (590 ^{0} C)
Absorption	Nil
Alkali Resistance	Excellent
Tensile Strength	85 ksi (585 MPa)
Length	2.1 in. (54 mm)
Aspect Ratio	67
Fiber Type	embossed
Material	100% virgin polypropylene
Chemical Resistance	Excellent

Figure 2.1- MasterFiber MAC Matrix synthetic fibers

2.3 Material and specimen

To determine the material properties of Syn-FRC, two mixtures with two different compressive strength values, 28 MPa (4,000 psi) and 34 MPa (5,000 psi), were selected. The mixture proportions for the concrete compressive strengths are given in Table 2.2 (a) and (b).

Table 2.2 (a) 28 MPa (4,000 psi) dry cast concrete mix design

Mixture ingredient	Quantity
Cement, kg/m3(lbs/yd3)	263 (444)
Fly ash, kg/m3(lbs/yd3)	67 (113)
Water, kg/m3(lbs/yd3)	151 (255)
Sand, kg/m3(lbs/yd3)	887 (1,496)
0.95 cm (3/8") aggregate, kg/m3(lbs/yd3)	1,052 (1,774)
W/C	0.46
Compressive strength, 7 days, MPa (psi)	28 (4,000)

Table 2.2 (b) 34 MPa (5,000 psi) dry cast concrete mix design

Mixture ingredient	Quantity
Cement, kg/m3(lbs/yd3)	474 (800)
Water, kg/m3(lbs/yd3)	166 (280)
Sand, kg/m3(lbs/yd3)	575 (970)
0.95 cm (3/8") aggregate, kg/m3(lbs/yd3)	1,180 (1,990)
Super Plasticizer, kg/m3(lbs/yd3)	0.453 (1)
W/C	0.36
Compressive strength, 7 days, MPa (psi)	34 (5,000)

In order to investigate the effect of synthetic fibers on concrete material properties, different fiber dosages were utilized as presented in Table 2.3.

Table 2.3 Synthetic fiber dosage

Fiber Dosage, kg/m^3 (lb/yd^3)	0	2.37 (4)	4.75 (8)	7.12 (12)	9.49 (16)
Volume Fraction (V.F) (%)	0	0.26	0.52	0.78	1.04

As shown in Figure 2.2, synthetic fibers were introduced into the mixer after all dry aggregates, sand, and stone were thoroughly mixed together. Then the water was added to the mixer gradually. After a good blend of water with aggregates and fibers, the cementitious materials introduced to the mixer (Figure 2.3). This approach was to ensure uniform distribution of the fibers throughout the entirety of the mixture.

Figure 2.2 - Introducing synthetic fibers into the mixer after all dry aggregates

Figure 2.3 - Adding cementations material to the mixer

Before casting the concrete, mold release has been applied to all the steel beam molds to make it easy unmolding process (Figure 2.4). A slump test has been conducted for each batch of concrete to make sure all testing is on zero-slump dry cast concrete (Figure 2.5 (a) and (b)). As shown in Figure 2.6, Fresh concrete was

poured into molds and externally vibrated with concrete vibrating table and compacted with rammers.

Figure 2.4 - A light coat of mold release used inside the molds

a) b)

Figure 2.5 - (a) slump test (b) zero-slump dry cast concrete

a) b)

Figure 2.6 - (a) pouring the concrete into molds (b) externally vibrating the concrete with vibrating table and compacting with rammers

For each mixture, six 100 mm (4 in.)-diameter × 200 mm (8 in.)-long cylinders were made for compression test in accordance with ASTM C39. Three 150 mm × 150 mm × 500 mm (6 in.× 6 in. × 20 in.) beams were cast for conducting flexure test based on ASTM C1609 and three 150 mm × 150 mm × 500 mm (6 in.× 6 in.× 20 in.) beams were cast for determination of shear capacity of concrete according to JSCE-SF6 (Table 4). After casting, the specimens were covered with plastic sheets for 24 hours and were consequently placed in curing room for a duration of 7 days (Figure 2.7).

Figure 2.7 - Placing specimens in curing room for a duration of 7 days

According to Table 2.4, the total number of beam tested is 60, and the total number of cylinders for compression test is 28.

The relative density of synthetic fibers is 0.91, and 908 kg/m3 (1530 lbs/yd3) of mass per volume value. Volume fraction calculated based on the relative density of water (1.0).

Table 2.4 Number of beams and cylinders used in this research

F'c, MPa (psi)	Vol. Fraction (%)	No. of beams for JSCE G-553 shear test	No. of beams for flexural test based on ASTM C1609	No. of cylinders for compression test
28 (4000)	0	3	3	6
	0.26	3	3	6
	0.52	3	3	6
	0.78	3	3	6
	1.04	3	3	6
34 (5000)	0	3	3	6
	0.26	3	3	6
	0.52	3	3	6
	0.78	3	3	6
	1.04	3	3	6
Total		**30**	**30**	**60**

2.4 Shear test setup

Since no standard shear test method has been documented in American Society for Testing and Materials (ASTM) or Canadian Standards Association (CSA), therefore the Japan Society of Civil Engineering (JSCE) test method (with some alterations) was selected for extracting shear properties of Syn-FRC. Figure 2.8 shows the schematic of the shear test setup used in this research. In this test method, the shear load was applied by a loading block with two loading edges 150 mm (5.9 in.) apart. To obtain the real behavior of Syn-FRC specimen in direct shear, a stiff plate and 4

adjustable bolts on each side were used to hold the end parts of the specimen against rotation [8]. The specimen was supported by two rigid blocks 155 mm (6.1 in.) apart. In order to capture the shear behavior of beam, a thin, 2.5 mm (0.1 in.)-wide with 10 mm (0.4 in.)-deep notch was sawed all around the beam (between the loading and support) as shown in Figure 2.9.

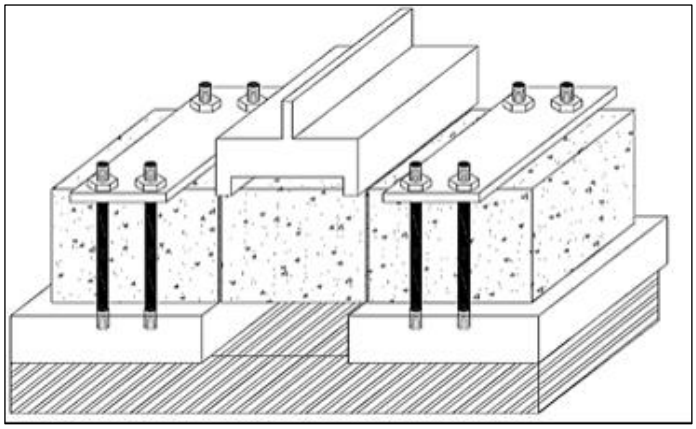

Figure 2.8 - Schematic of shear test used in this research

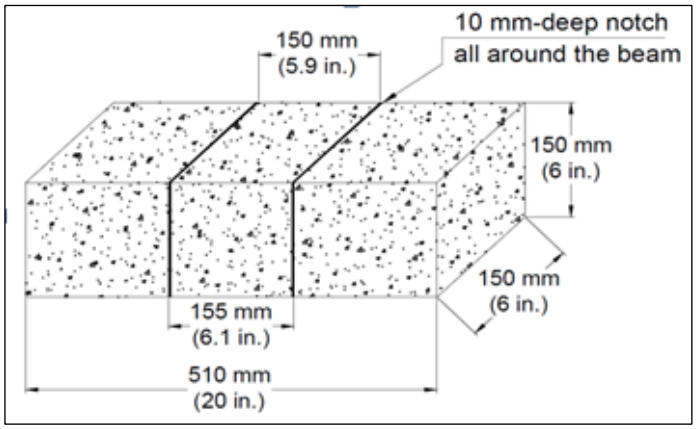

Figure 2.9 - The exact location of notch on the beam

The experiment was conducted using MTS machine with the capacity of 445 kN (100 kips) by applying displacement control with a rate of 0.001 mm/sec (0.00004 in/sec) [8].

The displacement of the specimen parallel to the shear plane in the middle of the beam was measured by two Linear Variable Displacement Transducers (LVDTs). Applied displacement and load were recorded at the frequency of 10 Hz. Figure 2.10 (a) shows the shear test setup and the fractured specimen at the end of the test. As shown in Figure 2.10 (b), the shear fracture occurred exactly in the predefined planes.

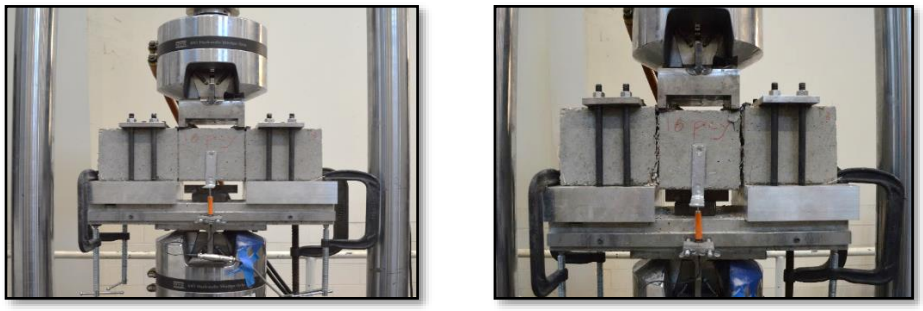

(a) (b)

Figure 2.10 - (a) Test setup for direct shear test and (b) Fractured specimen

2.5 Shear test results

The maximum shear strength of the beam was calculated based on Equation 1.

$$\tau_{Max} = \frac{P_{Max}}{2A} \qquad \text{Equation (1)}$$

Where Pmax is the maximum peak load supported by test specimen shown in Figure 2.10-(a) and A is the effective area of the shear plane on each side of the specimen. In this study, the shear toughness, which is equal to the area under the load-deflection curve, was calculated and further discussed.

The JSCE shear test results are presented in Figure 2.11 and Figure 2.12. The load-deflection curve for each fiber dosage was calculated based on the average of three beam test results. The mid-displacement was recorded by two LVDTs installed in the middle of the specimen, in both front and back of specimen, and was calculated as the average of the two readings. The LVDT installed in the middle of the front surface of the test setup is shown in Figure 2.10. As shown in Figure 2.11 and Figure 2.12, implementing the synthetic fibers in concrete changed the initial slope (considered as the rigidity of the specimen) slightly; however, the slope after failure changed more significantly. Subsequently, increasing the fiber dosage in concrete changed the sudden and brittle shear behavior to more ductile one which is a more desirable performance in concrete structures. The Photographs of each test and the observed failure are presented in Appendix A.

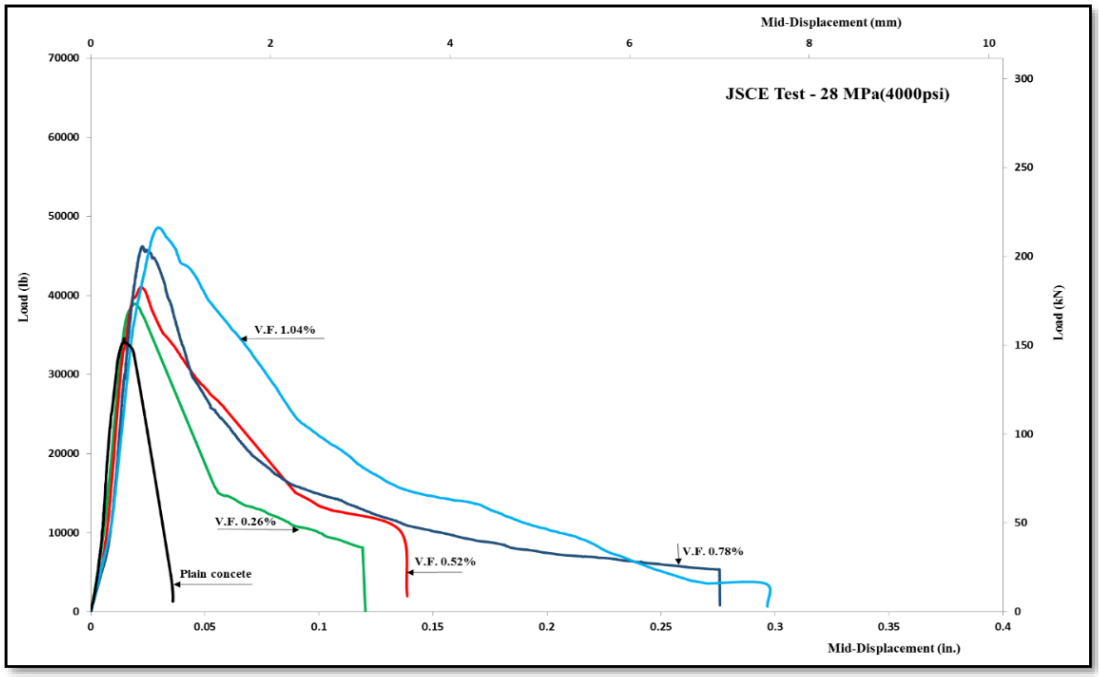

Figure 2.11 - Load-deflection curve based on JSCE shear test for concrete with 28 MPa compressive strength

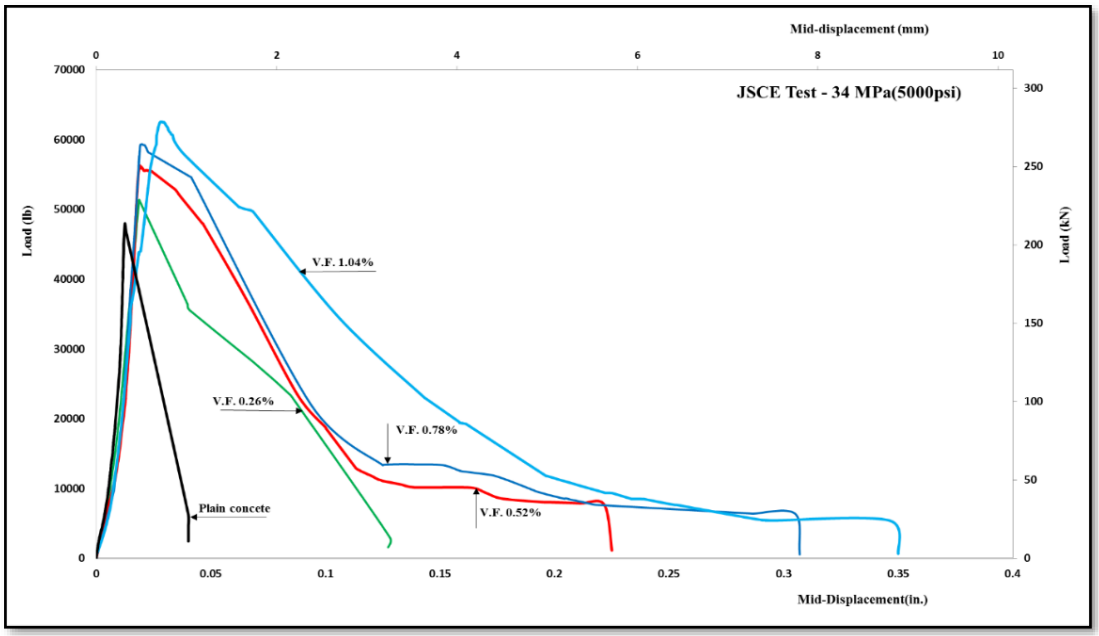

Figure 2.12 - Load-deflection curve based on JSCE shear test for concrete with 34 MPa compressive strength

Table 2.5 demonstrates shear test results for concrete with 28 MPa (4,000 psi) compressive strength. As shown in this table, by increasing the fiber dosage from V.F. = 0% to V.F. = 1.04%, the shear strength and shear toughness (the area under the shear load-deflection curve) enhanced up to 41% and 648%, respectively. Table 2.6 shows the shear test results for concrete with 34 MPa (5,000 psi) compressive strength equipped with different synthetic fiber dosages. As shown, the shear strength and shear toughness increased up to 43% and 736%, respectively by increasing the fiber dosage rates.

Table 2.5 Compare shear test results for concrete with different fiber dosage (28 MPa)

28 (4,000) concrete, MPa (psi)				
Vol. Fraction (V.F.), %	**Shear strength, MPa (psi)**	**Increase in shear strength (%)**	**Shear toughness, N.m (lb.in)**	**Increase in shear toughness (%)**
0	4.24 (615)	-	80 (708)	-
0.26	4.72 (685)	11	241.3 (2,136)	202
0.52	5.04 (731)	19	326.6 (2,891)	308
0.78	5.60 (812)	32	453 (4,010)	466
1.04	5.96 (865)	41	598.6 (5,298)	648

Table 2.6 Compare shear test results for concrete with different fiber dosage (34 MPa)

34 (5,000) concrete, MPa (psi)				
Vol. Fraction (V.F.), %	**Shear strength, MPa (psi)**	**Increase in shear strength (%)**	**Shear toughness, N.m (lb.in)**	**Increase in shear toughness (%)**
0	5.51 (800)	-	104.6 (926)	-
0.26	6.34 (920)	15	366.8 (3,247)	251
0.52	6.82 (990)	24	533.4 (4,721)	410
0.78	7.41 (1,075)	34	664.7 (5,883)	535
1.04	7.86 (1,140)	43	874.5 (7,740)	736

By comparing Table 2.5 and Table 2.6, it is seen that synthetic fibers have significant effect on the shear behavior of concrete with higher compressive strength. For instance, for 0.26% fiber volume fraction, the shear strength increased by 11% and 15% for 28 MPa (4,000 psi) and 34 MPa (5,000 psi) compressive strength values, respectively. It is also shown in Figure 2.13 that by increasing compressive strength from 28 MPa (4,000 psi) to 34 MPa (5,000 psi), the effect of increase in shear strength is more pronounced in lower fiber dosage concrete than higher ones. This basically means that the deviation of the increase in shear strength between the 28 MPa (4,000

psi) and 34 MPa (5,000 psi) concrete is higher for lower fiber dosages (i.e. V.F. = 0.26% and 0.52%) than higher ones. This is attributed to the complex relationship between the higher fiber dosages (i.e. V.F. = 0.78% and 1.04%) and different concrete mix strengths. For instance, for 0.26% fiber volume fraction, increase in shear strength enhanced from 11% to 15% (36% increase) for 28 MPa (4,000 psi) and 34 MPa (5,000 psi) compressive strength values, respectively, while for fiber volume fraction equals to 0.78%, this increase improved from 32% to 34% (6% increase) for 28 MPa (4,000 psi) and 34 MPa (5,000 psi) compressive strength values, respectively.

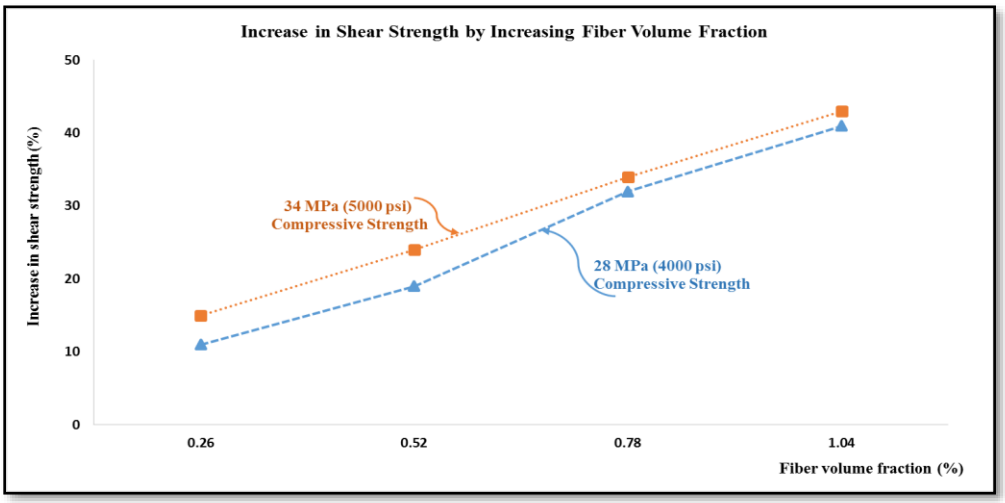

Figure 2.13 - Changing trends in the shear strength by increasing fiber volume fraction

2.6 Flexural and compression test setup

Flexural behavior of synthetic fiber reinforced concrete was investigated based on ASTM C1609 “Standard Test Method for Flexural Performance of Fiber-Reinforced Concrete (Using Beam with Third-Point Loading)” [27]. All the flexural beams were 150 mm × 150 mm × 500 mm (6 in. × 6 in.× 20 in.) in size and they all tested after 7 days of curing. From this test, first peak and peak load were determined as well as the load–deflection curve up to the specified deflection. From the given information, modulus of rupture and specimen toughness were determined. Figure 2.14 (a) and (b) show the flexural beam setup and the broken specimen at the end of the test. The Photographs of beams with different fiber dosage and the observed failure are presented in Appendix A.

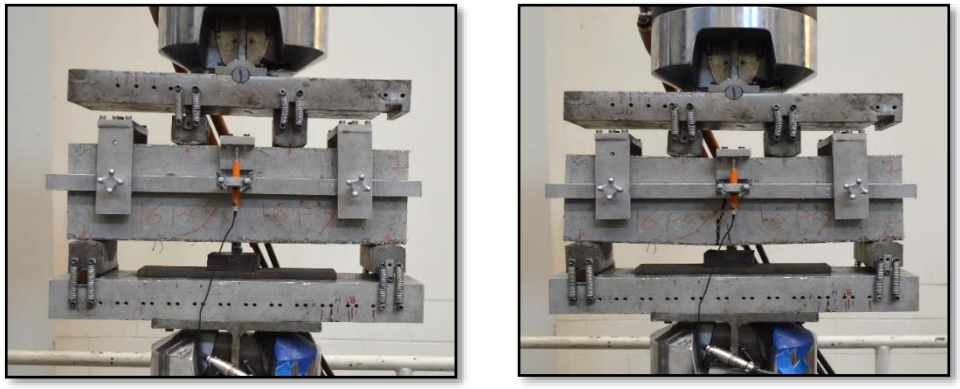

(a) (b)

Figure 2.14 - (a) Flexural test setup according to ASTM C1609 and (b) damaged specimen after L/150 deflection (1.04% Vol. Fraction)

To evaluate the compressive strength of fiber reinforced concrete, 6 cylinders were cast for each fiber dosage. After 7 days, all cylinders were capped according to ASTM

C617 “Standard Practice for Capping Cylindrical Concrete Specimens” [28] and were tested based on ASTM C39 “Standard Test Method for Compressive Strength of Cylindrical Concrete Specimens” [29]. From this testing, the maximum compressive load at failure was determined. The rate of loading was kept at 35 ± 7 psi/sec (0.25 ± 0.05 MPa/sec) as described in ASTM C39 [29]. Figure 2.15 shows compression test for each fiber dosage.

Figure 2.15 - Concrete compression test based on ASTM C39

2.7 Flexural test results

Based on ASTM C1609, the modulus of rupture (ft) is calculated according to the peak flexural load of a beam specimen in the three-point loading test. This material property was defined for each fiber dosage beam testing.

Figure 2.16 and Figure 2.17 show the load-deflection plots attained from the flexural test conducted on beam specimens with different fiber dosages and two different

target compressive strength values. Each curve was calculated as the average of the test results of three beam specimens.

The deflection was recorded by two LVDTs installed in the middle of the specimen, in both front and back surfaces, and was calculated as the average of the two readings.

The addition of synthetic fiber influences load-deformation response of the beam specimen as well the modulus of rupture. The modulus of rupture represents concrete flexural tensile strength at a moment of the first crack. Based on ASTM C1609, by considering the first peak load the modules of rupture has been calculated as follow:

$$f = \frac{PL}{b.d^2}$$

Where P – total peak load from MTS reading, [lbf];

L – the span length, [in];

b – the average width of the specimen at the fracture, [in];

d – the average depth of the specimen at the fracture, [in].

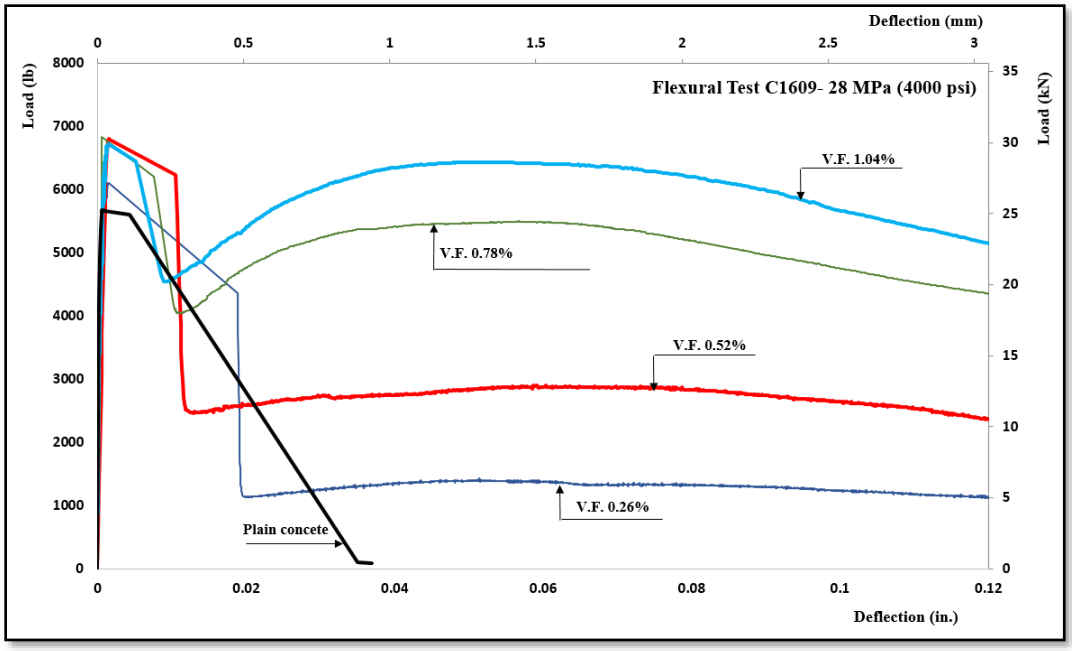

Figure 2.16 - Load-deflection plot based on ASTM C1609 for concrete with 28 MPa compressive strength

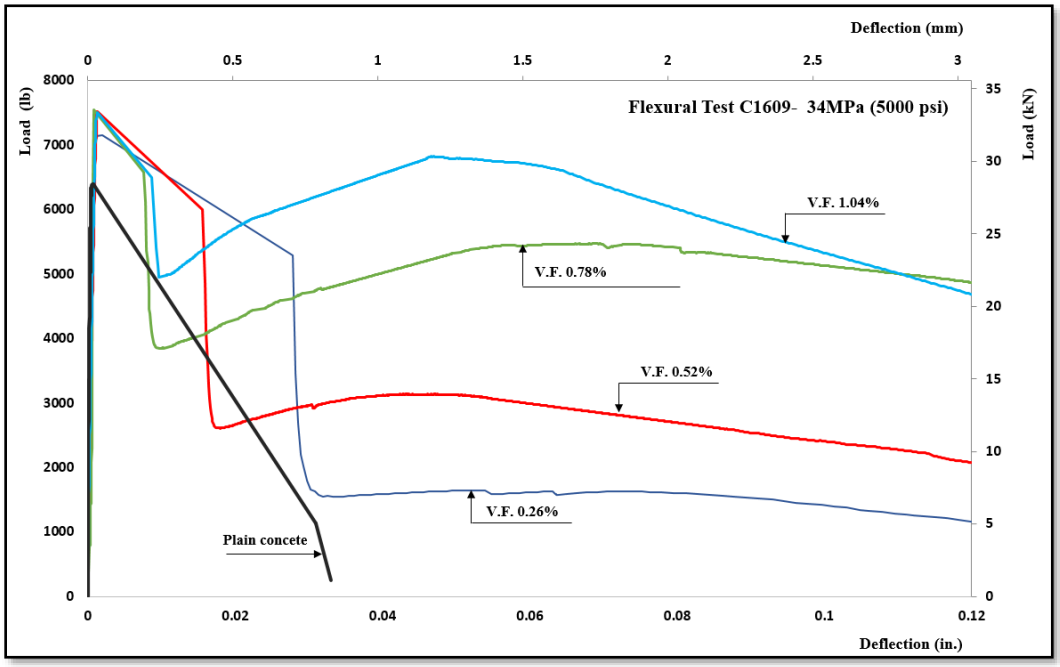

Figure 2.17 - Load-deflection plot based on ASTM C1609 for concrete with 34 MPa compressive strength

Flexural toughness was defined based on the area under the load-deflection curve up to a deflection of L/150 or 0.5 mm (0.12 in.). As shown in Figure 2.16 and figure 2.17, the load dropped after reaching the peak load, which happened at the same time of the crack initiation, and after that, the beam started to regain its stiffness due to the fibers engagement. In higher fiber dosages, after a slight drop of the load, once the peak-load reached, the beams took additional load (strain hardening) and the area under the curve (energy dissipation) improved more significantly.

Table 2.7 reveals the flexural test results for concrete with 28 MPa (4,000 psi) compressive strength and different fiber contents. As shown, by increasing the fiber dosage from V.F.=0% to V.F. = 1.04%, the modules of rupture increased up to 18% (V.F. = 0.78%). It can be seen that by increasing fiber volume fraction, the modules of rupture doesn't change with the same rate. As shown, the optimum fiber volume fraction value will be 0.52% which improved modules of rupture by 17%. After that, increasing the fiber dosages didn't have a considerable effect on changing the modules of rupture. As shown in Table 2.7, by increasing fiber volume fraction, flexural toughness increased up to 540%.

Table 2.8 illustrates the flexural test results for concrete with 34 MPa (5,000 psi) compressive strength and different fiber dosage rates. As shown in this table, by increasing fiber dosage, the modules of rupture increased up to 19% (V.F= 0.78%) but the changing rate is not constant. The optimum fiber volume fraction is 0.52% which enhanced modules of rupture up to 18%. As shown in Table 2.8, by increasing fiber volume fraction, flexural toughness enhanced up to 555%. By comparing the flexural test results for concrete with 28 MPa (4,000 psi) and 34 MPa (5,000 psi)

compressive strength values (Table 2.7 and Table 2.8), it can be seen that increasing the compressive strength by 25% (changing from 28 MPa to 34 MPa) doesn't have significant effect on modules of rupture and flexural toughness (except for 0.26% fiber volume fraction).

Table 2.7 Compare flexural test results for concrete with different fiber dosage

28 (4,000) concrete, MPa (psi)				
Vol. Fraction (V.F.), %	**Modules of rupture, MPa (psi)**	**Increase in modules of rupture (%)**	**Flexural toughness, N.m (lb.in)**	**Increase in flexural toughness (%)**
0	3.31 (480)	-	12.5 (111)	-
0.26	3.51 (513)	7	29 (256)	131
0.52	3.91 (560)	17	41.1 (364)	228
0.78	3.92 (569)	18	69.5 (615)	454
1.04	3.87 (561)	17	80.2 (710)	540

Table 2.8 Compare flexural test results for concrete with different fiber dosage

34 (5,000) concrete, MPa (psi)				
Vol. Fraction (V.F.), %	**Modules of rupture, MPa (psi)**	**Increase in modules of rupture (%)**	**Flexural toughness, N.m (lb.in)**	**Increase in flexural toughness (%)**
0	3.66 (532)	-	12.65 (112)	-
0.26	4.03 (585)	10	32.7 (289)	158
0.52	4.32 (626)	18	44 (389)	247
0.78	4.36 (631)	19	72 (637)	469
1.04	4.31 (625)	17	83 (734)	555

2.8 Compression test results

As shown in Tables 2.9 and 2.10, by increasing the fiber volume fraction from 0% to 0.52%, the concrete cylinders could resist 17% more compression load for both 28 MPa (4,000 psi) and 34 MPa (5,000 psi) compressive strength values. However, increasing the fiber volume fraction from 0.52% to 1.04% has less effect on compressive strength. As shown in Tables 2.9 and 2.10, for 1.04% fiber volume fraction, compressive strength increased 10% and 12% for 28 MPa (4,000 psi) and 34 MPa (5,000 psi) compressive strength values, respectively. Therefore, the

optimum fiber volume fraction values were shown to be 0.52% for both concrete mix design.

Table 2.9 Compressive strength for different fiber dosage after 7 days (28 MPa (4,000 psi) plain concrete)

Vol. Fraction (V.F.), %	Compressive strength, MPa (psi)	Increase in fc (%)
0	28.3 (4,100)	-
0.26	31.3 (4,544)	11
0.52	33.0 (4,780)	17
0.78	32.75 (4,750)	16
1.04	31.1 (4,510)	10

Table 2.10 Compressive strength for different fiber dosage after 7 days (34 MPa (5,000 psi) plain concrete)

Vol. Fraction (V.F.), %	Compressive strength, MPa (psi)	Increase in fc (%)
0	34.0 (4,940)	-
0.26	39.4 (5,700)	15
0.52	39.9 (5,790)	17
0.78	39.8 (5,770)	16
1.04	38.3 (5,550)	12

Based on the shear and flexural test results, increasing the compressive strength enhances the shear strength and shear toughness more remarkably than flexural strength and flexural toughness. Moreover, increasing the compressive strength has more influence on the lower fiber dosages concrete than the higher ones.

CHAPTER 3

EXPERIMENTAL PROGRAM ON BOX CULVERTS

3.1 Introduction

Full-scale experimental tests were performed on five box culverts with three different spans of 122 cm (4 ft), 244 cm (8 ft) and 366 cm (12 ft) designated as per ASTM C1433-05 and ASTM C1577 and equipped with 0.52% fiber volume fraction (8 PCY). The rise of all of the box culverts was 144 cm (4 ft). The wall and the slab thickness of box culverts were 20 cm (8 in) for 4'x4' and 8'x4' box culverts and 30 cm (12 in) for 12'x4' box culvert designed based on ASTM C1433 and for the other two ones followed ASTM C1577 design criteria. Boxes were manufactured in Northern Concrete Pipe Company in Michigan and Forterra and shipped to Civil Engineering Laboratory Building (CELB) at UTA in order to be tested in a more controlled environment. The instrumentation used during the test consisted of two wire potentiometers placed at two different locations (In the middle of the loading plate and also in the center of the box slab), data acquisition system, and an actuator connected to a fixed frame in CELB. The load was applied gradually in the form of displacement control.

Each test was performed with the assistance of a minimum of 3 researchers who identified and marked each crack in addition to scribing each event of each test. The

load-deflection plot, detailed report on crack formation/initiation, and discussion of the failure mode are reported.

3.2 Specimen preparation

The reinforcement cages were fabricated by the manufacturer as per design ASTM C1433 and ASTM C1577 with 34 MPa (5000 psi) concrete compressive strength and the fiber has been added to the concrete before casting. After curing, the boxes shipped to UTA for testing. Figure 3.1 shows the box culvert cages before casting and making them ready for curing process after casting.

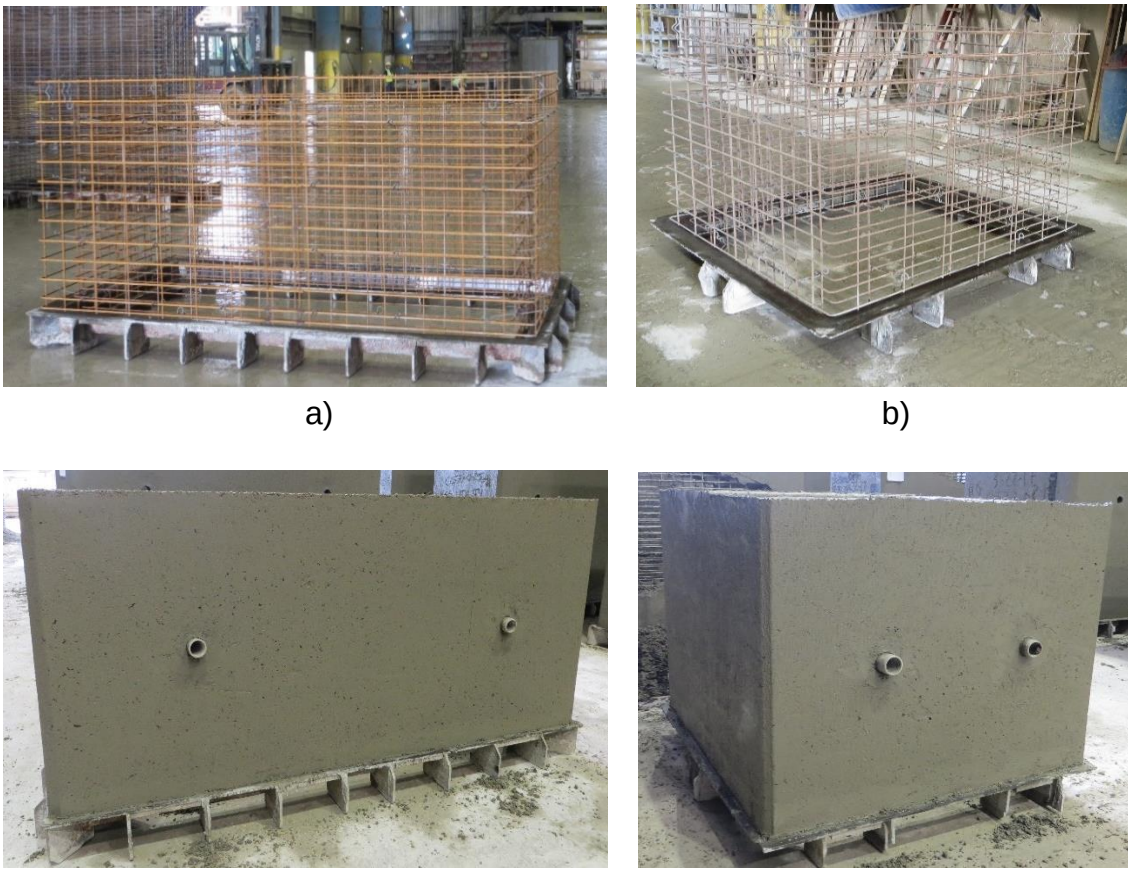

Figure 3.1- Box culverts manufacturing process, a) reinforcement cage box 8 ft by 4 ft, b) box culvert 4 ft by 4 ft, c and d) making boxes ready for curing after casting

After curing, the box culverts have been transferred to CELB by a trailer and moved to reaction room in CELB by using a crane with the capacity of 15 ton (30000 lb) and placed under actuator and made it ready for the test (Figure 3.2).

a)

b)

c)

d)

Figure 3.2 - Culverts handling at CELB a and b) Moving from plant to CELB c) unloading the trailer d) putting the culverts under actuator and make it ready for the test

3.3 Test set-up and instrumentation

A 25 cm x 51 cm x 2.54 cm (10 in x 20 in x 1 in) mild steel load plate supported by a 1.27 cm (1/2 in) thick rubber sheet, was placed on the top of the box culvert at the distance d from the tip of the haunch to the edge of the plate. This was done in order

to simulate the contact area of the wheel of a HS20 truck or tandem, having an axle load of 142 kN (32 kips) and wheel load of 71 kN (16 kips). A cylindrical stub column with 17.78 cm (7 in.) diameter and 50.8 cm (20 in.) length along with a beam with enough stiffener on its web has been placed on top of the load plate to transfer the load from the actuator to the plate (Figure 3.3). In order to introduce the maximum stress state in the culvert and to consider the most conservative behavior, each box culvert was placed directly on the top of the reaction floor. The load was applied gradually in the form of displacement control.

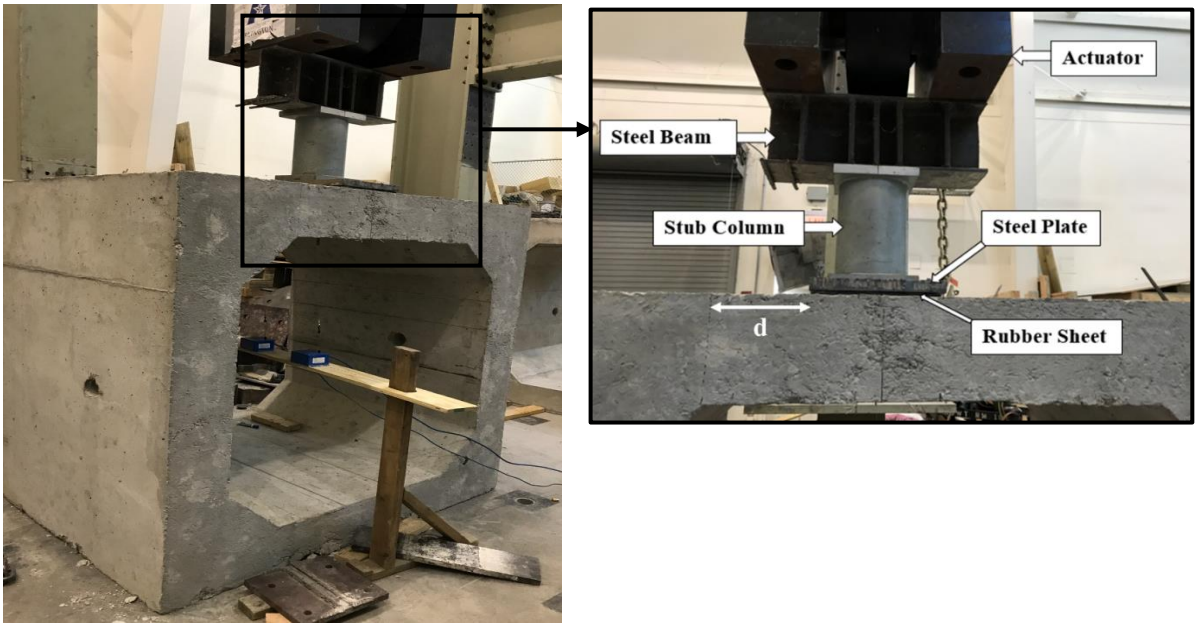

Figure 3.3 - Box culverts test set-up

A data acquisition system and two cable-Extension displacement sensors were used for recording the data. The load was applied in the form of displacement from the actuator to the middle of the steel plate and the culvert deflection was measured by two potentiometers, as shown in Figure 3.4. The load and deflection were recorded

by a data acquisition system as shown in Figure 3.5. The displacement sensors were connected to a scanner (Micro Measurement) and the Strainsmart 5000 software was used to acquire and store the data for each test. Figure 3.5-(b) shows the system used for controlling the actuator and moving it up and down manually or automatically.

a)

b)

Figure 3.4- Two cable-extension displacement sensors were placed under the top slab in order to measure slab deflection in middle of the steel plate and slab during the test

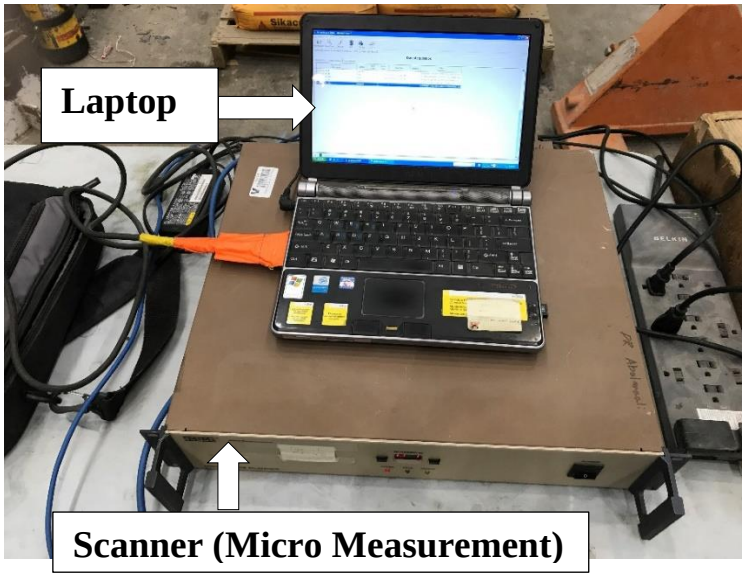

a)

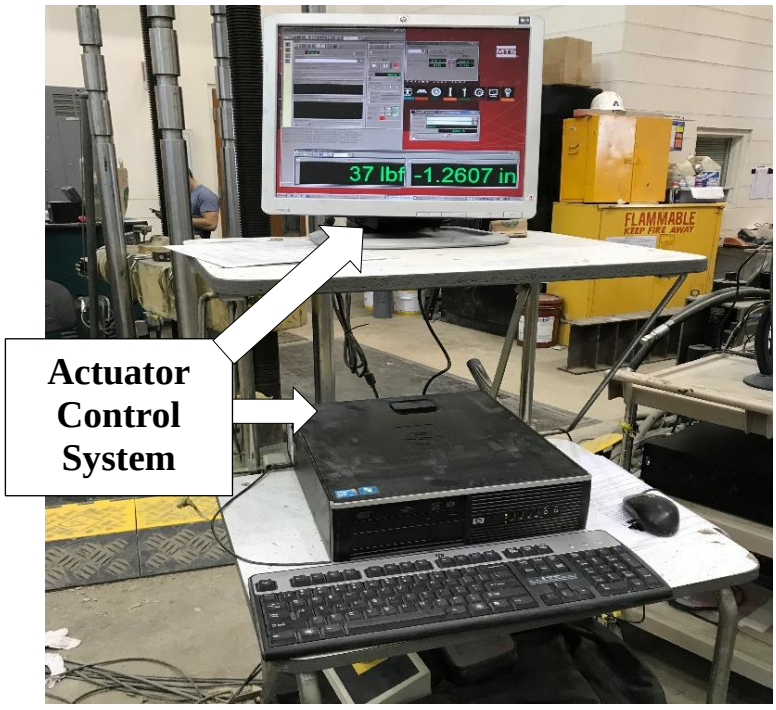

b)

Figure 3.5 – a) Data collection system and b) actuator control system

3.4 Box culvert sizes

Full-scale experimental tests were performed on five box culverts with spans of 122 cm (4 ft), 244 cm (8 ft) and 366 (12ft) designated as per ASTM C1433-05 and ASTM C1577 equipped with 0.52% fiber volume fraction (8 PCY). The rise of all of the box culverts was 144 cm (4 ft). The wall and the slab thickness of box culverts were 20 cm (8 in) for 4'x4' and 8'x4' box culverts and 30 cm (12 in) for 12'x4' box culvert designed based on ASTM C1433 and for the other two ones followed ASTM C1577 design criteria. The joint length of all boxes was 144 cm (4 ft). The geometric detail of all box culverts has been shown in Table 3.1. The plain welded wires were used for the reinforcement cages as per ASTM A 185. The sizes of the steel wires used for the reinforcement cages were W2.5 to W9.0 with the nominal area of 16.13 mm^2 (0.025 in^2) through 58.06 mm^2 (0.09 in^2) per reinforced wire. Typical spacing of wires was 5 cm (2 in), 7.5 cm (3 in), and 20 cm (8 in).

Table 3.1 Geometric properties of box culverts

Specimen	Code	Span m (ft)	Rise m (ft)	Joint m (ft)	Haunch cm (in)	Th $_{Topslab}$ cm (in)	Th $_{Botslab}$ cm (in)	Th $_{wall}$ cm (in)
Box 4'x4'-1433	ASTM C1433	1.22 (4)	1.22 (4)	1.22 (4)	20.32 (8)	20.32 (8)	20.32 (8)	20.32 (8)
Box 8'x4'-1433	ASTM C1433	2.44 (8)	1.22 (4)	1.22 (4)	20.32 (8)	20.32 (8)	20.32 (8)	20.32 (8)
Box 12'x4'-1433	ASTM C1433	3.66 (12)	1.22 (4)	1.22 (4)	30.48 (12)	30.48 (12)	30.48 (12)	30.48 (12)
Box 4'x4'-1577	ASTM C1577	1.22 (4)	1.22 (4)	1.22 (4)	12.70 (5)	19.05 (7.5)	15.24 (6)	12.70 (5)
Box 8'x4'-1577	ASTM C1577	2.44 (8)	1.22 (4)	1.22 (4)	20.32 (8)	20.32 (8)	20.32 (8)	20.32 (8)

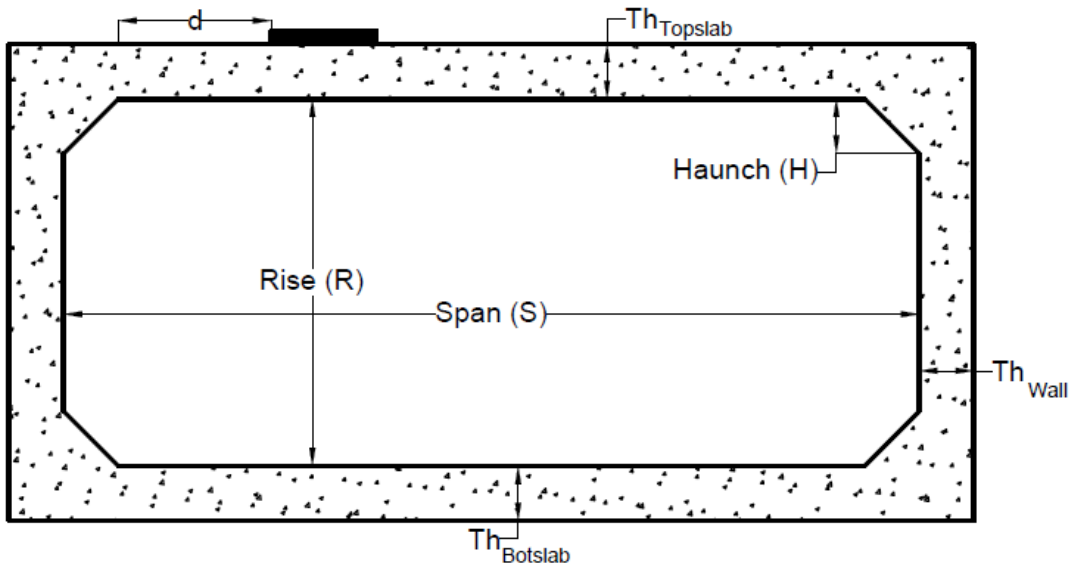

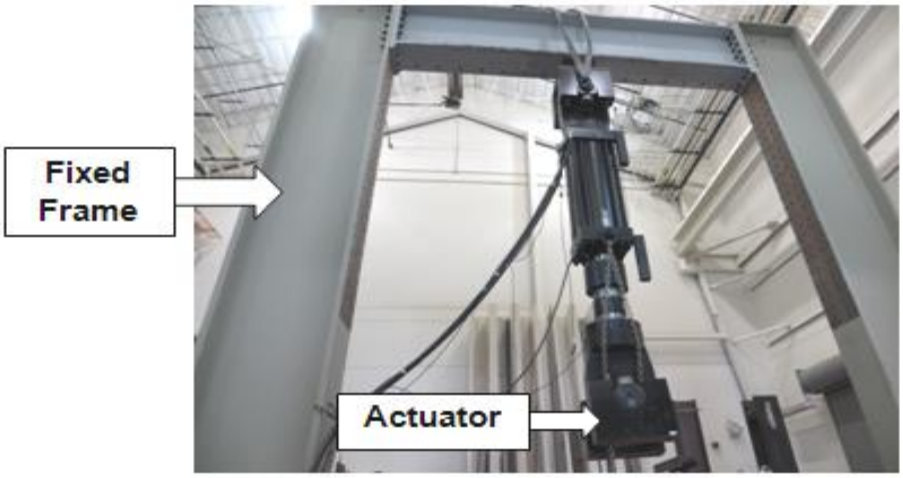

Figure 3.6 - Actuator connected to a fixed frame

3.5 Location of load

The scope of this experimental program was to investigate the shear strength of box culverts equipped with synthetic fiber and compared the results with the one without Fiber. In 2007, in a very comprehensive study, Anil Garg [24] had studied the shear behavior and capacity of 24 precast concrete box culverts subjected to HS 20 truck wheel load by applying the load at different distances from the tip of the haunch. Based on their investigation, the most critical place for putting the load plate (10 in.×20 in. ×1 in) is at a distance d from the tip of the haunch to the edge of the load plate (Figure 3.7). This study continued the previous investigation but this time by using the synthetic fiber in the concrete along with regular reinforcement.

Figure 3.7 -The steel plate placed at the distance d in order to investigate the shear capacity of box

3.6 Crack monitoring

During the test, after each crack occurred, a line parallel to each crack was drawn to identify the path of each crack on the slab or walls and the related load for each crack was written next to each one in kips for future evaluations (Figure 3.8).

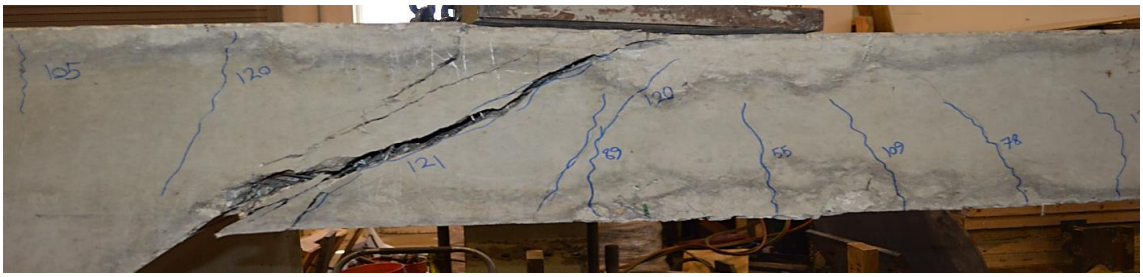

Figure 3.8 - Crack monitoring

3.7 Experimental results

3.7.1 Box of 244 cm (12 ft) span and 122 cm (4 ft) rise and joint length based on ASTM C1433

In all of the tests conducted, the load plate was placed on the left side of the culvert. The main events during the experimental test have been recorded and were shown in Table 3.2. The first crack was superficial flexural crack which occurred on the inside face of the top slab exactly under the load plate. Flexural cracks continued to arise in this area throughout the testing. At approximately 445 kN (100 kips), flexural cracks started to occur on the left wall of the box culvert. The main crack was a shear crack that occurred diagonally from tip of the left haunch to the middle of the load plate at approximately 930 kN (209 kips). The Load versus deflection at the center point of load plate was shown in Figure 3.9. The photographs of box culvert with the detail of cracking on slabs and walls occurred during the test have been presented in Figure 3.10. The Photographs of the setup and the observed failure are presented in Appendix A.

Table 3.2– Crack events for box of 366 cm (12 ft) span and 122 cm (4 ft) rise and joint length

Event No.	Event	Test load kN (kip)	Crack width mm (in)
1	The 1st superficial flexural crack detected on the inside face of the top slab under the load plate	**395 (89)**	**0.1 (0.0039)**
2	The 1st superficial flexural crack initiated on the outside face of the wall (left side)	**445 (100)**	**0.15 (0.0059)**
3	The 2nd superficial flexural crack detected on the inside face of the top slab on the right side of the load plate	**467 (105)**	**0.15 (0.0059)**
4	The 2nd superficial flexural crack initiated on the outside face of the left wall	**525 (118)**	**0.15 (0.0059)**
5	Flexural crack detected on the inside face of the top slab under the load plate	**538 (121)**	**0.15 (0.0059)**
6	The first negative flexural crack initiated on outside face of top slab and extended toward the left haunch	**538 (121)**	**0.1 (0.0039)**
7	Flexural crack detected on the outside face of the left wall	**596 (134)**	**0.2 (0.0079)**
8	The first shear flexural crack initiated on the right side of the load plate	**680 (153)**	**0.15 (0.0059)**
9	Flexural crack detected in the middle of the outside face of the left wall	**730 (164)**	**0.1 (0.0039)**
10	The first shear crack initiated on the right side of the load plate	**800 (180)**	**0.15 (0.0059)**
11	The 1st Flexural crack detected on the right wall	**800(180)**	**0.15 (0.0059)**
12	Flexural crack detected on the top part of the outside face of the left wall	**800(180)**	**0.5 (0.0197)**
13	The shear crack initiated on the left side of the load plate from tip of the haunch to the edge of the load plate	**805(181)**	**1 (0.0393)**
14	The shear flexural crack initiated on the left side of the load plate	**823(185)**	**0.25 (0.0098)**
15	A major shear crack detected at the tip of the haunch toward the center of the load plate.	**930(209)**	**6 (0.236)**

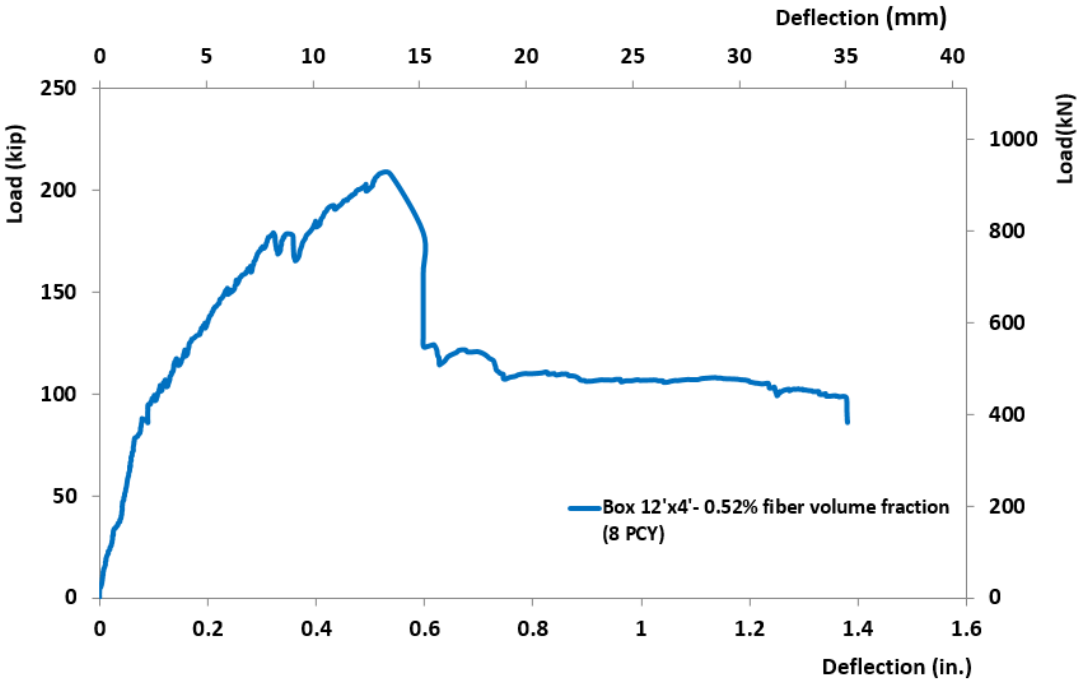

Figure 3.9 – Load versus deflection plot for box of 244 cm (8 ft) span and 122 cm (4ft) rise and joint length

a)


121
209
151
155
121
89
105
153
150

b)


125
120

c)


121
209
151
155
121
89
105

d)

e)

f)

g)

h)

Figure 3.10 -Experimental photographs: (a) uncrack box; (b) crack patterns under the load plate of top slab; (c) crack patterns on the right side of top slab; (d) Inside face of top slab; (e) outside face of top slab; (f) inside face of bottom slab (no crack); (g) outside face of left wall; (h) outside face of right wall.

3.7.2 Box of 244 cm (8 ft) span and 122 cm (4 ft) rise and joint length deigned based on ASTM C1433

This box culvert was designed based on ASTM C1433 and manufactured in Northern Concrete Pipe Company in Michigan In this box culvert, like the previous box culvert, the first crack was superficial flexural crack which occurred on the inside face of the top slab exactly under the load plate at approximately 245 kN (55 kips). Flexural cracks continued to occur under the load plate throughout the test. At approximately 355 kN (80 kips), flexural cracks started to occur on the sidewalls on box culvert. The main crack was a shear crack that occurred diagonally from tip of the left haunch to the middle of the load plate at approximately 540 kN (121 kips). The Load versus deflection at the center point of load plate was shown in Figure 3.11. The photographs of box culvert with the detail of cracking on slabs and walls occurred during the test have been illustrated in Figure 3.12. The Photographs of the setup and the observed failure are presented in Appendix B.

Table 3.3 – Crack events for box of 244 cm (8 ft) span and 122 cm (4 ft) rise and joint length

Event No.	Event	Test load kN (kip)
1	First superficial flexural crack detected on the inside face of the top slab under the load plate.	**245 (55)**
2	Second flexural crack detected on the inside face of the top slab near the middle of the slab and also first negative flexural crack detected on the outside face of the top slab close to the haunch.	**345 (78)**
3	First flexural crack initiated on the outside face of the wall (right side).	**355 (80)**
4	First flexural crack initiated on the outside face of the wall (left side, close to loading plate).	**427 (96)**
5	Flexural crack detected at the haunch on the outside face of the top slab.	**467 (105)**
6	First shear crack initiated at the loading end.	**535 (120)**
7	First Serviceability shear crack detected.	**540 (121)**
8	Failure	**300 (68)**

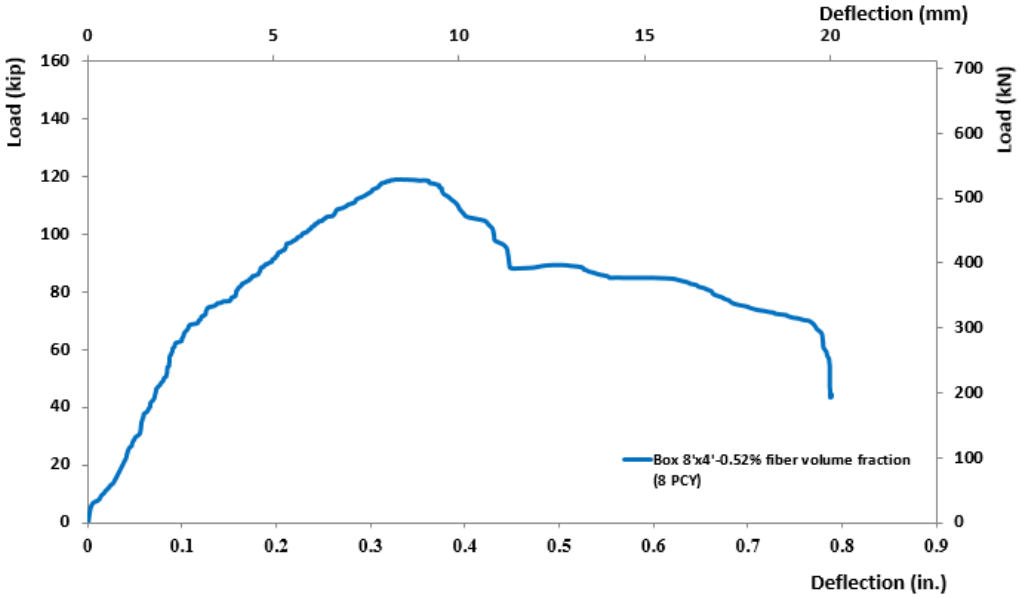

Figure 3.11 – Load versus deflection plot for box of 244 cm (8 ft) span and 122 cm (4ft) rise and joint length

a)

b)

c)

d)

e)

f)

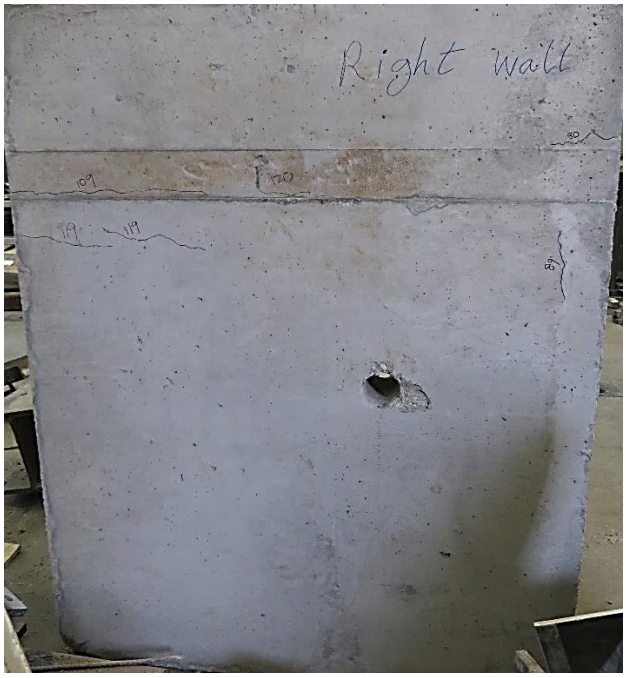

g) h)

Figure 3.12 -Experimental photographs: (a) uncrack box; (b) crack patterns under the load plate of top slab; (c) crack patterns on the right side of top slab; (d) Inside face of top slab; (e) outside face of top slab; (f) inside face of bottom slab (no crack); (g) outside face of left wall; (h) outside face of right wall

3.7.3 Box of 122 cm (4 ft) span, rise, and joint length designed based on ASTM C1433

This box culvert was also designed based on ASTM C1433 and manufactured in Northern Concrete Pipe Company in Michigan and shipped to UTA. In this box culvert, like the previous boxes, the first crack was superficial flexural crack which occurred on the inside face of the top slab exactly under the load plate at approximately 400 kN (90 kips). Flexural cracks continually occurred in this area throughout the test. At approximately 625 kN (140 kips), flexural cracks started to occur on the sidewalls on

box culvert. The main crack was the shear crack which occurred diagonally near the left haunch to the middle of the load plate at approximately 743 kN (167 kip). The detail of crack events was shown in Table 3.4. The Load versus deflection plot for this box culvert was shown in Figure 3.13. The photographs of box culvert with the detail of cracking on slabs and walls occurred during the test have been indicated in Figure 3.14.

Table 3.4 – Crack event for box of 122 cm (4 ft) span, rise, and joint length

Event No.	Event	Test load kN (kip)
1	First superficial flexural crack detected on the inside face of the top slab under the load plate.	**400 (90)**
2	Second flexural crack detected on the inside face of the top slab near the middle of the slab and also first negative flexural crack detected on the outside face of the top slab close to the haunch.	**423 (95)**
3	First flexural crack initiated on the outside face of the wall (right side).	**625 (140)**
4	First flexural crack initiated on the outside face of the wall (left side, close to loading plate).	**625 (140)**
5	Flexural crack detected at the haunch on the outside face of the top slab.	**588 (132)**
6	First shear crack initiated at the loading end.	**743 (167)**
7	First Serviceability shear crack detected.	**796 (179)**
8	Failure	**267 (60)**

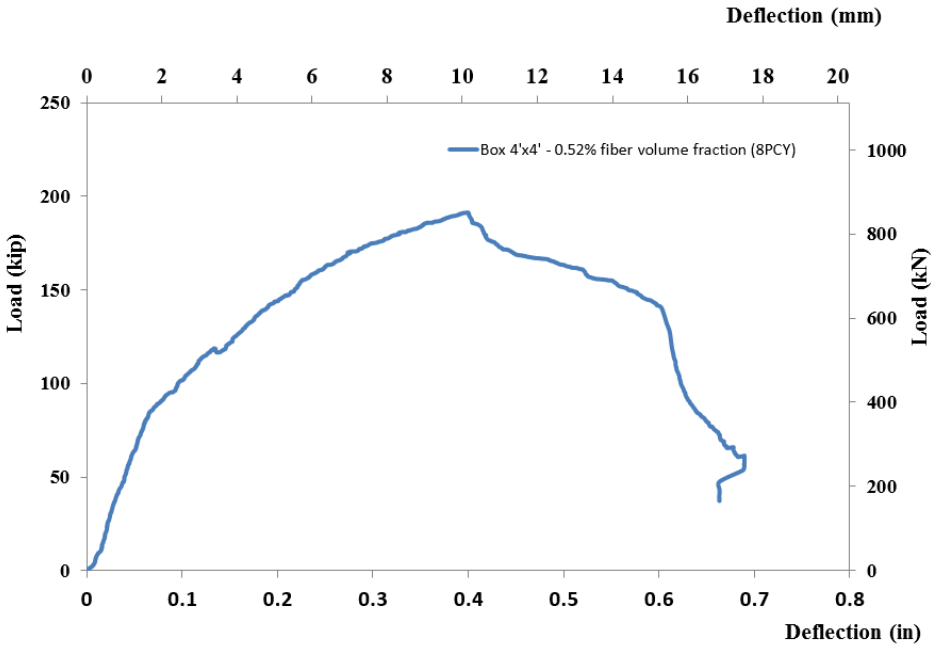

Figure 3.13- Load versus deflection plot for box of 122 cm (4 ft) span, rise and joint length

a)

b)

c)

d)

e)

f)

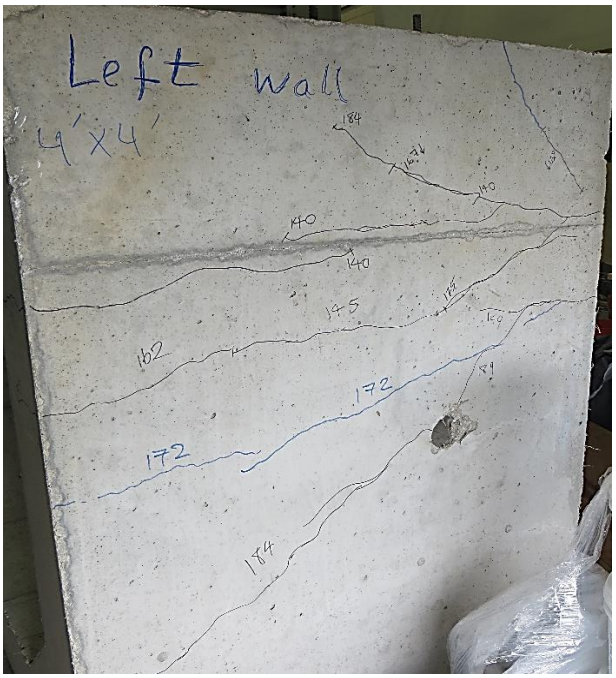

g)

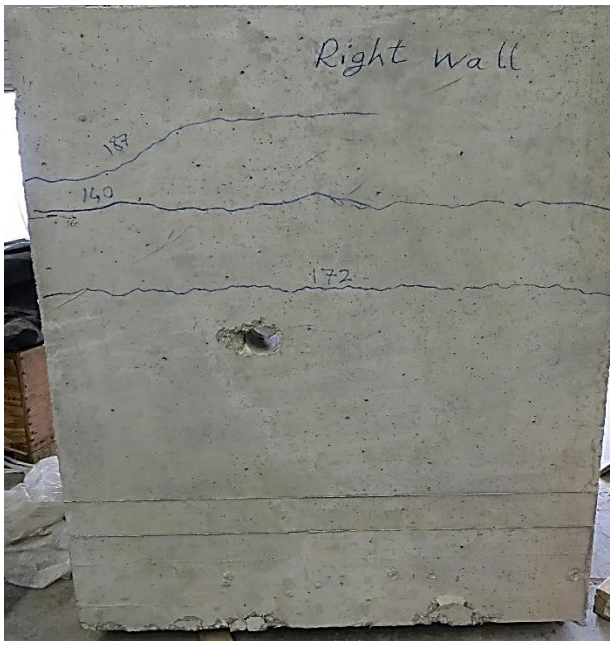

h)

Figure 3.14 - Experimental photographs: (a) uncrack box; (b) crack patterns under the load plate of top slab; (c) crack patterns on the right side of top slab; (d) inside face of top slab; (e) outside face of top slab; (f) inside face of bottom slab (no crack); (g) outside face of left wall; (h) outside face of right wall.

3.7.4 Box of 244 cm (8 ft) span and 122 cm (4 ft) rise and joint length deigned based on ASTM C1577

This box culvert was designed based on ASTM C1577 and manufactured at Forterra. The crack pattern was similar to the previous box culverts. In this box culvert, the first crack was superficial flexural crack which occurred on the inside face of the top slab exactly under the load plate at approximately 298 kN (67 kips). Flexural cracks continued to occur under the load plate throughout the test. At approximately 365 kN (82 kips), flexural cracks started to occur on the sidewalls on box culvert. The main

crack was a shear crack that occurred diagonally from tip of the left haunch to the middle of the load plate at approximately 650 kN (146 kips). The Load versus deflection at the center point of load plate was shown in Figure 3.15. The photographs of box culvert with the detail of cracking on slabs and walls occurred during the test have been illustrated in Figure 3.16. The Photographs of the setup and the observed failure are presented in Appendix B.

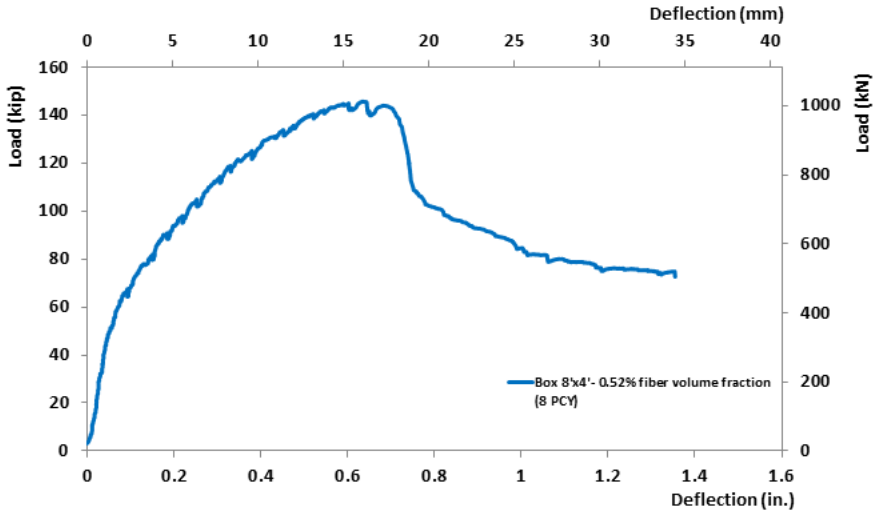

Figure 3.15– Load versus deflection plot for box of 244 cm (8 ft) span and 122 cm (4ft) rise and joint length designed based on ASTM C1577

Table 3.5- Crack Event for box of 244 cm (8 ft) span and 122 cm (4 ft) rise and joint length

Event No.	Event	Test load kN (kip)	Crack width mm (in)
1	First superficial flexural crack detected on the inside face of the top slab under the load plate.	**298 (67)**	**0.1 (0.0039)**
2	Second flexural crack detected on the right side of top slab close to haunch	**298 (67)**	**0.1 (0.0039)**
3	Second superficial flexural crack detected on the inside face of the top slab under the load plate.	**365 (82)**	**0.1 (0.0039)**
4	First flexural crack initiated on the outside face of the wall (right side)	**365 (82)**	**0.1 (0.0039)**
5	First flexural-shear crack detected on the top slab, left side close to haunch	**400 (90)**	**0.15 (0.0059)**
6	Flexural crack detected on the right side of loading plate	**431 (97)**	**0.1 (0.0039)**
7	Second flexural crack initiated on the outside face of the wall (right side)	**431 (97)**	**0.1 (0.0039)**
8	Flexural crack detected on the right side of top slab	**467 (105)**	**0.1 (0.0039)**
9	First flexural crack initiated on the outside face of the wall (left side)	**530 (119)**	**0.1 (0.0039)**
10	First Serviceability shear crack detected	**650 (146)**	**1.5 (0.059)**
11	Failure	**355 (80)**	**2 (0.078)**

a)

b)

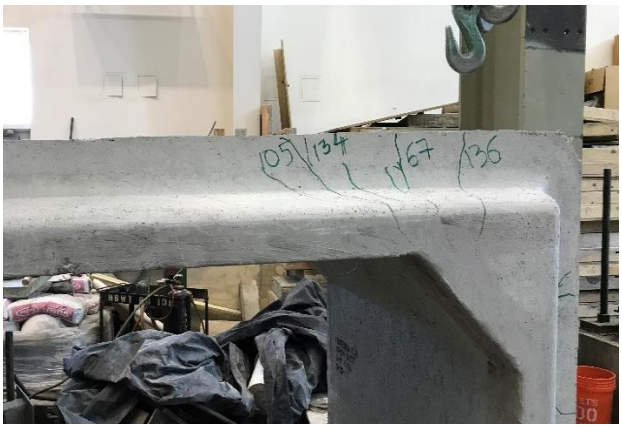

c)

d)

e)

f)

g)

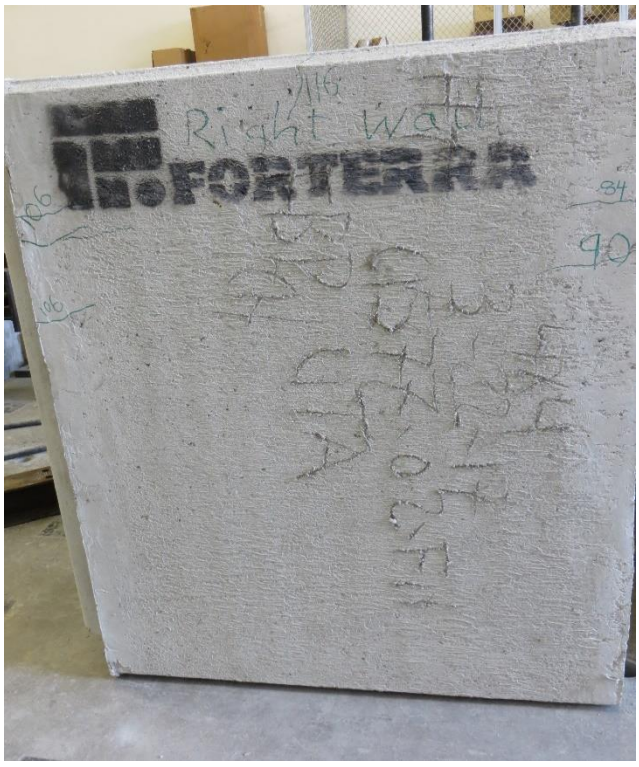

h)

Figure 3.16 -Experimental photographs: (a) uncrack box; (b) crack patterns under the load plate of top slab; (c) crack patterns on the right side of top slab; (d) inside face of top slab; (e) outside face of top slab; (f) inside face of bottom slab (no crack); (g) outside face of left wall; (h) outside face of right wall.

3.7.5 Box of 122 cm (4 ft) span, rise, and joint length designed based on ASTM C1577

In this box culvert, like the previous boxes, the first crack was superficial flexural crack which occurred on the inside face of the top slab exactly under the load plate at approximately 315 kN (61 kips). Flexural cracks continually occurred in this area throughout the test. At approximately 625 kN (71 kips), flexural cracks started to occur on the sidewalls on box culvert. The main crack was the shear crack which occurred diagonally near the left haunch to the middle of the load plate at approximately 525 kN (118 kip). The detail of crack events was shown in Table 3.6. The Load versus deflection plot for this box culvert was shown in Figure 3.17. The photographs of box culvert with the detail of cracking on slabs and walls occurred during the test have been indicated in Figure 3.18. The Photographs of the set up and the observed failure are presented in Appendix B.

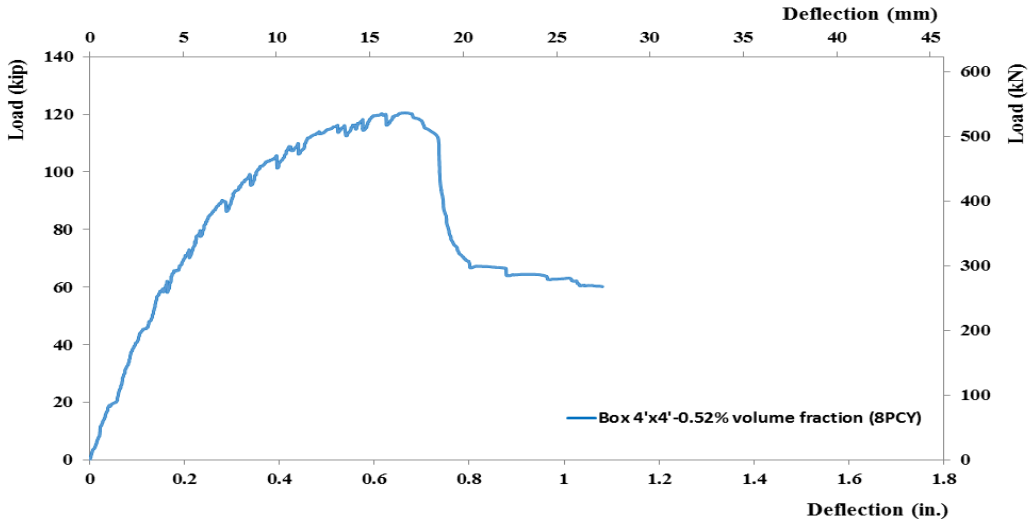

Figure 3.17 - Load versus deflection plot for box of 122 cm (4 ft) span, rise and joint length

Table 3.6 – Crack event for box of 122 cm (4 ft) span, rise and joint length

Event No.	Event	Test load kN (kip)	Crack width mm (in)
1	First superficial flexural crack detected on the inside face of the top slab under the load plate.	**271 (61)**	**0.1 (0.0039)**
2	Second flexural crack detected on the top slab near the middle of the slab	**315 (71)**	**0.1 (0.0039)**
3	First flexural crack initiated on the outside face of the wall (left side).	**315 (71)**	**0.1 (0.0039)**
4	First flexural-shear crack detected on the top slab close to haunch	**355 (80)**	**0.15 (0.0059)**
5	First flexural crack initiated on the outside face of the wall (Right side)	**373 (84)**	**0.1 (0.0039)**
6	First shear crack detected on the top slab close to haunch	**431 (90)**	**0.15 (0.0059)**
7	Flexural crack initiated on the outside face of the wall (Right side)	**431 (90)**	**0.15 (0.0059)**
8	Flexural crack and shear crack observed under the load plate and on the right side of loading plate respectively	**472 (106)**	**0.15 (0.0059)**
9	First main shear crack initiated at the loading end.	**490 (110)**	**1.0 (0.039)**
10	First Serviceability shear crack detected.	**525 (118)**	**1.5 (0.059)**
11	Failure	**267 (60)**	**2 (0.078)**

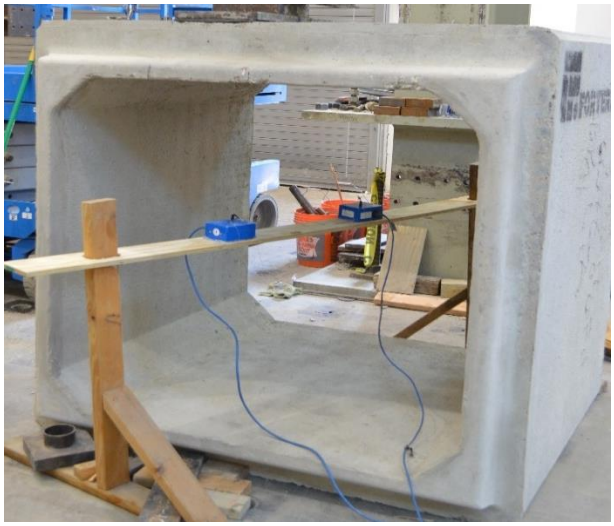

a)

b)

c)

d)

e)

f)

g)

h)

Figure 3.18 - Experimental photographs: (a) uncrack box; (b) crack patterns under the load plate of top slab; (c) crack patterns on the right side of top slab; (d) inside face of top slab; (e) outside face of Top Slab; (f) inside face of bottom slab (no crack); (g) outside face of left wall; (h) outside face of right wall.

3.8 Least square data fitting

One of statistical regression techniques used for data analysis is Least squares fitting. By establishing a relation between the independent and dependant variables, we can predict the data. In measuring the experimental data, there are generally some error or uncertainty. Error can be human error or due to the limitation in the equipment being used to do the measurement. For representing the experimental data by some functional expression, we may pick a particular form of function (or a particular form of formula).

If experimental data seeks to get an unknown functional relationship like y = f(x), for each varying values of x, like $x_1, x_2, \dots, x_n$, there is a corresponding set of values for y. If the actual measurements be donated by $y_1, y_2, \dots, y_n$, then the unknown measurement errors is equal to

$$\epsilon_i = f(x_i) - y_i$$

In order to use this concept for box culvert experimental data, we assume

$$\delta = \frac{p}{\frac{E^{\alpha} I^{\beta}}{L^3}} = \frac{p}{k}$$

in which:

$p =$ Applied load

$E =$ Modulus of Elasticity

$I =$ Moment of Inertia

$L =$ Effective length (Span of box culvert by considering haunches)

$$\frac{E^{\alpha}I^{\beta}}{L^3} = k = \text{stiffness}$$

For finding α and β, there are three different ways:

1) Choose α and β so as to minimize an average approximation error

$$\frac{1}{n}\sum_{i=1}^{n}|f(x_i) - y_i|$$

2) Choose α and β so as to minimize an average approximation error called root mean square error

$$E = \sqrt{\frac{1}{n}\sum_{i=1}^{n}[f(x_i) - y_i]^2}$$

3) Choose α and β so as to minimize the maximum error of approximation

$$\max_{1\le i\le n}|f(x_i) - y_i|$$

Among all these three methods, #2 is the most common one used for calculating α and β. Therefore, we have

$$E = \sqrt{\frac{1}{n}\sum_{i=1}^{n}[\delta_{pred} - \delta_{exact}]^2}$$

$$E = \sqrt{\frac{1}{n}\sum_{i=1}^{n}[\frac{p_i}{\frac{E^{\alpha}I^{\beta}}{L^3}} - \delta_i]^2}$$

For minimize the E, α and β need to satisfy the below equation

$$G(\alpha,\beta) = [\frac{p_i}{\frac{E^{\alpha} I^{\beta}}{L^3}} - \delta_i]^2$$

$$\frac{\partial G(\alpha,\beta)}{\partial \alpha} = 0 \, , \frac{\partial G(\alpha,\beta)}{\partial \beta} = 0$$

$$\frac{\partial G}{\partial \alpha} = 0 \;\rightarrow\; 2 * \sum_{i=1}^{n} \left(\frac{p_i \, L^3}{E^{\alpha} I^{\beta}} - \delta_i \right) * \left(\frac{-p_i \, L^3 \ln E}{E^{\alpha} I^{\beta}} \right) = 0$$

$$\rightarrow \qquad \sum (\ln E) p_i \delta_i - \sum \left(\frac{L^3 \ln E}{E^{\alpha} I^{\beta}} \right) * p_i^2 = 0$$

Figure 3.19 to Figure 3.22 show the normalization results conducted on the box culvert experimental data based on the least square data fitting method. As shown there is a good agreement between the experimental results of box culverts produced by Forterra and for boxes manufactured by Northern concrete except 8'x4' box, there is a good agreement between the experimental results of the other two boxes.

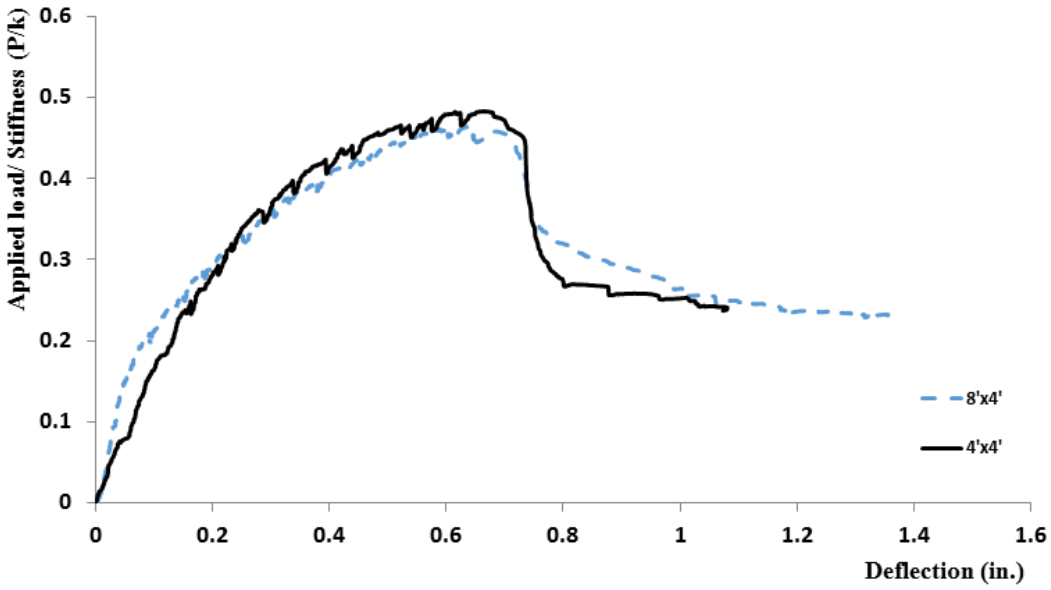

Figure 3.19 - Results of normalization on Forterra box culverts

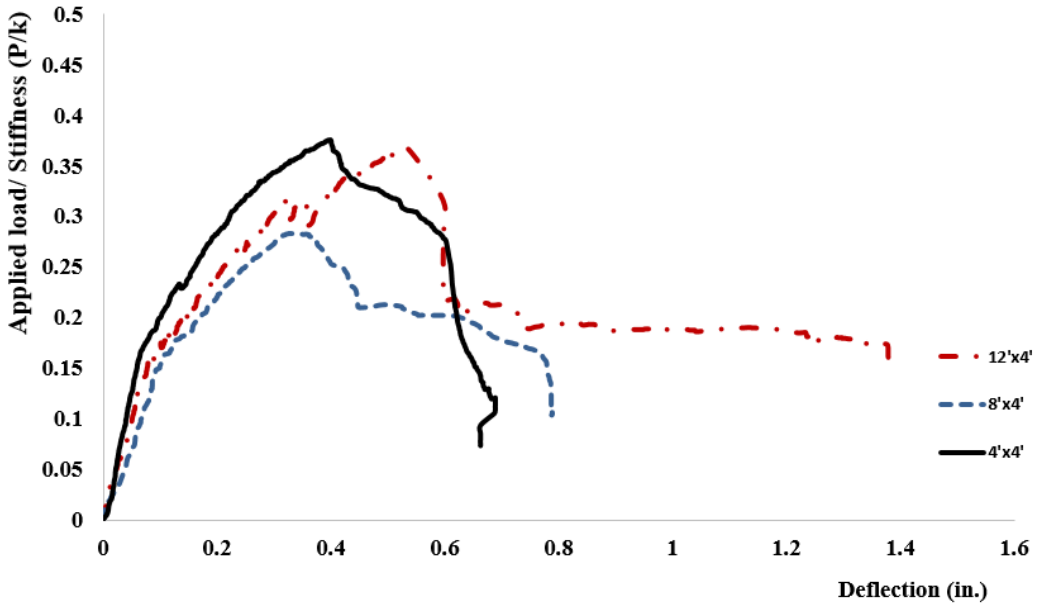

Figure 3.20 - Results of normalization on Northern Concrete box culverts

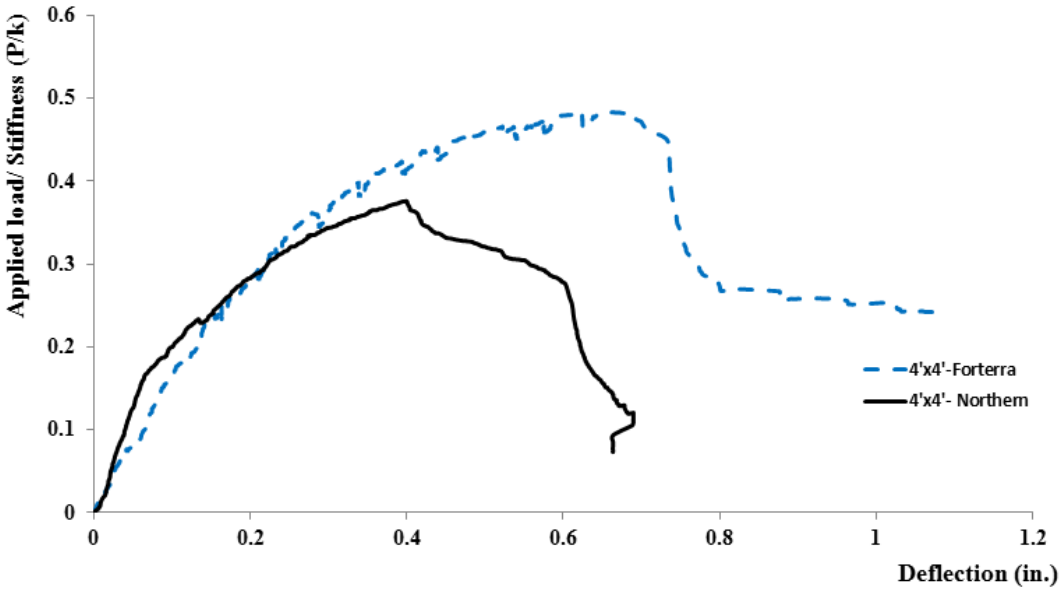

Figure 3.21 - Comparison between normalization results of 4'x4' boxes

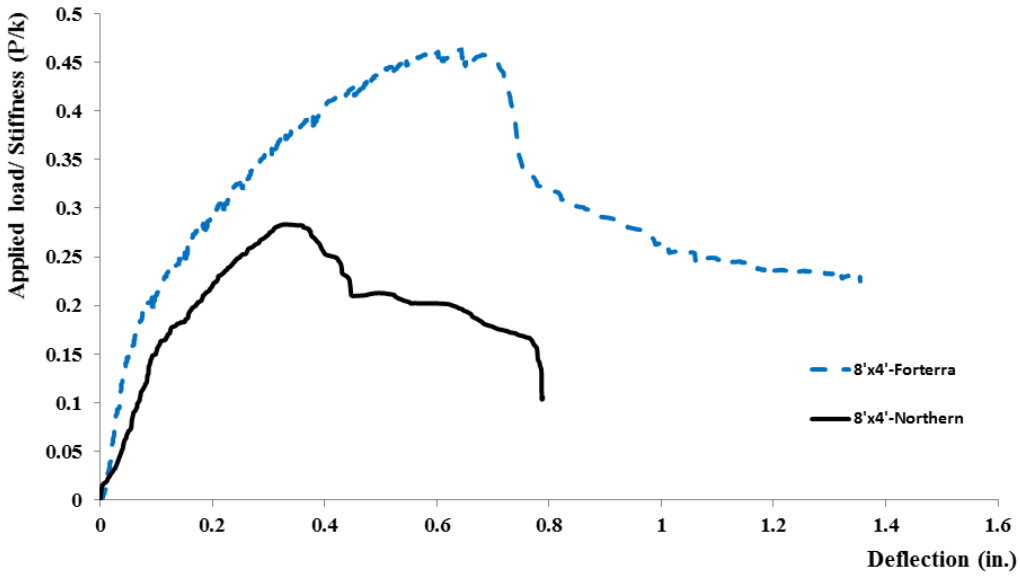

Figure 3.22 - Comparison between normalization results of 8'x4' boxes

CHAPTER 4

FINITE ELEMENT ANALYSIS ON SHEAR BEAM

4.1 Introduction

This chapter describes the finite element modeling of synthetic fiber reinforced concrete beam in ABAQUS in order to capture the shear capacity of this material by using interface element and compare the FEM results with JSCE shear test results.

A three dimensional full-scale model was built based on the experimental test. Three dimensional solid elements with geometric and material non-linearities were used for the beam. The presence of synthetic fibers in notch area was modeled through the introduction of an interface element in notch area of the beam. The model also included two loading strips with the dimension of 0.6 in. x 6 in. (127 mm x 127 mm) for displacement application to the beam and two supports with dimension 8 in. x 8 in. at the bottom of the beam in both sides for holding the beam from moving down and also two plates (4.5 in. x 8 in.) on top of the beam for keeping the beam from the rotation (Similar to the real test set-up). The FEM model met all the boundary conditions in JSCE shear test.

Concrete damaged plasticity has been used for the whole beam except the notch areas with a density of 2400 kg/m3 (150 pcf), Modulus of Elasticity of 24870 MPa (4000 ksi) and 27405 MPa (5000 ksi) and Poisson's ratio 0.2, total strain 0.003 and cohesive behavior has been defined for notch areas.

Finite element model verification was achieved for two different concrete compressive strength values and compared the results of FEM to that of the experimental results to develop the shear capacity of synthetic fiber reinforced concrete with 7000 psi strength.

4.2 Elements

4.2.1 Solid element

In modeling the beam, Eight-noded isoparametric solid elements with hourglass control and reduced integration algorithm were used. For reducing computational time, reduced integration used in lower order integration to form the element stiffness. It is also referred to as uniform strain or centroidal strain elements with hourglass control.

These elements use linear interpolation in each direction and called first-order elements, shown in Figure 4.1.

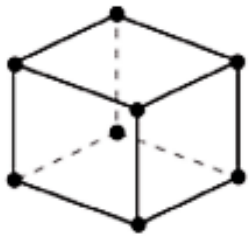

Figure 4.1 - Eight-noded linear brick with reduced integration [30]

Since using second order brick elements increase the computational time significantly. In this research first order elements have been used for the beam part

which could predict results in non-linear analysis involving large deformation and plasticity accurately.

4.2.2 Cohesive element

In modeling the notch area, an 8-node three dimensional cohesive element (COH3D) with small amount of viscosity has been used to simulate mode II fracture of concrete equipped with synthetic fiber. As shown in Figure 4.2, the cohesive element with a very small thickness in compared with other dimensions has been used in notch area.

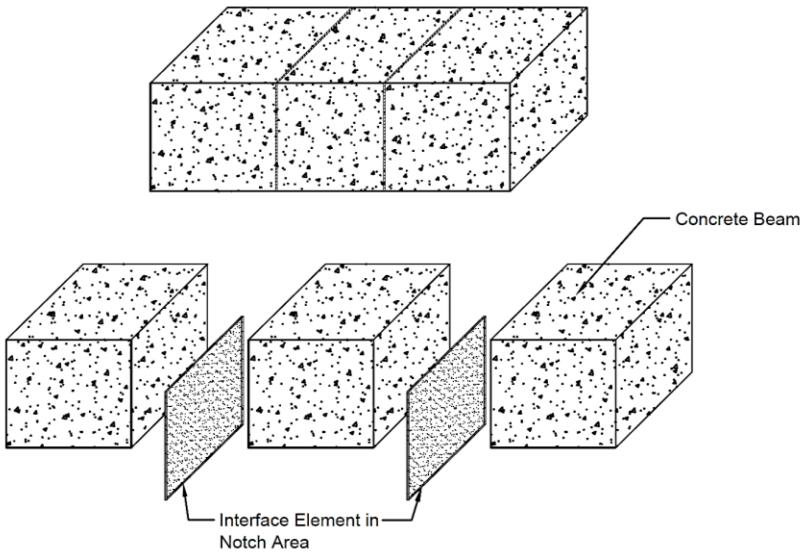

Figure 4.2 - Assigning cohesive element in notch area in finite element analysis

Interface elements have been tied up to the beam parts on both sides in order to act with master element nodes.

4.3 Boundary conditions and load application

To provide the exact boundary condition in finite element analysis like the JSCE modified shear test, two loading strips with the dimension of 0.6 in. x 6 in. (127 mm x 127 mm) for applying displacement has been modeled with surface-to-surface contact property. Two blocks with dimension 8 in. x 8 in. have been modeled in both sides of the beam in order to keep the beam from moving down. A surface-to-surface contact property has also been assigned between the beam and two supports. To keep the beam from rotation, two plates (4.5 in. x 8 in.) on top of the beam at both sides have been modeled and the same contact property has been defined for these two plates as well. For all the contacts, the strong surface was made as master surface, and the other side was assigned as slave surface. All the boundary conditions and surface interactions have been shown in Figure 4.3.

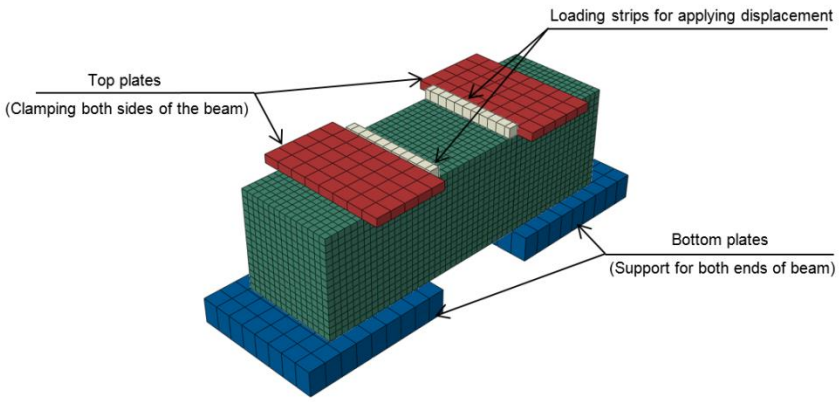

Figure 4.3 - Different parts has been modeled in the JSCE shear test FE analysis

The contact property between concrete beam and top and bottom plates were surface-to-surface contact with both tangential and normal behaviors.

As shown in Figure 4.4, load has been applied to the model by doing displacement control and through two loading strips distanced 5.9 in. far from each other on top of the beam.

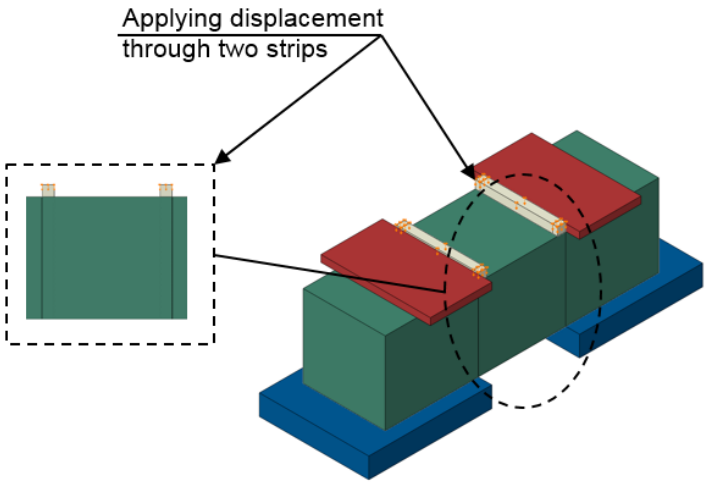

Figure 4.4 - Applying load in the form of displacement control

4.4 Material properties

Concrete damaged plasticity has been used for the whole beam except the notch areas with a density of 2400 kg/m3 (150 pcf), Modulus of Elasticity of 24870 MPa (4000 ksi) and 27405 MPa (5000 ksi) and Poisson's ratio 0.2, total strain 0.003.

4.4.1 Concrete damage plasticity

Concrete Damaged Plasticity (CDP) provides a capability for modeling concrete and other quasi-brittle materials in different part of structures like beams, columns, foundation, etc. This model considers the degradation of elastic stiffness caused by plastic straining in both tension and compression. In cyclic loading, it has the ability to recover the stiffness after each cycle [30]. Tensile cracking and compressive crushing of the concrete have been considered as two main failure mechanisms in this model. In this model, two hardening variables $\tilde{\varepsilon}_t^{pl}$ (Tensile equivalent plastic strain) and $\tilde{\varepsilon}_c^{pl}$ (Compressive equivalent plastic strain) control the evolution of yield surface. The concrete damaged plasticity model assumes nonassociated potential plastic flow. The flow potential G used for this model is the Drucker-Prager hyperbolic function [30].

$$G = \sqrt{(\in \sigma_{t0} \tan \varphi)^2 + \bar{q}^2} - \bar{p} \tan \varphi$$

$\varphi\ (\theta, f_i)$ Dilation angle in the p-q plane.

$\in (\theta, f_i)$ Flow potential eccentricity, a small positive number that defines the rate at which the hyperbolic flow potential approached its asymptote. The default is 0.1.

$\sigma_{to}(\theta, f_i)$ The uniaxial tensile stress at failure, taken from the user-specified tension stiffening data.

$$\bar{p} = -\frac{1}{3}\ trace\ (\bar{\sigma})$$

The plastic flow potential function and yield surface make use of two stress invariants of the effective stress tensor, namely the hydrostatic pressure stress,

$$\bar{\sigma} = D_0^{el} : (\varepsilon - \varepsilon^{pl})$$

And the Mises equivalent effective stress,

$$\bar{q} = \sqrt{\frac{3}{2}(\bar{S} : \bar{S})}$$

Where $\bar{S}$ is the effective stress deviator, defined as

$$\bar{S} = \bar{\sigma} + \bar{p}I$$

The choice of tension stiffening parameters is important because, generally, more tension stiffening makes it easier to obtain numerical solutions. Too little tension stiffening will cause the local cracking failure in the concrete to introduce temporarily unstable behavior in the overall response of the model [30].

4.4.2 Concrete tension stiffening behavior

By using tension stiffening, the post-failure behavior for direct straining is modeled that allows defining the strain-softening behavior for cracked concrete. Tension stiffening is essential in the concrete damaged plasticity model. There are two ways

for defining the tension stiffening, 1) by means of a postfailure stress-strain relation, shown in Figure 4.5 or 2) by considering a fracture energy cracking criterion. Concrete tensile cracking strain, $\tilde{\varepsilon}_t^{ck}$, which is equal to total strain minus the elastic strain related to the undamaged material. The data that is given in ABAQUS is in terms of tensile damage and concrete cracking strain and then the plastic strain is automatically calculated by using the below equation:

$$\tilde{\varepsilon}_t^{pl} = \tilde{\varepsilon}_t^{ck} - \frac{d_t}{1 - d_t}\frac{\sigma_t}{E_0}$$

d_t Tensile damage variable

$\tilde{\varepsilon}_t^{pl}$ Tensile equivalent plastic strain

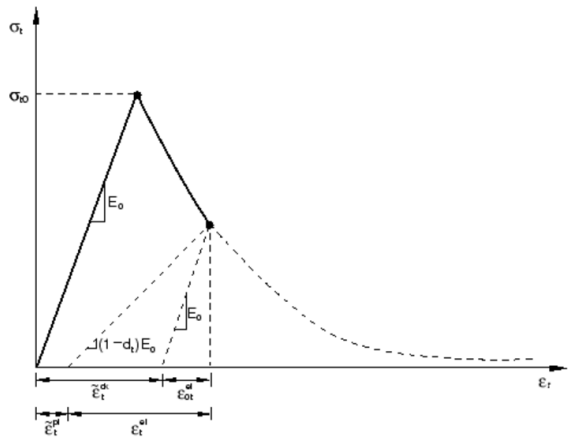

Figure 4.5 - Defining tension stiffening in CDP model [30]

An error message will be issued by ABAQUS if the calculated plastic strain values are negative and/or decreasing with increasing cracking strain, which normally shows that the tensile damage curves are not correct [30].

Too little tension stiffening will create the local cracking failure in the concrete and cause temporarily unstable behavior in the model. Therefore, it is very important to choose appropriate tension stiffening parameters to get numerical solutions.

4.4.3 Uniaxial compression behavior

The stress-strain behavior of plain concrete in uniaxial compression in the form of inelastic strain ($\tilde{\varepsilon}_c^{ck}$) need to be introduced in the ABAQUS as compression behavior of concrete, shown in Figure 4.6.

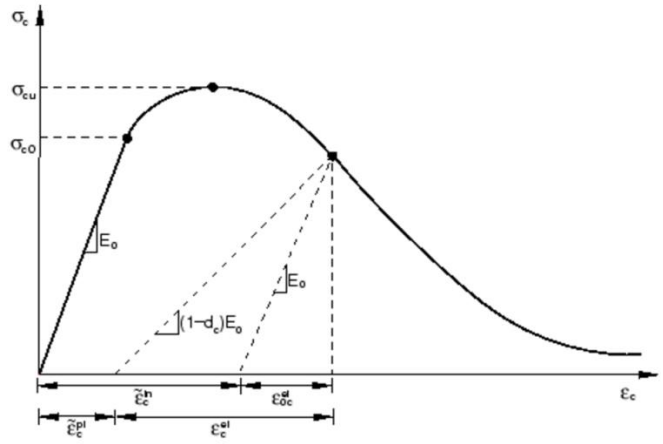

Figure 4.6 - Defining Compression behavior in CDP model [30]

In defining the compression behavior, like the tension behavior, the data is given in ABAQUS in the form of compression stress after failure and inelastic strain.

$$\tilde{\varepsilon}_c^{pl} = \tilde{\varepsilon}_c^{in} - \frac{d_c}{1 - d_c}\frac{\sigma_c}{E_0}$$

d_c Compressive damage variable

$\tilde{\varepsilon}_c^{pl}$ Compressive equivalent plastic strain

An error message will be issued by ABAQUS if the calculated plastic strain values are negative and/or decreasing with increasing inelastic strain, which normally shows that the compressive damage curves are not correct [30]. When the compressive damage is not defined the ABAQUS considers $\tilde{\varepsilon}_c^{pl} = \tilde{\varepsilon}_c^{in}$.

4.4.4 Cohesive behavior

As mentioned above, interface element with cohesive behavior has been defined in the notch areas on both sides of the beam.

Cohesive behavior assumes that by increasing degradation of the material stiffness, the failure of the elements is considered, which is determined by a damage process and it also allows multiple damage mechanisms as well as specification of material data such as the fracture energy as a function of the ratio of normal to shear deformation (mode mix) at the interface [30].

4.4.4.1 Defining elasticity for cohesive elements

The linear elastic behavior of cohesive elements can be written in the form of a matrix that relates the nominal stresses to the nominal strains all along the interface.

The linear elastic behavior of cohesive element can be written as:

$$\sigma = \begin{bmatrix} \sigma_n \\ \sigma_s \\ \sigma_t \end{bmatrix} = \begin{bmatrix} E_{nn} & E_{ns} & E_{nt} \\ E_{ns} & E_{ss} & E_{st} \\ E_{tn} & E_{ts} & E_{tt} \end{bmatrix} \times \begin{bmatrix} \varepsilon_n \\ \varepsilon_s \\ \varepsilon_t \end{bmatrix} = E.\varepsilon$$

σ_n, σ_s, σ_t are stresses in normal and two shear directions respectively, shown in Figure 4.7.

ε_n, ε_s, ε_t are strains in normal and two shear directions respectively.

In ABAQUS the cohesive elements can be used for modeling the bonded interface and both coupled and uncoupled behaviors are supported [30]. In uncoupled behavior, the element behavior is more specific and each traction component depends only on its associated normal strain and the off-diagonal terms in the elasticity matrix to zero while the coupled behavior is more general and all the components in elastic matrix will be considered.

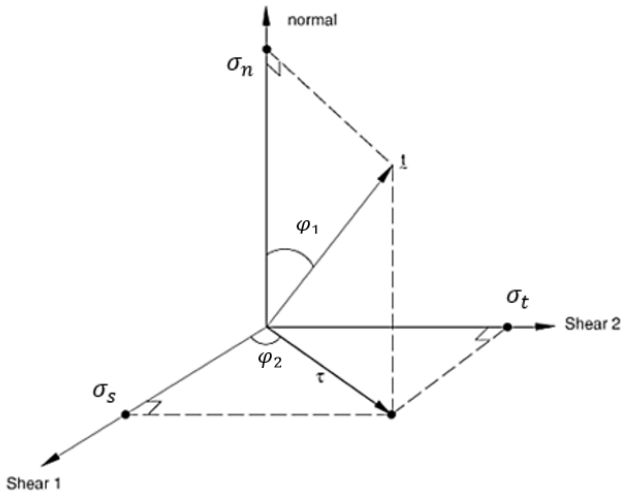

Figure 4.7 - Normal and two shear stress directions [30]

4.4.4.2 Modeling damage in cohesive elements

When cohesive element material is defined as traction-separation, the Maxs damage initiation criteria is used for predicting the damage initiation and it can estimate the stress ratios between a given stress value and the peak nominal stress value. The Maxs criterion considers the maximum value of the nominal stresses in three directions shown in Figure 4.8 [30].

Damage modeling in cohesive elements is very similar to the conventional materials. In this framework, the combination of several damage mechanisms acting concurrently on one material are allowed.

As mentioned above, the initial behavior is considered linear elastic until it reaches to the damage point that the user defines in ABAQUS based on damage evolution law. Once it meets the damage initiation criterion the material stiffness starts degradation. If the element is under pure compression, the damage will not occur. Figure 4.8 shows typical failure mechanism in cohesive elements.

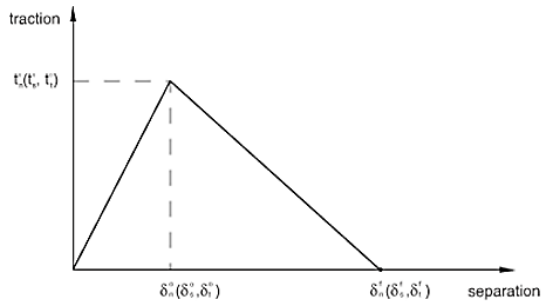

Figure 4.8 - Typical traction-separation behavior in cohesive elements [30]

The stiffness degradation begins when the stresses and/or strains meet certain damage initiation criteria which specified by user in ABAQUS. In maximum nominal stress and/or strain criterion, damage is assumed to start when the maximum nominal stress and/or strain ratio (as shown in below equations) reaches a value of one [30].

$$max\left\{\frac{\langle\sigma_n\rangle}{\sigma_n^0},\frac{\sigma_s}{\sigma_s^0},\frac{\sigma_t}{\sigma_t^0}\right\}=1$$

σ_n^0, σ_s^0, σ_t^0 are the maximum value of nominal stress when the deformation is totally normal to the interface or in the first or the second shear direction, respectively.

$$max\left\{\frac{\langle\varepsilon_n\rangle}{\varepsilon_n^0},\frac{\varepsilon_s}{\varepsilon_s^0},\frac{\varepsilon_t}{\varepsilon_t^0}\right\}=1$$

ε_n^0, ε_s^0, ε_t^0 are the maximum value of nominal strain when the deformation is totally normal the interface or in the first or the second shear direction, respectively. By assuming the initial thickness is equal to 1, the nominal strain components are equal to relative displacement in normal and the first and second shear direction (δ_n, δ_s, δ_t). By defining an effective displacement which is a combination of normal and shear deformation along the interface, the damage evolution will be assigned in the model. The effective displacement can be calculated based on below equation:

$$\delta_n=\sqrt{\langle\delta_n\rangle^2+{\delta_s}^2+{\delta_t}^2}$$

The mode mix of the deformation for cohesive material in ABAQUS can be defined based on energies measurement or tractions measurement. In this study, the mode mix was assigned based on the tractions in which the damage will be evaluated.

In the mode mix based on traction components, the effective shear traction will be measured based on below equation.

$$\tau = \sqrt{\sigma_s^2 + \sigma_t^2}$$

And the angle φ_1 and φ_2 shown in Figure 4.9 can be calculated based on below equations before it got normalized by factor $\frac{2}{\pi}$.

$$\varphi_1 = (\frac{2}{\pi}) \tan^{-1}(\frac{\tau}{\langle \sigma_n \rangle})$$

$$\varphi_2 = (\frac{2}{\pi}) \tan^{-1}(\frac{\sigma_t}{\sigma_s})$$

There are two ways for defining the damage improvement in cohesive elements, first is by specifying the effective displacement at complete failure, δ_m^f, compared with the effective displacement at the initiation of damage, δ_m^0 and the second is the energy degenerated due to failure, G^c, as shown in Figure 4.9.

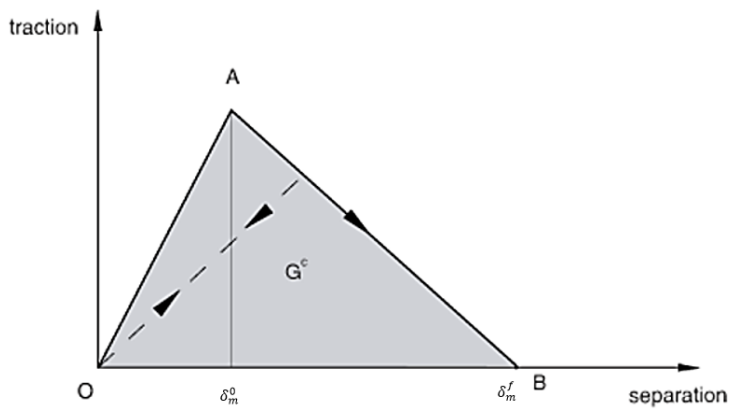

Figure 4.9 - Damage progress in cohesive elements [30]

The nature of damage progress can also be defined for cohesive elements in ABAQUS as linear or exponential softening laws or even in the form of tabular function of the effective displacement relative to the effective displacement at the damage origination. In this study, the damage evolution has been considered as exponential softening law and the FEM results showed better agreement with the experimental results.

In this study the mode mix based on traction has been selected. By specifying the fracture energy (G^c) versus φ_1 and φ_1 in tabular format the mode of failure can be assigned. φ_1 equals to zero shows pure normal deformation and φ_1 equals to 1 shows pure shear deformation.

4.5 Typical FEM results obtained with interface elements

Based on the JSCE-G553 shear test results, the FEA model has been calibrated for both 28 MPa (4,000 psi) and 34 MPa (5,000 psi) concrete compressive strength with different fiber volume fractions and then shear property of 7000 psi concrete compressive strength with different fiber volume fraction has been developed.

4.5.1 Deflected shape

The deflected shape of the specimen can be checked in visualization module in ABAQUS. Figure 4.10 shows the typical beam deflection after application of load. The deformation is magnified 3 times. As shown in Figure 4.10, upon applying the load on both sides of beam, through the load plates with the distance 5.9 in far from each other, the beam starts to get load until it reached to the ultimate load. After that, the middle part of the beam starts moving down exactly similar to what has been observed in experimental test and then the load starts decreasing.

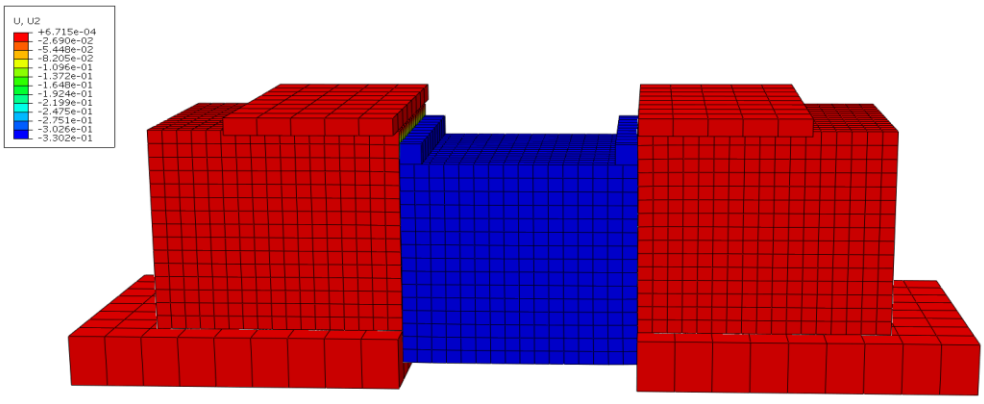

Figure 4.10 -Typical Deflection Shape of the JSCE beam in FEM

4.5.2 Load-deformation response

Typical results of JSCE-G553 shear beam for 48 MPa (7000 psi) concrete compressive strength have been discussed in this section. As mentioned above, the load-deformation curves for concrete equipped with different fiber dosages have been derived based on shear test results for concrete with two compressive strength values, 28 MPa (4,000 psi) and 34 MPa (5,000 psi).

As shown in Figure 4.11, there is a good agreement between the FEM results and test results for both 28 MPa (4,000 psi) and 34 MPa (5,000 psi) concrete compressive strength. The shear strength of plain concrete with 48 MPa (7000 psi) compressive strength has been developed based on the calibrated FEM results of two target concrete compressive strength, 28 MPa (4,000 psi) and 34 MPa (5,000 psi). The FEM results also confirm the accuracy of JSCE test method for investigating the shear property of synthetic fiber reinforced concrete.

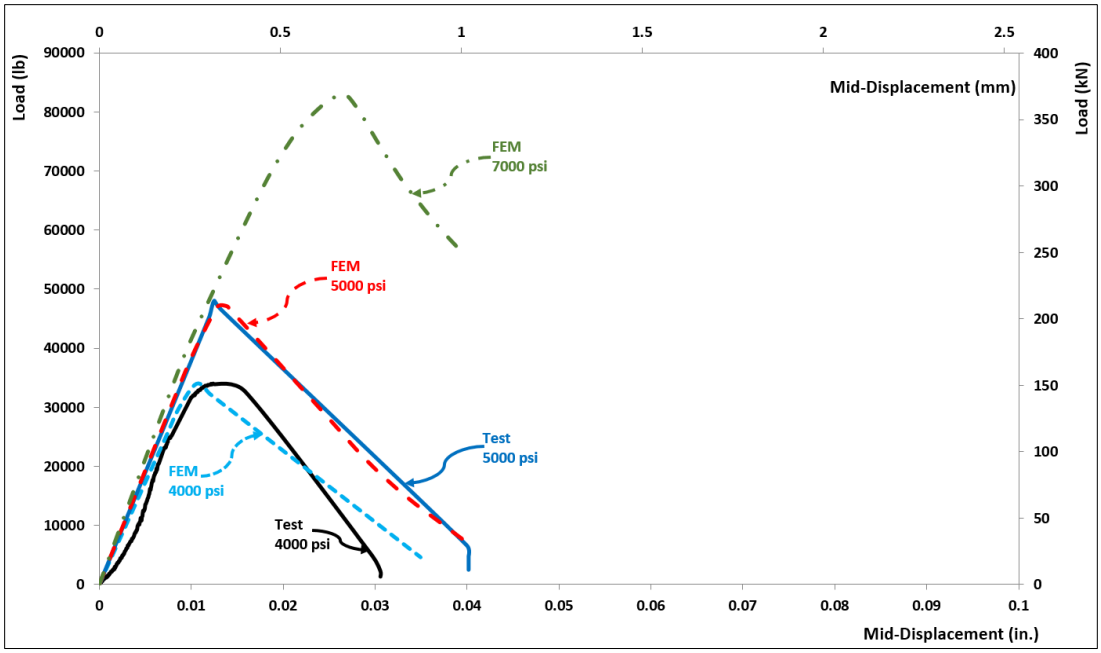

Figure 4.11 - FEM results of plain concrete with three target compressive strength values

Figure 4.12 through Figure 4.15 show the finite element results for 0.26%, 0.52%, 0.78% and 1.04% fiber volume fraction for concrete with three different compressive strength values. As mentioned above for concrete with 48 MPa (7000 psi) compressive strength, the FEM results have been developed based on finite element results of two other compressive strength values, 28 MPa (4,000 psi) and 34 MPa (5,000 psi), which their obtained FEM results closely match the values of test results. However, some direct shear tests need to be conducted on concrete with 48 MPa (7000 psi) compressive strength with different fiber volume fractions to consider the accuracy of FEM data.

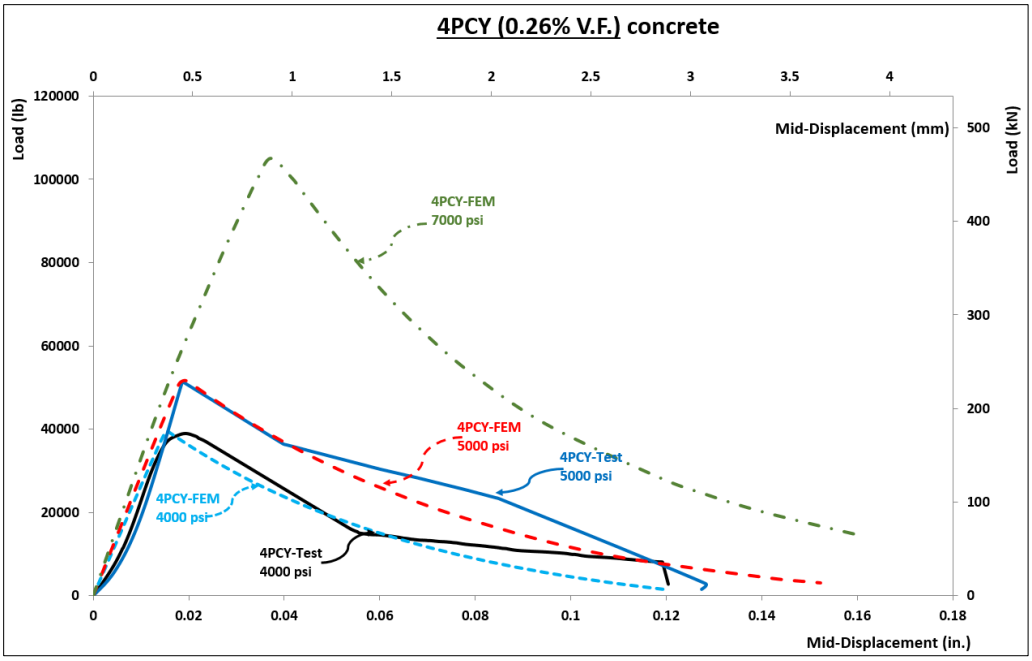

Figure 4.12 - FEM results of 4 PCY (0.26% V.F.) concrete with three target compressive strength values

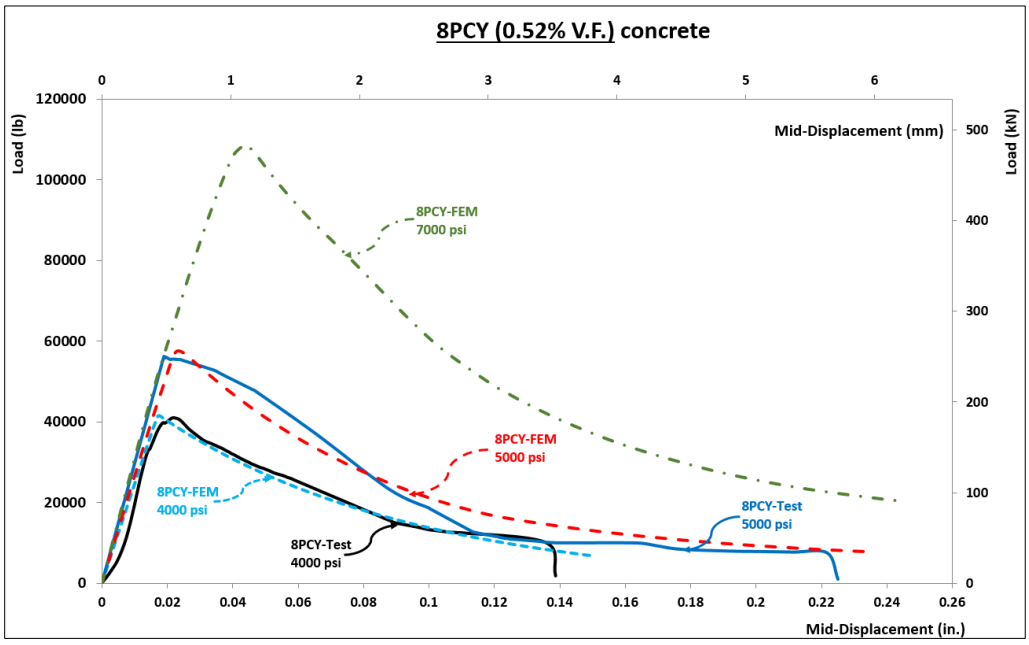

Figure 4.13 - FEM results of 8 PCY (0.52% V.F.) concrete with three target compressive strength values

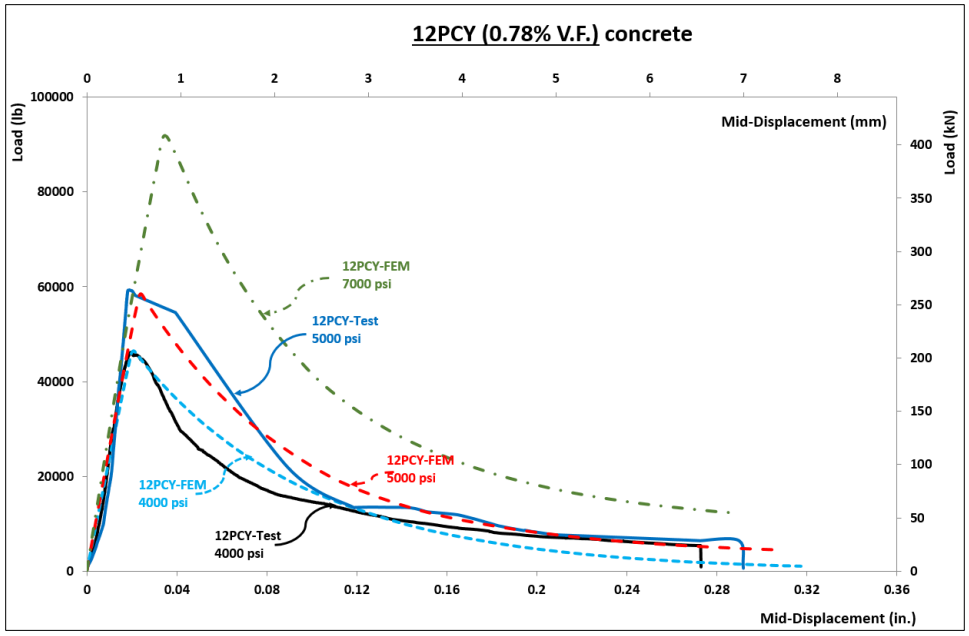

Figure 4.14 - FEM results of 12 PCY (0.78% V.F.) concrete with three target compressive strength values

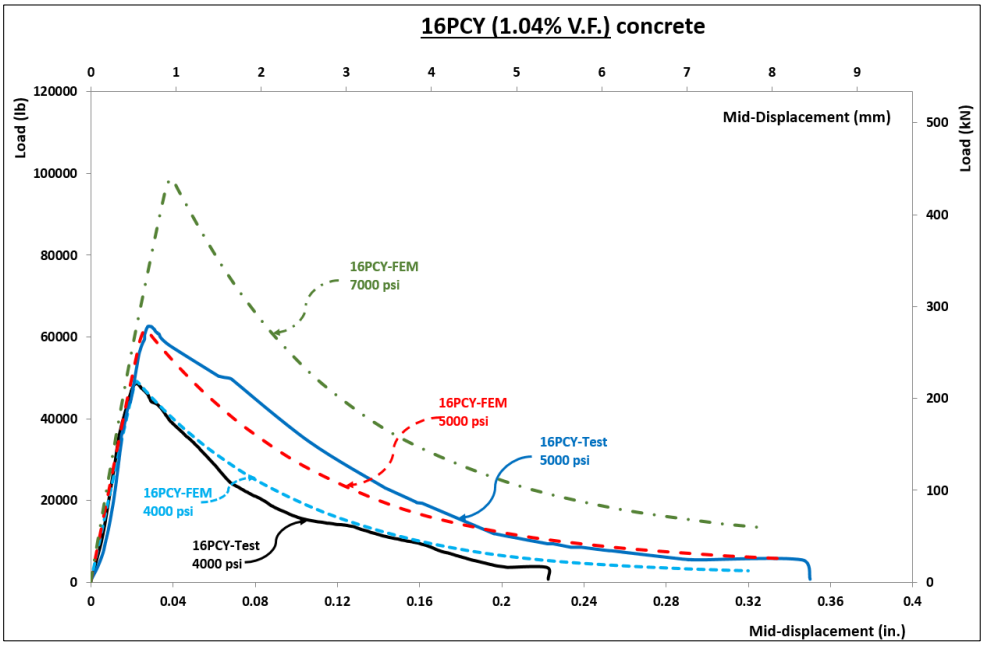

Figure 4.15 - FEM results of 12 PCY (1.04% V.F.) concrete with three target compressive strength values

Overall, using interface element with cohesive property in notch areas in JSCE shear test method is an appropriate method to use in FEM for getting the shear property of synthetic fiber reinforced concrete and also predicting the shear properties of concrete with higher compressive strength.

CHAPTER 5

FINITE ELEMENT ANALYSIS ON BOX CULVERTS

5.1 Introduction

To study the shear behavior of box culverts equipped with synthetic fiber Reinforced Concrete (Syn-FRC), three dimensional finite element models were prepared for all the standard sizes of box culverts studied by Anil Garg in 2007. This part of the research has been completed in order to calibrate the geometry and boundary conditions of box culverts modeled in FEM with the experimental test data. For defining the material property of Syn-FRC in FEM by using concrete brittle cracking, a series of finite element analysis has been done based on ASTM C1609 test setup for different fiber volume fractions and the results of FEM have been compared with ASTM C1609 test results.

In 2007, in a very comprehensive study, Anil Garg [24] had studied the shear behavior and capacity of 24 precast concrete box culverts subjected to HS 20 truck wheel load by applying the load at different distances from the tip of the haunch. Based on their investigation, the most critical place for putting the load plate (10 in.×20 in. ×1 in) is at a distance d from the tip of the haunch to the edge of the load plate. The dimension of load plate has been selected based on wheel load print. 15 out of 24 tested box culverts has been loaded at a distance d from tip of the haunch and in this research the behavior of these 15 box culverts has been analyzed in finite element program.

All the box culverts subjected to zero depth fill. Figure 5.1 through Figure 5.3 show a typical box culvert reinforcement arrangement used finite element analysis based on Anil's study.

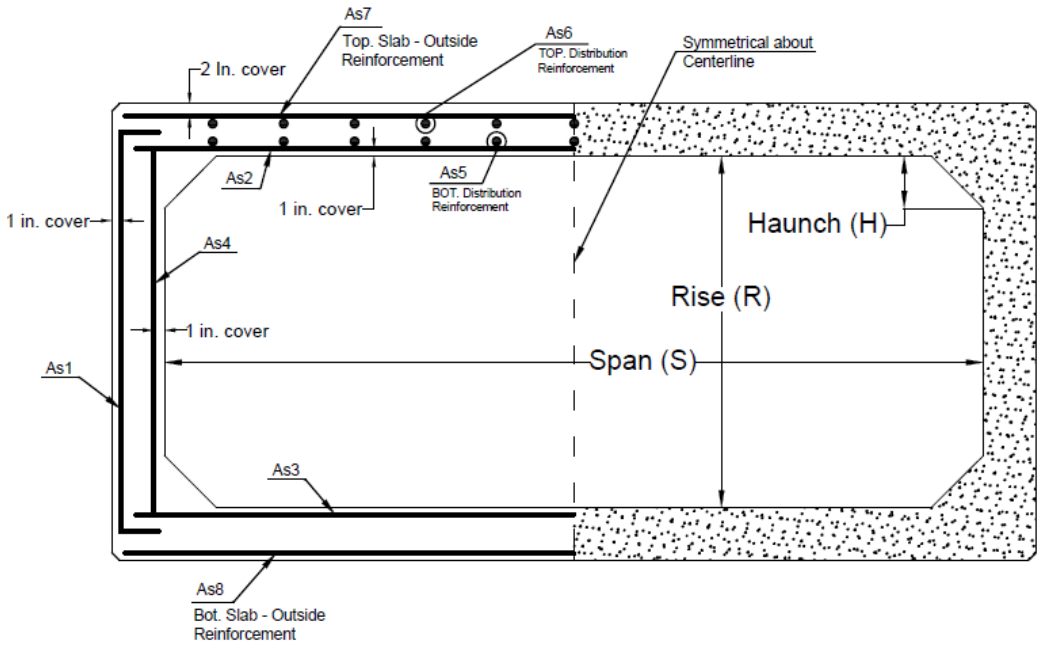

Figure 5.1 - Typical reinforcement arrangement in Box culverts

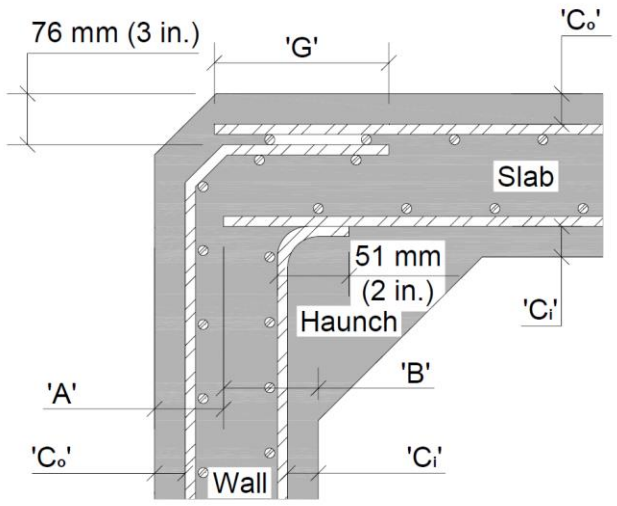

Figure 5.2 - Haunch reinforcement detail [23]

Two box culverts are connected together by placing the spigot into the bell as shown in Figure 5.3.

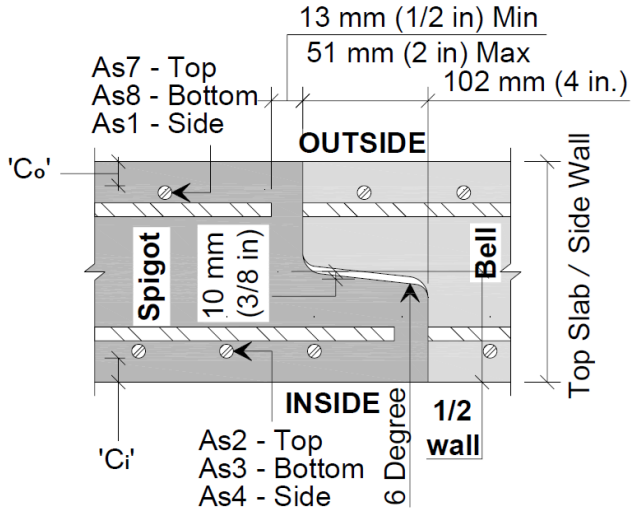

Figure 5.3 – Connecting two box culverts through bell and spigot [23]

The box culverts modeled as 3-D solid elements and the horizontal and vertical reinforcement modeled as truss element embedded in the box culvert. In all models, the material and geometry nonlinearities has been considered. The base support of box culvert is modeled as a rectangular block and the contact between the box and block is defined as surface-to-surface contact elements.

After completing a comprehensive finite element analysis on different sizes of box culverts equipped with steel reinforcement and also calibrating the material properties of Syn-FRC by conducting FE analysis on ASTM C1609, the behavior of concrete box culverts equipped with different fiber volume fractions has been investigated.

5.2 Box culverts nomenclature

The experimental results that have been used in this section were on both the spigot and the bell end of box culverts. The box culverts were also equipped with or without top slab compression distribution steel (AS6). The following nomenclature has been used for describing each box culvert identification in more detail. Since the critical place for putting the load plate is at the distance d from the tip of the haunch to the edge of the plate, in all the finite element analysis, this distance is kept constant as d [23].

SP or BL _ S-R-L _ N or Y

Where designations are:

SP – Spigot end

BL – Bell end

S-R-L – Dimension of the box culvert in cm (ft) (span, rise, and the joint length)

N – No distribution reinforcement (AS6)

Y – With distribution reinforcement (AS6)

For instance SP_122-122-244_Y (SP_4-4-8_Y), identifies a spigot-end box culvert with the dimensions of: Span = 122 cm (4 ft); Rise = 122 cm (4 ft) and Joint Length = 244 cm (8 ft) with distribution steel AS6. As mentioned above, the edge of the load plate for all box culverts was placed at the distance d from the tip of the haunch.

5.3 Elements

5.3.1 Solid element

Solid elements are the standard volume elements in Abaqus and can be presented as a single homogeneous material. If distortion doesn't happen particularly in quadrilaterals and hexahedra, these elements will be accurate. In this study for modeling the box culverts, Eight-noded isoperimetric solid elements with hourglass control and reduced integration algorithm were used for modeling box culvert, base support and also loading plate. For reducing computational time, reduced integration used in lower order integration to form the element stiffness. It is also referred to as uniform strain or centroidal strain elements with hourglass control.

In Abaqus/Explicit solid element library, there are first-order (linear) interpolation elements and modified second-order interpolation elements in two or three

dimensions [30]. Since using second order brick elements increase the computational time significantly, in this research, first order elements have been used for the box culvert, loading plate and also the base support which could predict results in non-linear analysis involving large deformation and plasticity accurately.

5.3.2 Truss elements

Truss elements are long, slender structural members that only can carry the axial force and they can't support any forces or moments perpendicular to the centerline. The 3-node truss element can be used for modeling reinforcement in regular concrete structures or modeling tendons in prestressed ones. Figure 5.4 shows how truss elements are named in Abaqus.

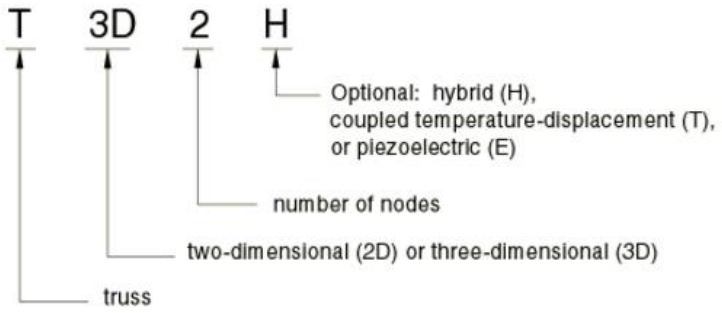

Figure 5.4 - How truss elements are called in Abaqus [30]

In this study, T3D2, a 2-node linear 3-D truss element used for modeling the reinforcement in box culvert. All the reinforcement has been embedded in the box culverts.

5.4 Boundary condition

In all the FEM models, the mechanical contact properties between the beam and supports, Box culvert and reaction floor and also load plate and box culvert have been assigned as a surface to surface contact with tangential and normal properties. The strong surface was assigned as master surface, and the other side was assigned as slave surface. As shown in Figure 5.5, in node to surface contact property, the contact is assigned between a slave node and master surface facets local to the node, while in surface to surface contact property, the contact is assigned between a slave node and a large number of master surface facets around that node (Figure 5.6).

The normal behavior has been assigned as “Hard” contact that use the classical Lagrange multiplier method of constraint enforcement in an Abaqus/Standard analysis and to use penalty contact enforcement in an Abaqus/Explicit analysis. The tangential behavior has been selected as “Penalty” contact that use a stiffness method that permits some relative motion of the surfaces when they should be sticking [30].

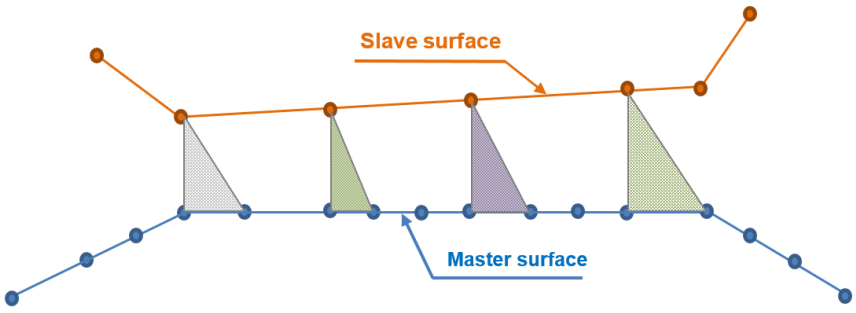

Figure 5.5 – Node to surface contact property in ABAQUS

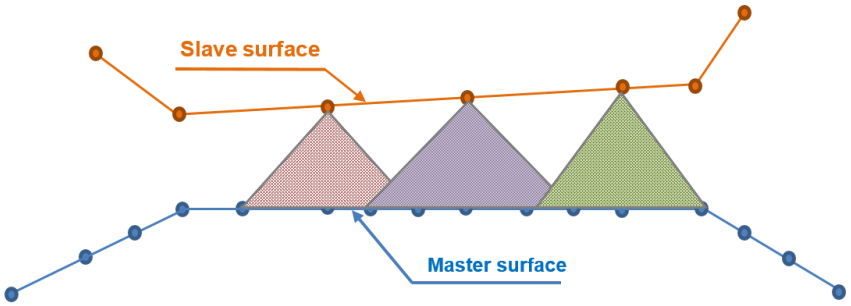

Figure 5.6 – Surface to surface contact property in ABAQUS

5.4.1 Contact surface weighting

In Abaqus/Explicit, there are two contact algorithms, the pure master-slave and the balanced master-slave contact. For any given contact pair based on the nature of the two surfaces, Abaqus/Explicit by default will decide which algorithm to use forming the contact pair and whether kinematic or penalty enforcement of contact constraints is used. In some cases, we can override the defaults [30].

5.4.1.1 Default choices for the contact pair weighting

Abaqus/Explicit uses the pure master-slave, kinematic contact algorithm, by default, in the following situations:

- When a rigid surface contacts a deformable surface;
- When an element-based surface contacts a node-based surface; or

- When a surface based on continuum elements contacts a surface based on shell or membrane elements.

By default, Abaqus/Explicit uses the balanced master-slave, kinematic contact algorithm in the following situations:

- When a single surface contacts itself (referred to as self-contact or single-surface contact); or
- When two deformable surfaces that are meshed with similar elements (i.e., either both surfaces have shells or membranes or both have continuum elements) contact each other.

If the penalty contact algorithm is specified, Abaqus/Explicit uses pure master-slave weighting, by default, in the following situations:

- When an analytical rigid surface contacts a deformable surface; or
- When an analytical rigid surface or an element-based surface contacts a node-based surface.

If the penalty contact algorithm is specified, Abaqus/Explicit chooses balanced master-slave weighting, by default, in the following situations:

- When a single surface contacts itself (referred to as self-contact or single-surface contact); or
- When two element-based surfaces contact each other.

Balanced master-slave weighting means that the corrections produced by both sets of contact calculations are weighted equally [30].

The details of contact properties used in FEM have been shown in Appendix C.

5.5 Material properties

Concrete brittle cracking has been used for the whole box culverts with a density of 2400 kg/m3 (150 pcf), Modulus of Elasticity of 27405 MPa (5000 ksi) and Poisson's ratio 0.25, total strain 0.003. For the base support and loading plate, a normal steel property with a density of 7800 kg/m^3 (0.28 lb/cu^3), young's modulus of 200 GPa (29,000,000 psi) and poison's ratio of 0.3 has been selected.

The details of material properties used for modeling ASTM C1609 beams equipped with different fiber volume fractions (0%, 0.26%, 0.52%, 0.78% and 1.04%) have been presented in Appendix C.

5.5.1 Concrete brittle cracking

The concrete brittle cracking model has been used in finite element analysis. This model has a capability for modeling concrete in all types of structures like beam, trusses, shells and solids and it is designed for applications in which the behavior is controlled by tensile cracking [30]. The brittle cracking is run in Abaqus/Explicit environment and in this model, the concrete compression behavior is considered linear elastic. A smeared crack model is considered in concrete brittle cracking and it doesn't track individual macro crack but a continuum of micro-cracks in the

neighborhood of the points the stress and material stiffness associated with that point affected [30].

Detecting crack initiation is based on simple Rankine criterion. Based on this criterion, the crack starts when the maximum principle tensile stress exceeds the tensile strength of the brittle material. Rankine criterion in the deviatoric plane, Meridian plane and plane stress have been shown in Figure 5.7, 5.8 and 5.9, respectively. When the Rankine criterion for crack formation has been met, the first crack will occur and the crack surface will be considered normal to the direction of the maximum tensile principle stress. Following cracks will occur with crack surface normal in the direction of maximum principle tensile stress and is orthogonal to the directions of any present crack surface. Although Mode I purely detect crack, ensuing cracked behavior includes both Mode I (tension softening) and Mode II (shear softening/retention) behavior [30].

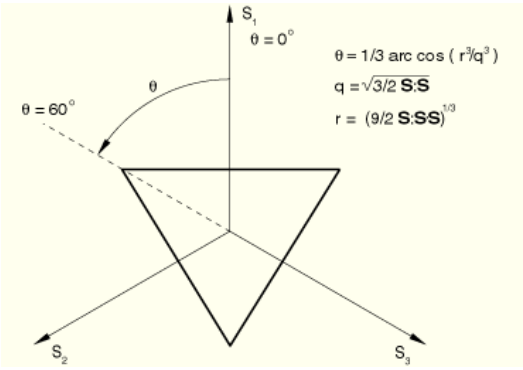

Figure 5.7 – Rankine criterion in the deviatoric plane [30]

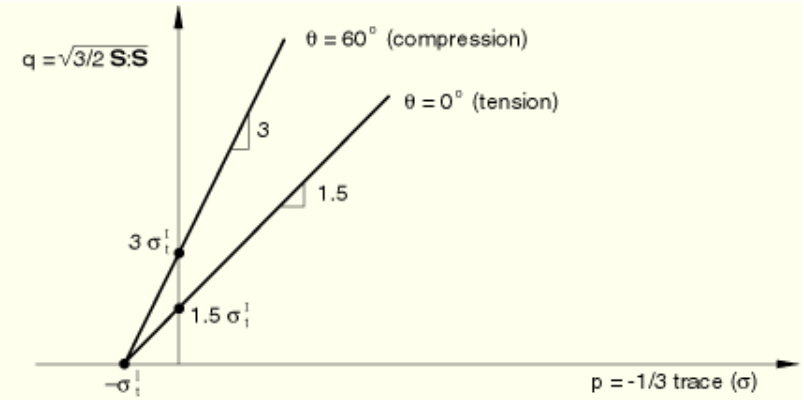

Figure 5.8 – Rankine criterion in the Meridian plane [30]

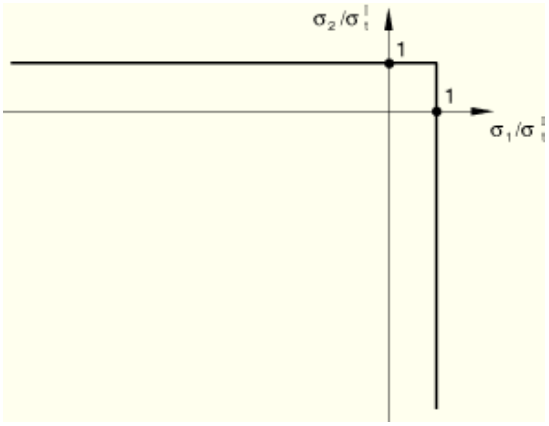

Figure 5.9 – Rankine criterion in plane stress [30]

5.5.1.1 Abaqus Explicit vs Abaqus Standard

The Newton-Raphson method is used in Abaqus/Standard to obtain solutions for nonlinear problems. In a nonlinear analysis, the solution usually cannot be calculated by solving a single system of equations, as would be done in a linear problem. Instead, by applying the specified loads slowly and incrementally working toward the final solution, the answer is found. Therefore, Abaqus/Standard breaks the simulation

into a number of load increments and finds the approximate equilibrium configuration at the end of each load increment. It often takes Abaqus/Standard several iterations to determine an acceptable solution to a given load increment. The sum of all of the incremental responses is the approximate solution for the nonlinear analysis. Thus, Abaqus/Standard mixes incremental and iterative procedures for solving nonlinear problems [30].

Abaqus/Explicit determines a solution to the dynamic equilibrium equation $M\ddot{u} = P - I$ without iterating by explicitly advancing the kinematic state from the end of the previous increment. Solving a problem explicitly does not require the formation of tangent stiffness matrices. The explicit central-difference operator satisfies the dynamic equilibrium equations at the beginning of the increment, t; the accelerations calculated at time t are used to advance the velocity solution to time $t + {\Delta t}/{2}$ and the displacement solution to time $t + \Delta t$. For linear and nonlinear problems alike, explicit methods require a small time increment size that depends solely on the highest natural frequency of the model and is independent of the type and duration of loading. Simulations typically require a large number of increments; however, due to the fact that a global set of equations is not solved in each increment, the cost per increment of an explicit method is much smaller than that of an implicit method. The small increments characteristic of an explicit dynamic method make Abaqus/Explicit well suited for nonlinear analysis [30].

5.5.1.2 Tension stiffening

In modeling the reinforced concrete in Abaqus, the rebars are usually introduced with elastic-plastic material behavior. The concrete cracking behavior is considered with no effect of rebars. The effect of bond slip and dowel action associated with the rebar/ concrete interface is modeled by introducing tension stiffening into the concrete cracking model, for simulating the role of rebars in transferring the load to the concrete [30].

Tensile stiffening can be specified by means of a postfailure stress-strain relation or by applying a fracture cracking criterion. In this research, the tensile stiffening has been assigned in the form of postfailure stress-strain relation [30].

5.5.1.3 Postfailure stress-strain relation

By assigning the postfailure stress as a function of strain across the crack, the postfailure behavior will be assigned in Abaqus. Figure 5.10 shows a typical stress-strain behavior as postfailure property of concrete [30].

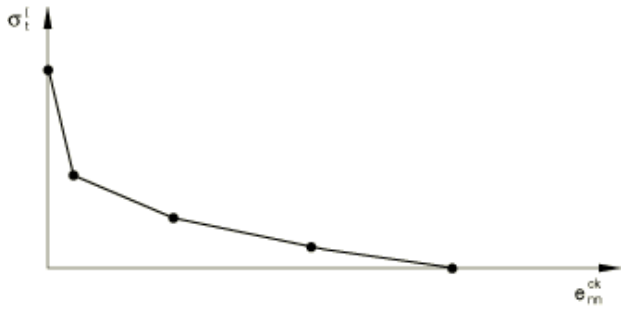

Figure 5.10- Stress-strain curve as typical postfailure of concrete [30]

5.5.1.4 Shear retention model

Although crack initiation in this model is based on mode I, postcracked behavior includes mode II as well as Mode I. The shear behavior is based on the observation of crack opening. Shear retention model is an offer in Abaqus/Explicit for defining the postcracked shear stiffness as the function the crack opening across the crack. Figure 5.11 shows a linear relation between the crack opening strain and shear retention [30].

$$G_c = \rho\left(e_{nn}^{ck}\right)G$$

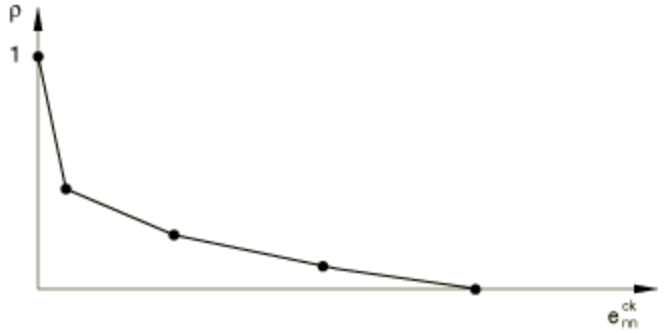

Figure 5.11- Shear retention model in linear form [30]

G, Uncracked shear Stiffness

G_c, post cracked shear stiffness

$\rho\left(e_{nn}^{ck}\right)$, Shear retension factor and depends on the crack opening strain, e_{nn}^{ck}

As another alternative, the shear retention can also be defined in the power law form:

$$\rho\left(e_{nn}^{ck}\right) = (1 - \frac{e_{nn}^{ck}}{e_{max}^{ck}})^{p}$$

p and e_{max}^{ck} are material parameters.

$e_{nn}^{ck} \to 0, \rho \to 1, \text{before crack starting}$

$e_{nn}^{ck} \to e_{max}^{ck}, \rho \to 0, \text{complete loss of aggregate}$

Figure 5.12 shows the power law form can be used for modeling the shear retention.

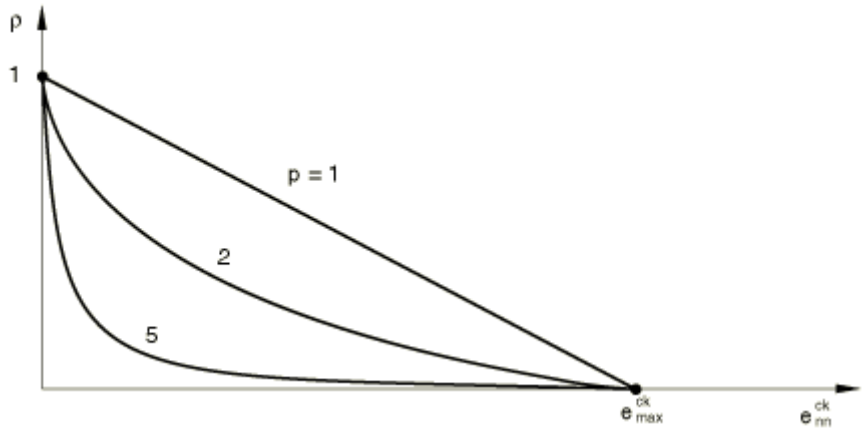

Figure 5.12- Power law form of the shear retention model [30]

In this study, the shear retention factor has been defined based on shear test results.

5.5.1.5 Brittle failure criterion

In expressing the brittle failure of the material, when one, two or all the three local direct cracking strain (displacement) elements get the value stated as the failure strain (displacement), all the stress components get zero and the failure happens in the material [30].

When stress versus strain is considered as the postfailure relation, the failure strain has to be assigned as the failure criterion. However, if postfailure is expressed in terms of stress versus displacement or stress versus fracture energy, for stating the failure criteria, the failure displacement has to be assigned to material property [30].

5.6 Calibration of concrete brittle cracking model used in FEM for different fiber volume fractions

To capture the tensile behavior of concrete equipped with different fiber volume fractions, a three dimensional full-scale model was built in ABAQUS based on ASTM C1609 beam test and concrete brittle cracking model was used for presenting the mechanical behavior of synthetic fiber reinforced concrete in ABAQUS. To calibrate the material model defined in ABAQUS, the results of FEM were compared with experimental data. Three dimensional solid elements with geometric and material non-linearities were used for the ASTM beam. The model also included two narrow loading strips with the dimension of 0.3 in. x 6 in. (127 mm x 127 mm) for displacement application to the beam and two supports with the same dimension at the bottom of the beam in both sides for holding the beam from moving down. As shown in Figure 5.13, The FEM model met all the boundary conditions in ASTM C1609 test setup.

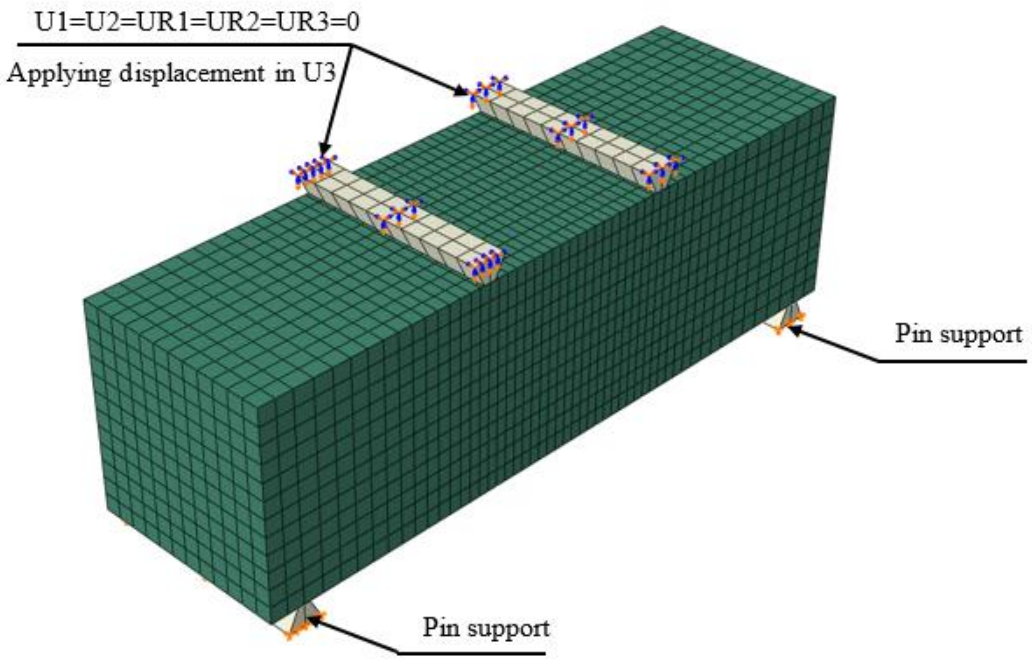

Figure 5.13 – Meeting all the boundary condition in FEM based on ASTM C1609 beam test

Concrete Brittle Cracking has been used for the whole beam with a density of 2400 kg/m3 (150 pcf), Modulus of Elasticity of 28665 MPa (4157.2 ksi) and Poisson's ratio 0.25.

Finite element model verification was achieved for concrete with 5000 psi compressive strength, and the results of FEM have been compared with that of the experimental ones in order to calibrate the material property of concrete with different fiber volume fractions.

The details of material properties used for modeling ASTM C1609 beams equipped with different fiber volume fractions (0%, 0.26%, 0.52%, 0.78% and 1.04%) have been presented in Appendix C.

5.6.1 Deflected shape

The deflected shape of specimen can be checked in visualization module in ABAQUS. Figure 5.9 shows the typical beam deflection after application of load. The deformation is magnified 15 times. As shown in Figure 5.14, upon applying the load on both sides of beam, through the load plates with the distance 6 in. far from each other, the beam starts getting load until it reached to the ultimate load. After that a crack will occur in the middle part of the beam exactly similar to what has been observed in experimental test and then the load decreased quickly.

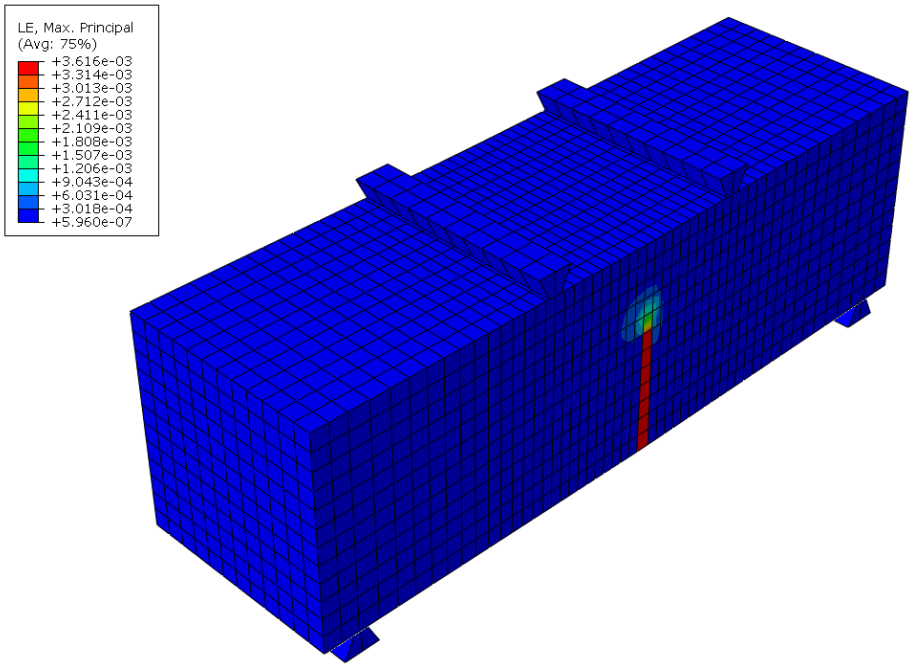

Figure 5.14 - Typical Deflected Shape and crack propagation in ASTM C1609 beam

5.6.2 Load-deformation response

Typical FEM results of ASTM C1609 flexural beam test with 34 MPa (5000 psi) concrete compressive strength and different fiber volume fractions have been discussed in this section. The load-deformation curve for any target fiber volume fraction has been derived based on the results of ASTM C1609 finite element analysis.

As shown in Figure 5.15 through Figure 5.19, there is a good agreement between the FEM and test results for 34 MPa (5,000 psi) concrete compressive strength and the defined concrete brittle cracking model satisfies the tensile behavior of concrete with various fiber volume fractions.

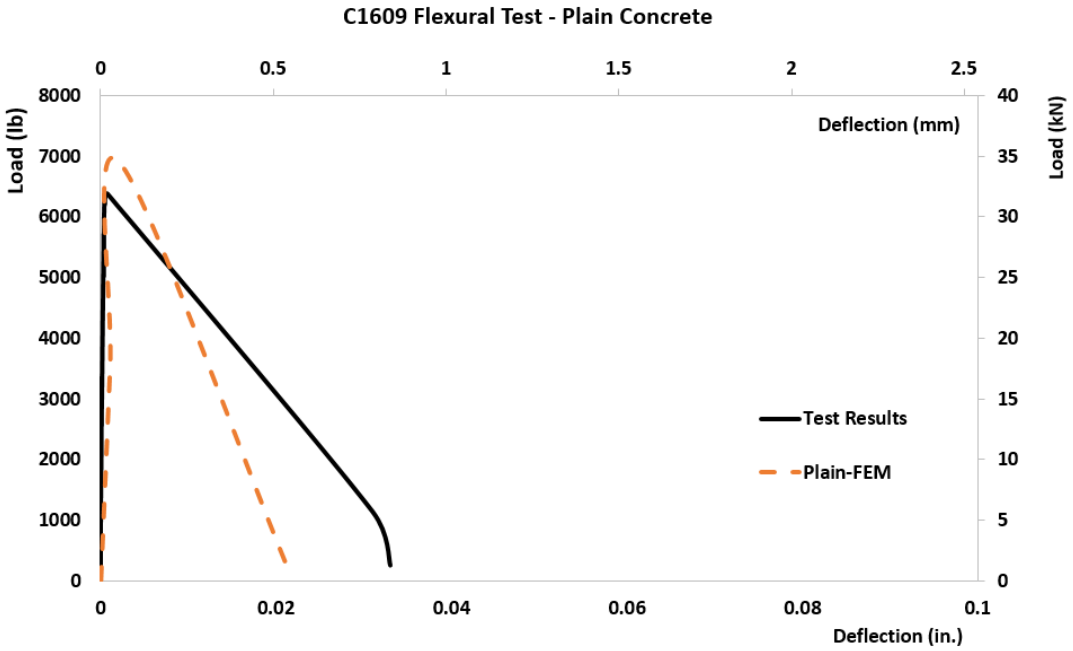

Figure 5.15 - Comparison between FEM and ASTM C1609 test results- Plain

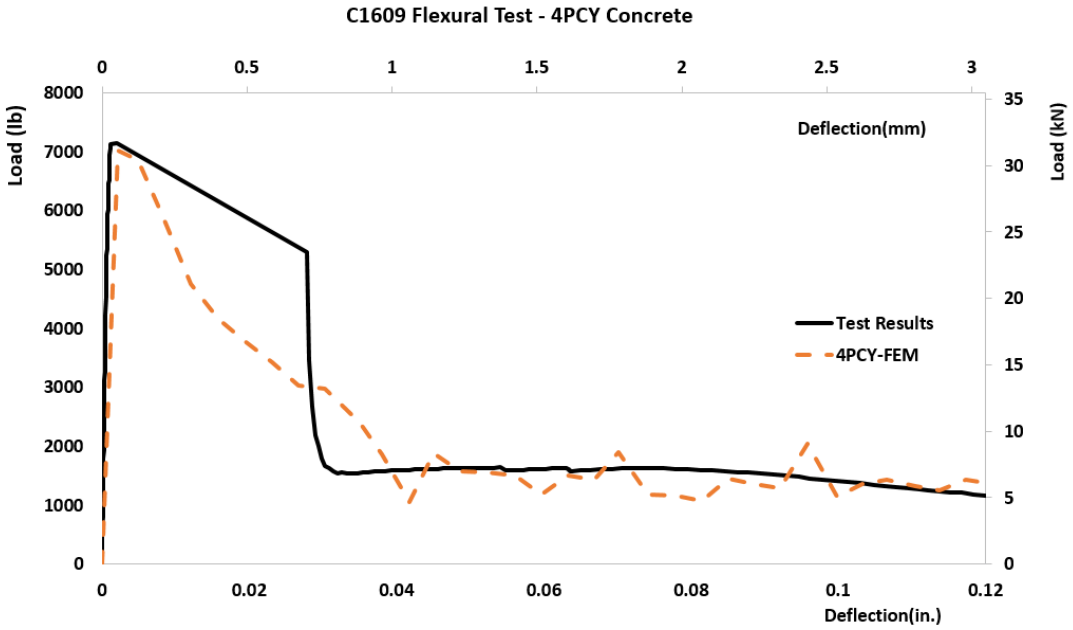

Figure 5.16 - Comparison between FEM and ASTM C1609 test results- 4PCY

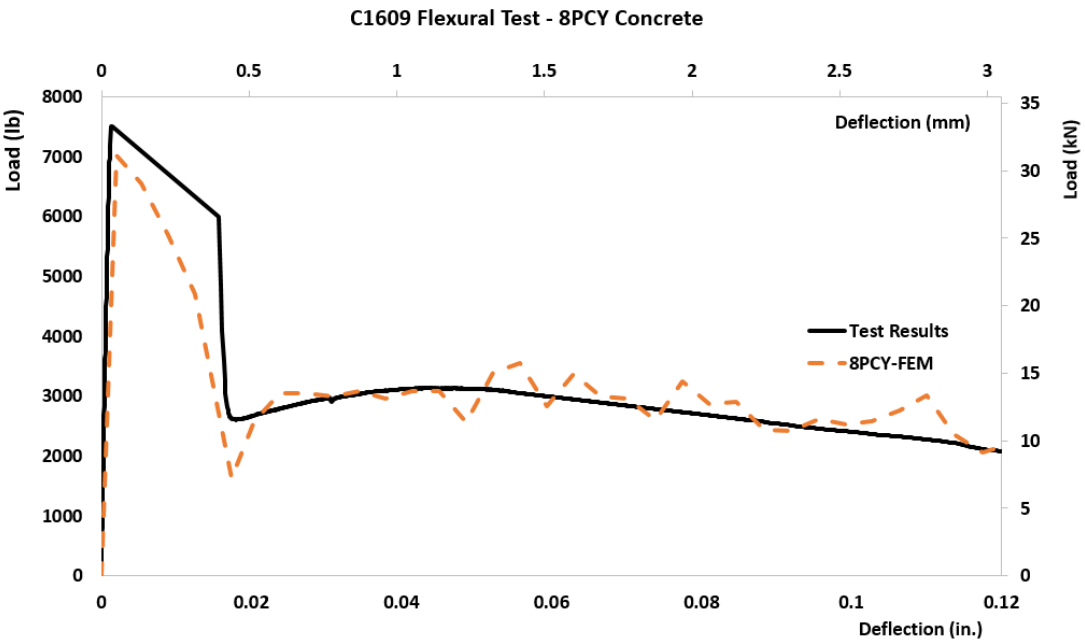

Figure 5.17 - Comparison between FEM and ASTM C1609 test results- 8PCY

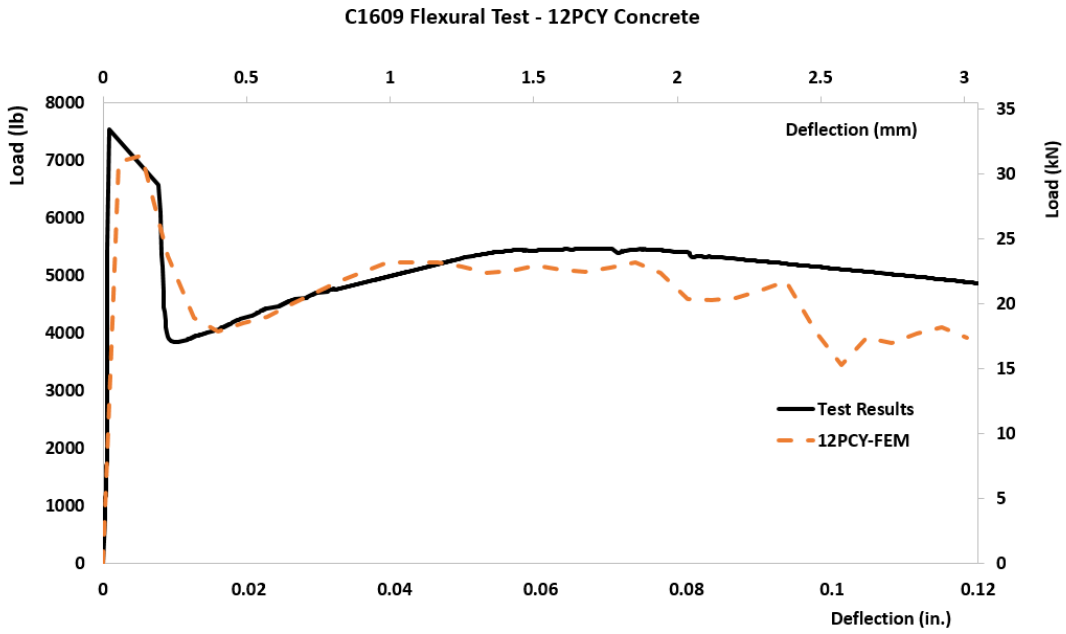

Figure 5.18 - Comparison between FEM and ASTM C1609 test results- 12PCY

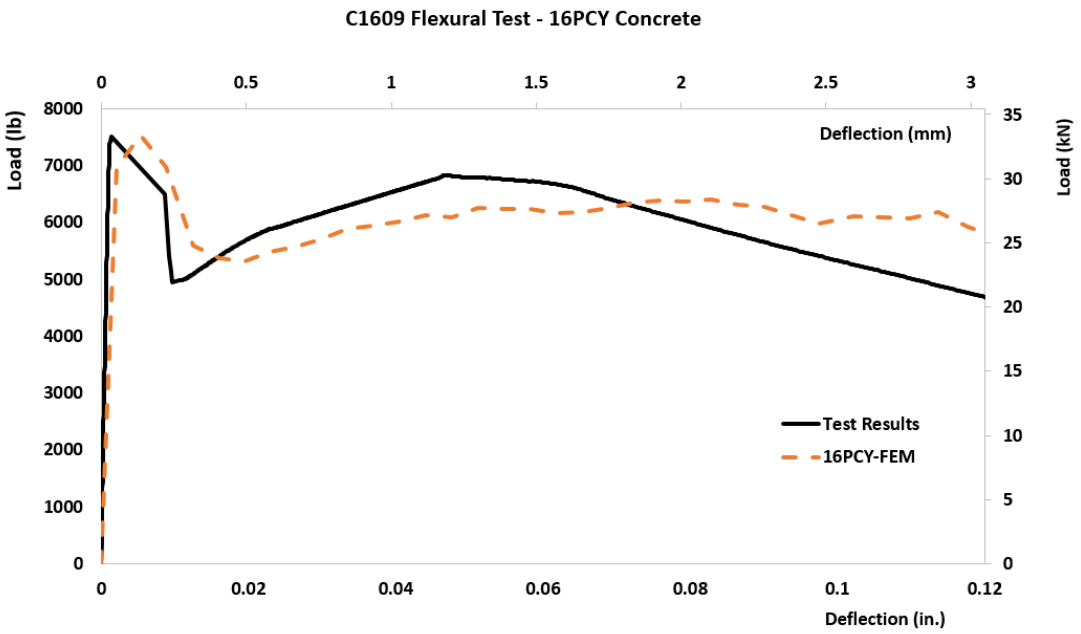

Figure 5.19 - Comparison between FEM and ASTM C1609 test results- 16PCY

As shown in above figures, using concrete brittle cracking could accurately predict the flexural behavior of ASTM C1609 beam. An appropriate tensile strain-softening behavior has been defined for each fiber volume fractions by carrying out a comparison between obtained FEM results and existing experimental results on ASTM C1609. Based on the previous published work on fiber reinforced concrete [31], the compressive behavior of fiber reinforced concrete can be safely considered to be similar to that of plain concrete.

5.7 Model calibration

The load-deflection plots obtained experimentally for zero and 0.52% fiber volume fractions (8PCY) are compared with the FEM analysis in order to calibrate the box culvert model. As shown in Figure 5.15 through Figure 5.19, there is a good agreement between the FEM and test results for 34 MPa (5,000 psi) concrete compressive strength for two specified fiber volume fractions. It can be concluded that the defined concrete brittle cracking model for various fiber volume fractions satisfies the tensile behavior of concrete and can be used to predict the structural behavior of box culverts equipped with different fiber volume fractions.

5.7.1 Boundary conditions and load application

To provide the exact boundary condition in finite element analysis like the real test setup, a rectangular block has been modeled as base support with surface-to-surface contact property for holding the box culvert from moving down and also lateral movement. A loading plate with dimension 10 in. x 20 in. have been modeled for applying wheel load to box culvert. A surface-to-surface contact property has also been assigned between the box culvert and load plate. In order to provide the same experimental loading condition in FEM analysis, a cylinder has also been model on top of the load plate with surface-to-surface contact property in order to play the actuator role in experimental test (Figure 5.20). For all the contacts, the strong surface was made as master surface and the other side was assigned as slave surface. All the boundary conditions and surface interactions have been shown in Figure 5.21.

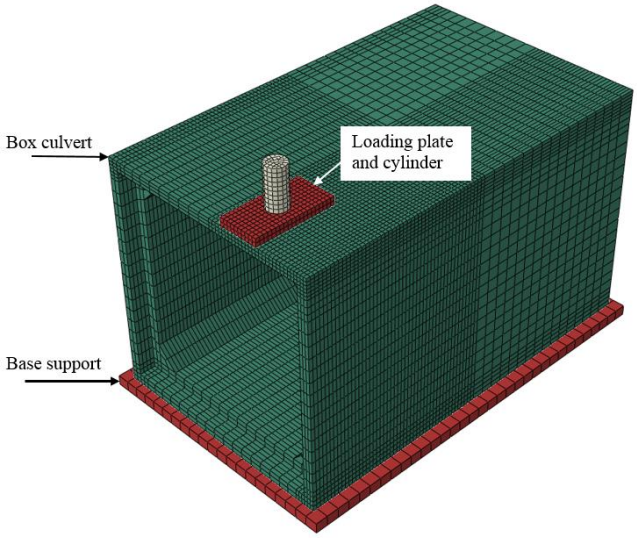

Figure 5.20 - Different parts has been modeled in FEM based on experimental test

The contact property between box culvert and top and bottom plates were surface-to-surface contact with both tangential and normal behaviors.

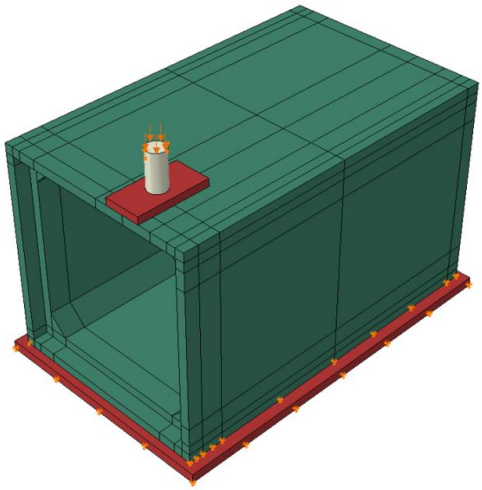

Figure 5.21 - Applying load through the cylinder in the form of displacement control

As shown in Figure 5.21, load has been applied to the model by doing displacement control and through cylinder part that has been modeled on top of the loading plate. The cylinder is playing the role of actuator that has been used in experimental test for applying load.

5.8 Comparison of experimental and FEM results on box culvert with conventional reinforcement and with no synthetic fiber

By using the visualization module in ABAQUS, the results of finite element analysis have been read and compared with related test results. As shown in following figures, there is a good agreement between the FEM and experimental data. In these series of finite element analysis, no fiber has been introduced to the box culverts.

5.8.1 Deflected shape

The deflected shape of box culvert can be checked in visualization module in ABAQUS. Figure 5.22 shows the typical box culvert deflection after application of load through the attached cylinder in the form of displacement control. The deformation is magnified 10 times. The load plate has been placed at a distance d from tip of the haunch to the side of the plate. As shown in Figure 5.23, the box culvert started getting load until it reached to the ultimate load. After that the box culvert slab started moving down exactly similar to what has been observed in experimental test and then the load started decreasing.

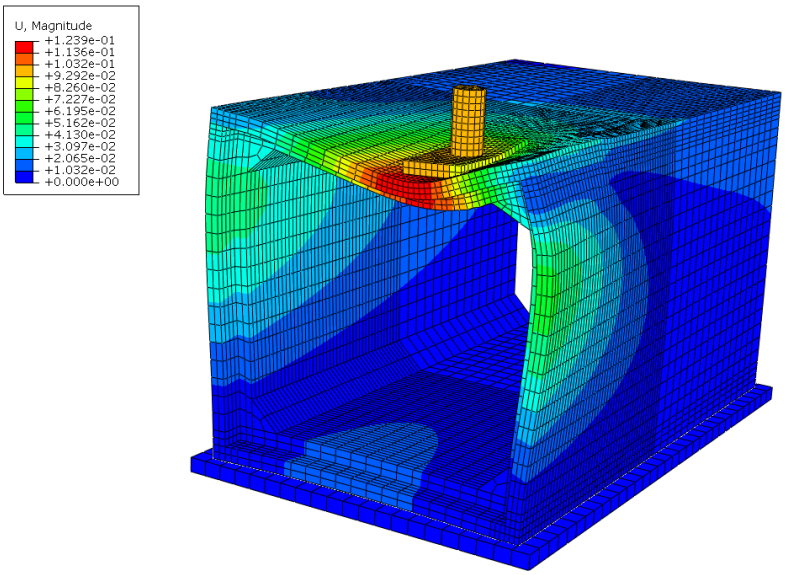

Figure 5.22 - Typical deformed shaped of box culverts (BL-4-4-8-Y)

As shown in Figure 5.23 and Figure 5.24, there is a relatively good coincidence between experimental results and finite element analysis on location of crack on top slab of box culvert.

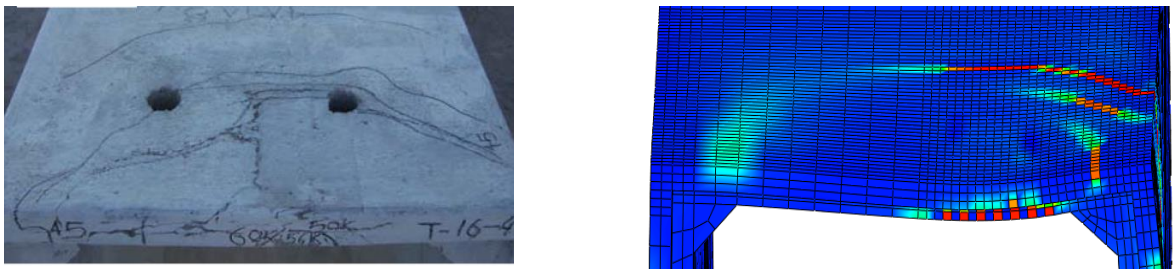

a) b)

Figure 5.23 - Location of crack on top slab of box culvert (BL-4-4-8-Y) (a) experimental test (b) FEM

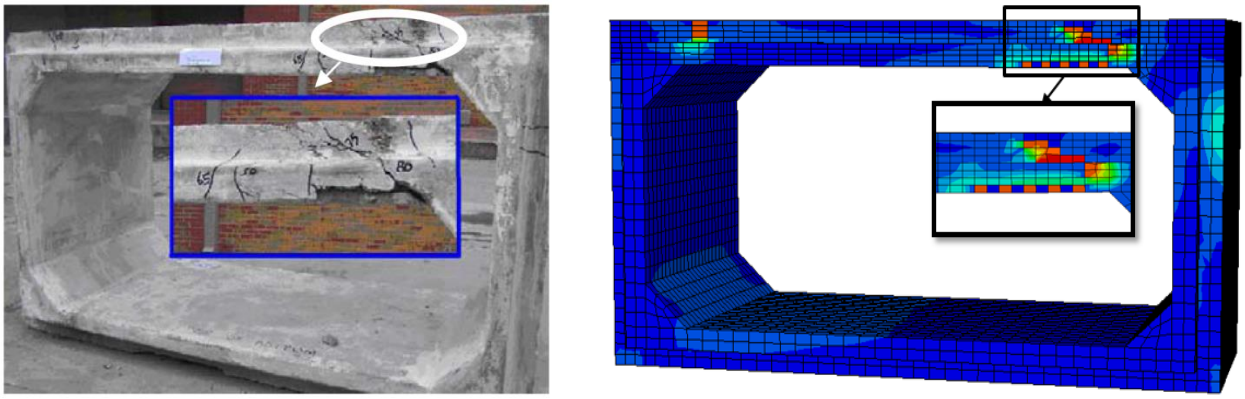

a) b)

Figure 5.24 - Location of crack on top slab of box culvert (SP-8-4-4-N) (a) experimental test (b) FEM

5.8.2 Load-deformation response

Typical results of finite element analysis of box culverts with 34 MPa (5000 psi) concrete compressive strength and with no fiber have been discussed in this section. As shown in Figure 5.25 to Figure 5.32, there is a good agreement between the FEM results and obtained test results for 34 MPa (5,000 psi) concrete compressive strength.

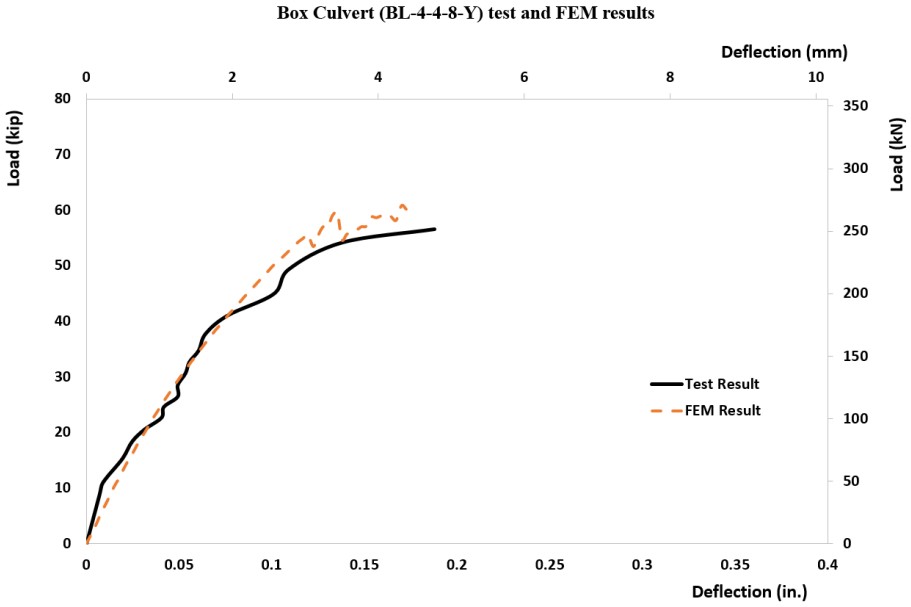

Figure 5.25 - Comparison between FEM and experimental results for BL-4-4-8-Y

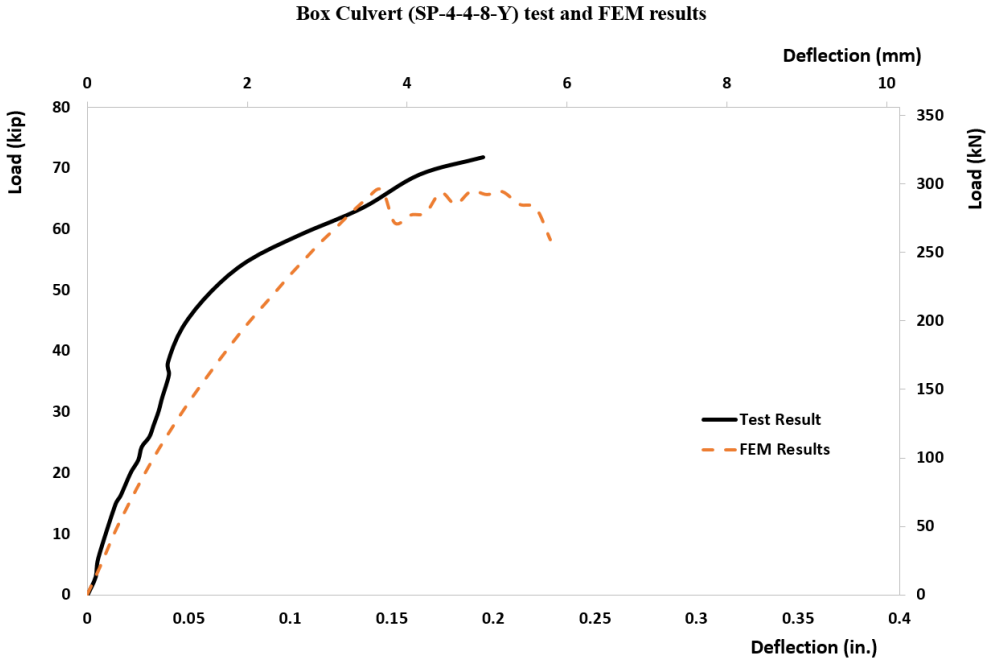

Figure 5.26 - Comparison between FEM and experimental results for SP-4-4-8-Y

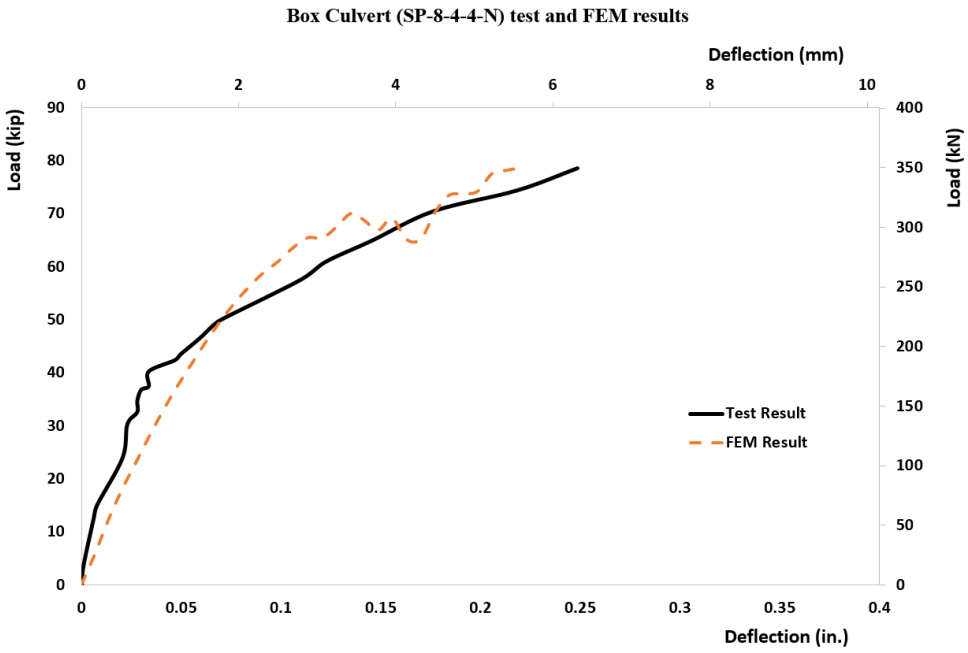

Figure 5.27 - Comparison between FEM and experimental results for SP-8-4-4-N

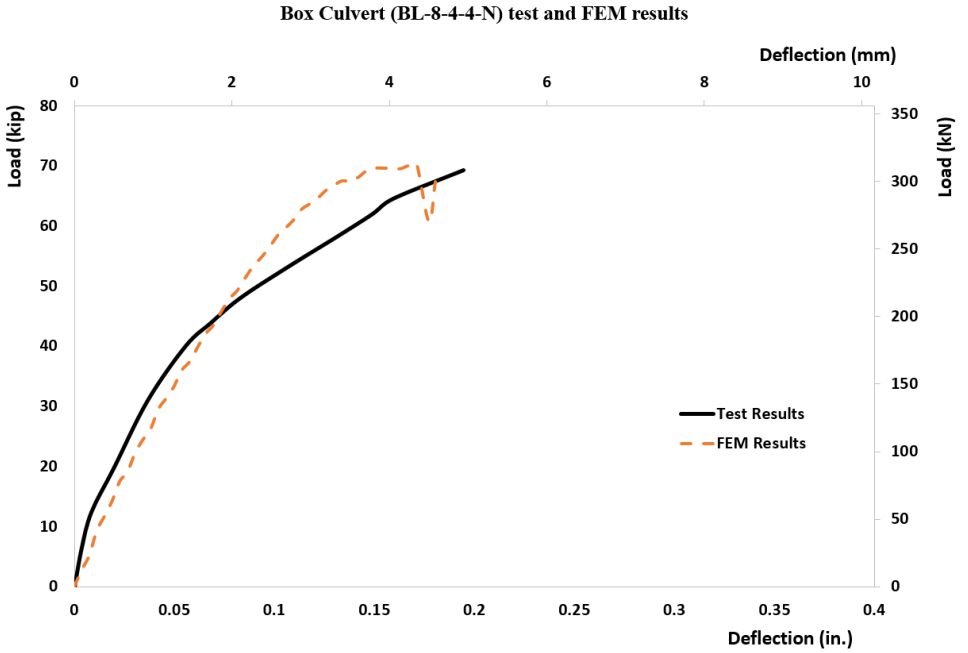

Figure 5.28 - Comparison between FEM and experimental results for BL-8-4-4-N

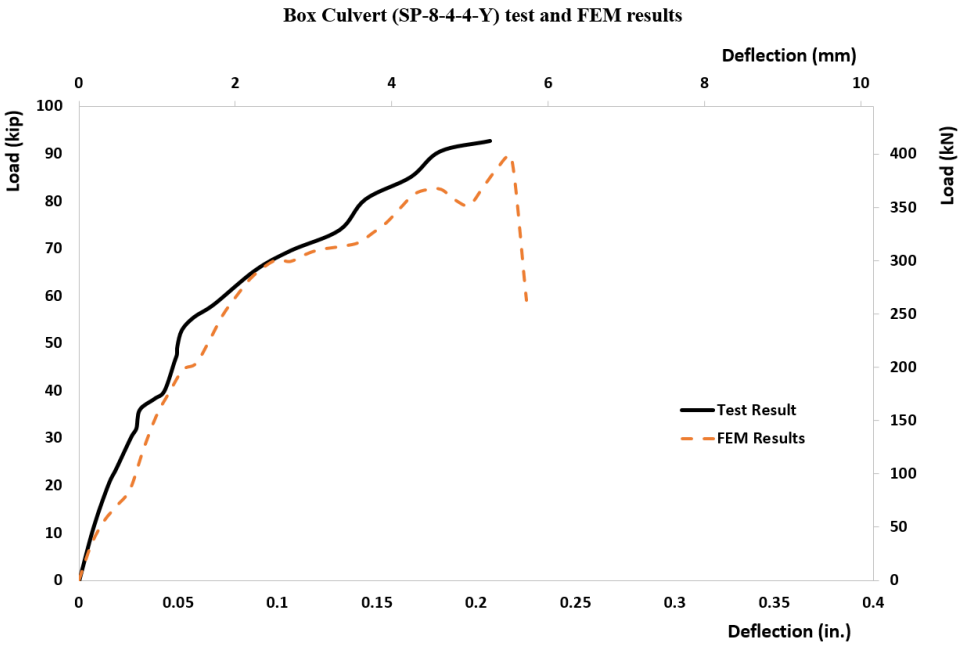

Figure 5.29 - Comparison between FEM and experimental results for SP-8-4-4-N

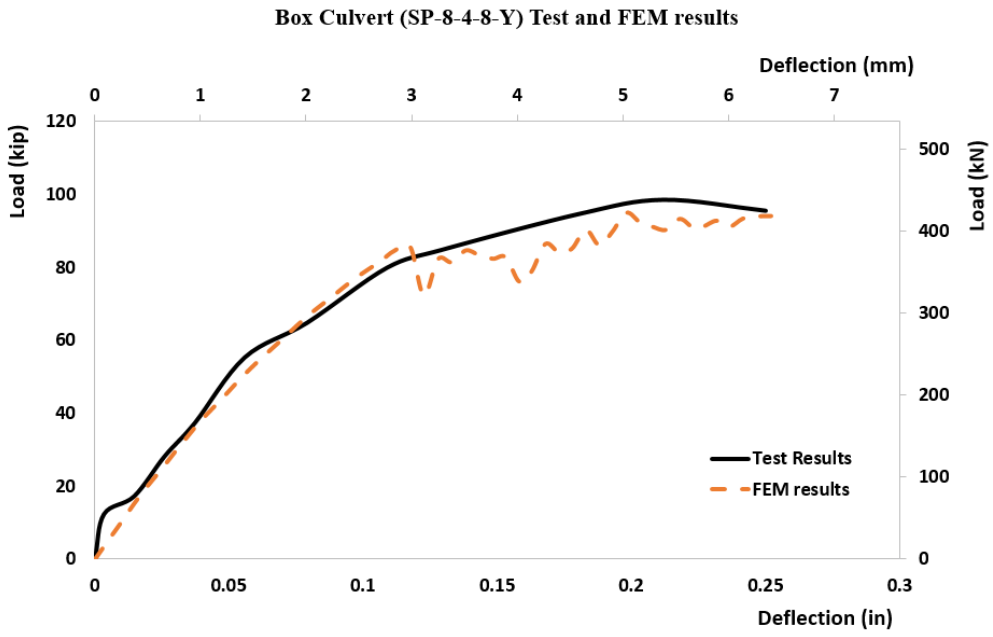

Figure 5.30 - Comparison between FEM and experimental results for SP-8-4-8-Y

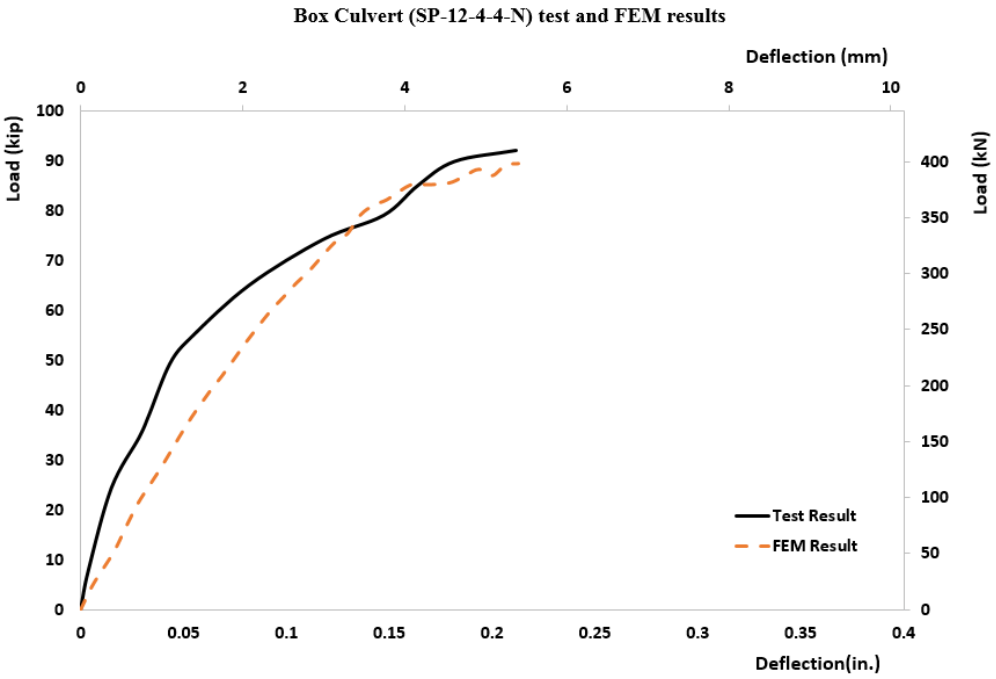

Figure 5.31 - Comparison between FEM and experimental results for SP-12-4-4-N

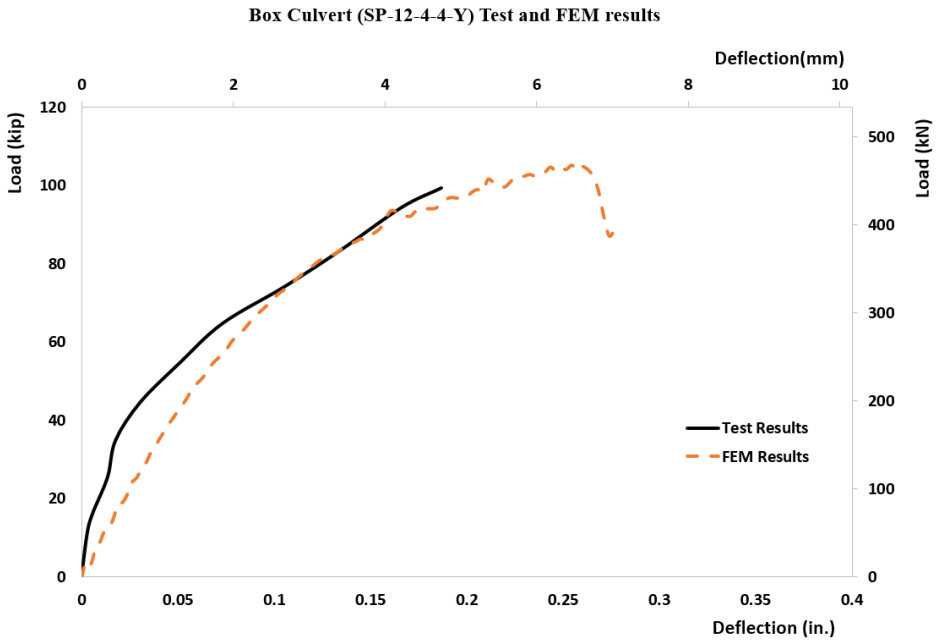

Figure 5.32 - Comparison between FEM and experimental results for SP-12-4-4-Y

5.9 Comparison of experimental and FEM results on box culvert with conventional reinforcement and with 0.52% fiber volume fraction

By using the visualization module in ABAQUS, the results of finite element analysis have been read and compared with related test results. As shown in following figures, there is a good agreement between the FEM and experimental data. In these series of finite element analysis, 0.52% fiber volume fraction (8PCY) concrete has been assigned as material used for the box culverts. The FEM algorithm used for modeling one of the box culverts has been presented in Appendix D.

5.9.1 Deflected shape

The deflected shape of box culvert can be checked in visualization module in ABAQUS. Figure 5.33 shows the 4'x4' box culvert deflection after application of load through the attached cylinder in the form of displacement control. The deformation is magnified 5 times. The load plate has been placed at a distance d from tip of the haunch to the side of the plate. As shown in Figure 5.33, the box culvert started getting load until it reached to the ultimate load. After that the box culvert slab started moving down exactly similar to what has been observed in experimental test and then the load started decreasing but this time slowly because of the strong bond exist between the fibers and the matrix.

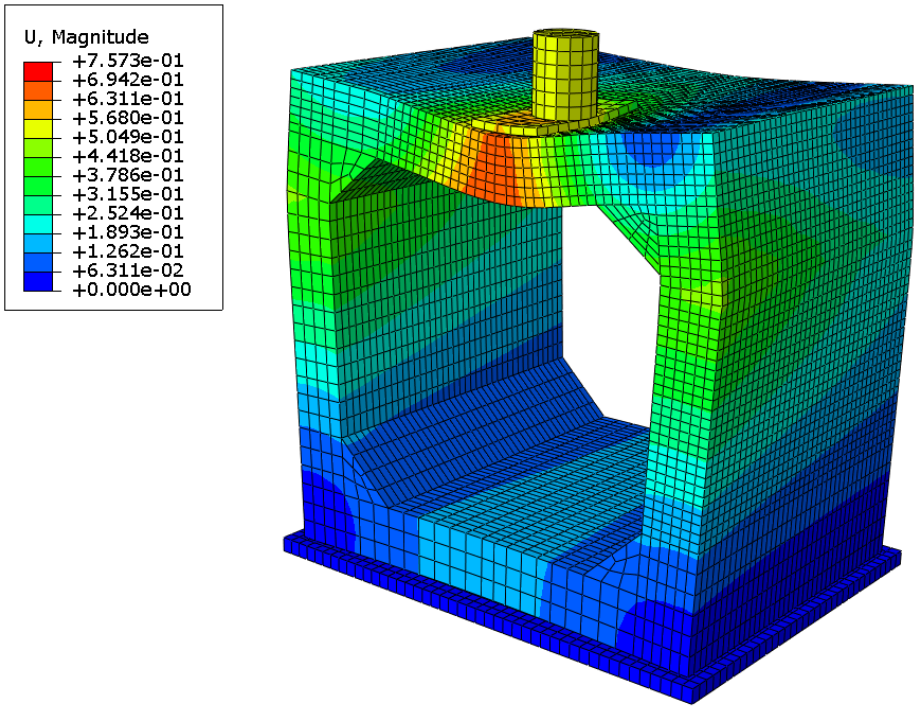

Figure 5.33 - Deformed shape of box culvert 4'x4'

As shown in Figure 5.34 and Figure 5.35, there is a relatively good coincidence between experimental results and finite element analysis on the location of crack on top slab of box culvert.

The FEM analysis generally displays initial cracks on the inside face of the top slab and with the increase in load the cracks are detected on the outside face of the side walls. With further increase of load, cracks are predicted on the outside face of the top slab. Similar behavior was observed in all experimental investigations.

a)

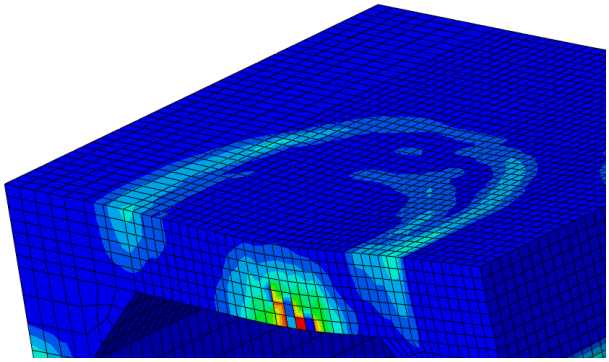

b)

Figure 5.34 - Location of crack on top slab of box culvert 4'x4' (a) experimental test (b) FEM

a)

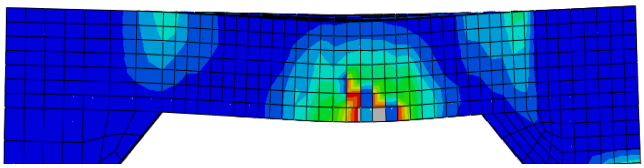

b)

Figure 5.35 - Location of crack on top slab of box culvert 4'x4' (a) experimental test (b) FEM

5.9.2 Load-deformation response

Typical results of finite element analysis of box culverts with 34 MPa (5000 psi) concrete compressive strength have been discussed in this section. As shown in Figure 5.36 to Figure 5.39, there is a close relationship between the FEM and experimental results for 34 MPa (5,000 psi) concrete compressive strength with 0.52% fiber volume fraction.

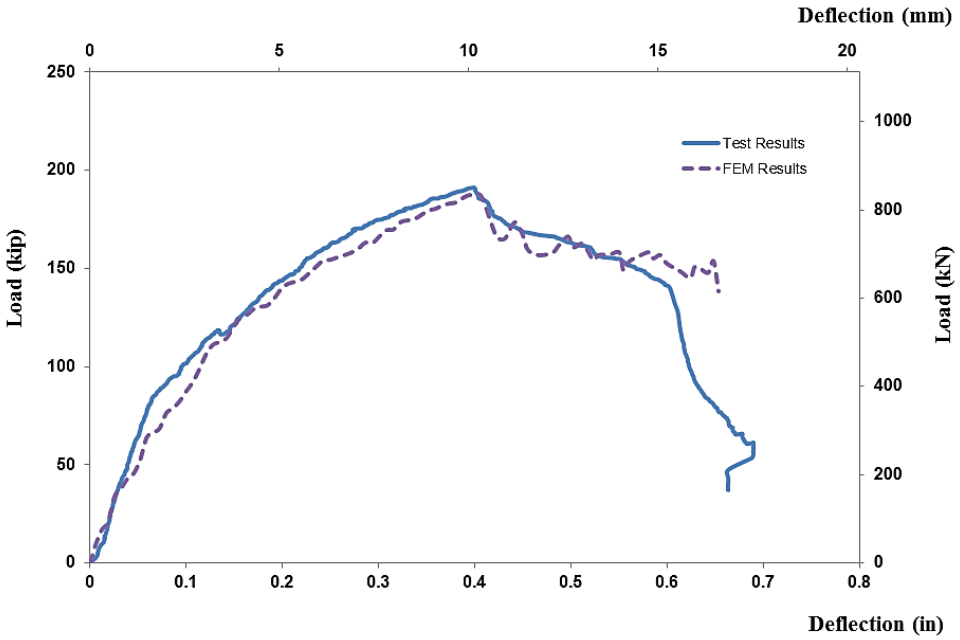

Figure 5.36 - Comparison between FEM and experimental results for Box culvert 4'x4' Manufactured by Northern Concrete

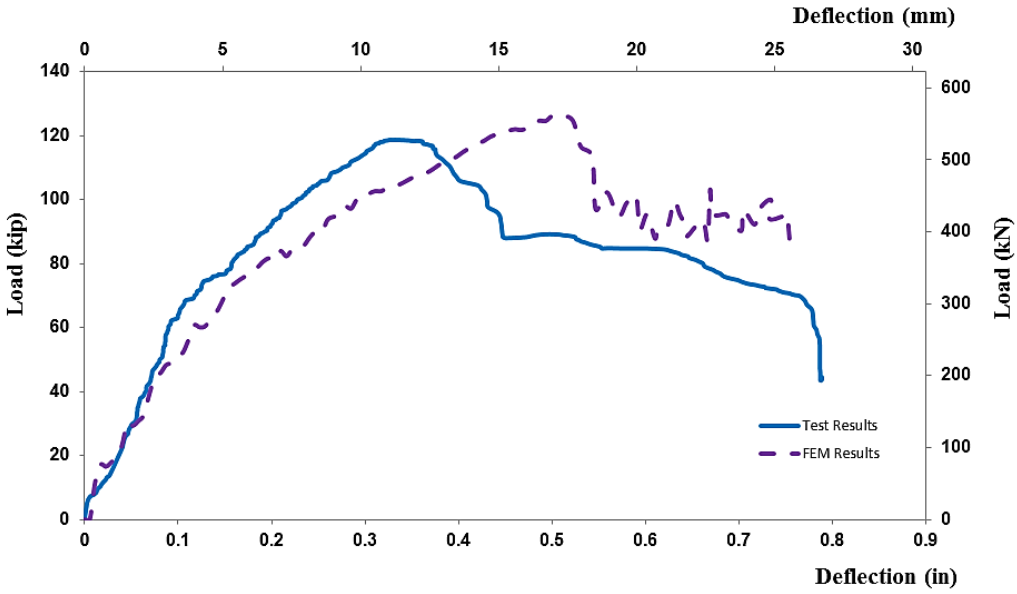

Figure 5.37 - Comparison between FEM and experimental results for Box culvert 8'x4' Manufactured by Northern Concrete

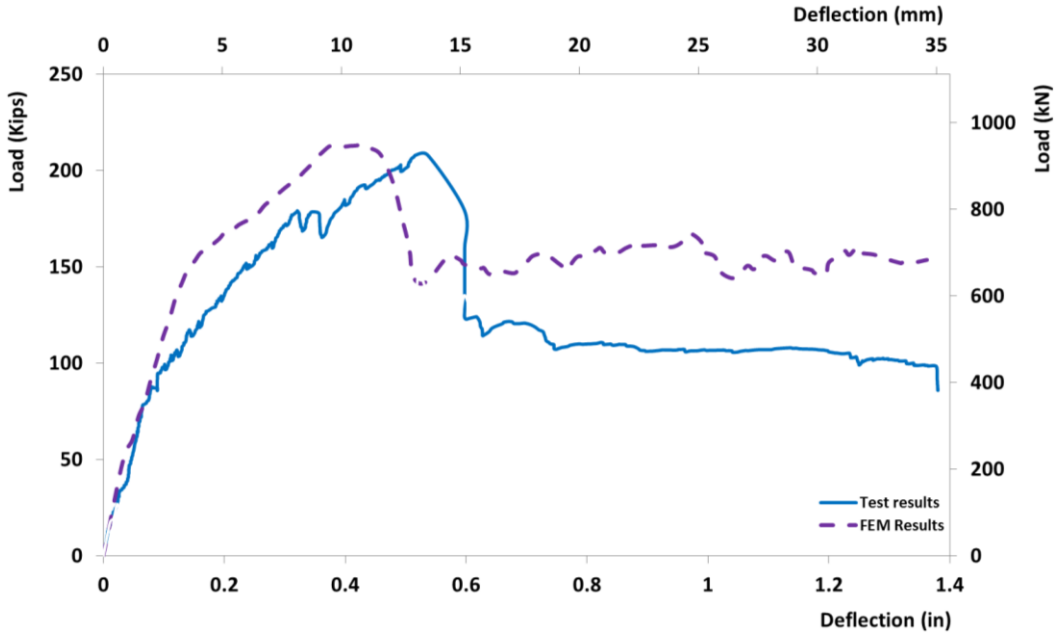

Figure 5.38 - Comparison between FEM and experimental results for Box culvert 12'x4' Manufactured by Northern Concrete

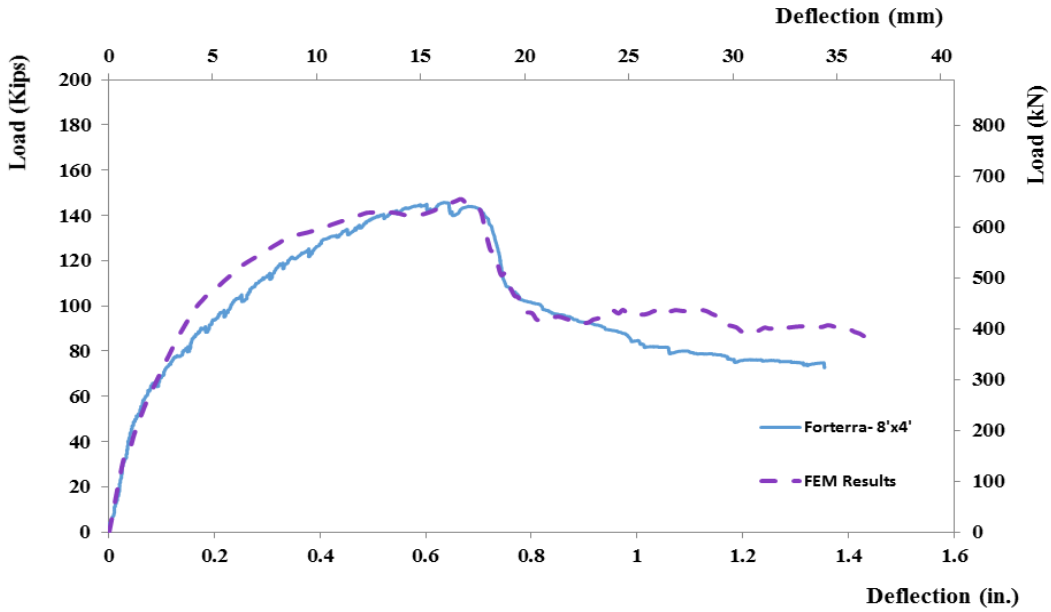

Figure 5.39 - Comparison between FEM and experimental results for Box culvert 8'x4' Manufactured by Forterra

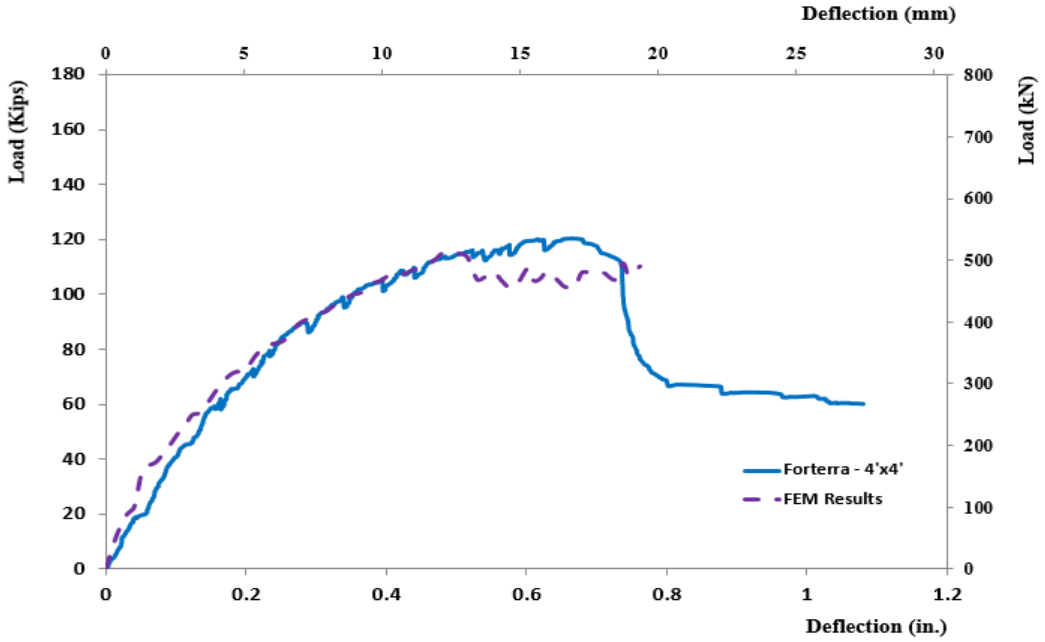

Figure 5.40 - Comparison between FEM and experimental results for Box culvert 4’x4’ Manufactured by Forterra

CHAPTER 6

FINITE ELEMENT ANALYSIS ON SHEAR CAPACITY OF ASTM C1577 PRECAST BOX CULVERTS EQUIPPED WITH DIFFERENT FIBER VOLUME FRACTIONS

6.1 Introduction

To study the shear behavior of box culverts equipped with synthetic fiber Reinforced Concrete (Syn-FRC), three dimensional finite element models were prepared for all the sixty-five standard sizes of ASTM C1577 box culverts. The geometric properties of all of the box culverts has been presented in Table 6.1.

This part of the research has been completed after calibrating the geometry, material property of Syn-FRC and also boundary conditions of box culverts modeled in FEM with the experimental test data explained in previous chapters. The box culverts modeled as 3-D solid elements and the horizontal and vertical reinforcement modeled as truss element embedded in the box culvert. In all of the models, the material and geometry nonlinearities have been considered. The base support of box culvert is modeled as a rectangular block and the contact between the box and block is defined as surface-to-surface contact elements. In all the FEM analysis of ASTM C1577 box culverts, the load plate was placed at the distance “d” from the tip of the haunch to the edge of the load plate.

After completing a comprehensive finite element analysis on all the different sizes of ASTM C1577 box culverts equipped with Syn-FRC, the shear capacity of concrete

box culverts equipped with different fiber volume fractions has been investigated. The peak shear force for each box culvert equipped with different fiber volume fractions (0%, 0.26%, 0.52% and 0.78%) was identified based on the load-deflection results for each box culvert. The load-deflection results of all the boxes are presented in Appendix E.

Table 6.1- Geometric properties of ASTM C1577 box culverts

ASTM C1577 Cases	Span in.	Rise in.	Thickness in.	Rein. Ratio
3 ft X 2 ft X 4 in.	36	24	4	0.69
3 ft X 3 ft X 4 in.	36	36	4	0.75
4 ft X 2 ft X 5 in.	48	24	5	0.56
4 ft X 3 ft X 5 in.	48	36	5	0.65
4 ft X 4 ft X 5 in.	48	48	5	0.69
5 ft X 2 ft X 6 in.	60	24	6	0.45
5 ft X 3 ft X 6 in.	60	36	6	0.52
5 ft X 4 ft X 6 in.	60	48	6	0.55
5 ft X 5 ft X 6 in.	60	60	6	0.58
6 ft X 2 ft X 7 in.	72	24	7	0.38
6 ft X 3 ft X 7 in.	72	36	7	0.43
6 ft X 4 ft X 7 in.	72	48	7	0.47
6 ft X 5 ft X 7 in.	72	60	7	0.51
6 ft X 6 ft X 7 in.	72	72	7	0.53
7 ft X 2 ft X 8 in.	84	24	8	0.33
7 ft X 3 ft X 8 in.	84	36	8	0.37

7 ft X 4 ft X 8 in.	84	48	8	0.40
7 ft X 5 ft X 8 in.	84	60	8	0.43
7 ft X 6 ft X 8 in.	84	72	8	0.45
7 ft X 7 ft X 8 in.	84	84	8	0.48
8 ft X 2 ft X 8 in.	96	24	8	0.37
8 ft X 3 ft X 8 in.	96	36	8	0.42
8 ft X 4 ft X 8 in.	96	48	8	0.45
8 ft X 5 ft X 8 in.	96	60	8	0.48
8 ft X 6 ft X 8 in.	96	72	8	0.50
8 ft X 7 ft X 8 in.	96	84	8	0.52
8 ft X 8 ft X 8 in.	96	96	8	0.54
9 ft X 2 ft X 9 in.	108	24	9	0.31
9 ft X 3 ft X 9 in.	108	36	9	0.34
9 ft X 4 ft X 9 in.	108	48	9	0.38
9 ft X 5 ft X 9 in.	108	60	9	0.40
9 ft X 6 ft X 9 in.	108	72	9	0.42
9 ft X 7 ft X 9 in.	108	84	9	0.44
9 ft X 8 ft X 9 in.	108	96	9	0.45
9 ft X 9 ft X 9 in.	108	108	9	0.46
10 ft X 2 ft X 10 in.	120	24	10	0.26
10 ft X 3 ft X 10 in.	120	36	10	0.29
10 ft X 4 ft X 10 in.	120	48	10	0.31
10 ft X 5 ft X 10 in.	120	60	10	0.33
10 ft X 6 ft X 10 in.	120	72	10	0.35
10 ft X 7 ft X 10 in.	120	84	10	0.37
10 ft X 8 ft X 10 in.	120	96	10	0.38

10 ft X 9 ft X 10 in.	120	108	10	0.39
10 ft X 10 ft X 10 in.	120	120	10	0.41
11 ft X 2 ft X 11 in.	132	24	11	0.23
11 ft X 3 ft X 11 in.	132	36	11	0.25
11 ft X 4 ft X 11 in.	132	48	11	0.28
11 ft X 5 ft X 11 in.	132	60	11	0.29
11 ft X 6 ft X 11 in.	132	72	11	0.30
11 ft X 7 ft X 11 in.	132	84	11	0.32
11 ft X 8 ft X 11 in.	132	96	11	0.33
11 ft X 9 ft X 11 in.	132	108	11	0.35
11 ft X 10 ft X 11 in.	132	120	11	0.38
11 ft X 11 ft X 11 in.	132	132	11	0.39
12 ft X 2 ft X 12 in.	144	24	12	0.22
12 ft X 3 ft X 12 in.	144	36	12	0.22
12 ft X 4 ft X 12 in.	144	48	12	0.23
12 ft X 5 ft X 12 in.	144	60	12	0.25
12 ft X 6 ft X 12 in.	144	72	12	0.27
12 ft X 7 ft X 12 in.	144	84	12	0.30
12 ft X 8 ft X 12 in.	144	96	12	0.31
12 ft X 9 ft X 12 in.	144	108	12	0.33
12 ft X 10 ft X 12 in.	144	120	12	0.34
12 ft X 11 ft X 12 in.	144	132	12	0.36
12 ft X 12 ft X 12 in.	144	144	12	0.37

6.2 Parametric study

A parametric study was conducted on the sixty-five standard sizes of ASTM C1577 box culverts to investigate the effect of adding synthetic fibers on shear capacity of concrete box culverts with different sizes. Span, rise and top slab thickness were the parameters that considered in this study. Figure 6.1 to 6.3 show the relation between increasing the span, rise and top slab thickness of box culverts and shear capacity of box culverts with different fiber volume fractions.

As shown in Figure 6.1, by increasing the span length, the shear load increased and the enhancement was more pronounced by adding more fibers to the boxes.

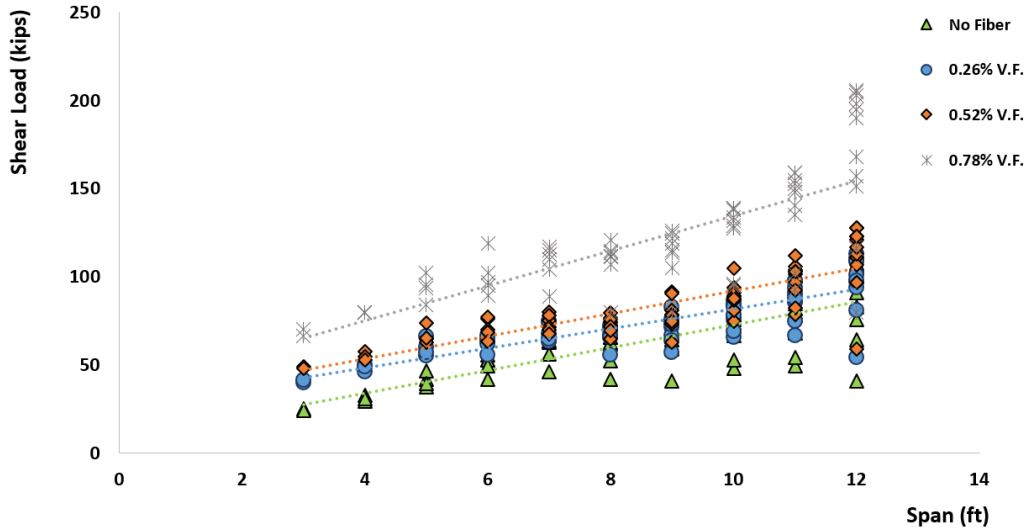

Figure 6.1 - Shear load versus span length of ASTM C1577 boxes

Figure 6.2 shows the relation between increasing the rise of box culverts and shear capacity of boxes for different fiber volume fractions. As shown, by increasing the rise

length, the shear load increased and the improvement was more pronounced for 0.78% fiber volume fraction compared with 0.26% and 0.52% fiber volume fractions.

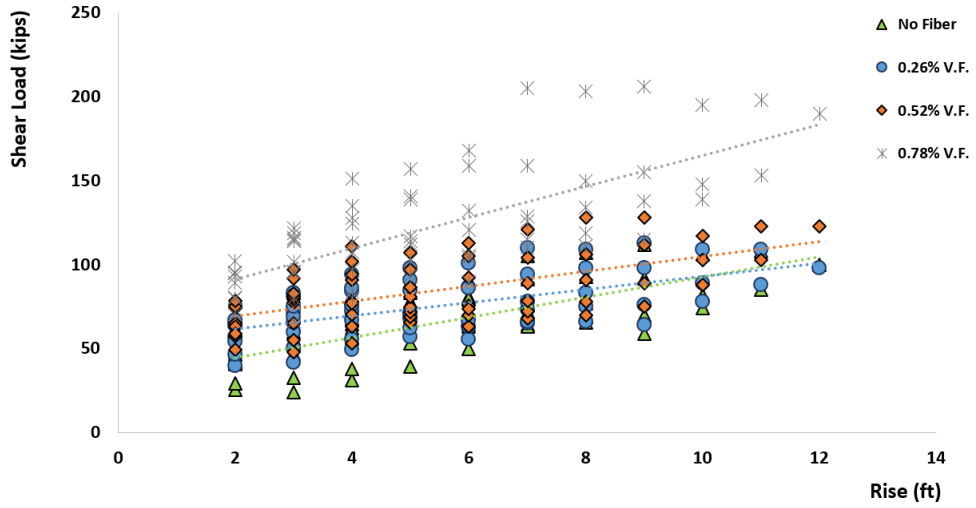

Figure 6.2 - Shear load versus rise length of ASTM C1577 boxes

Figure 6.3 presents the relation between increasing the top slab thickness and shear capacity of boxes for different fiber volume fractions. As shown, by increasing the slab thickness, the shear load increased and the improvement was more noticeable for 0.78% fiber volume fraction compared with 0.26% and 0.52% fiber volume fractions.

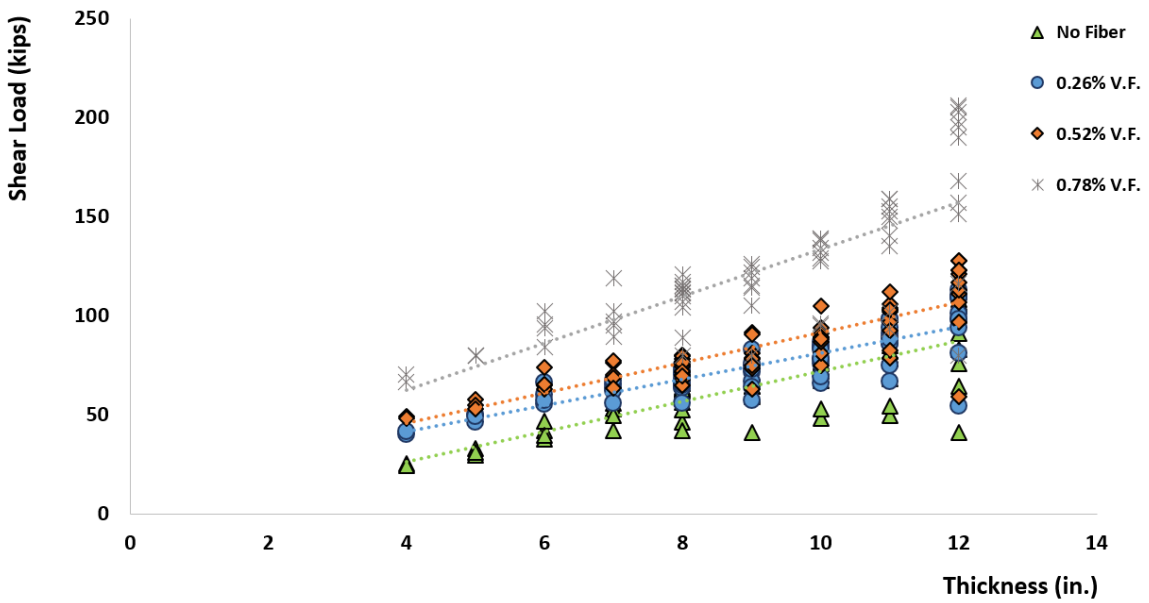

Figure 6.3 - Shear load versus top slab thickness of ASTM C1577 boxes

Figure 6.4 shows that the reinforcement ratios of all of the ASTM C1577 box culverts have been limited within 0.2% to 0.6% and based on ACI 318-08, the minimum and maximum reinforcement ratio in box culverts are 0.2% and 2.2%, respectively. Therefore, the effect of reinforcement ratio in shear capacity of box culverts has been neglected in this study.

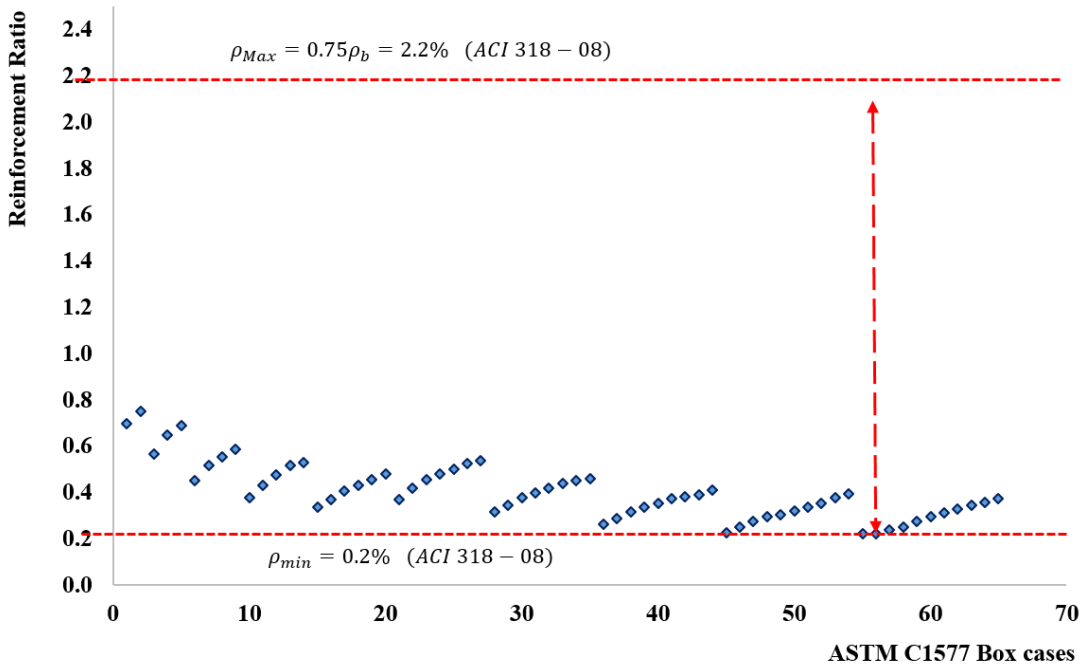

Figure 6.4 - Required reinforcement ratio for ASTM C1577 box culverts

Figure 6.5 through Figure 6.7 compared the shear capacity of ASTM C1577 box culverts equipped with three different fiber volume fractions with conventional reinforced boxes. As shown, adding synthetic fibers to the concrete increased the shear capacity of short span boxes (3, 4, 5 or 6 ft.) more than large span boxes (9, 10, 11 and 12 ft.). For boxes with same span length, adding more fiber had more effect on low-rise boxes more than high-rise boxes.

Figure 6.5 demonstrates that adding 0.26% fiber volume fractions to the concrete enhanced the shear capacity of boxes up to 1.6 times in comparison with boxes with conventional reinforcement. It also displays that for large span boxes (9, 10, 11 and 12 ft.), it enhances the shear capacity no more than 1.3 times compared with conventional reinforced boxes.

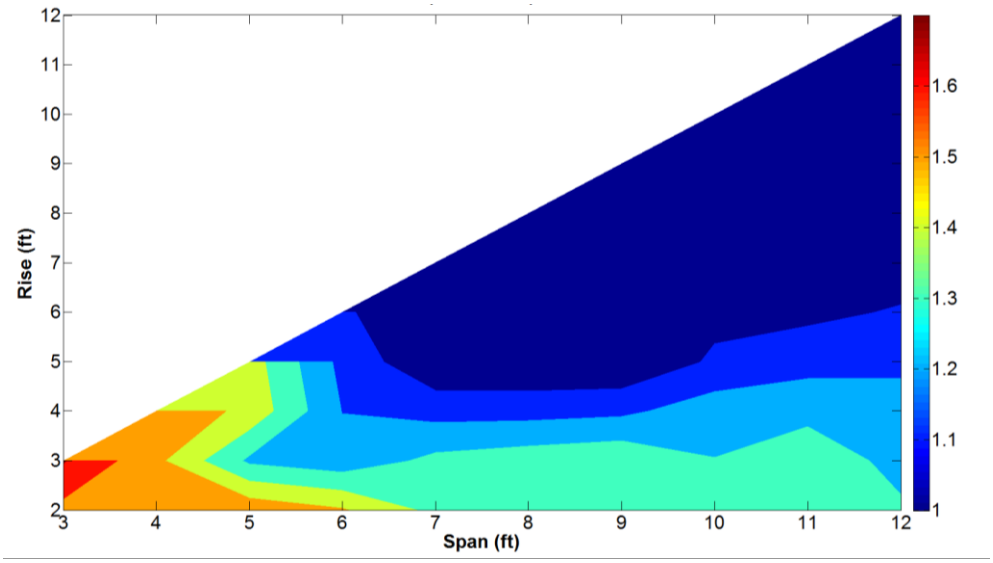

Figure 6.5 - Increase in Shear Capacity of Syn-FRC boxes (V.F. = 0.26%) compared with RC Boxes (VFRC/VRC)

Figure 6.6 displays that increasing the fiber volume fractions to 0.52% enhanced the shear capacity of boxes up to 1.9 times in comparison with boxes with traditional reinforcement. It also shows that for large span boxes (9, 10, 11 and 12 ft.), it enhances the shear capacity up to 1.6 times compared with conventional reinforced boxes. For boxes with large spans and high rises, applying synthetic fiber has less effect and it enhanced the shear capacity not more than 1.1 times in comparison with conventional boxes.

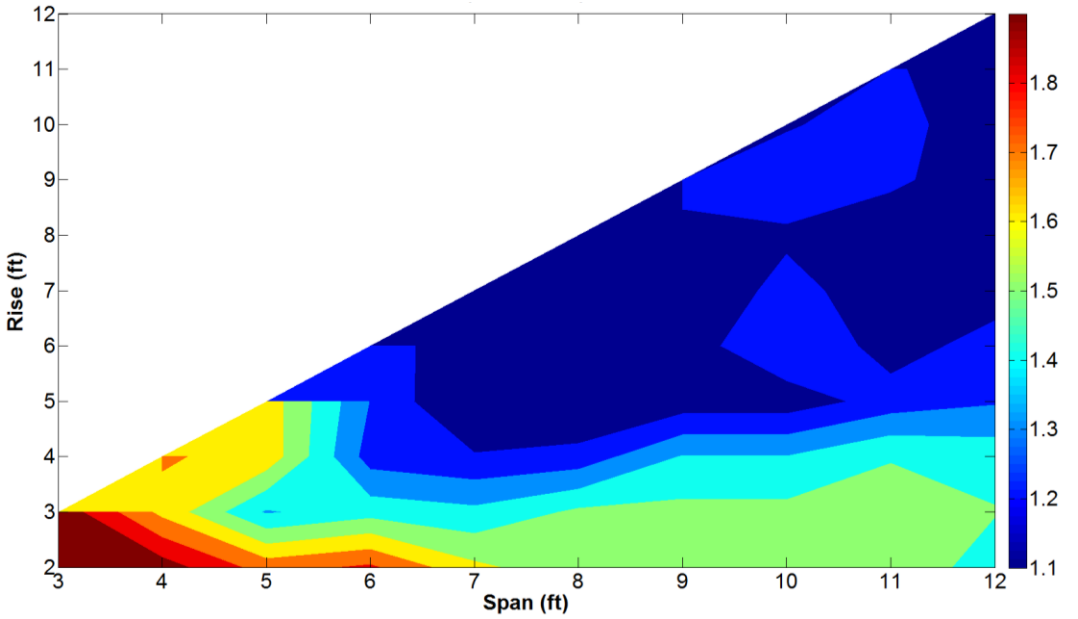

Figure 6.6 - Increase in Shear Capacity of Syn-FRC boxes (V.F. =0.52%) compared with RC Boxes (VFRC/VRC)

Figure 6.7 shows that addition of synthetic fibers at 0.78% volume fraction to the box culverts improved the shear capacity of boxes up to 2.8 times. It also displays that for large span boxes (9, 10, 11 and 12 ft.) it enhanced the shear capacity up to 1.9 times compared with traditional reinforced boxes. For boxes with large span and high rises, applying synthetic fiber has less effect and it enhanced the shear capacity not more than 1.6 times in comparison with conventional boxes.

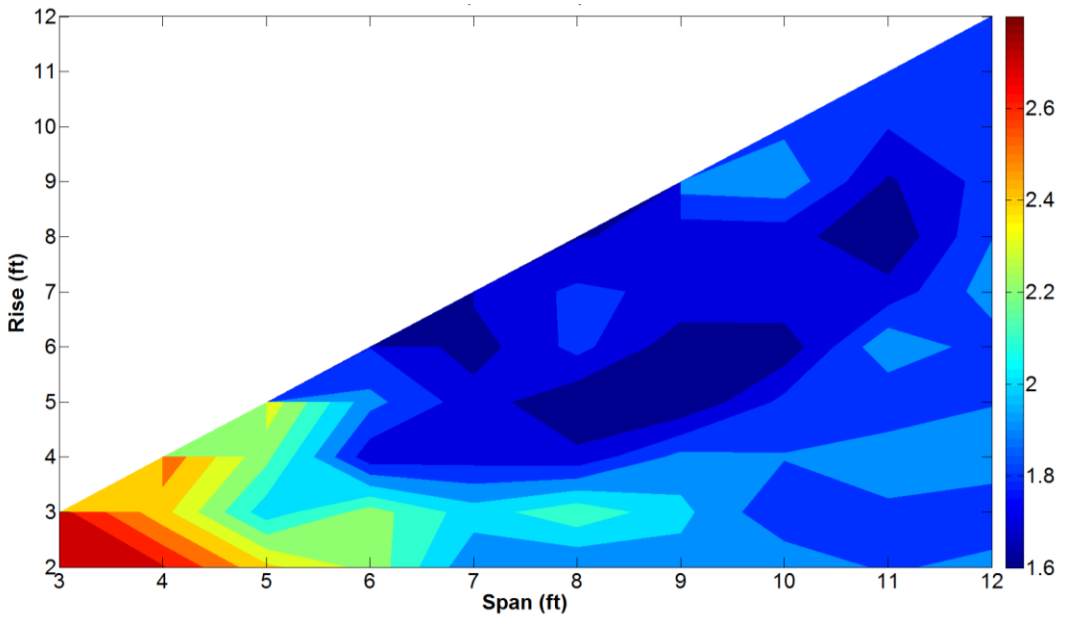

Figure 6.7 - Increase in Shear Capacity of Syn-FRC boxes (V.F. =0.78%) compared with RC Boxes (VFRC/VRC)

Figure 6.8 exhibits the effect of increasing synthetic fiber dosages (0.26%, 0.52% and 0.78%) in improving the shear capacity of all of the ASTM C1577 box culvert cases. As shown, increasing fiber volume fraction to 0.78%, enhanced the shear capacity of boxes up to 2.8 times. It also shows that the low dosage synthetic fiber (0.26% V.F.) has almost no effect in increasing shear capacity of 10 out of 65 cases. Increasing in shear capacity of box culverts was more noticeable when fiber volume fraction changed from 0.52% to 0.78% than from 0.52% to 0.78%.

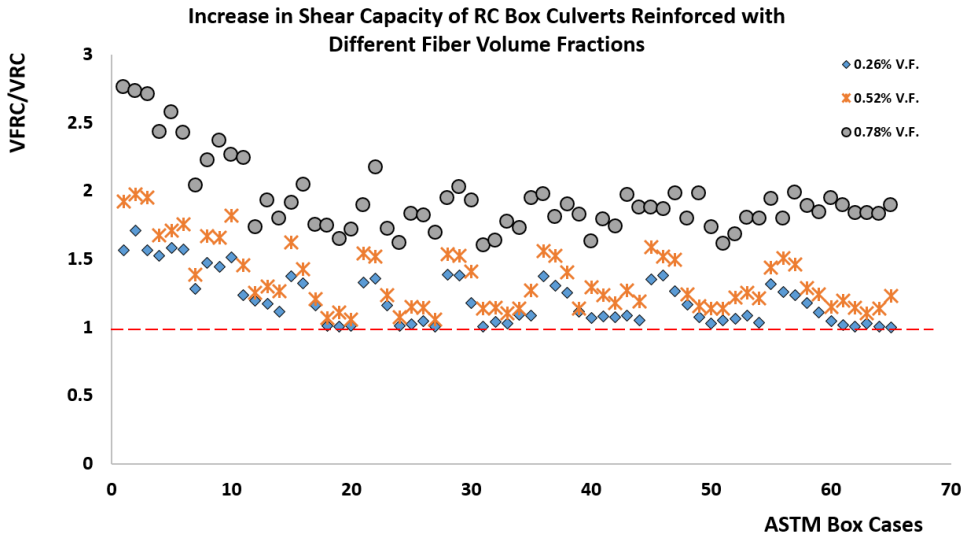

Figure 6.8 - Increase in shear capacity of ASTM Syn-FRC box culverts with 3 different fiber volume fractions

CHAPTER 7

SUMMARY, CONCLUSIONS, AND RECOMMENDATIONS

7.1 Summary

This research evaluated the shear behavior of synthetic fiber reinforced concrete and also the shear capacity of the precast concrete box culverts equipped with synthetic fibers and subjected to HS 20 truck wheel load. In all box culverts, the load plate was placed at the distance “d” from the tip of the haunch to the edge of the load plate. Two major phases were considered to complete the study, which included: (1) Material test for two different concrete compressive strength values (4000 and 5000 psi) and developing shear strength for 7000 psi concrete compressive strength with different fiber volume fractions by using Finite Element Analysis (FEA); (2) Finite Element Analysis (FEA) on all the ASTM C1577 box culverts equipped with different synthetic fiber dosages along with experimental tests in order to evaluate the FEM results.

7.2 Phase 1- Material tests

The first phase is consist of three different material tests with more focus on shear test. The Japan Society of Civil Engineering (JSCE) test method (with some alterations) was selected for extracting shear properties of SYN-FRC. The concrete used in this study was zero-slump, dry-cast one which is typically used for mass productions like concrete pipe, manhole and box culverts because the forms can be striped as soon as the concrete has been consolidated. The total number of 60 beams

have been tested based on JSCE-G553 and ASTM 1609 for two different concrete compressive strength values. After finishing the material tests, Finite Element Analysis (FEA) has been conducted for developing the shear strength of 7000 psi concrete compressive strength with different fiber volume fractions based on the shear test results for 28 MPa (4,000 psi) and 34 MPa (5,000 psi) concrete compressive strength values. The results of this phase have been utilized to develop the material behavior of Syn-FRC using finite element analysis in order to model and analyze the various sizes of the Syn-FRC box culverts.

7.3 Phase 2- Shear behavior of box culverts equipped with synthetic fiber

After implementing phase I, phase II started which had more focus on the shear behavior of box culverts equipped with synthetic fibers along with conventional reinforcement. Full-scale experimental tests were performed on five box culverts with three different spans of 122 cm (4 ft), 244 cm (8 ft) and 366 cm (12 ft) designated as per ASTM C1433-05 and ASTM C1577 and equipped with 0.52% fiber volume fraction (8 PCY). The rise of all of the box culverts was 144 cm (4 ft). The wall and the slab thickness of box culverts were 20 cm (8 in) for 4'x4' and 8'x4' box culverts and 30 cm (12 in) for 12'x4' box culvert designed based on ASTM C1433 and for the other two ones followed ASTM C1577 design criteria. Different span sizes and slab thicknesses were considered to cover a variety of geometrical dimensions. The experimental tests were conducted in order to calibrate the geometry, material property of Syn-FRC and also boundary conditions of box culverts modeled in FEM.

The verified model and the calibration parameters were used to perform complete 3-D FEM analysis of the ASTM-C1577 boxes equipped with different fiber volume fractions. The box culverts modeled as 3-D solid elements and the horizontal and vertical reinforcement modeled as truss elements embedded in the box culvert. Concrete brittle cracking model has been used for the whole box culverts with a density of 2400 kg/m3 (150 pcf), Modulus of Elasticity of 27405 MPa (5000 ksi). For the base support and loading plate, a normal steel property with a density of 7800 kg/m^3 (0.28 lb/cu^3), young's modulus of 200 GPa (29,000,000 psi) and poison's ratio of 0.3 has been selected. In all models, the material and geometry nonlinearities have been considered. The base support of box culvert is modeled as a rectangular block and the contact between the box and block is defined as surface-to-surface contact elements. In all boxes, the load plate placed at the distance "d" from the tip of the haunch to the edge of the load plate on the outside face of the top slab to transfer the load from the load cylinder and the load cell to each test culvert.

After finalizing a comprehensive finite element analysis on all the different sizes of ASTM C1577 box culverts equipped with Syn-FRC, the shear capacity of box culverts equipped with different fiber volume fractions (0%, 0.26%, 0.52% and 0.78% V.F.) has been investigated. In all the FEM analysis of ASTM C1577 box culverts, the peak shear force for each box culvert was identified based on the load-deflection plot for each box culvert. The step-by-step test events along with photographs of the test specimens including crack marks were recorded and are presented in Chapter 3.

7.4 Conclusion

The conclusion of this study advances in the following forefronts:

Phase I:

- A total of 60 beams were cast and tested based on JSCE G-553 and ASTM C1609 for evaluating the effect of synthetic fibers on shear capacity and flexural behavior of concrete with two different target compressive strength values. Based on shear test results, increasing the fiber dosage from V.F. = 0% to V.F. = 1.04% improved shear strength of concrete up to 41% and 43% for 28 MPa (4000 psi) and 34 MPa (5000 psi) concrete compressive strength, respectively. Additionally, shear toughness in concrete equipped with synthetic fibers improved by 648% and 736% for 28 MPa (4000 psi) and 34 MPa (5000 psi) concrete compressive strength values, respectively. It is also shown that by increasing compressive strength from 28 MPa (4000 psi) to 34 MPa (5000 psi) (25% increase), shear strength enhancement is more noticeable in lower fiber dosages concrete (i.e. V.F.= 0.26% and 0.52%) than higher ones.
- Based on the results from flexural tests, increasing the fiber dosages in concrete improved the flexural strength and flexural toughness significantly. This improvement is remarkable in lower fiber volume fractions (V.F. = 0.26% and 0.52%). By comparing the flexural test results for concrete with 28 MPa (4000 psi) and 34 MPa (5000 psi) compressive strength values, it is shown that increasing

the compressive strength has more influence on modules of rupture of concrete with lower fiber volume fractions (i.e. V.F= 0.26%) than higher fiber contents.

- In order to evaluate the effect of synthetic fibers on compressive behavior of dry-cast concrete, 60 cylinders were cast and tested according to ASTM C39. Based on this study, by increasing the fiber dosage, the compressive strength of concrete enhanced considerably. The optimum fiber volume fraction is 0.52% that increased the compressive strength up to 17% for both objective compressive strength values; however, increasing fiber dosages more than 0.52%, has less effect on concrete compressive strength.
- Increasing the compressive strength by 25% has more effect on shear and flexural strength of concrete equipped with 0.26% and 0.52% fiber volume fractions than 0.78% and 1.04% ones. Furthermore, the increase in compressive strength by 25%, has more significant influence on shear toughness than flexural toughness of synthetic fiber reinforced concrete.
- By carrying out a comparison between obtained FEM results and existing experimental results on ASTM C1609 beams, using concrete brittle cracking could accurately predict the flexural behavior of ASTM C1609 beam equipped with different fiber volume fractions. It can be concluded that the defined concrete brittle cracking model for various fiber volume fractions satisfies the tensile behavior of concrete and can be used to predict the structural behavior of box culverts equipped with different fiber volume fractions.

Phase II:

- The experimental results of all five box culverts showed that the flexural cracks formed initially on the inside face of the top or bottom slab, which extended to the middle of the load plate. Flexural cracks continually occurred in this area throughout the test. The second series of cracks were negative moment cracks which formed on the wall closest to the load plate.
- In all box culverts, the shear cracks were among the final cracks observed. These cracks initiated independently (not initiated at the tip of the flexural cracks) from the tip of the haunch and stretched toward the edge of the load plate. All of the shear cracks were detected after flexural cracks in all of the specimens tested.
- The crack width measured in some of the box culverts showed that the minimum crack width started from 0.1 mm (0.0039 in.) which was related to superficial flexural cracks and then reached to 2 mm (0.078 in.) which was related to shear crack at failure.
- The normalization results conducted on the box culvert experimental data based on the least square data fitting method showed that there is a good agreement between the experimental results of box culverts produced by Forterra and for boxes manufactured by Northern concrete.
- There was a close correlation between the experimental results and FE analysis conducted on box culverts produced by two different manufacturers.

- Based on the FEM results conducted on sixty five ASTM box culverts, by increasing the span length, the shear load increased and the enhancement was more pronounced by adding more fibers to the boxes.
- Adding synthetic fibers to the concrete increased the shear capacity of short span boxes (3, 4, 5 or 6 ft.) more than large span boxes (9, 10, 11 and 12 ft.). For boxes with same span length, adding more fiber had more influence on low rise boxes more than high rise boxes.
- For boxes with large span and high rises, applying synthetic fiber has less effect and it enhanced the shear capacity not more than 1.3 times in comparison with conventional boxes.
- Increasing fiber volume fraction to 0.78%, enhanced the shear capacity of boxes up to 2.8 times. The low dosage synthetic fiber (0.26% V.F.) has almost no effect in increasing shear capacity of 10 out of 65 cases. Increasing fiber volume fraction from 0.26% to 0.52% enhanced the shear capacity of boxes but not as much as increasing the fiber dosage from 0.52% to 0.78% volume fraction.

7.5 Recommendations

This study recommends the following future research studies to complement the work presented here:

- This study investigated the shear capacity of all the ASTM C1577 precast box culverts without considering the effect of soil load. The effect of surrounding soil load needs to be studied.

- The synthetic fiber material model for using in finite element analysis has been calibrated based on the experimental results of box culverts equipped with 0.52% fiber volume fraction. The material model for 0.26% and 0.78% fiber volume fraction also need to be calibrated by conducting the experimental tests on boxes equipped with the mentioned fiber volume fractions.

- Carry out a long-term fiber box culvert performance evaluation on installed box culverts in order to compare long-term load responses between fiber reinforced box culverts and RC boxes as measure by deflections.

APPENDIX A: MATERIAL TESTS PHOTOGRAPHS

a)

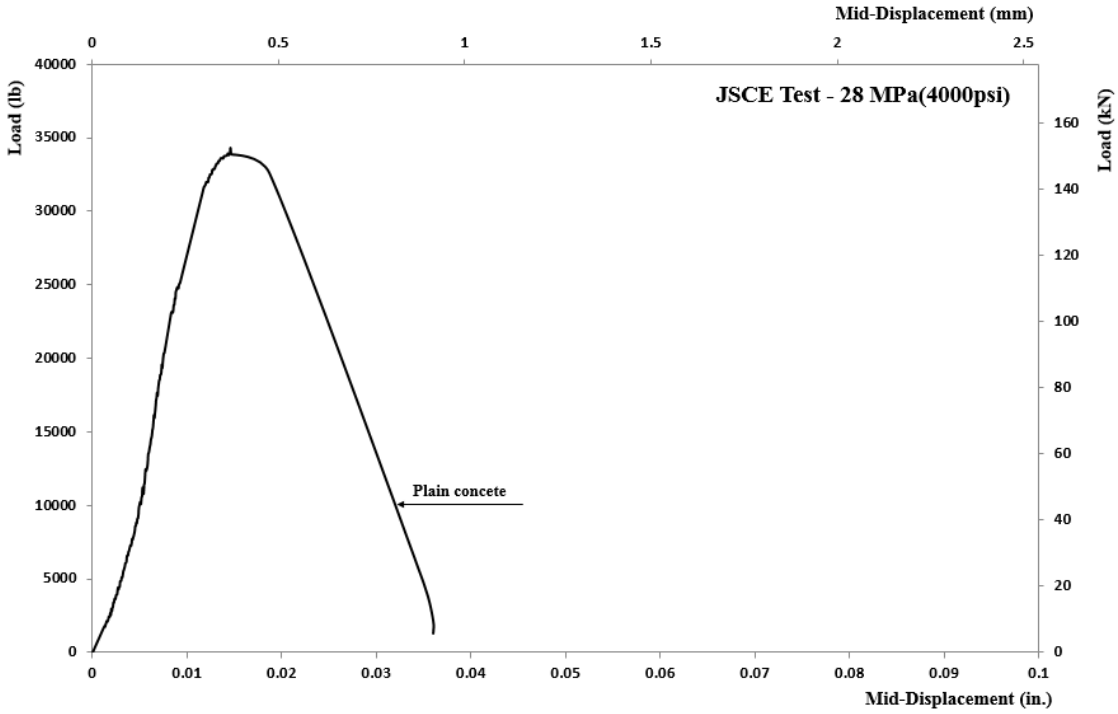

b)

Figure A-1 (a) Crack Propagation, (b) Load-Deformation Plot (V.F. = 0%)

a)

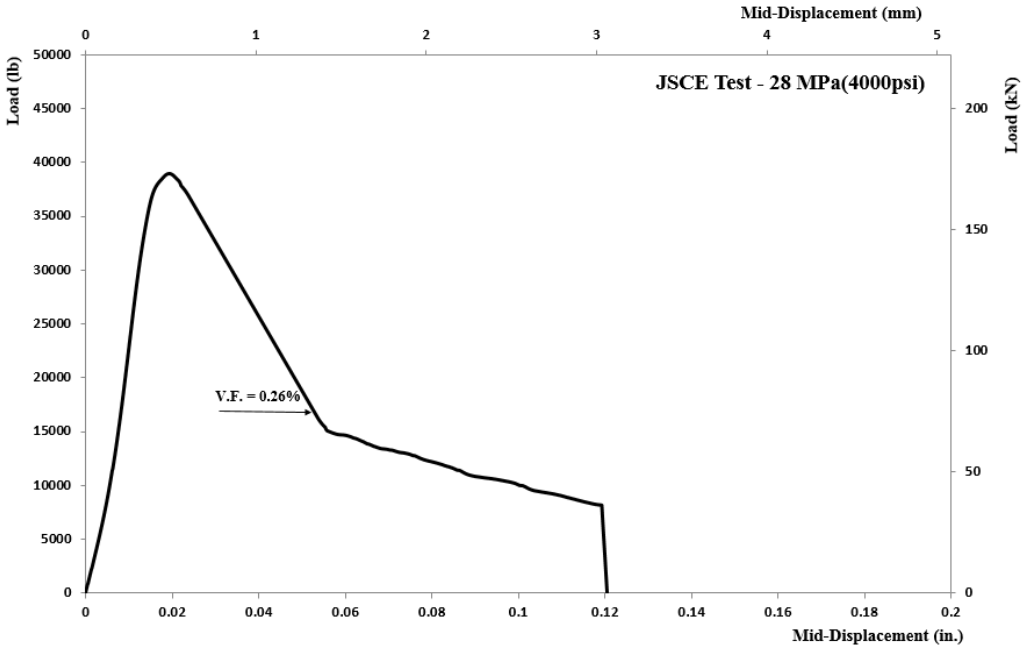

b)

Figure A-2 (a) Crack Propagation, (b) Load-Deformation Plot (V.F. = 0.26%)

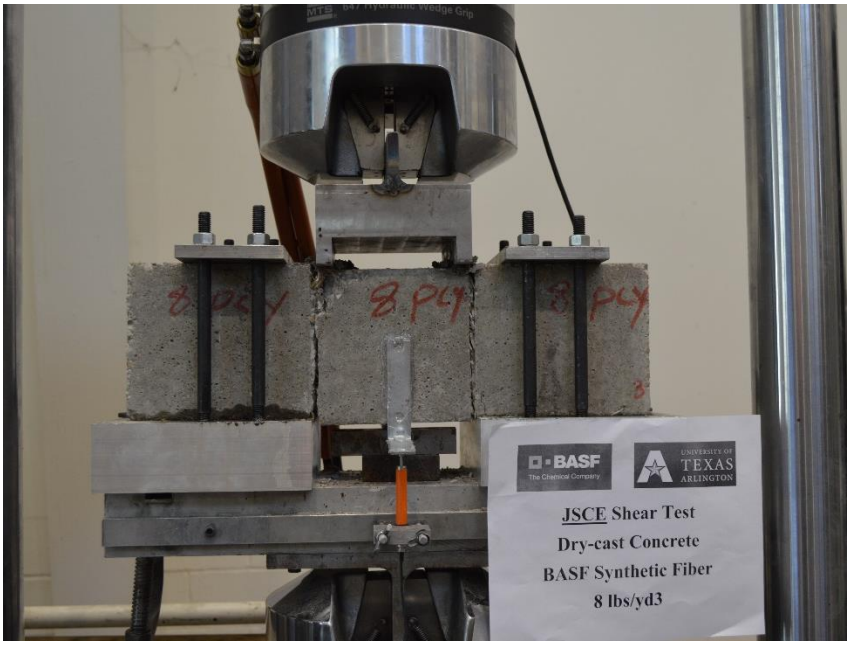

a)

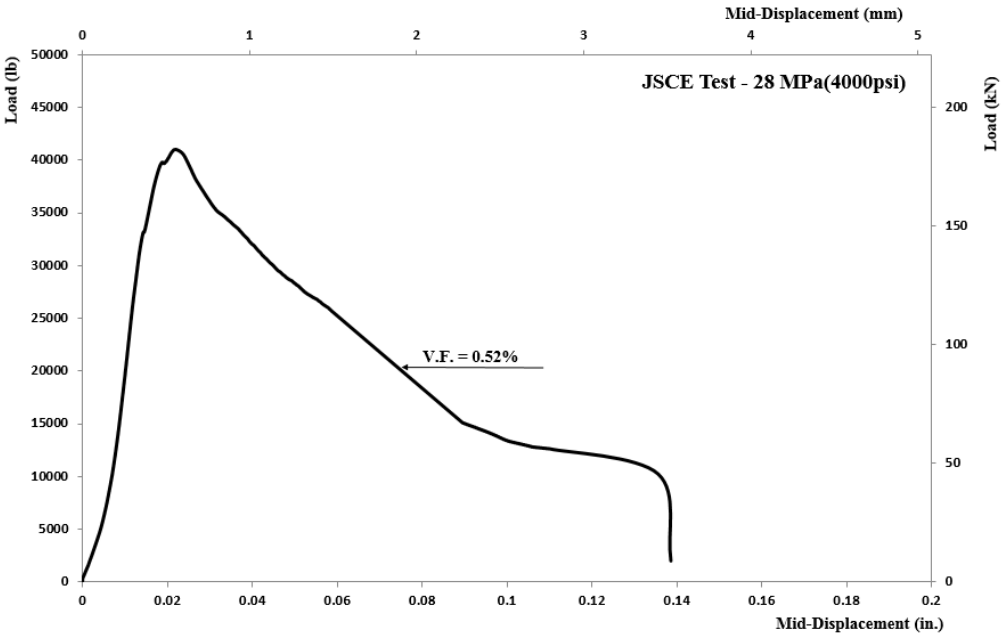

b)

Figure A-3 (a) Crack Propagation, (b) Load-Deformation Plot (V.F. = 0.52%)

a)

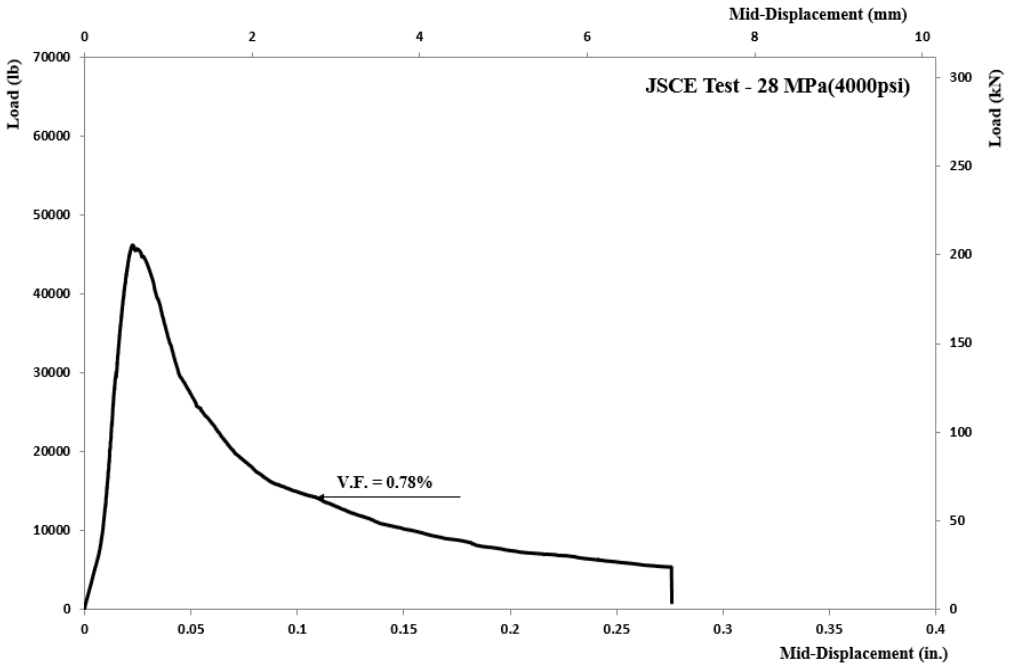

b)

Figure A-4 (a) Crack Propagation, (b) Load-Deformation Plot (V.F. = 0.78%)

a)

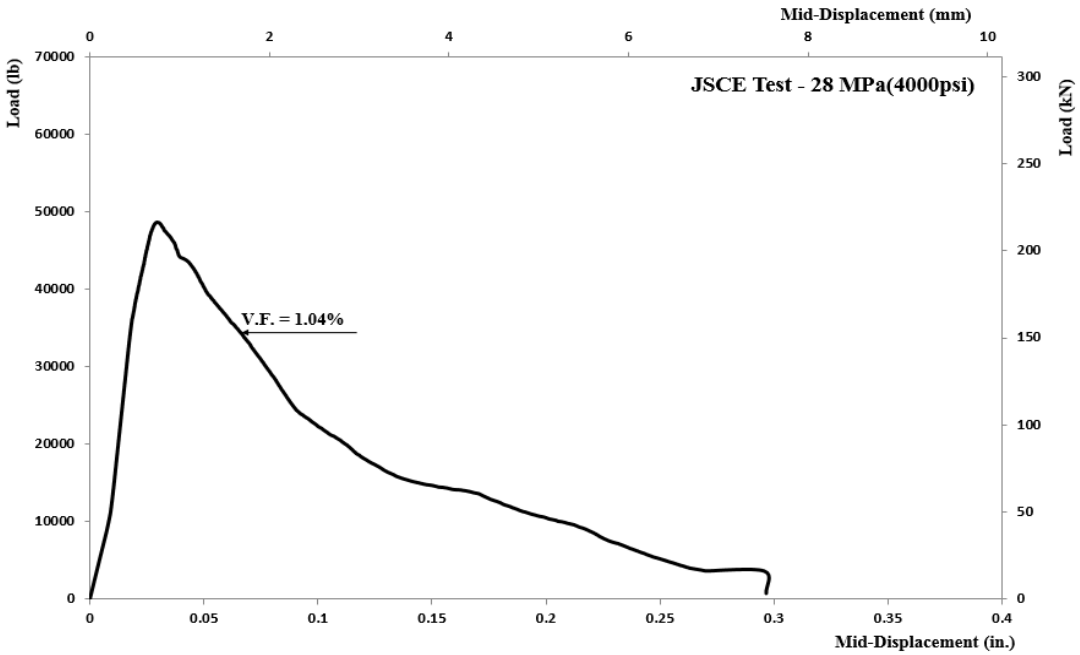

b)

Figure A-5 (a) Crack Propagation, (b) Load-Deformation Plot (V.F. = 0.78%)

a)

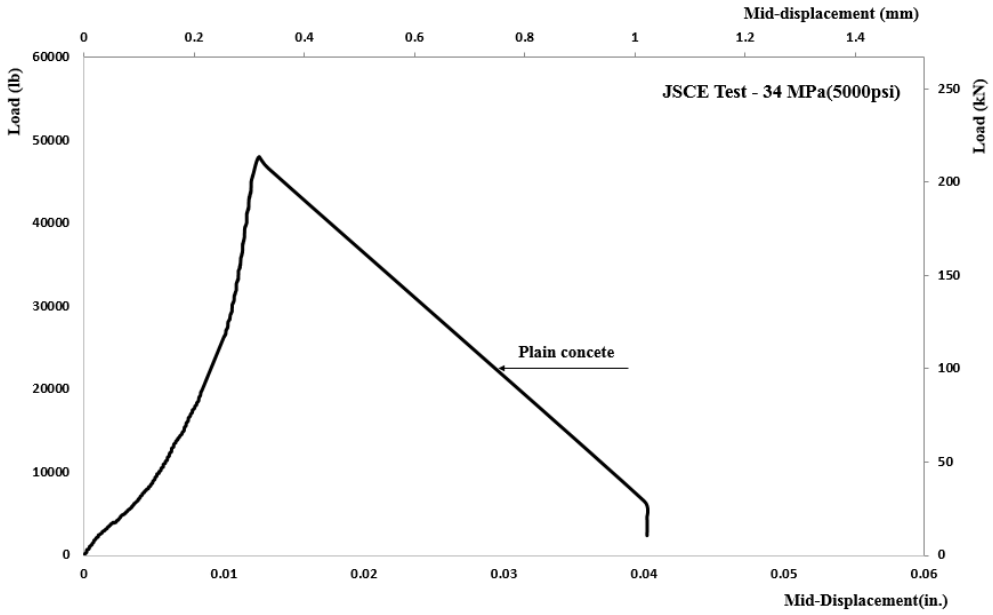

b)

Figure A-6 (a) Crack Propagation, (b) Load-Deformation Plot (V.F. = 0%)

a)

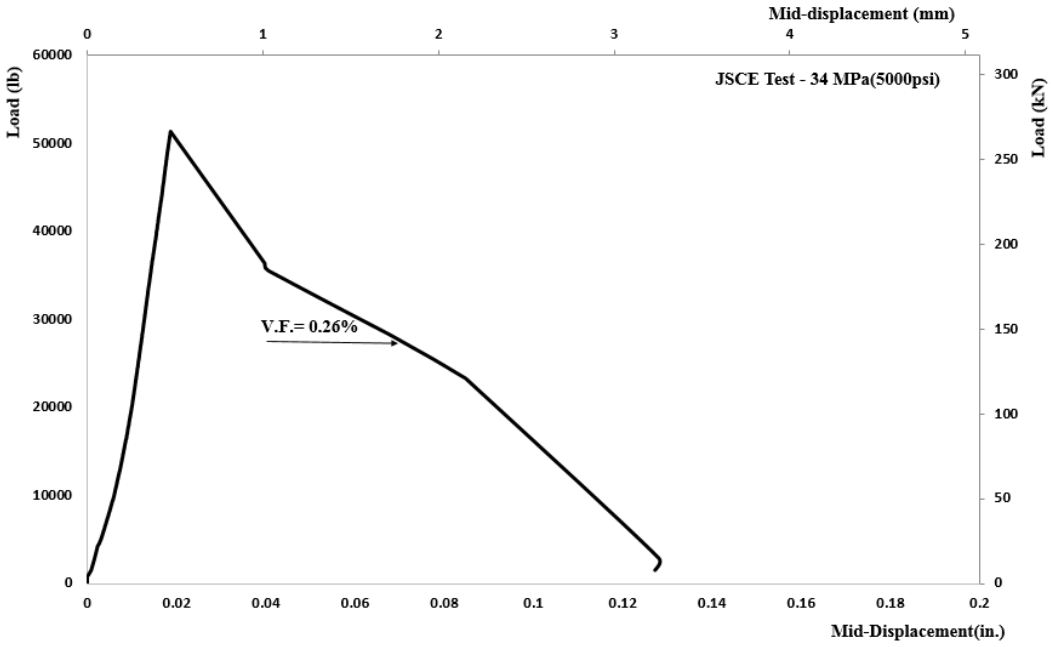

b)

Figure A-7 (a) Crack Propagation, (b) Load-Deformation Plot (V.F. = 0.26%)

a)

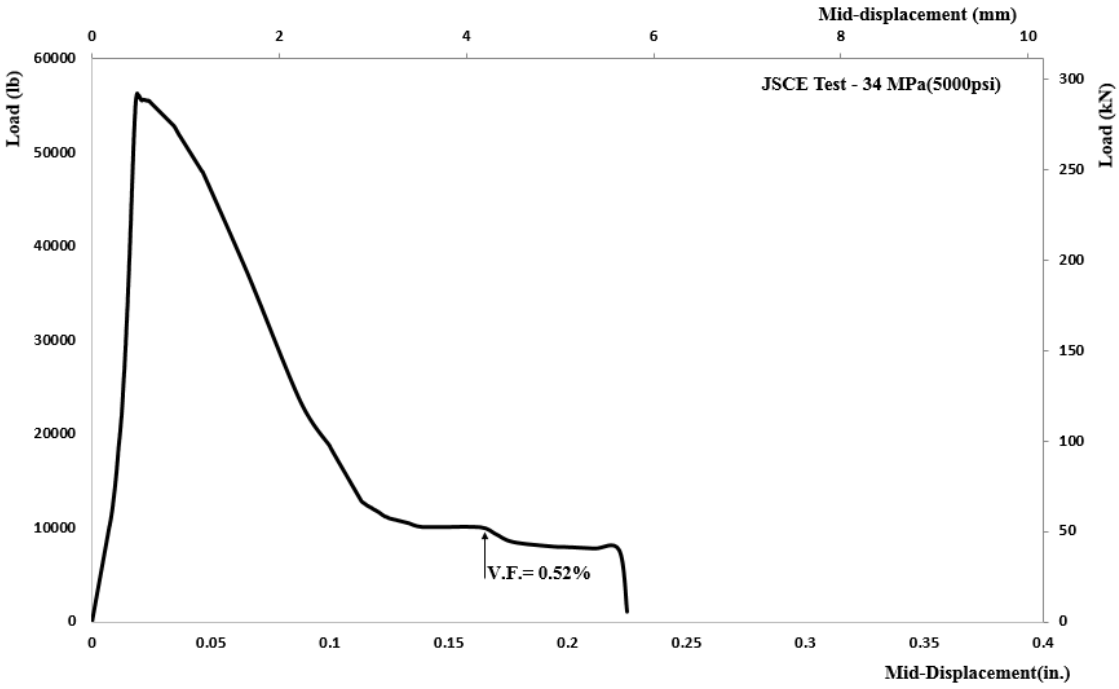

b)

Figure A-8 (a) Crack Propagation, (b) Load-Deformation Plot (V.F. = 0.52%)

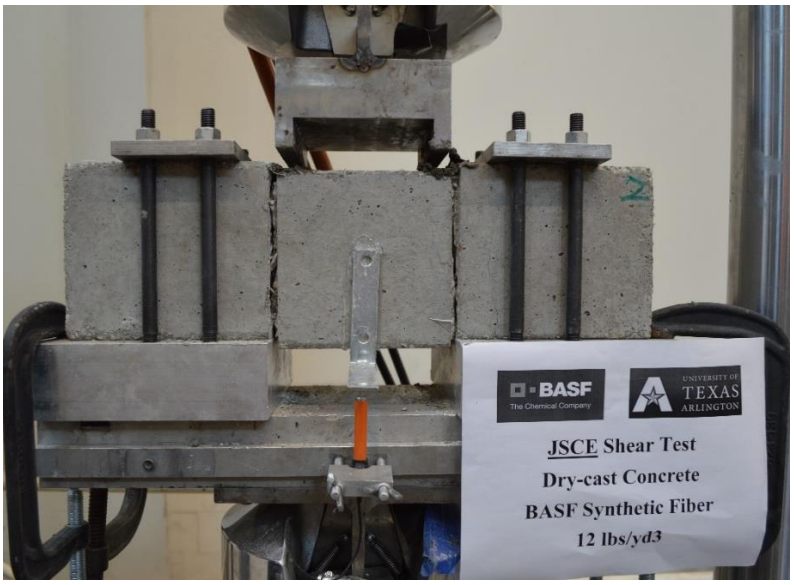

a)

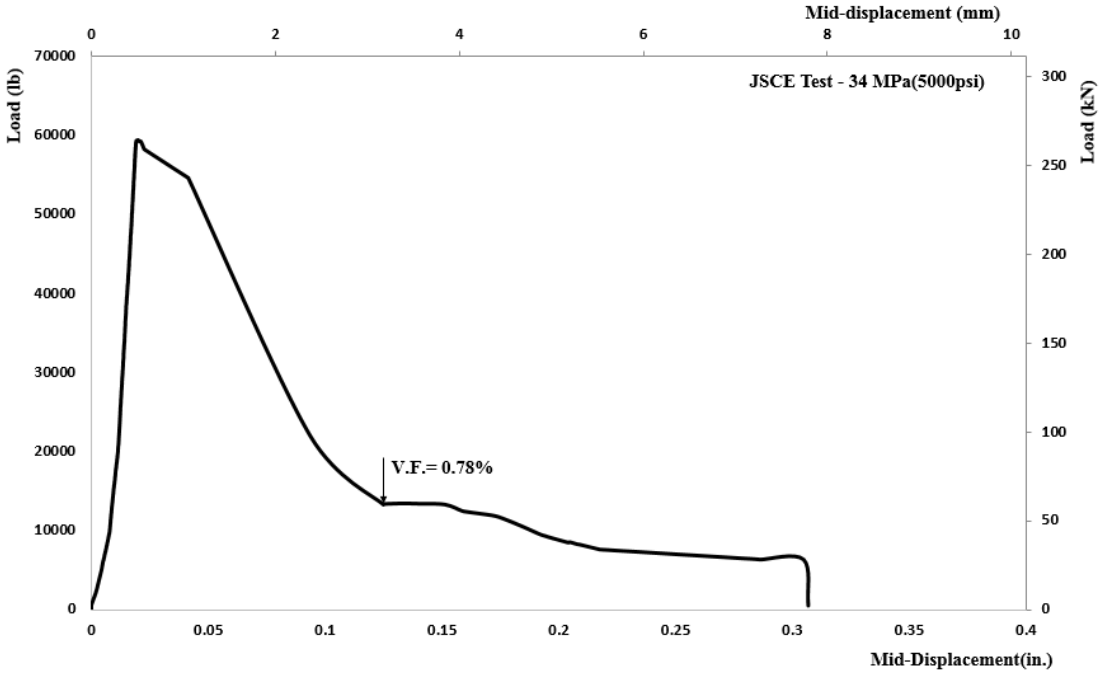

b)

Figure A-9 (a) Crack Propagation, (b) Load-Deformation Plot (V.F. = 0.78%)

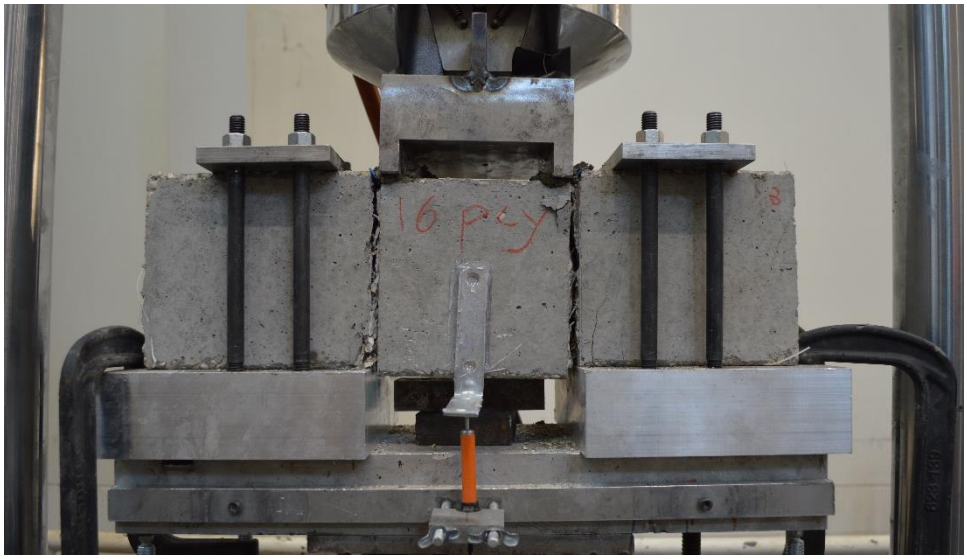

a)

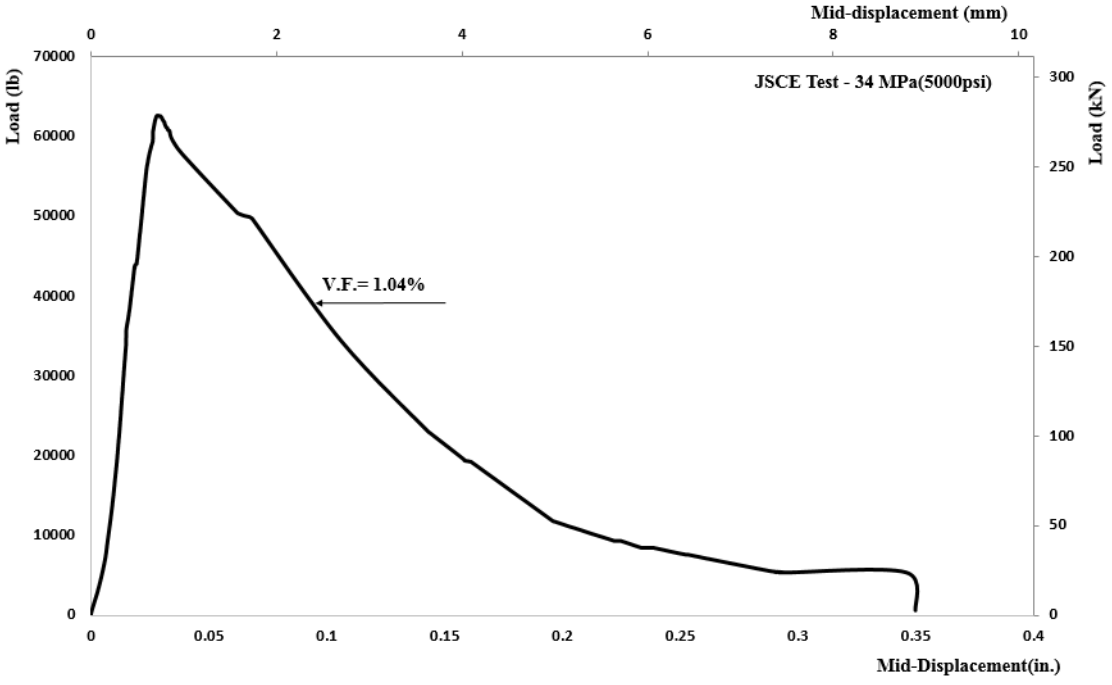

b)

Figure A-10 (a) Crack Propagation, (b) Load-Deformation Plot (V.F. = 0.78%)

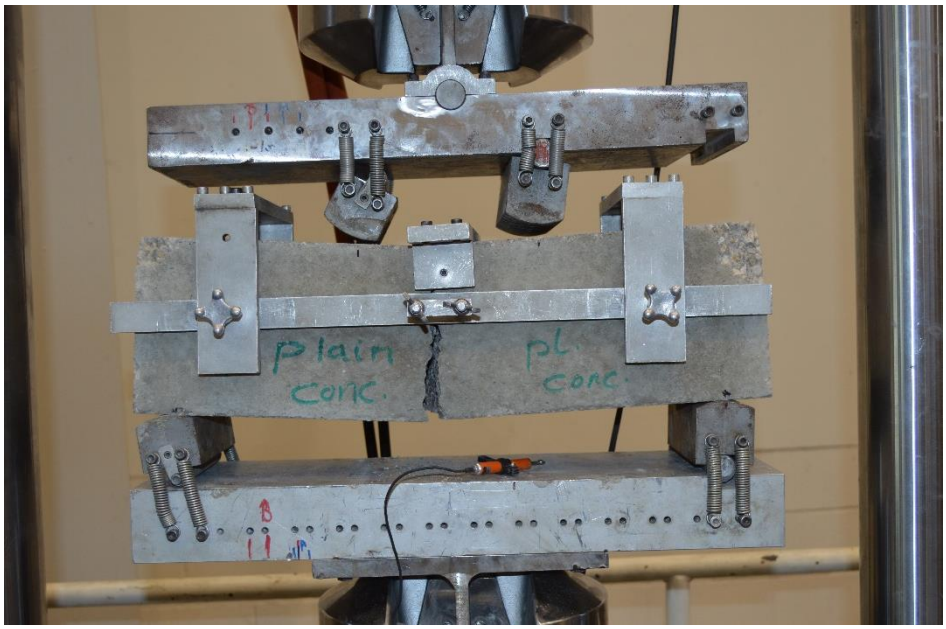

a)

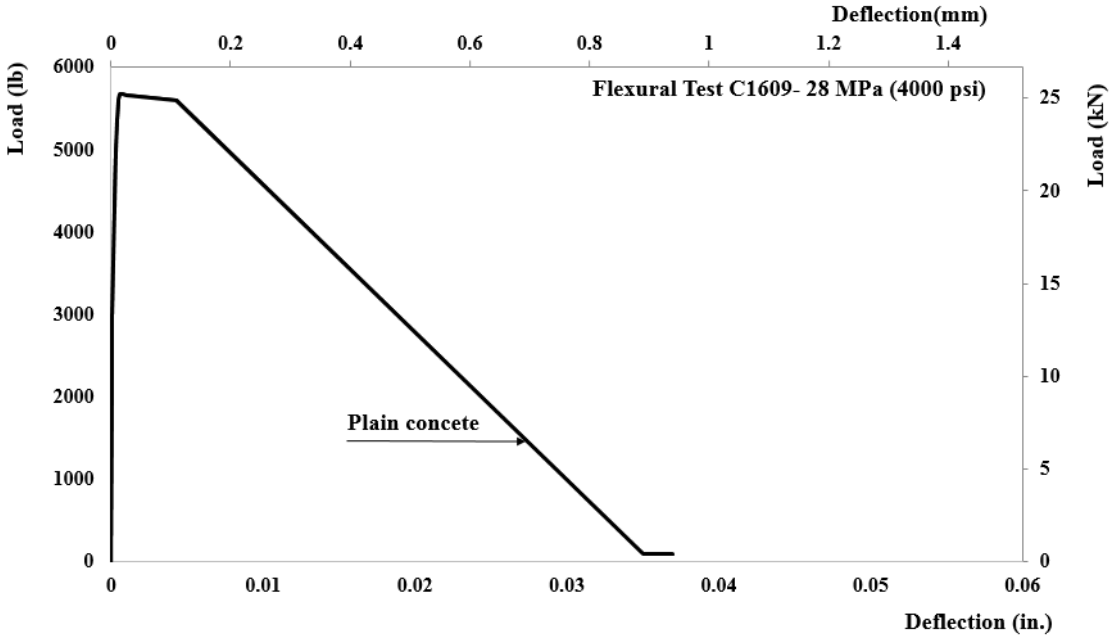

b)

Figure A-11 (a) Crack Propagation, (b) Load-Deformation Plot (V.F. = 0%)

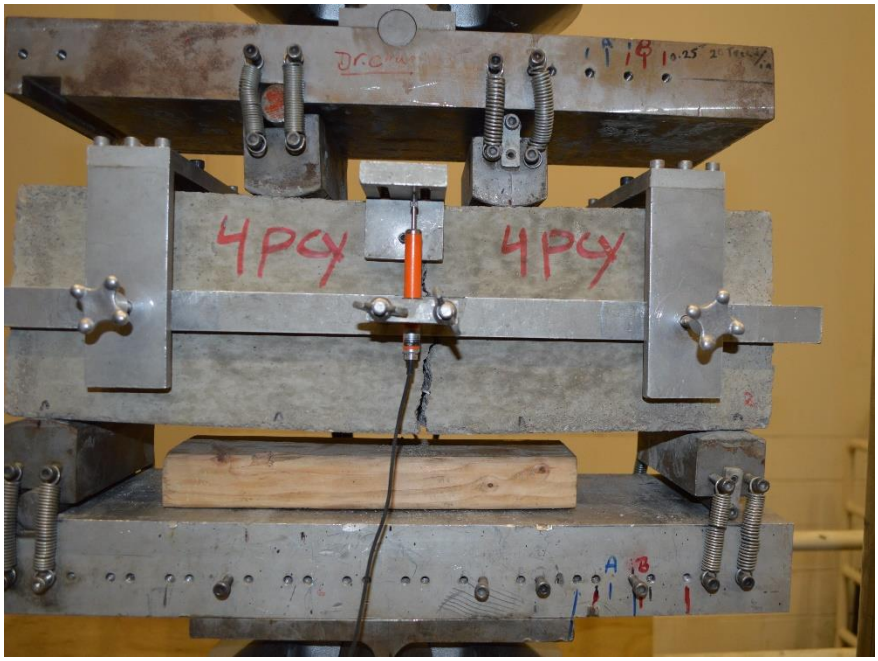

a)

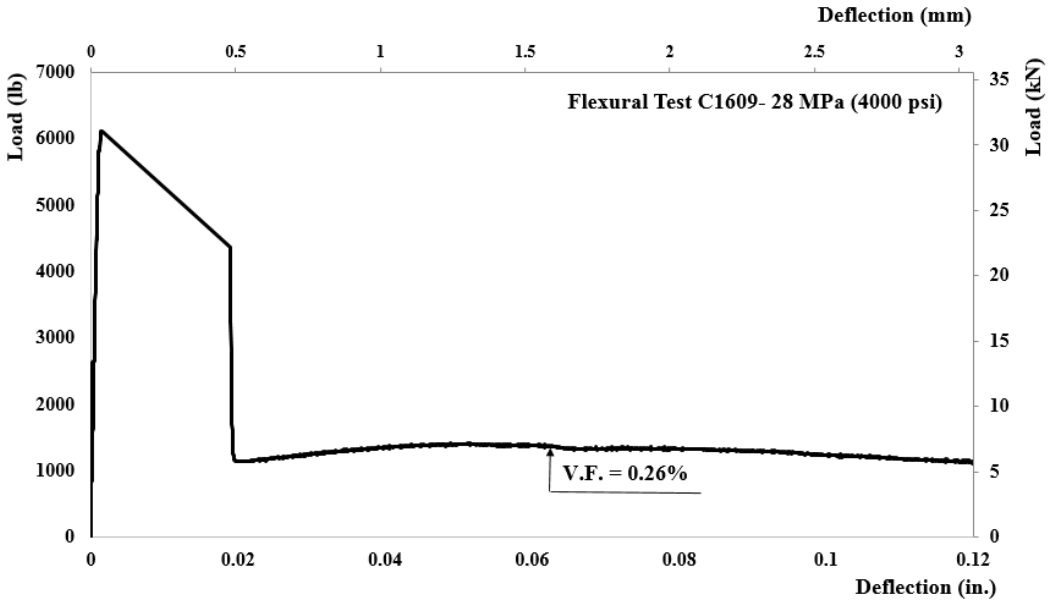

b)

Figure A-12 (a) Crack Propagation, (b) Load-Deformation Plot (V.F. = 0.26%)

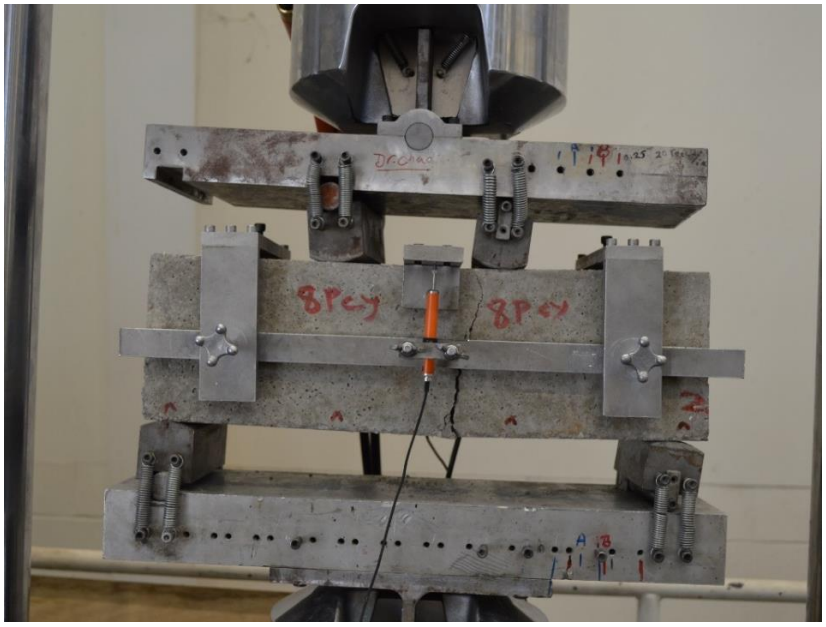

a)

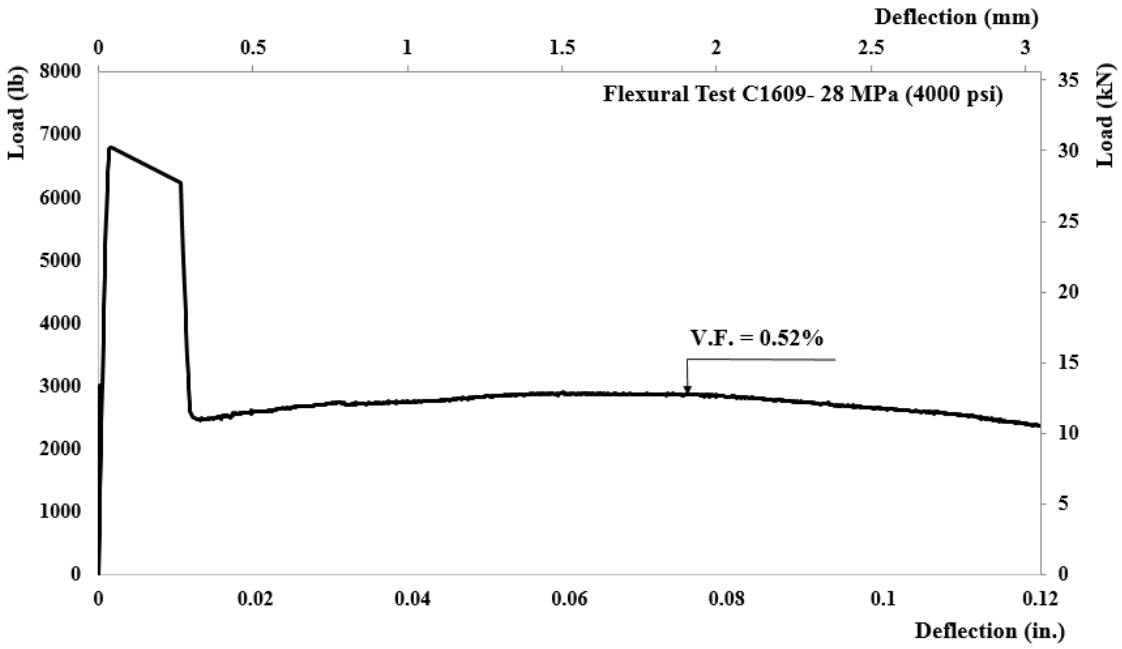

b)

Figure A-13 (a) Crack Propagation, (b) Load-Deformation Plot (V.F. = 0.52%)

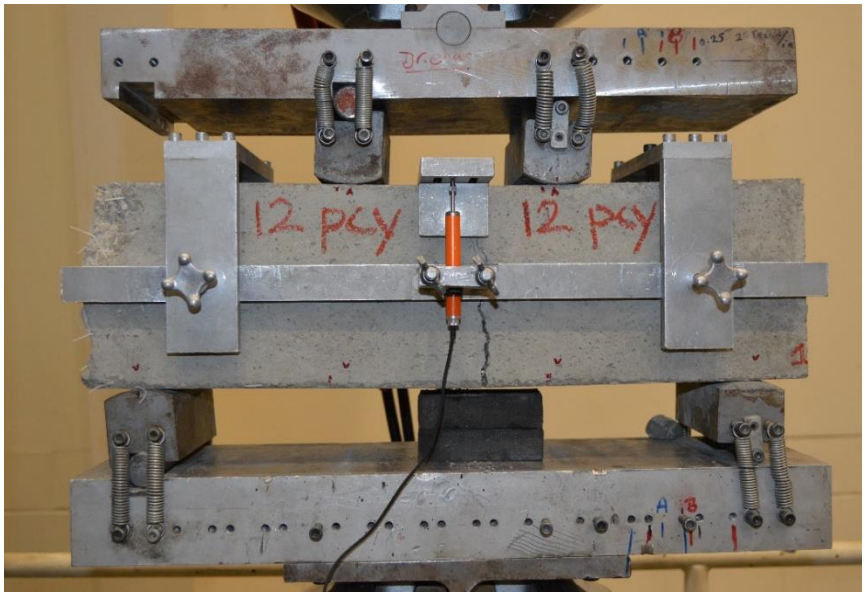

a)

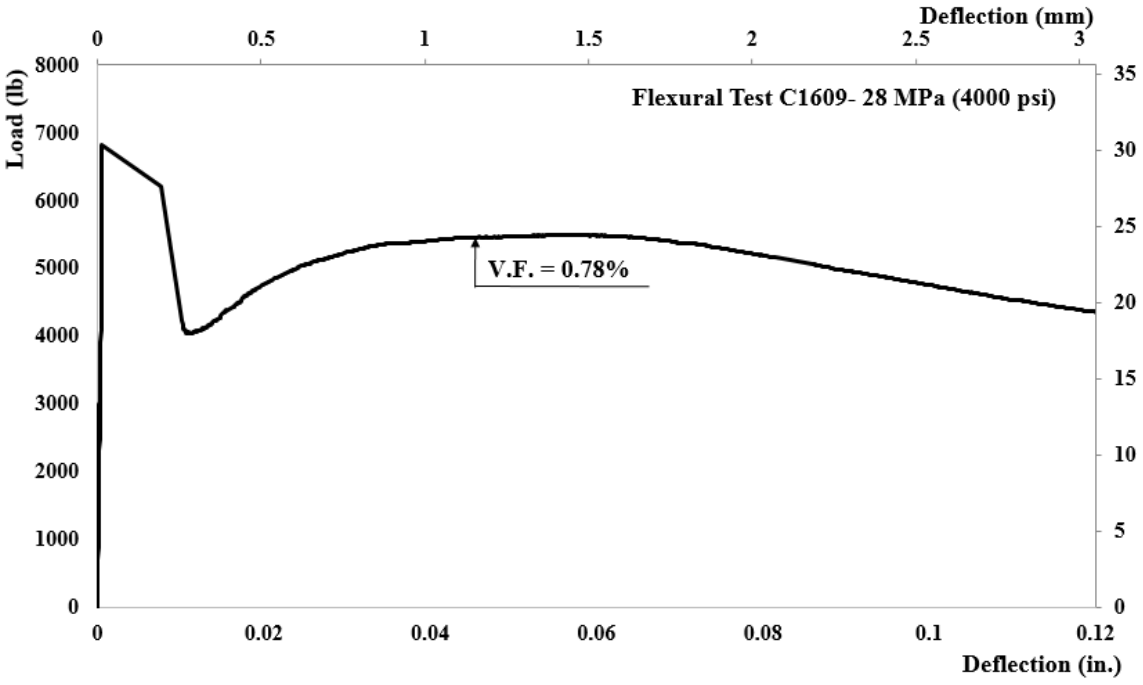

b)

Figure A-14 (a) Crack Propagation, (b) Load-Deformation Plot (V.F. = 0.78%)

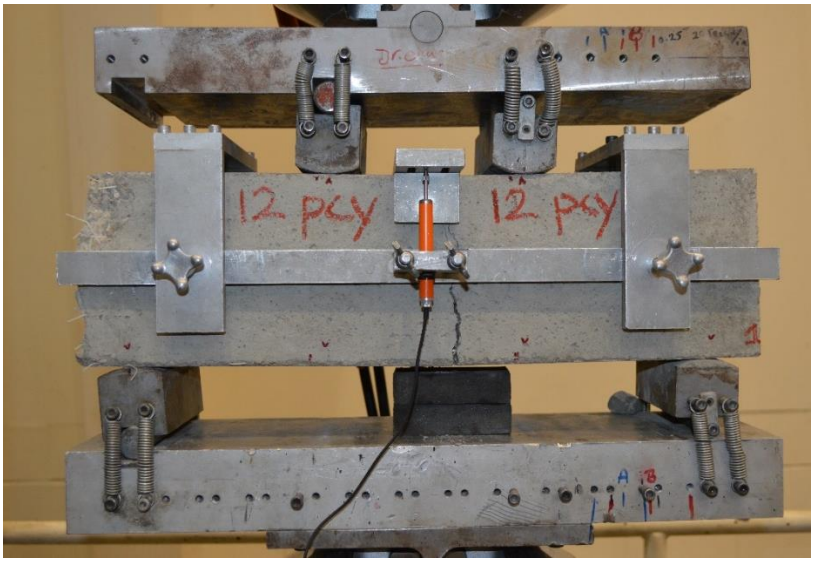

a)

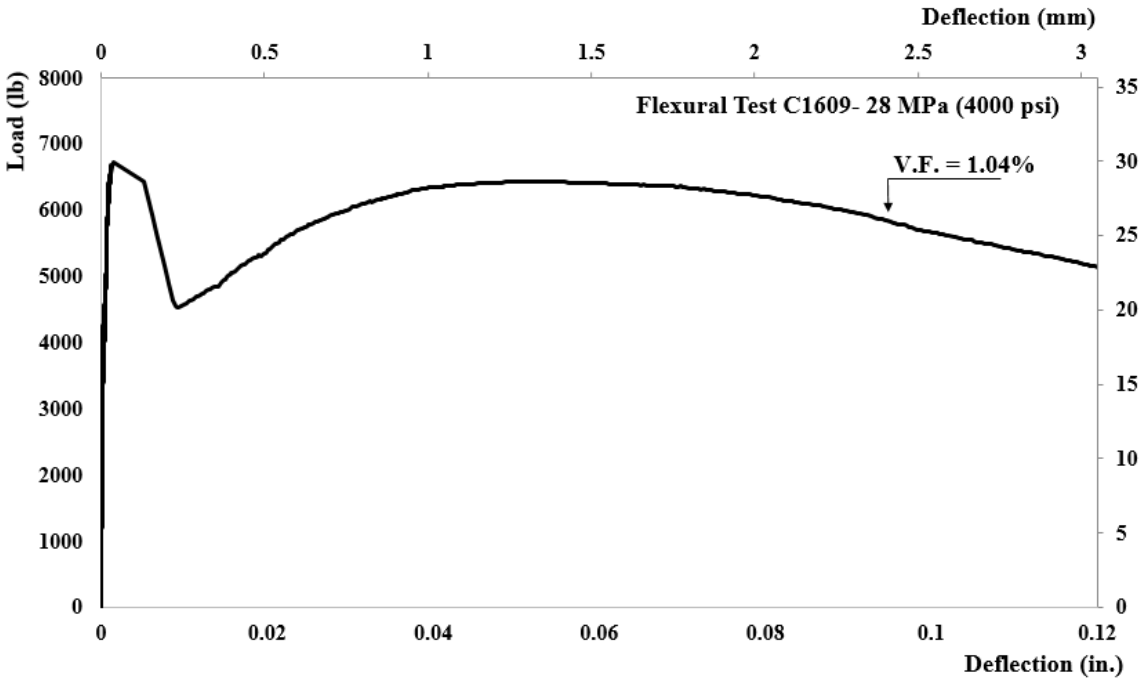

b)

Figure A-15 (a) Crack Propagation, (b) Load-Deformation Plot (V.F. = 1.04%)

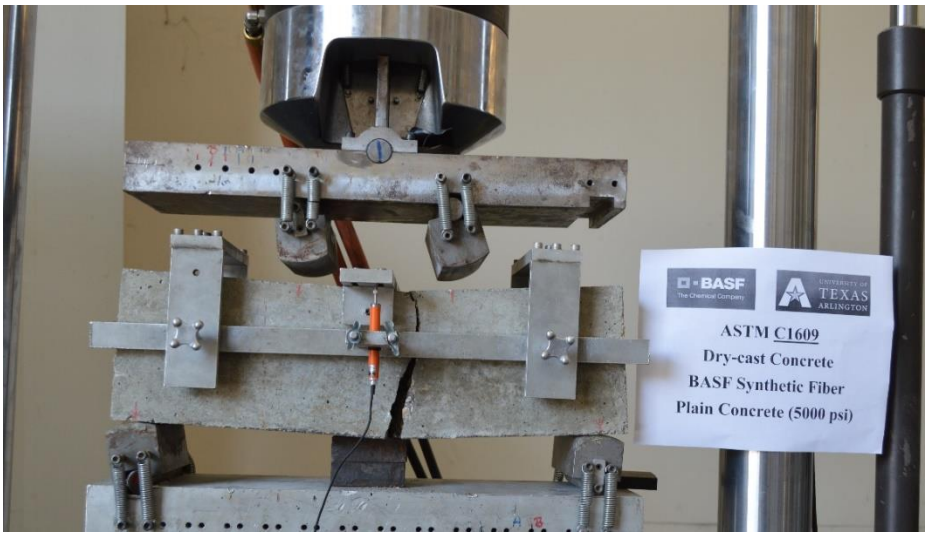

a)

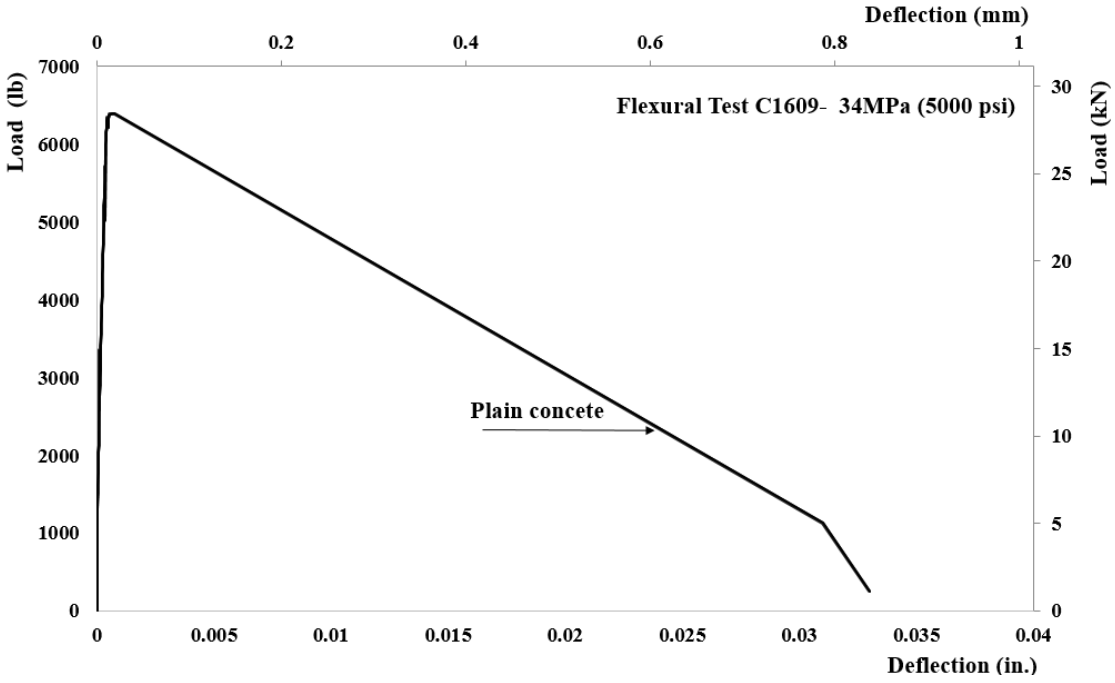

b)

Figure A-16 (a) Crack Propagation, (b) Load-Deformation Plot (V.F. = 0%)

a)

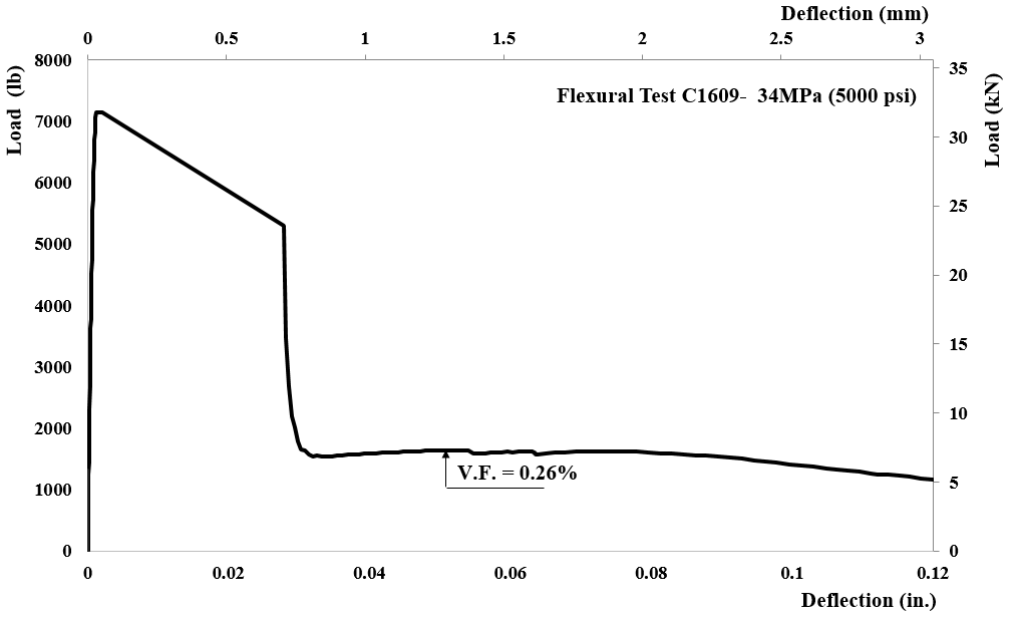

b)

Figure A-17 (a) Crack Propagation, (b) Load-Deformation Plot (V.F. = 0.26%)

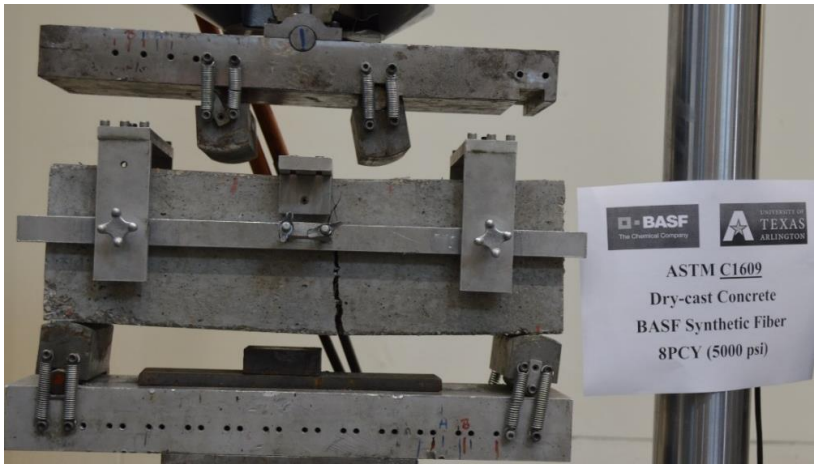

a)

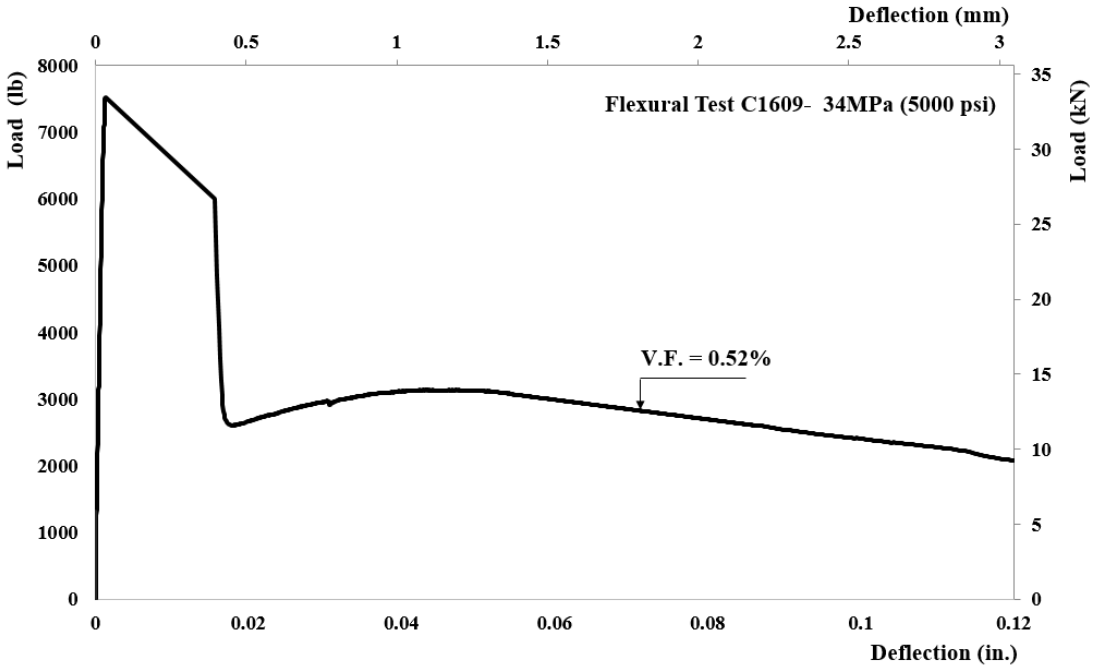

b)

Figure A-18 (a) Crack Propagation, (b) Load-Deformation Plot (V.F. = 0.52%)

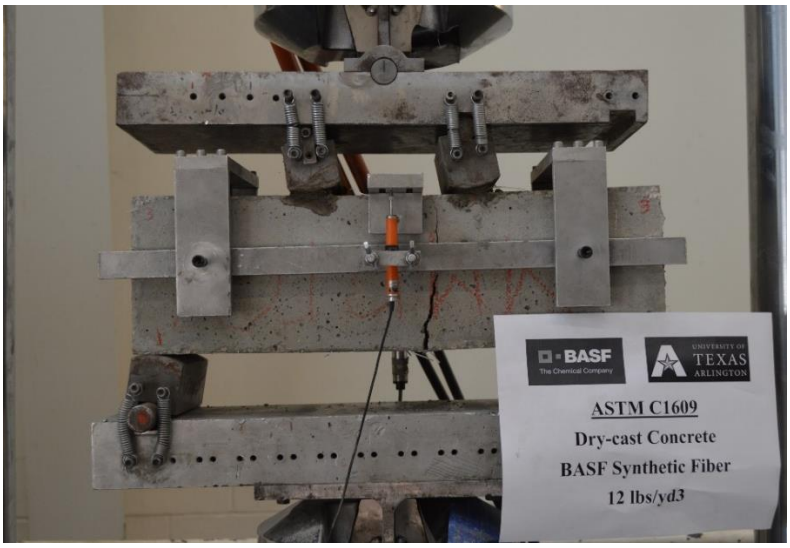

a)

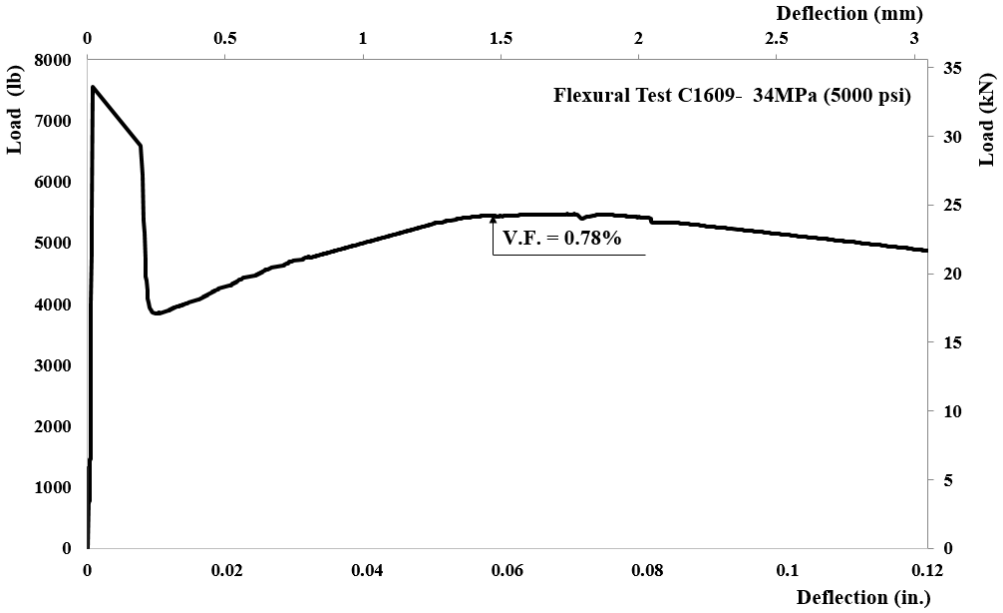

b)

Figure A-19 (a) Crack Propagation, (b) Load-Deformation Plot (V.F. = 0.78%)

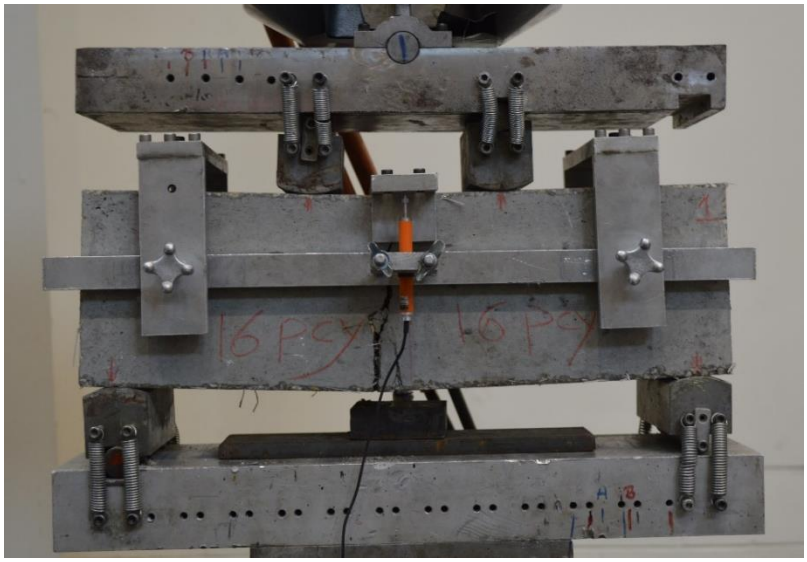

a)

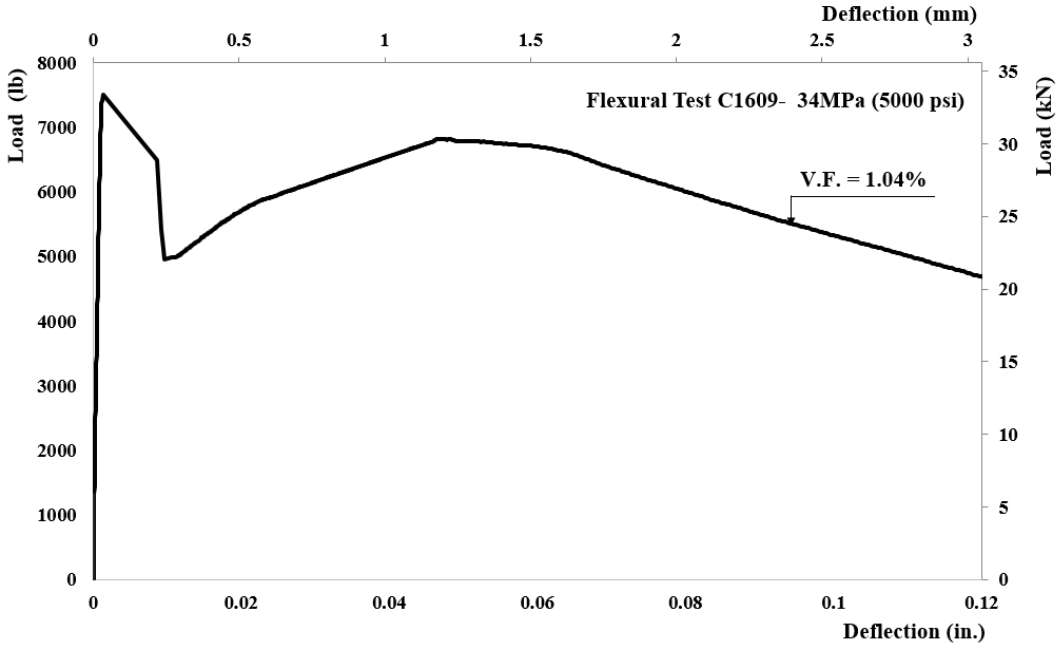

b)

Figure A-20 (a) Crack Propagation, (b) Load-Deformation Plot (V.F. = 1.04%)

APPENDIX B: EXPERIMENTAL PHOTOGRAPHS

a)

b)

c)

d)

e) **f)**

Figure B-1 Experimental photographs, Box 12’x4’x12” Northern Concrete: (a) shear crack; (b) crack patterns on the right side of load plate; (c) crack patterns under the top slab; (d) measuring the deflection under the load plate; (e) Top slab crack pattern; (f) Deformed shape of box culvert

a)

b)

c)

d)

e) **f)**

Figure B-2 Experimental photographs, Box 8'x4'x8" Northern Concrete: (a) shear crack; (b) crack patterns on the right side of load plate; (c) crack patterns under the top slab; (d) Measuring the deflection under the load plate; (e) Top slab crack pattern; (f) Deformed shape of box culvert

a)

b)

c)

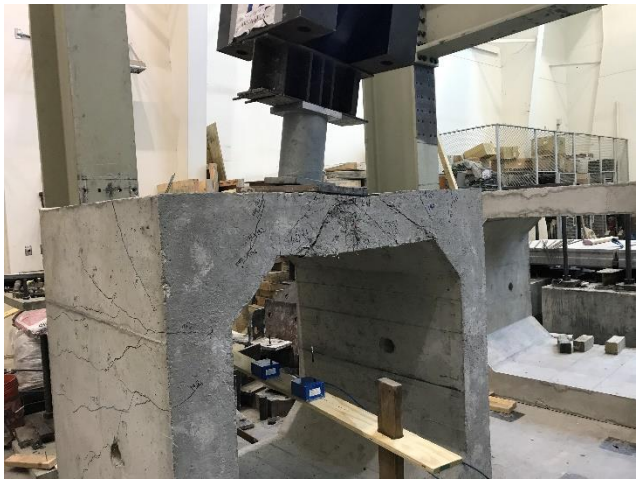

d)

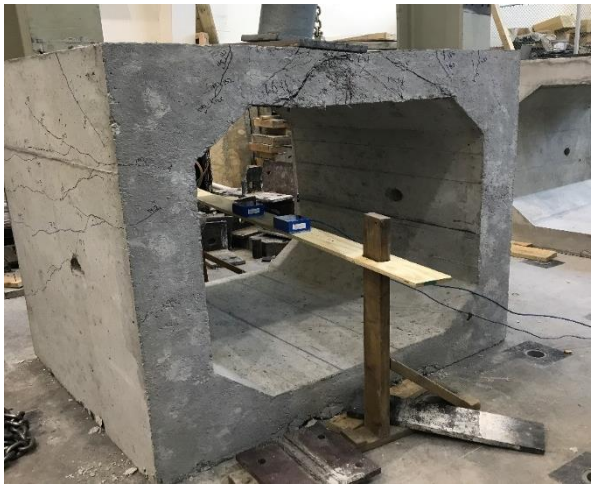

e) **f)**

Figure B-3 Experimental photographs, Box 4’x4’x8” Northern Concrete: (a) shear crack; (b) crack patterns on the right side of load plate; (c) crack patterns under the top slab; (d) Measuring the deflection under the load plate; (e) Top slab crack pattern; (f) Deformed shape of box culvert

a)

b)

c)

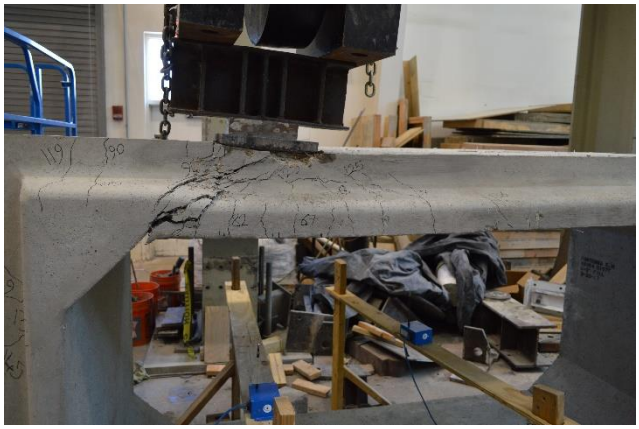

d)

e) **f)**

Figure B-4 Experimental photographs, Box 8’x4’x8” Forterra: (a) shear crack; (b) crack patterns on the right side of load plate; (c) crack patterns under the top slab; (d) Measuring the deflection under the load plate; (e) Top slab crack pattern; (f) Deformed shape of box culvert

a)

b)

c)

d)

e) **f)**

Figure B-5 Experimental photographs, Box 4'x4'x5" Forterra: (a) shear crack; (b) crack patterns on the right side of load plate; (c) crack patterns under the top slab; (d) Measuring the deflection under the load plate; (e) Top slab crack pattern; (f) Deformed shape of box culvert

APPENDIX C: ASTM C1609 FINITE ELEMENT ANALYSIS

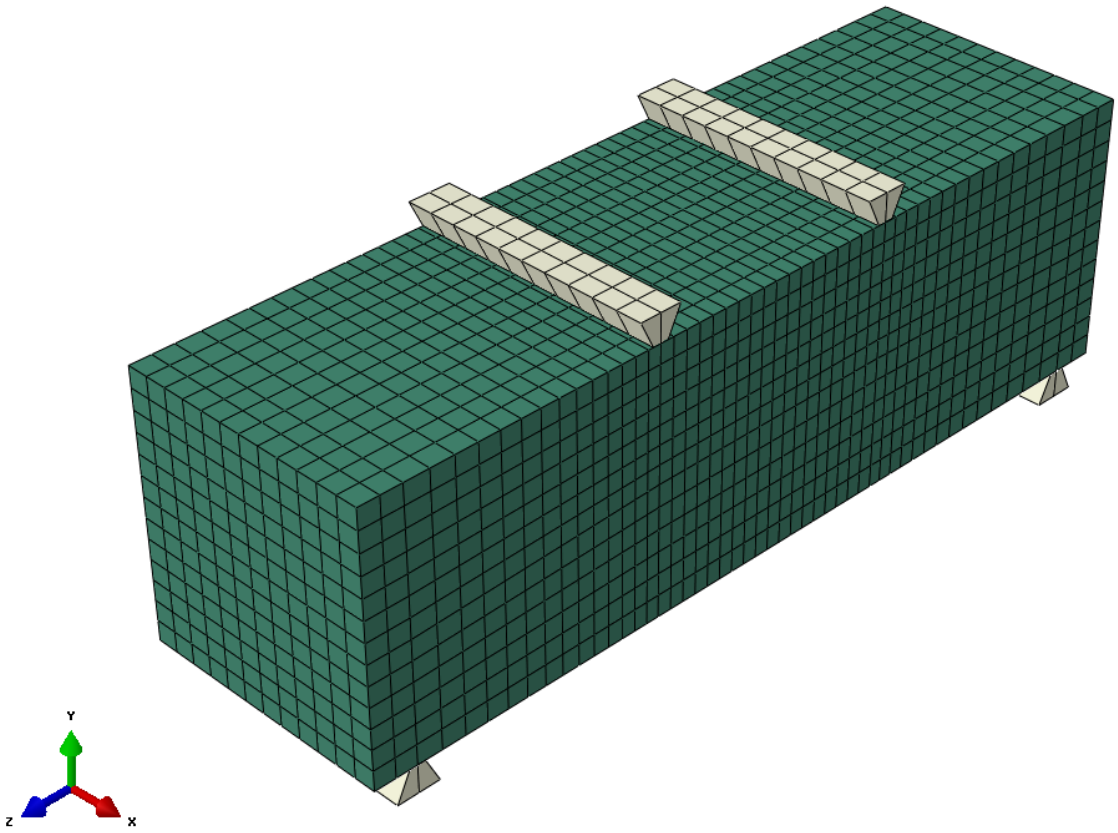

Figure C-1 Dividing the beam to 7800 linear hexahedral elements of type C3D8R

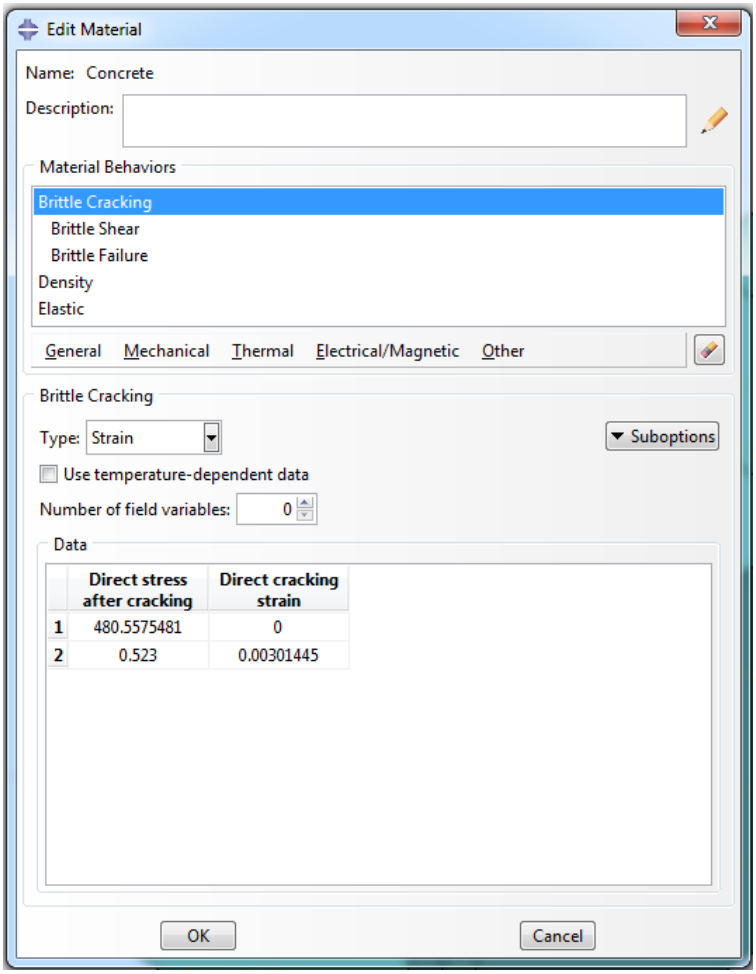

Figure C-2 Material properties used for 0.0% (Plain) fiber volume fraction

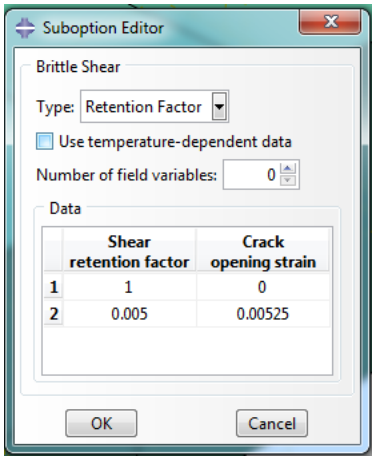

Figure C-3 Retention factor used for 0.0% (Plain) fiber volume fraction

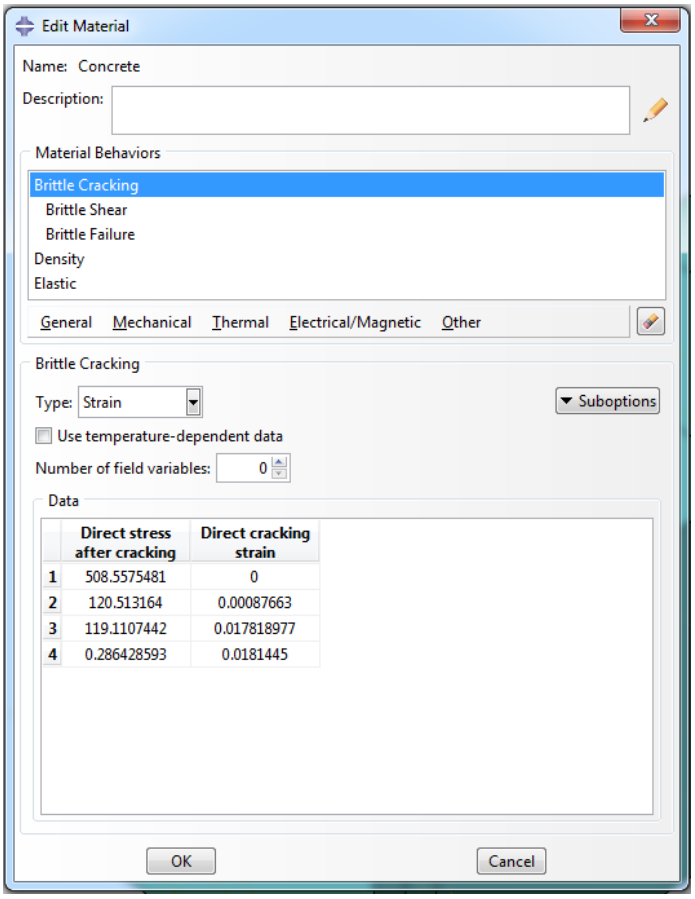

Figure C-4 Material properties used for 0.26% (4 PCY) fiber volume fraction

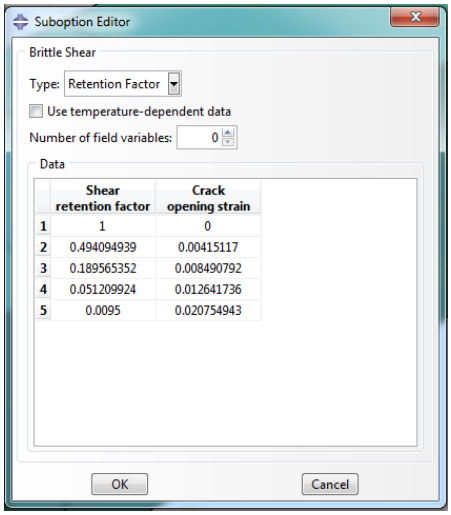

Figure C-5 Retention factor used for 0.26% (4 PCY) fiber volume fraction

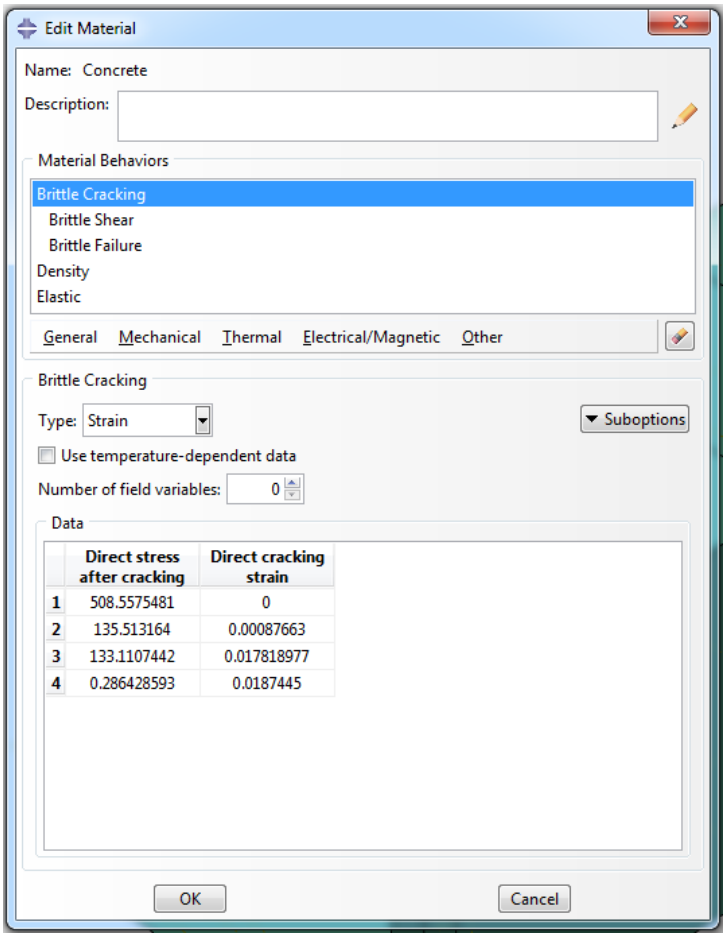

Figure C-6 Material properties used for 0.52% (8 PCY) fiber volume fraction

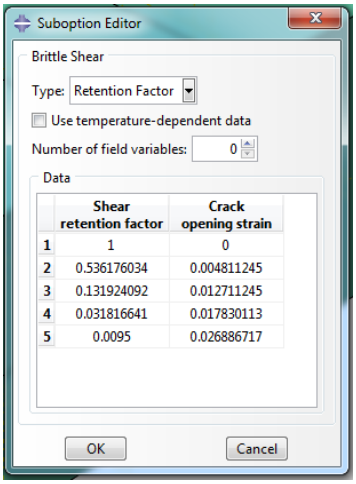

Figure C-7 Retention factor used for 0.52% (8 PCY) fiber volume fraction

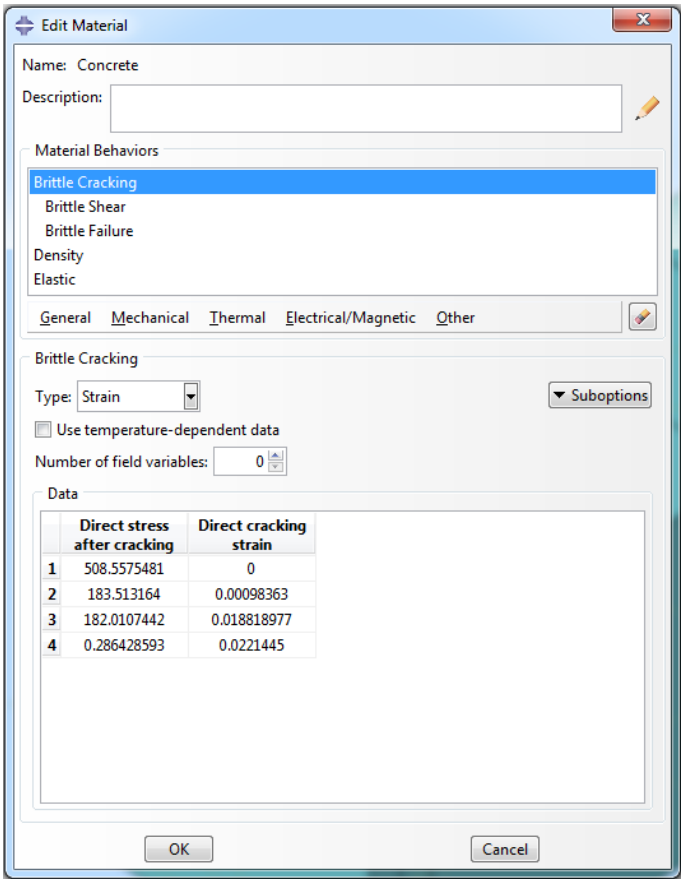

Figure C-8 Material properties used for 0.78% (12 PCY) fiber volume fraction

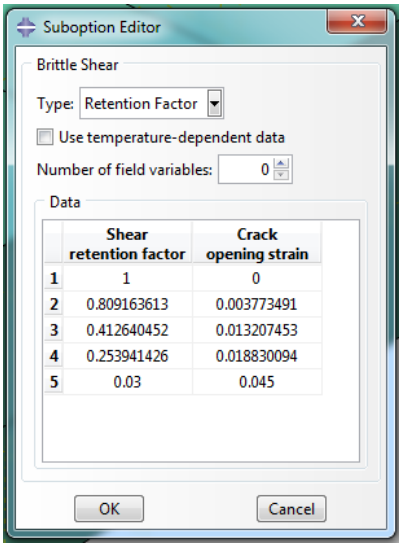

Figure C-9 Retention factor used for 0.78% (12 PCY) fiber volume fraction

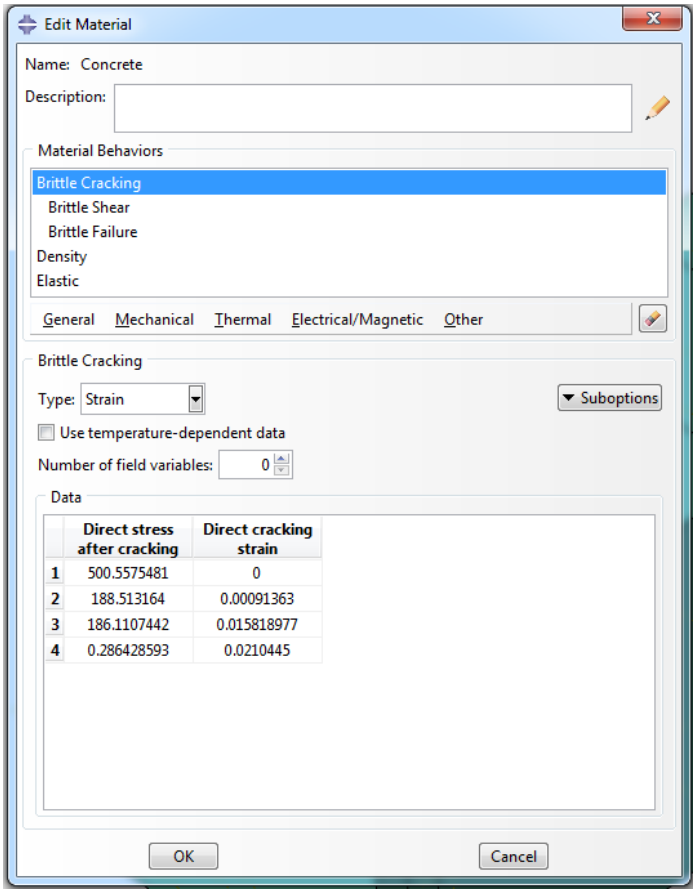

Figure C-10 Material properties used for 1.04% (16 PCY) fiber volume fraction

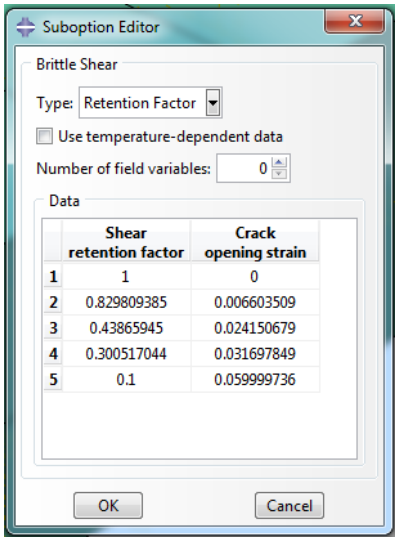

Figure C-11 Retention factor used for 1.04% (16 PCY) fiber volume fraction

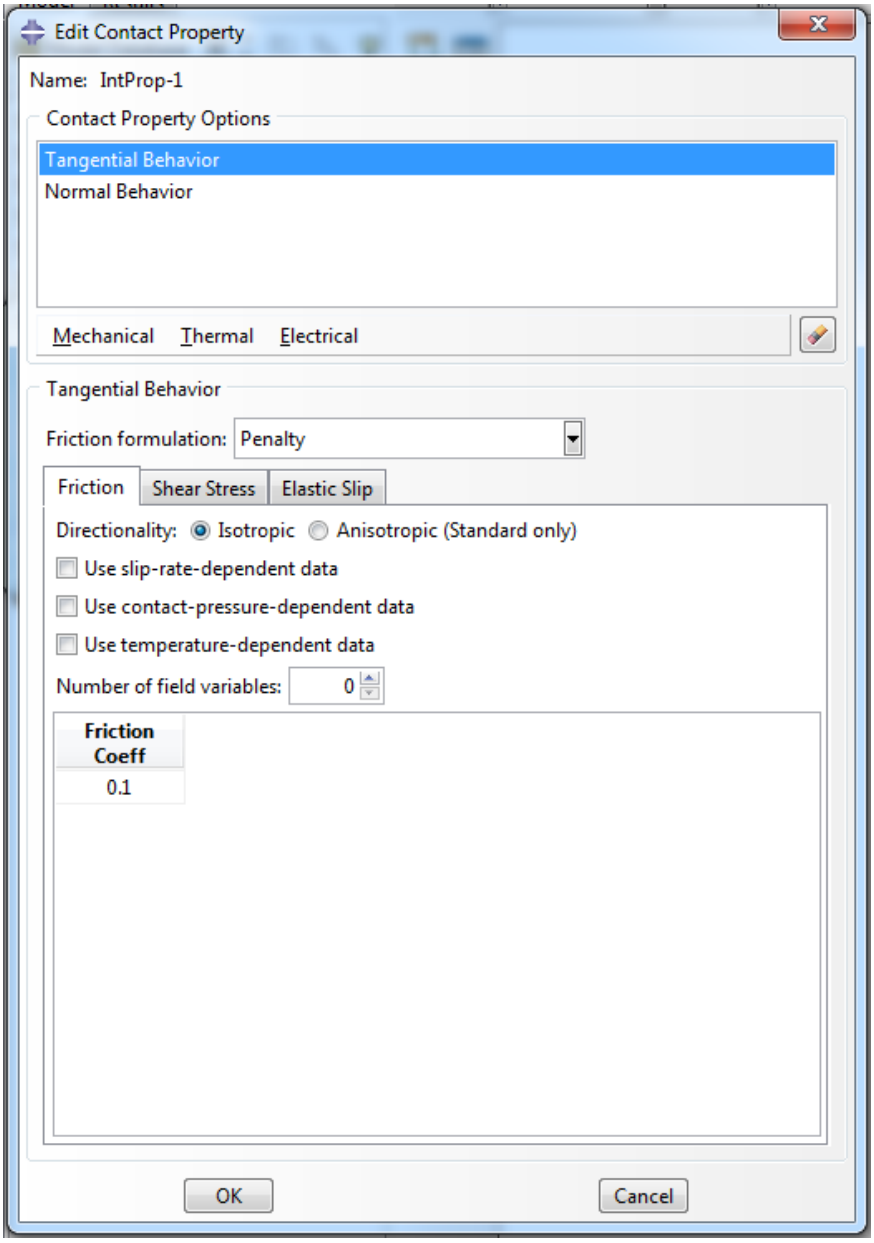

Figure C-12 Tangential contact property used between the beam and supports

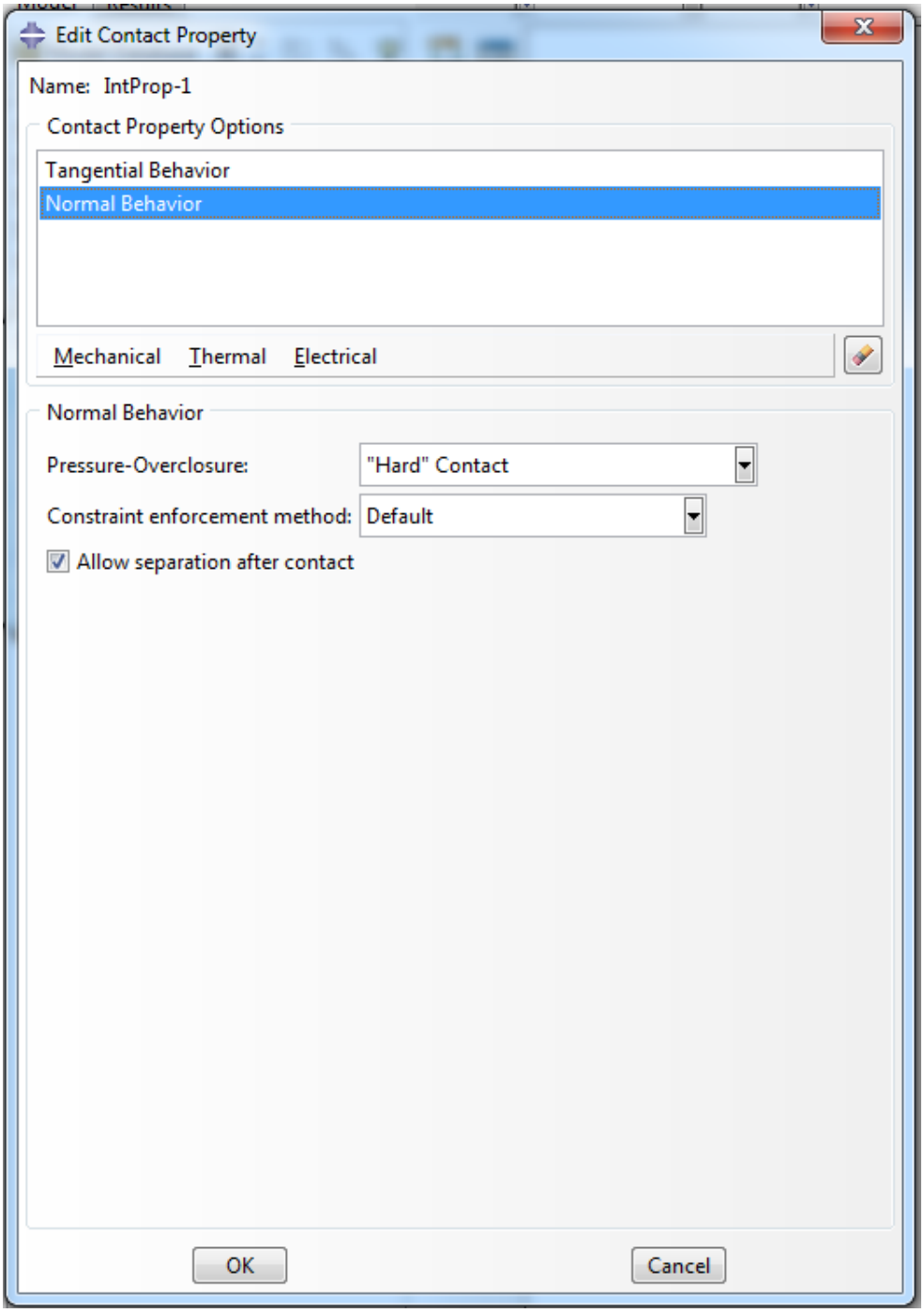

Figure C-13 Normal contact property used between the beam and supports

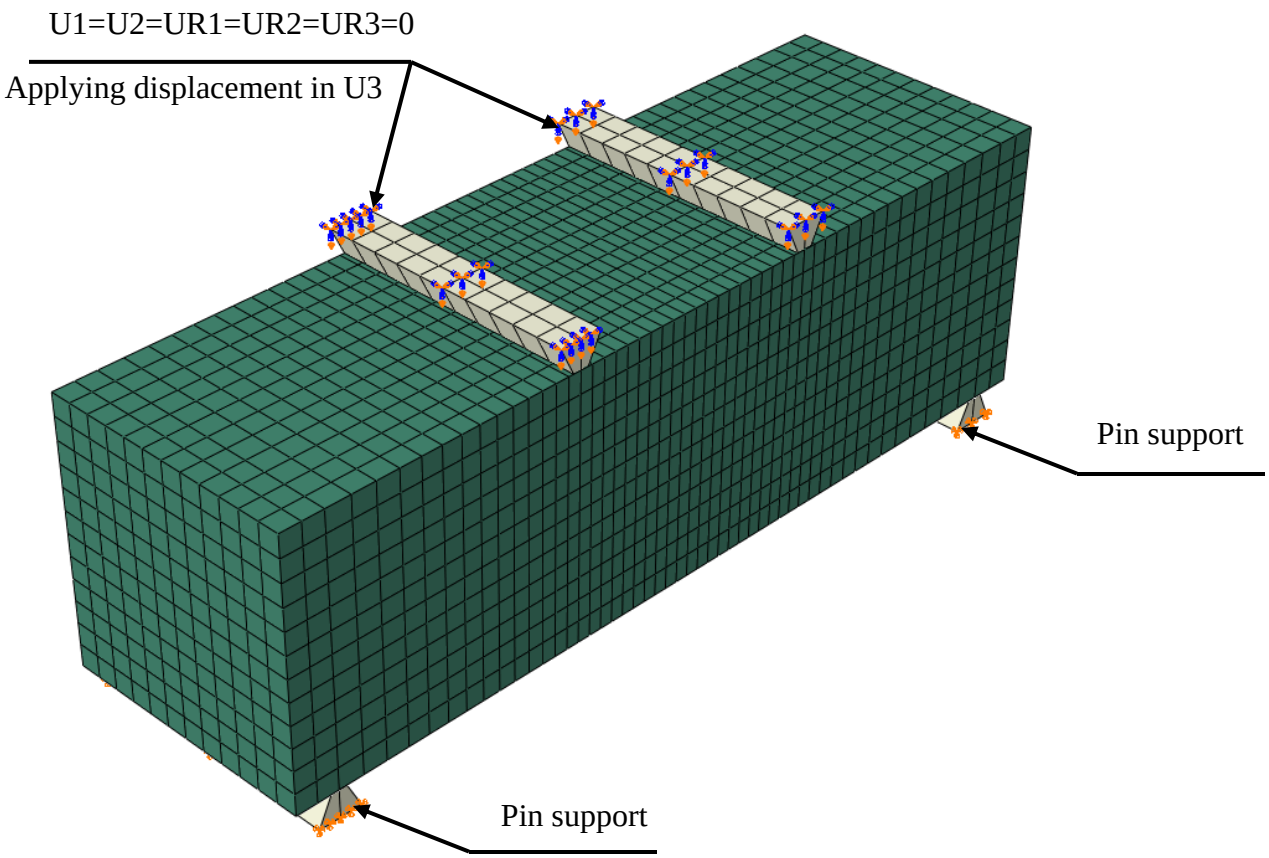

Figure C-14 Boundary condition and load application to ASTM C1609 beams

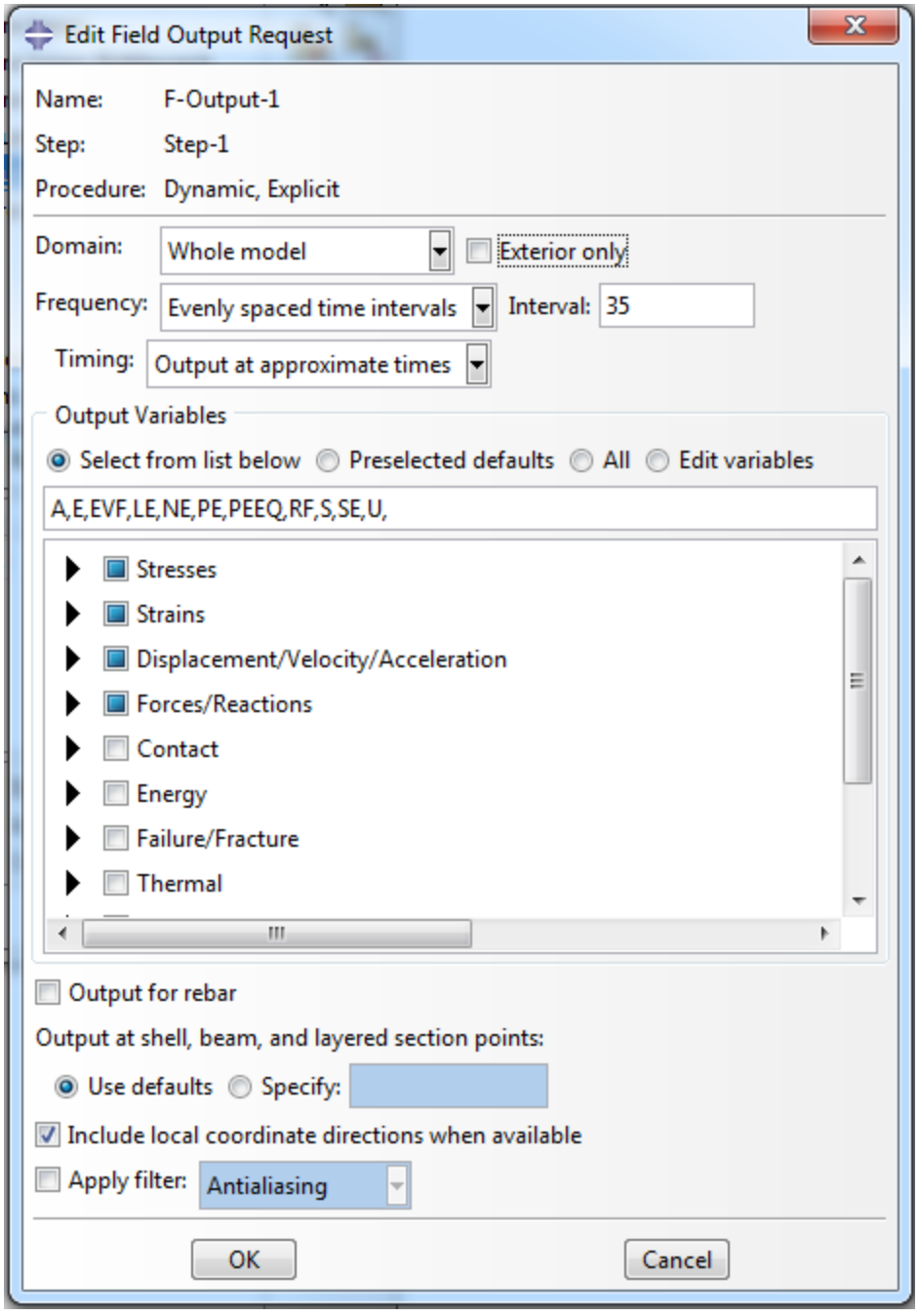

Figure C-15 Requesting output for the whole model

APPENDIX D: BOX CULVERT 8’X4’- FORTERRA FINITE ELEMENT ANALYSIS

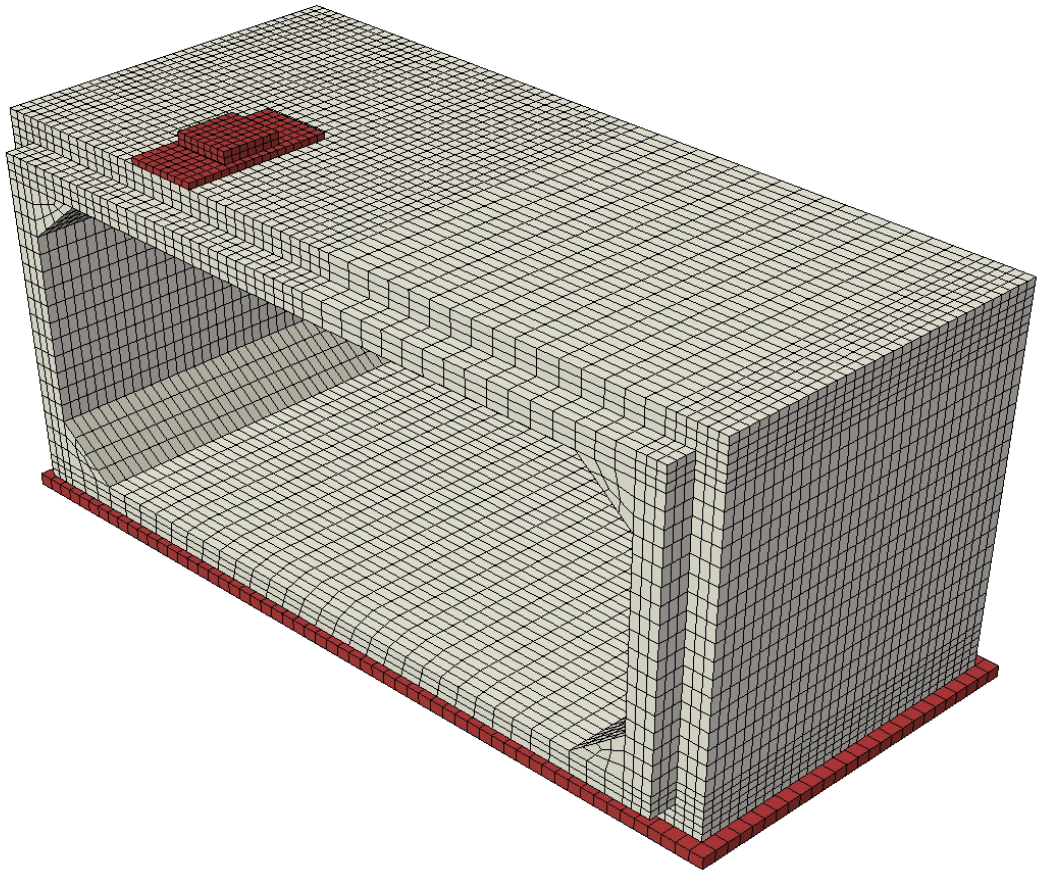

Figure D-1 Dividing the box culvert to 30640 linear hexahedral elements of type C3D8R

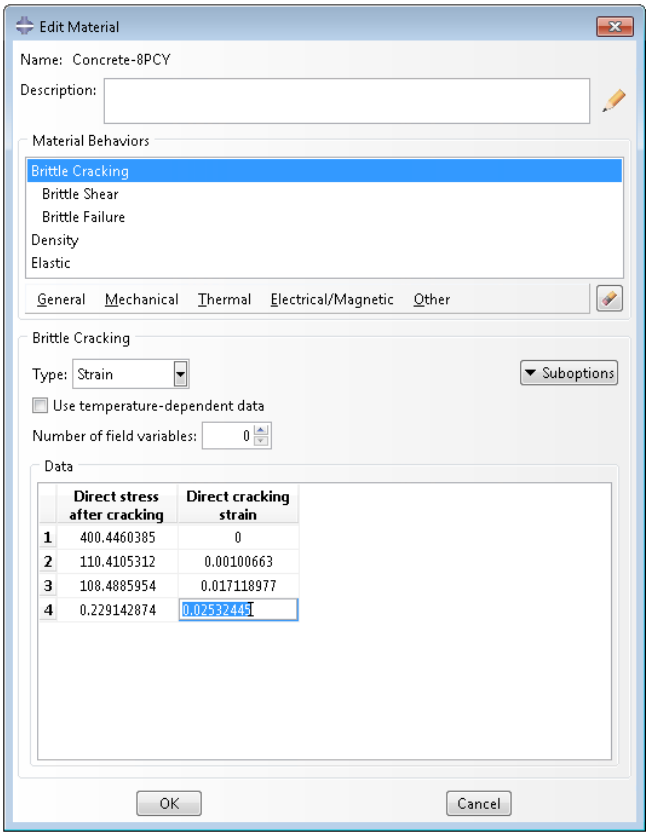

Figure D-2 Material properties used in the box culvert

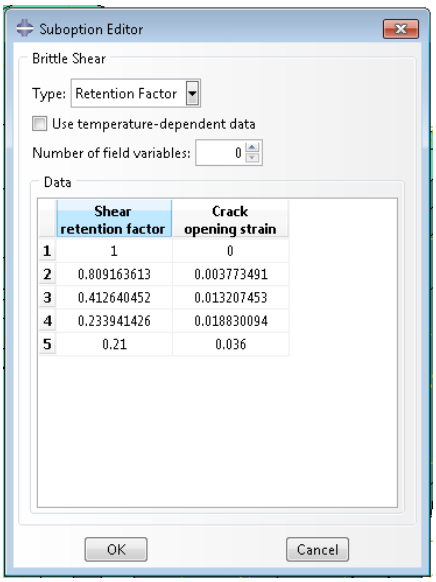

Figure D-3 Retention factor used in the box culvert

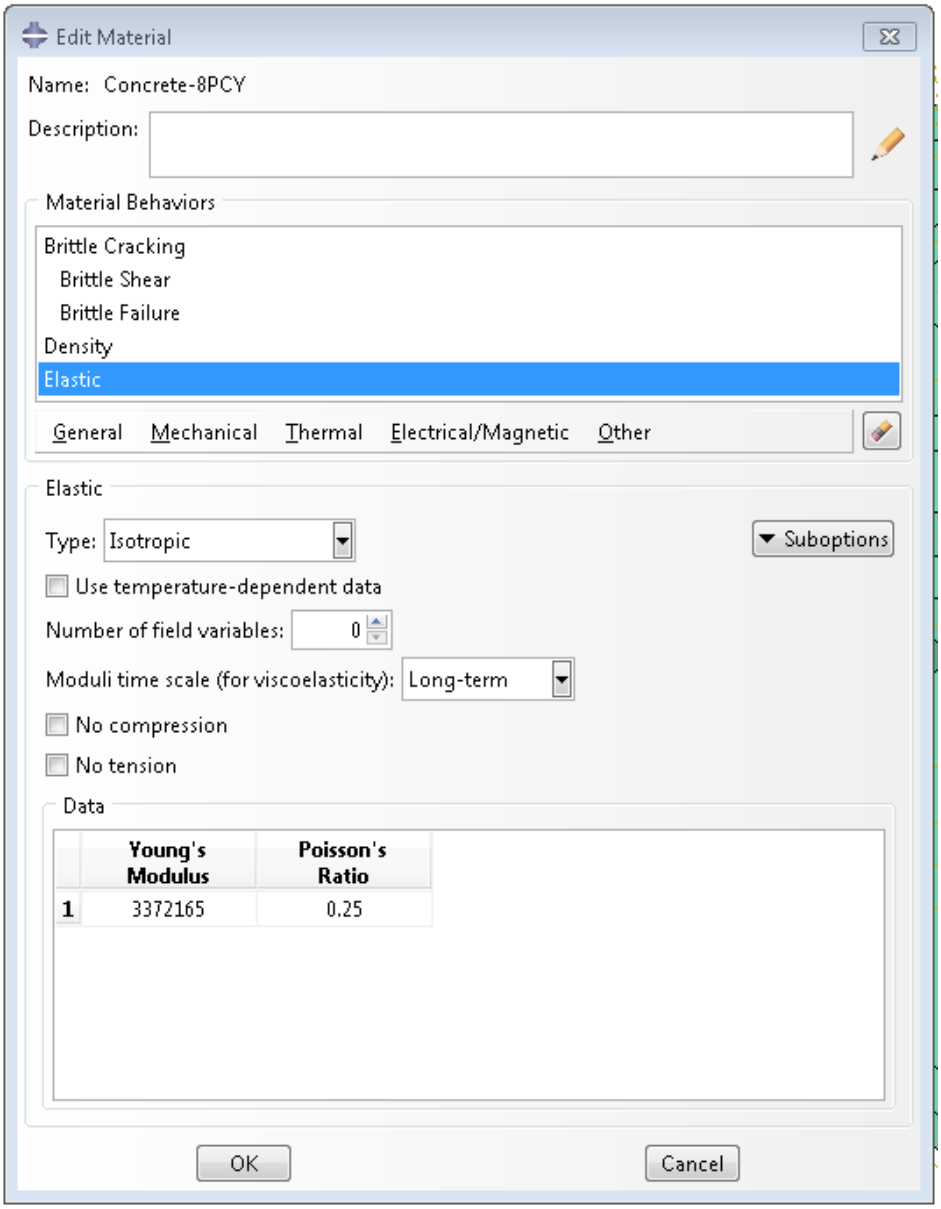

Figure D-4 Young's modulus and Poisson's ratio used in the box culvert

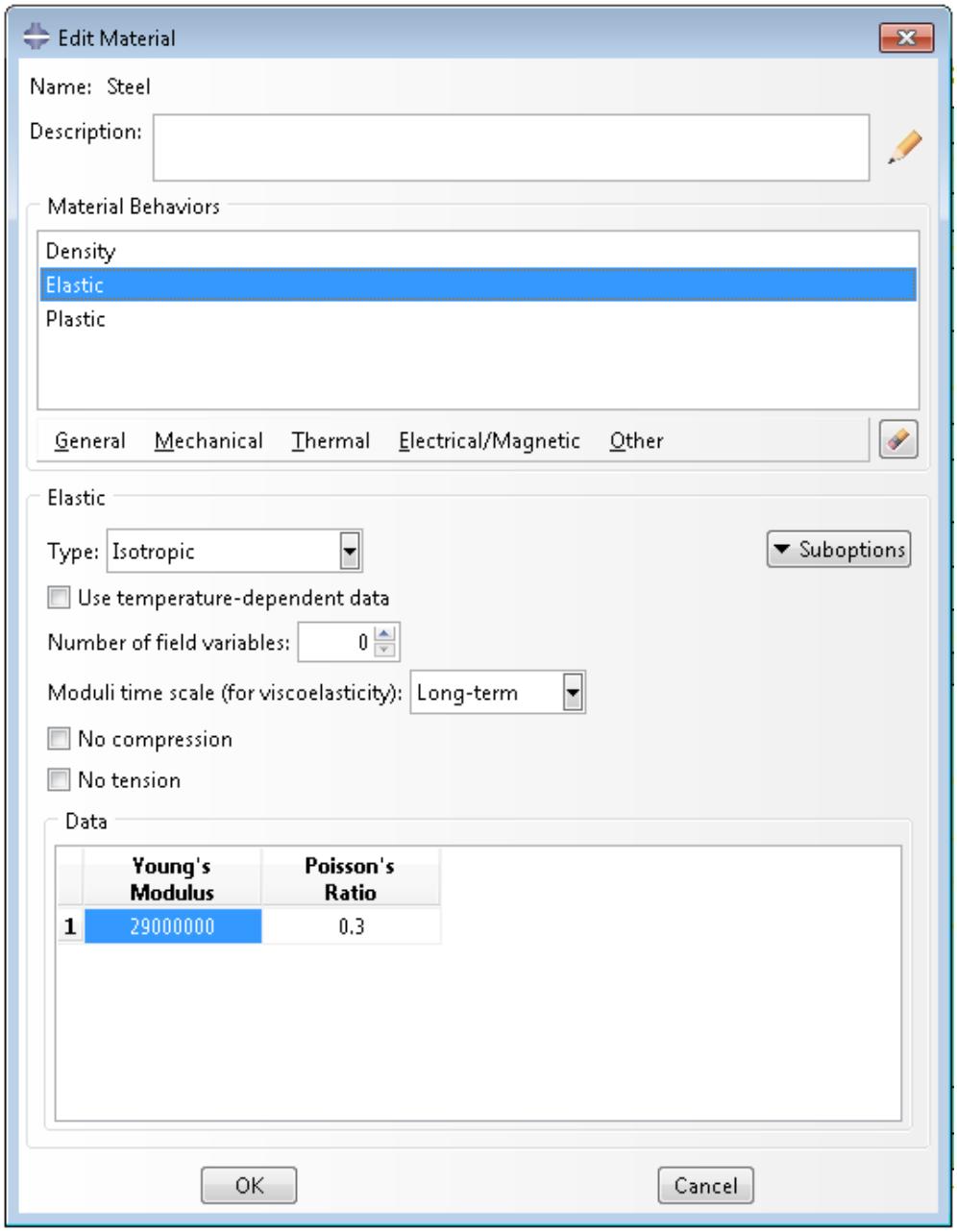

Figure D-5 Young's modulus and Poisson's ratio used for reinforcement embedded in box culvert

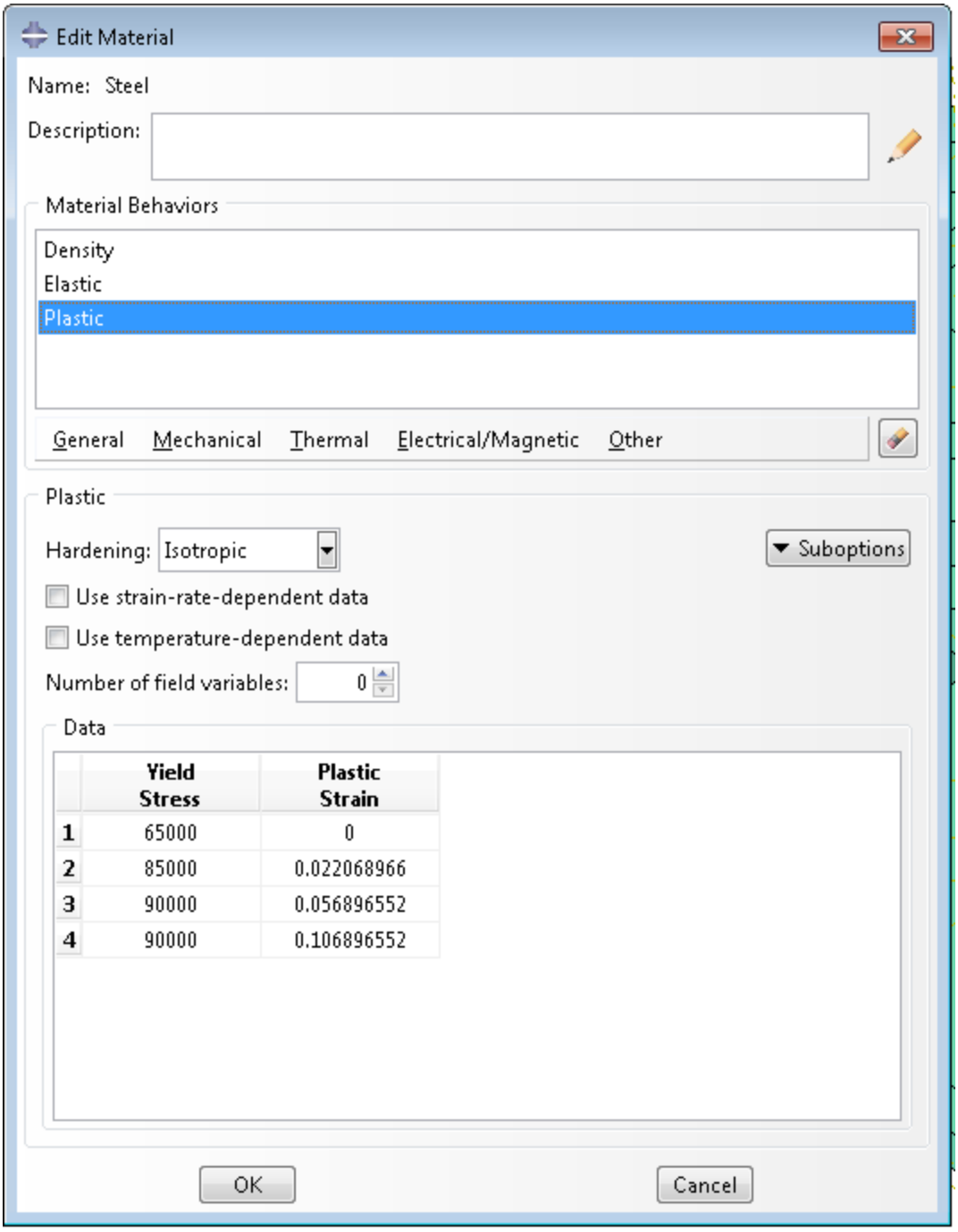

Figure D-6 Yield stress and Plastic strain used for reinforcement embedded in box culvert

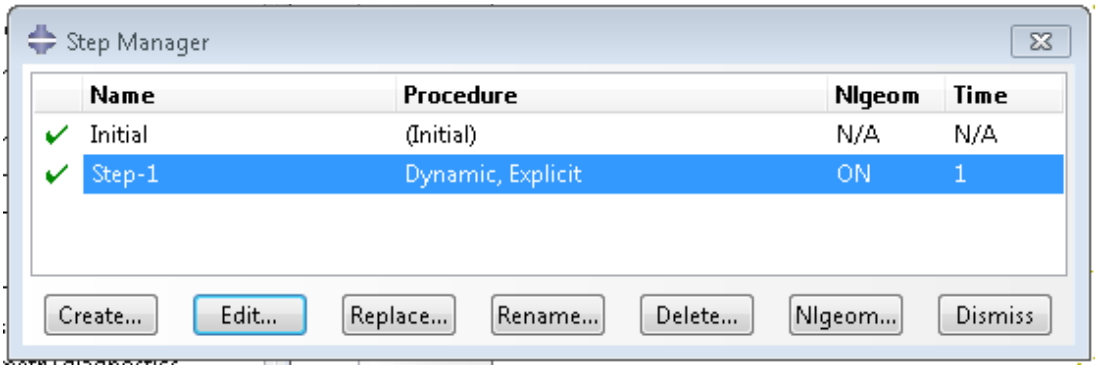

Figure D-7 Running the FEM model in ABAQUS/EXPLICIT

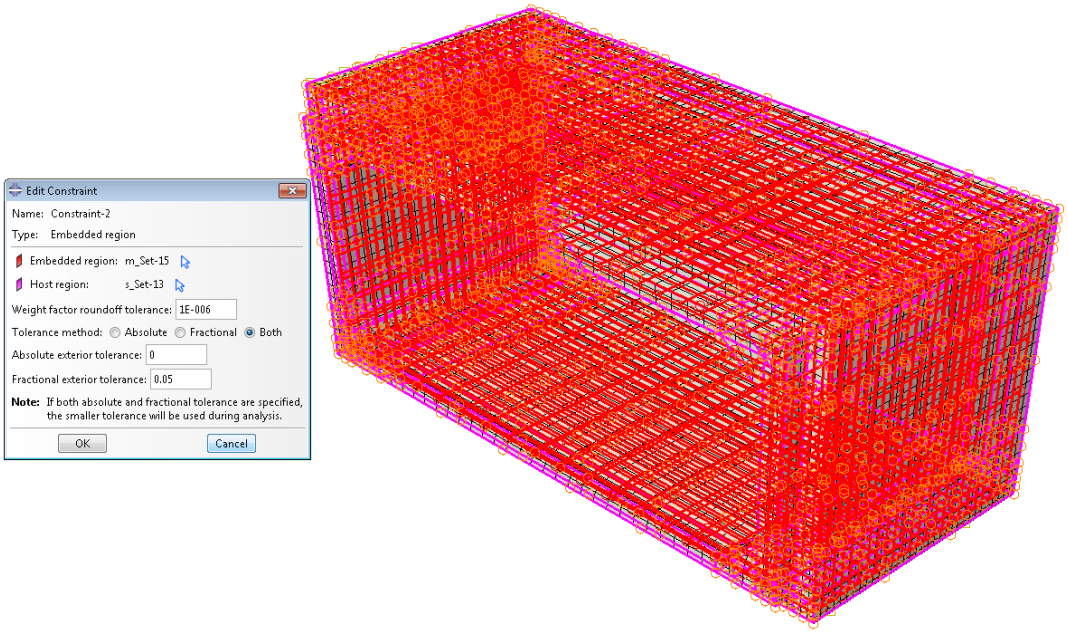

Figure D-8 Embedding reinforcement in box culvert

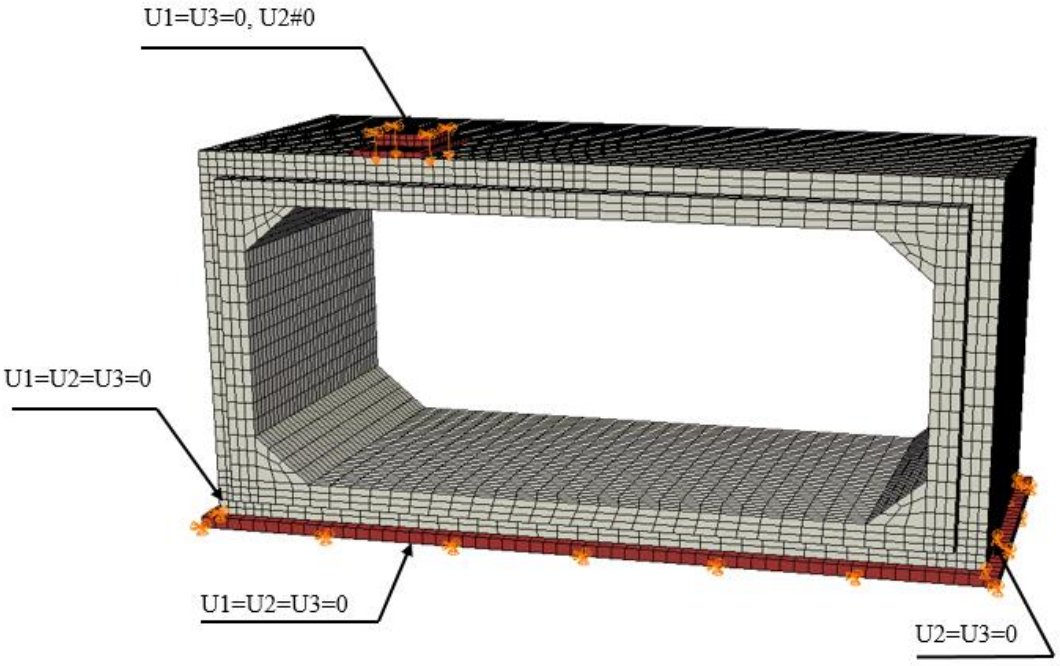

Figure D-9 Boundary condition and load application used in FE modeling

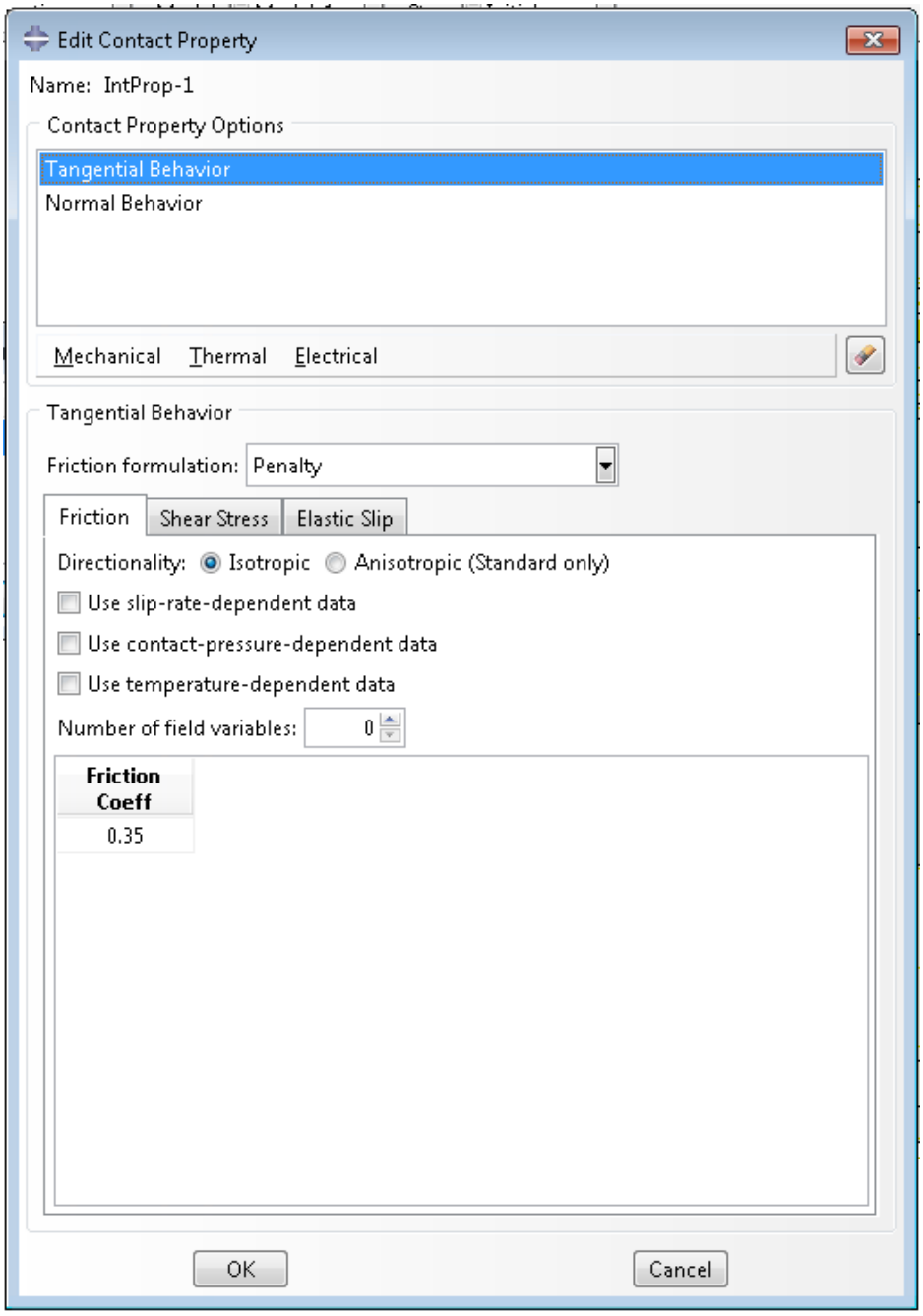

Figure D-10 Tangential contact property used between the box culvert, base support and loading plate

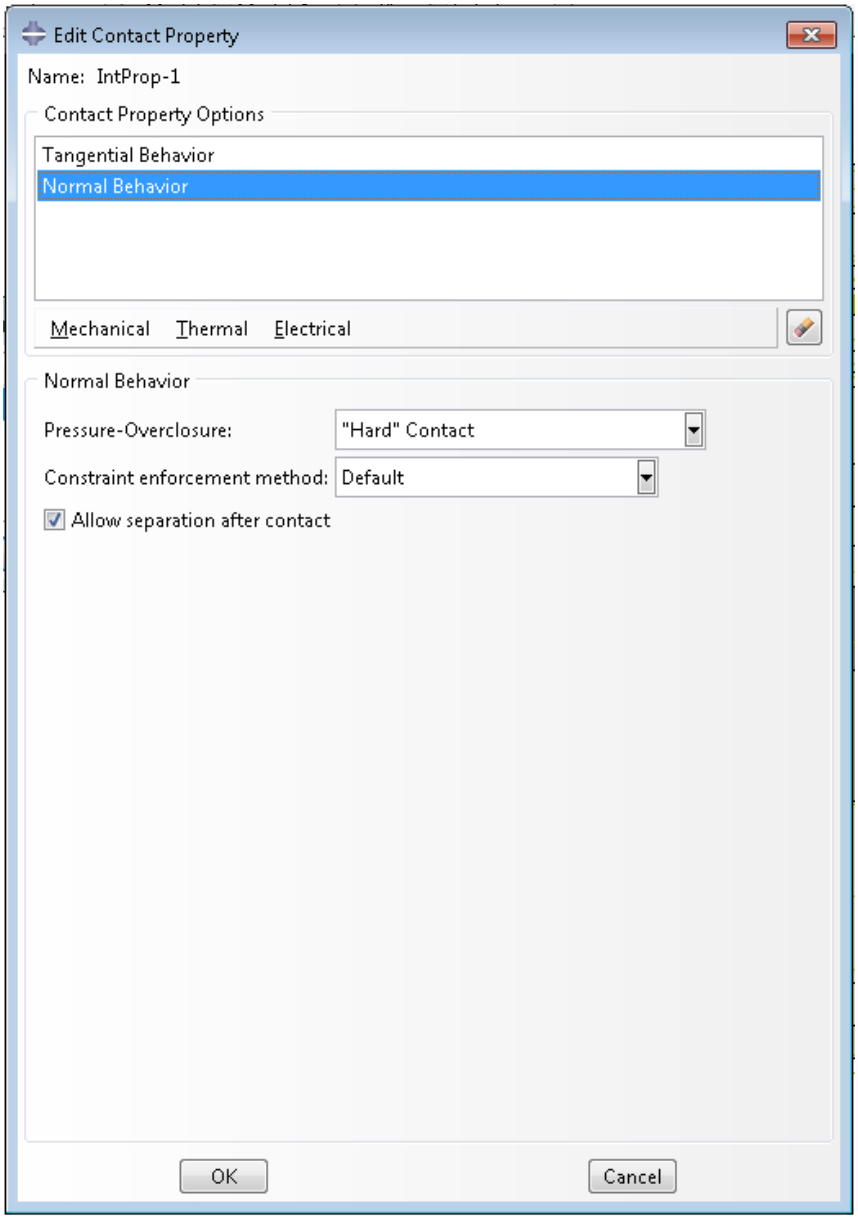

Figure D-11 Normal contact property used between the box culvert, base support and loading plate

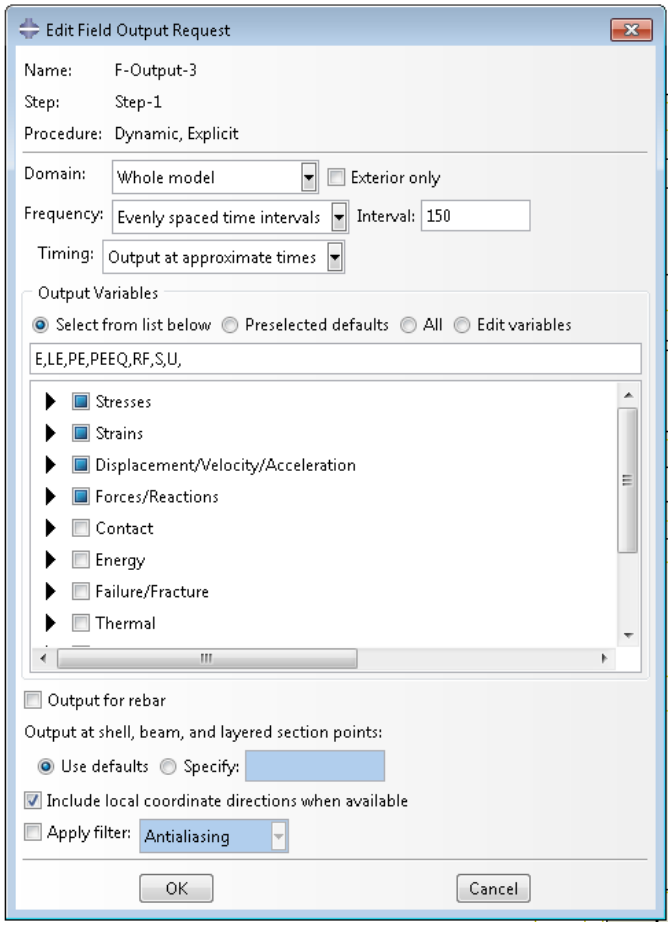

Figure D-12 Requesting field output from FEM

APPENDIX E: ASTM C1577 BOX CULVERTS FEM RESULTS

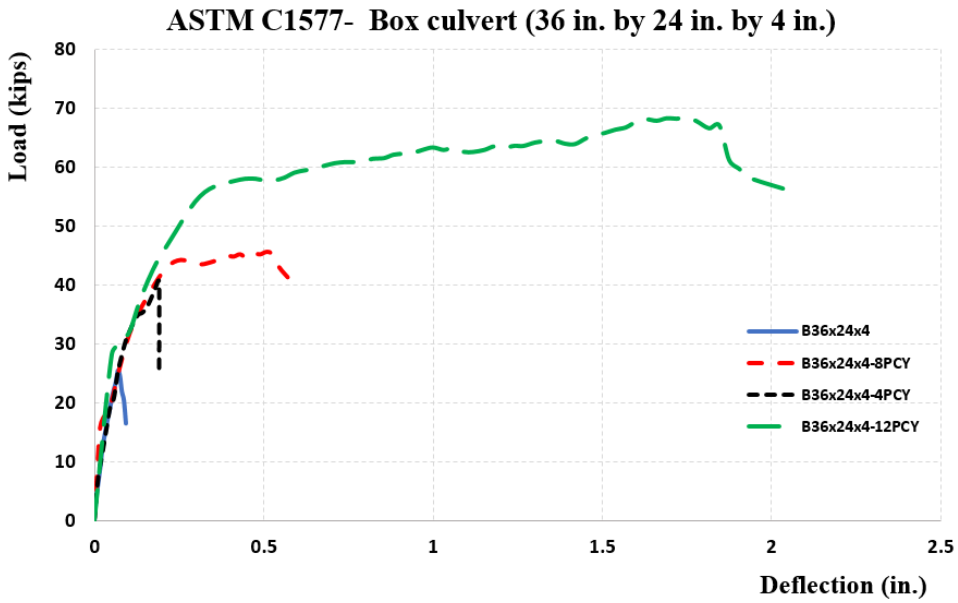

Figure E-1 Load-deflection plot for box culvert 3ft by 2 ft by 4 in.

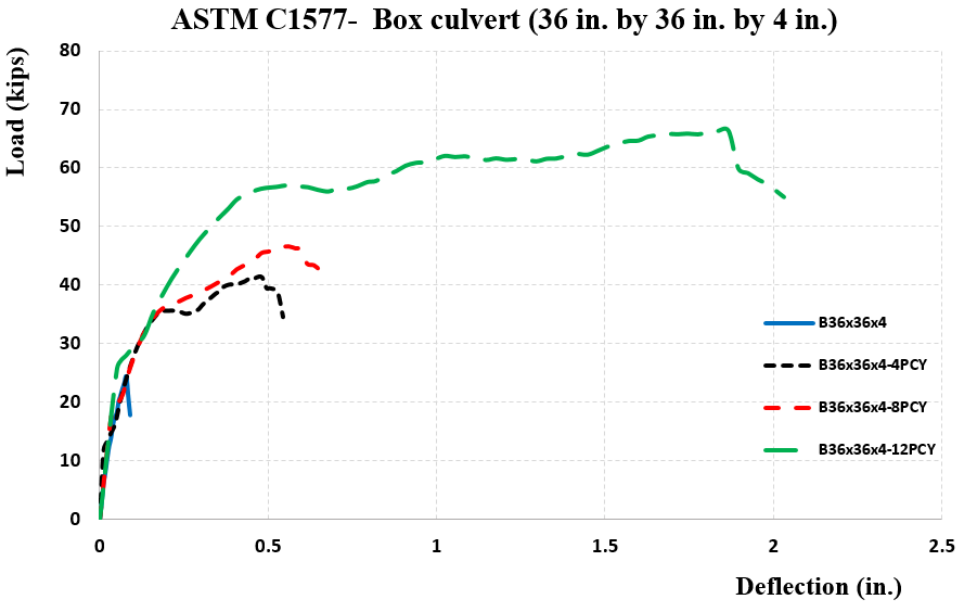

Figure E-2 Load-deflection plot for box culvert 3ft by 3 ft by 4 in.

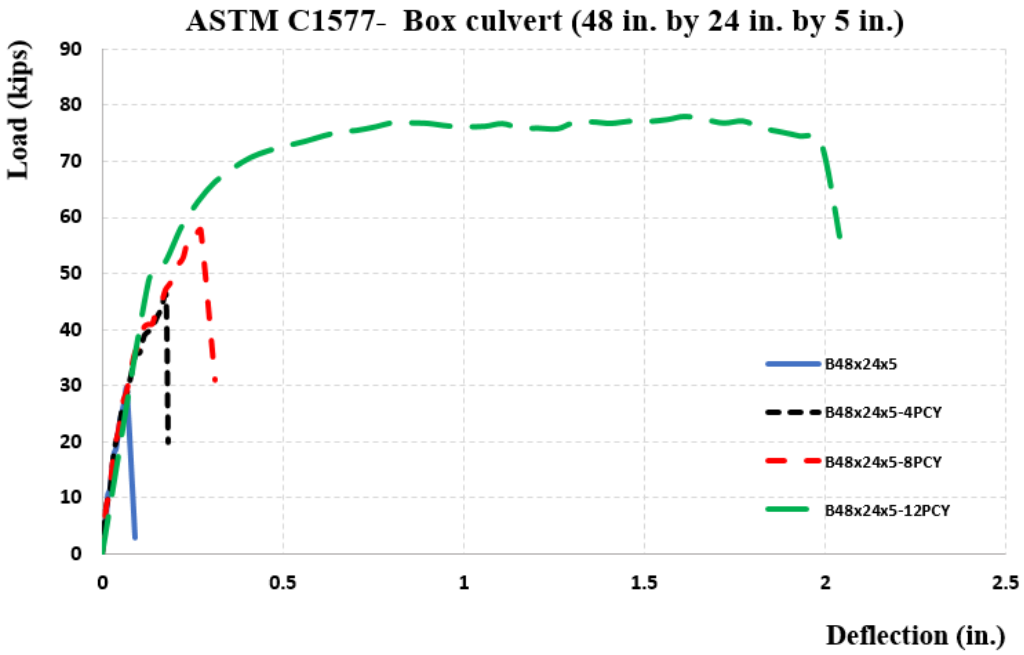

Figure E-3 Load-deflection plot for box culvert 4ft by 2 ft by 5 in.

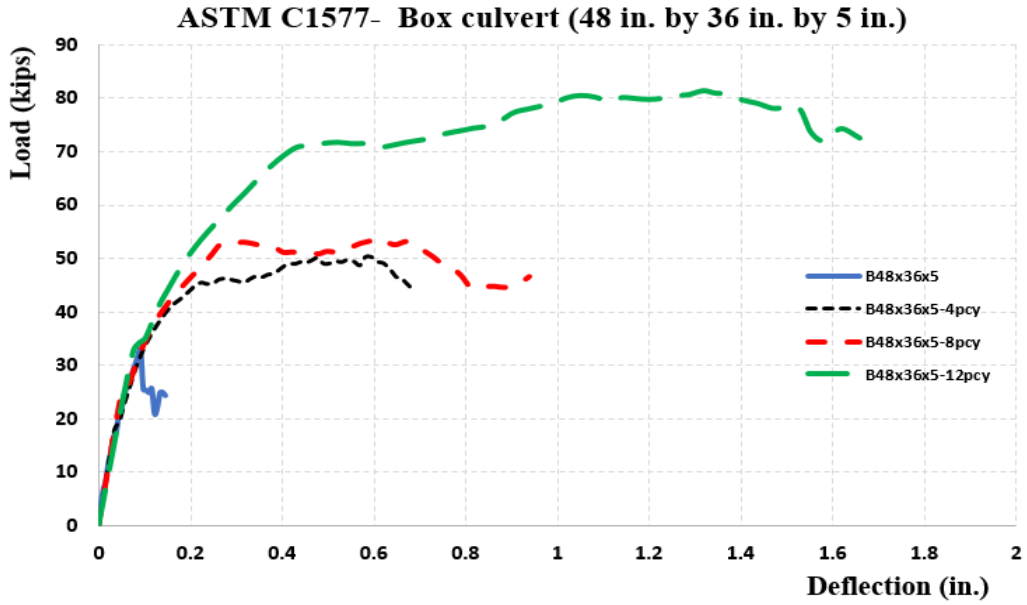

Figure E-4 Load-deflection plot for box culvert 4ft by 3 ft by 5 in.

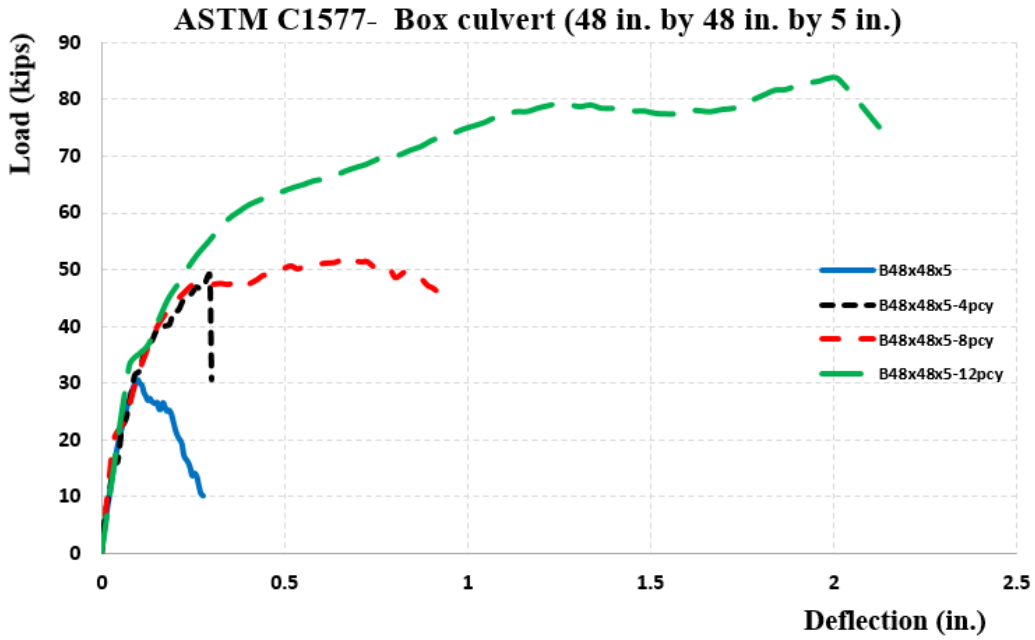

Figure E-5 Load-deflection plot for box culvert 4ft by 4 ft by 5 in.

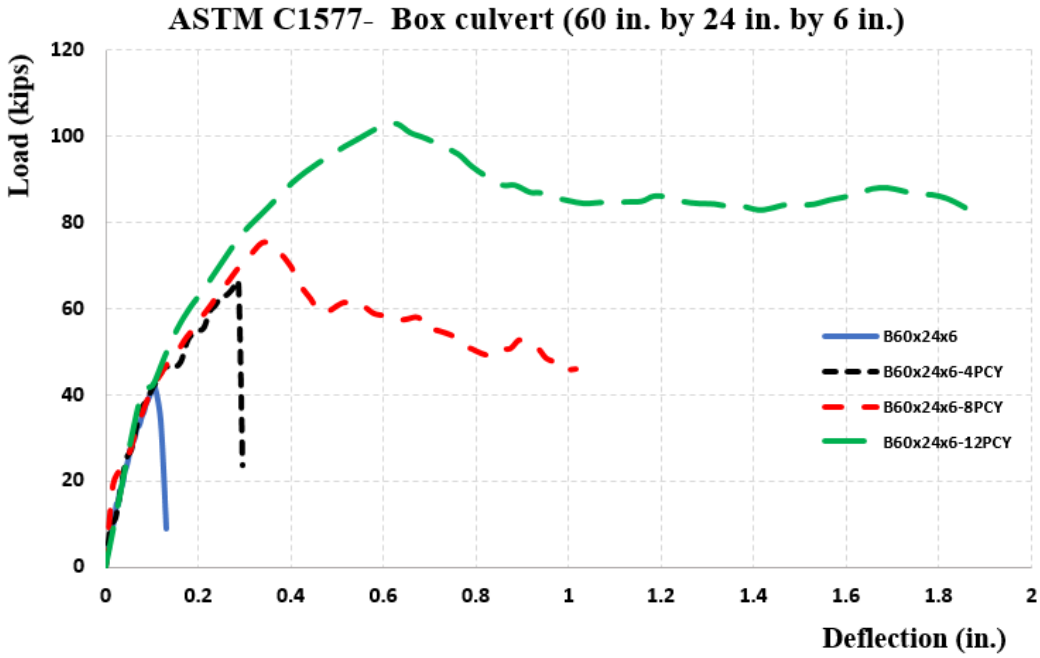

Figure E-6 Load-deflection plot for box culvert 5 ft by 2 ft by 6 in.

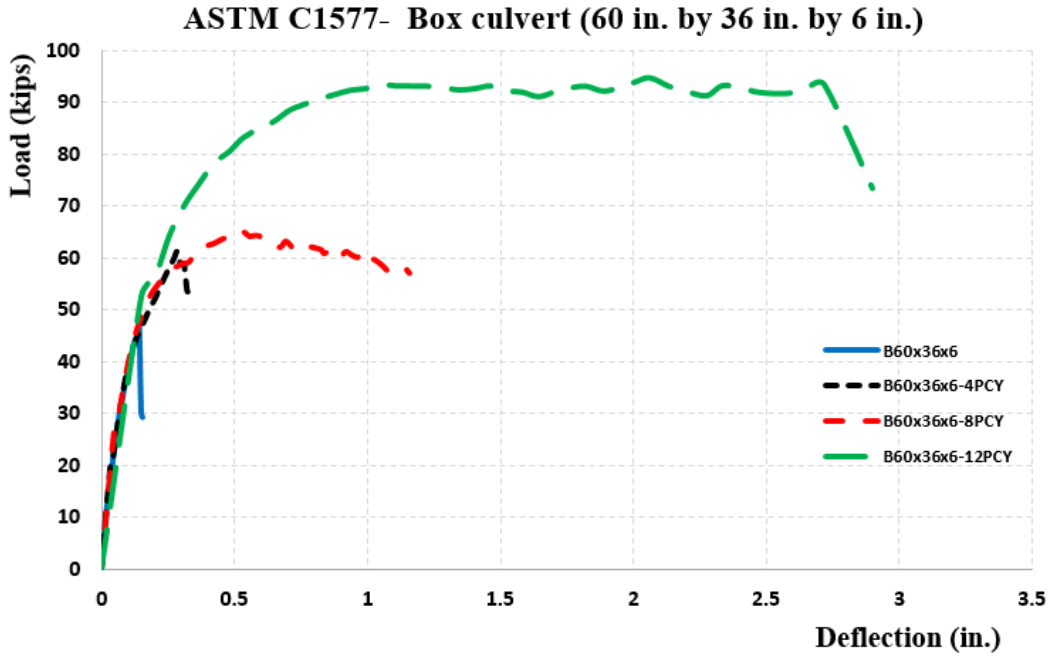

Figure E-7 Load-deflection plot for box culvert 5 ft by 3 ft by 6 in.

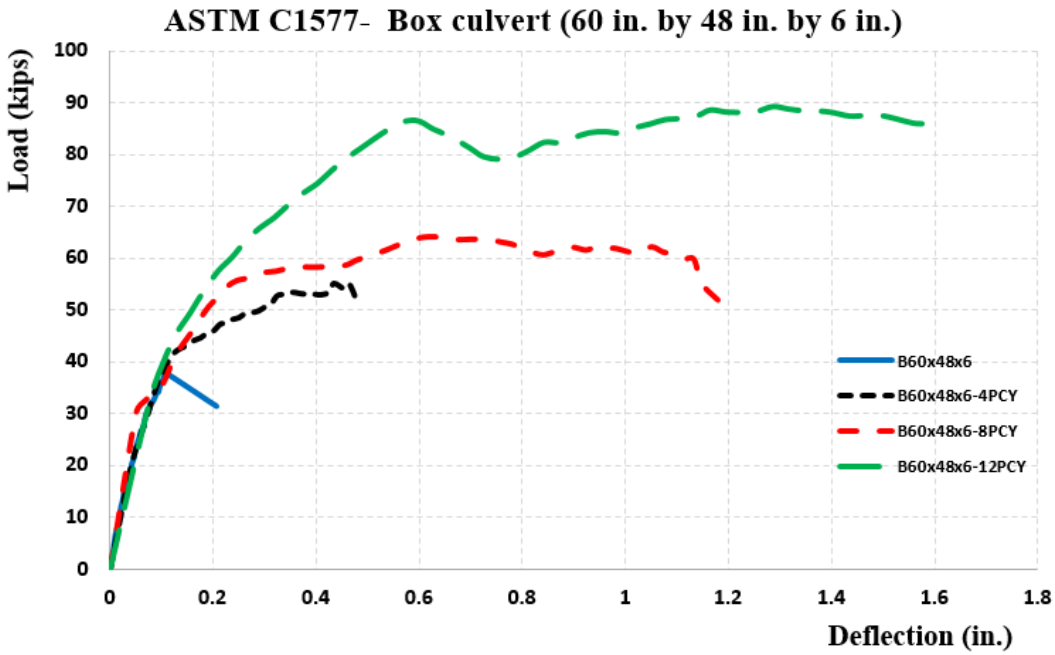

Figure E-8 Load-deflection plot for box culvert 5 ft by 4 ft by 6 in.

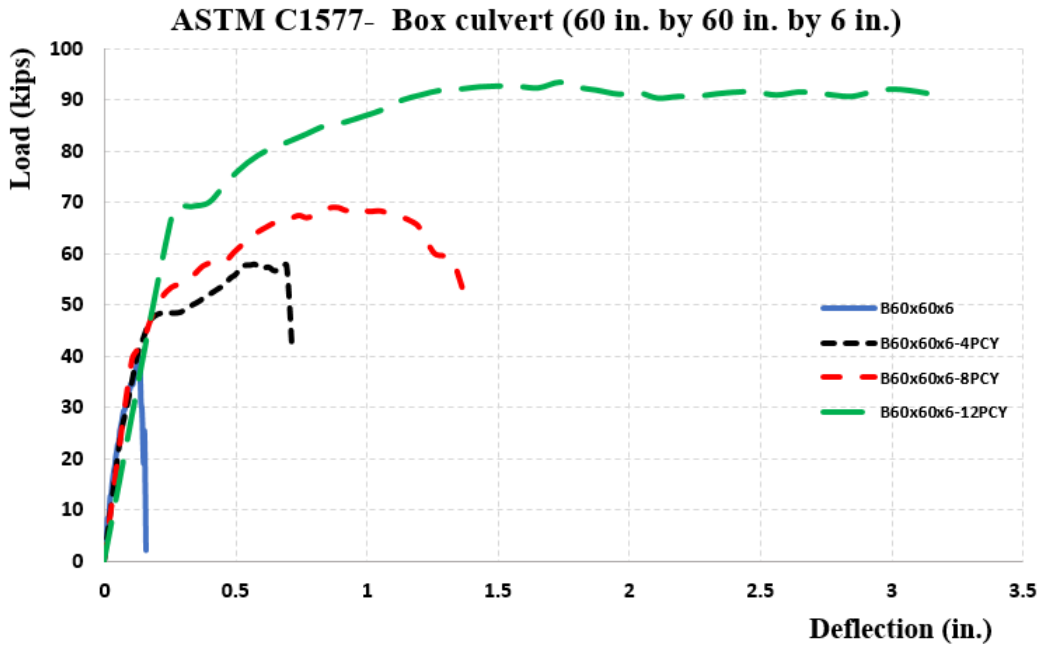

Figure E-9 Load-deflection plot for box culvert 5 ft by 5 ft by 6 in.

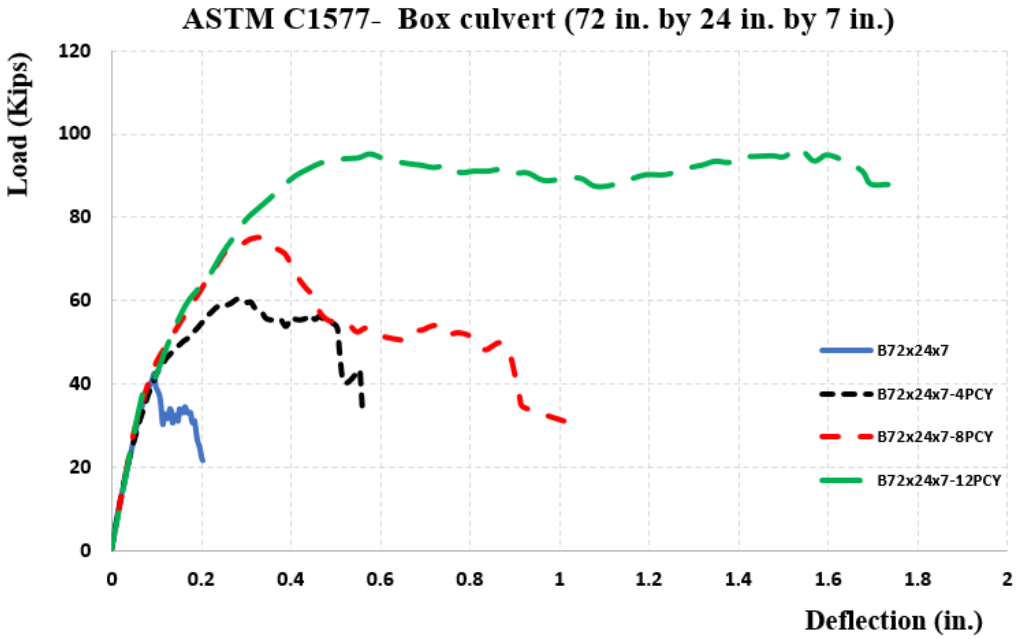

Figure E-10 Load-deflection plot for box culvert 6 ft by 2 ft by 7 in.

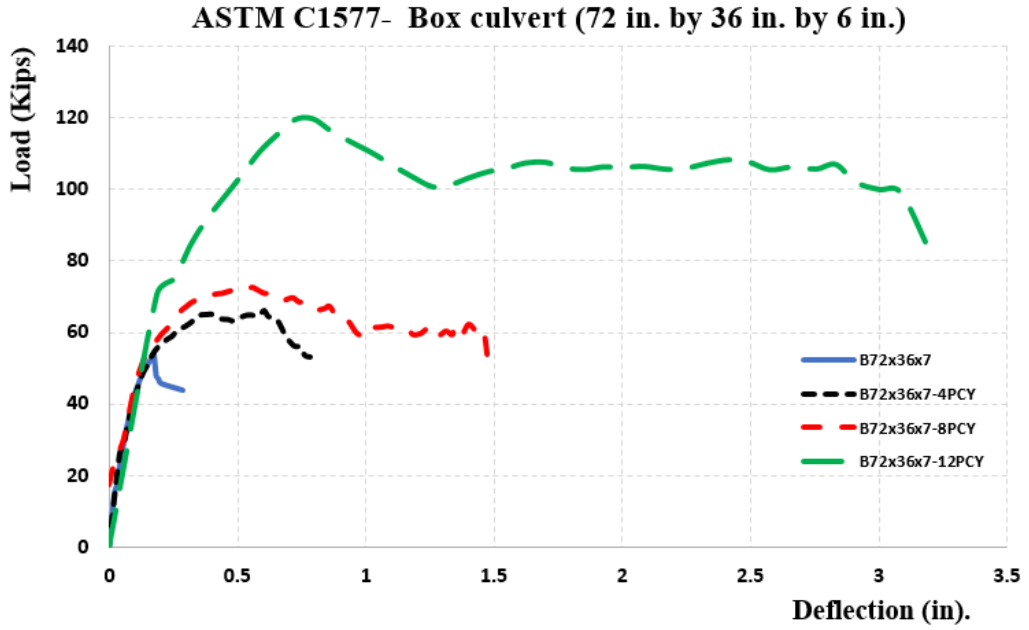

Figure E-11 Load-deflection plot for box culvert 6 ft by 3 ft by 7 in.

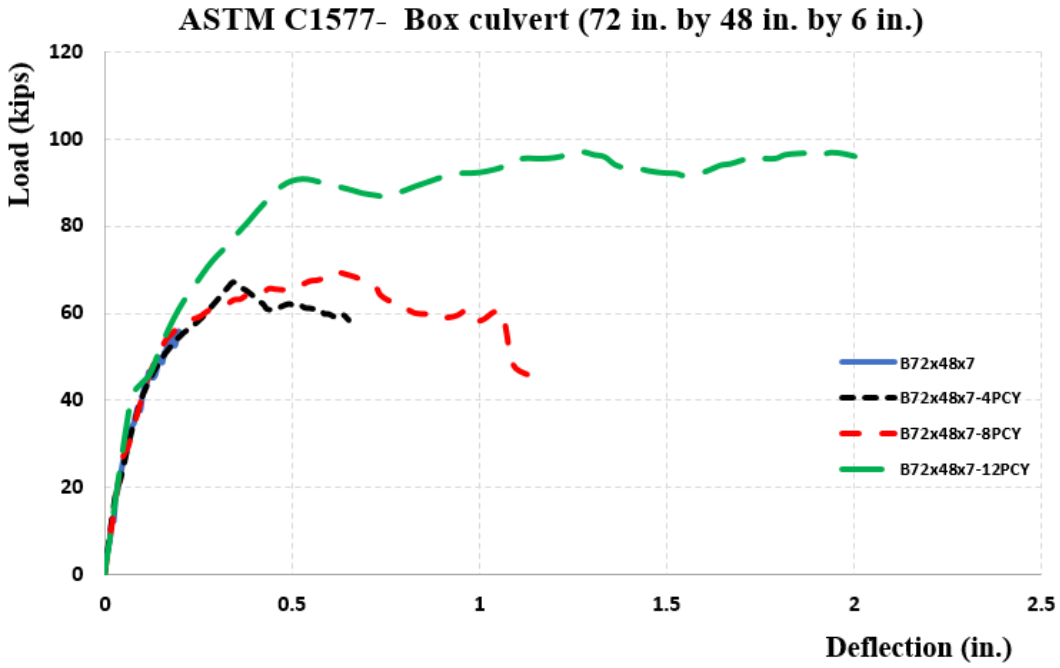

Figure E-12 Load-deflection plot for box culvert 6 ft by 4 ft by 7 in.

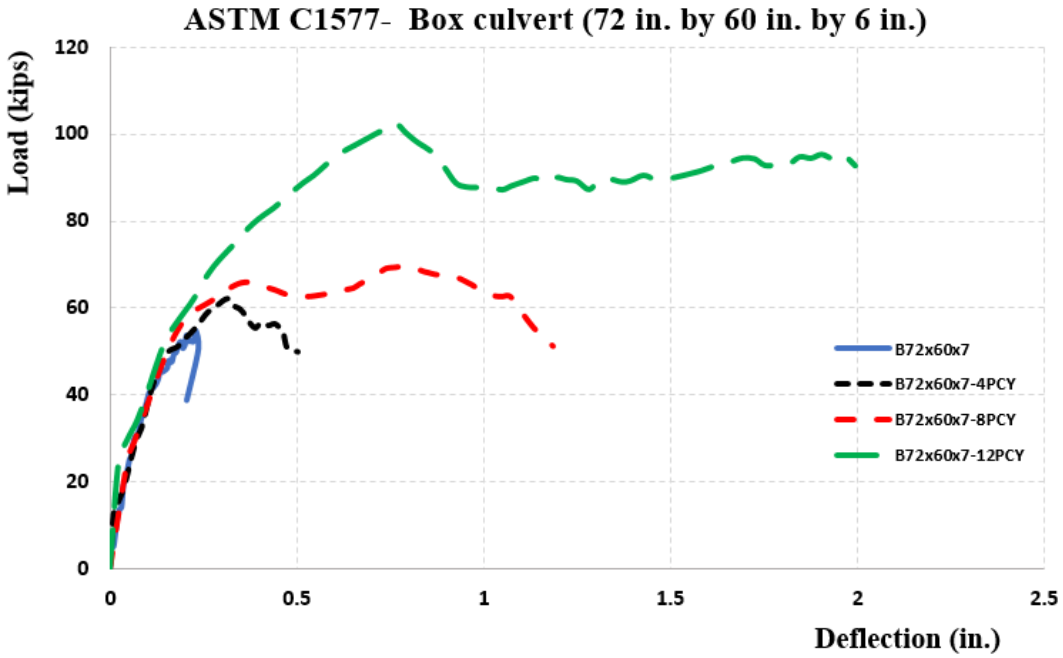

Figure E-13 Load-deflection plot for box culvert 6 ft by 5 ft by 7 in.

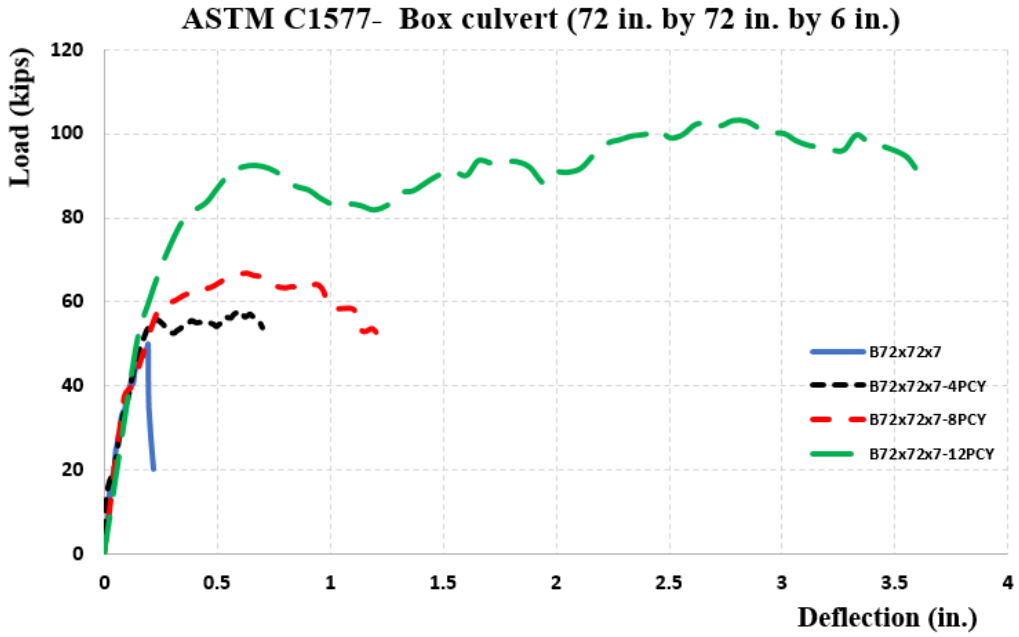

Figure E-14 Load-deflection plot for box culvert 6 ft by 6 ft by 7 in.

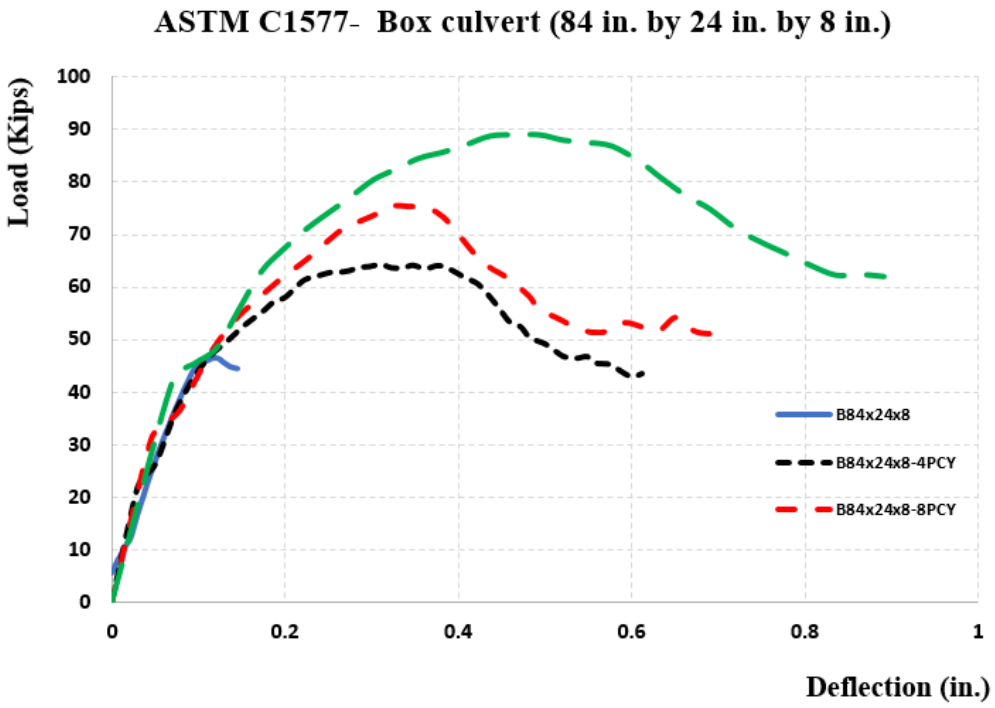

Figure E-15 Load-deflection plot for box culvert 7 ft by 2 ft by 8 in.

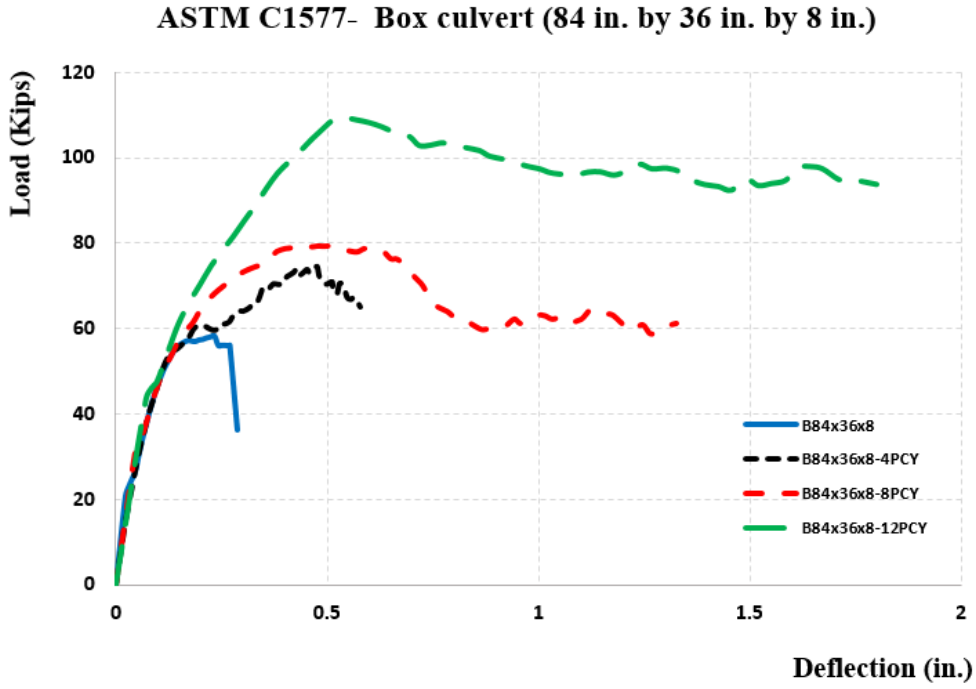

Figure E-16 Load-deflection plot for box culvert 7 ft by 3 ft by 8 in.

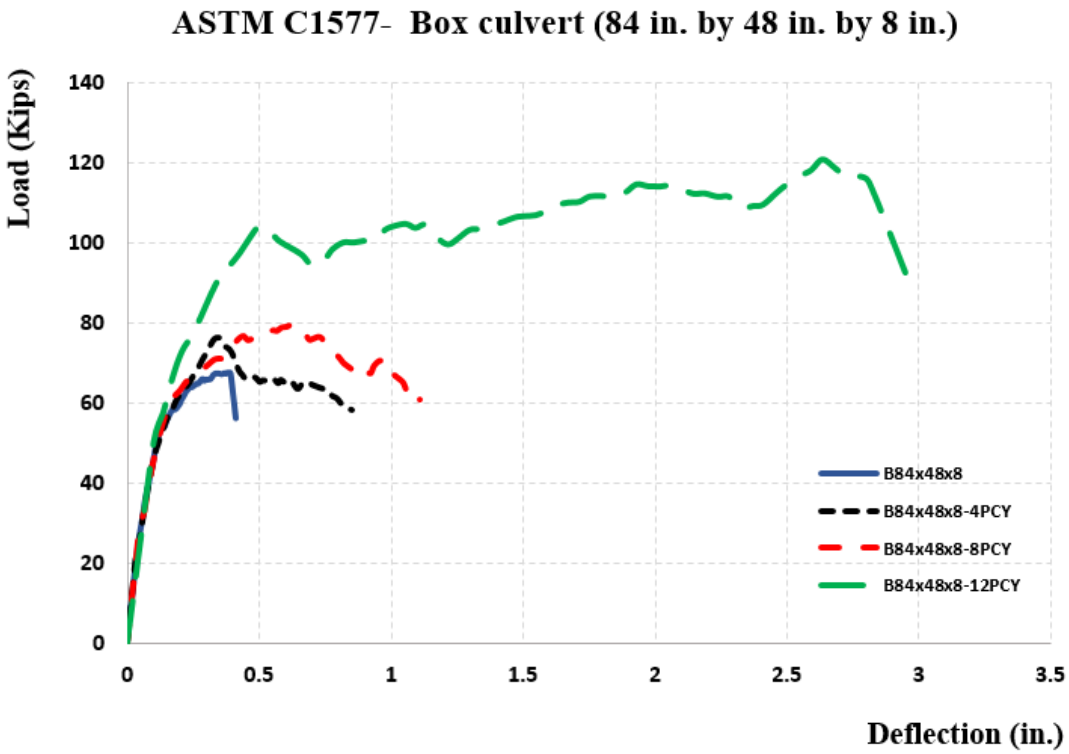

Figure E-17 Load-deflection plot for box culvert 7 ft by 4 ft by 8 in.

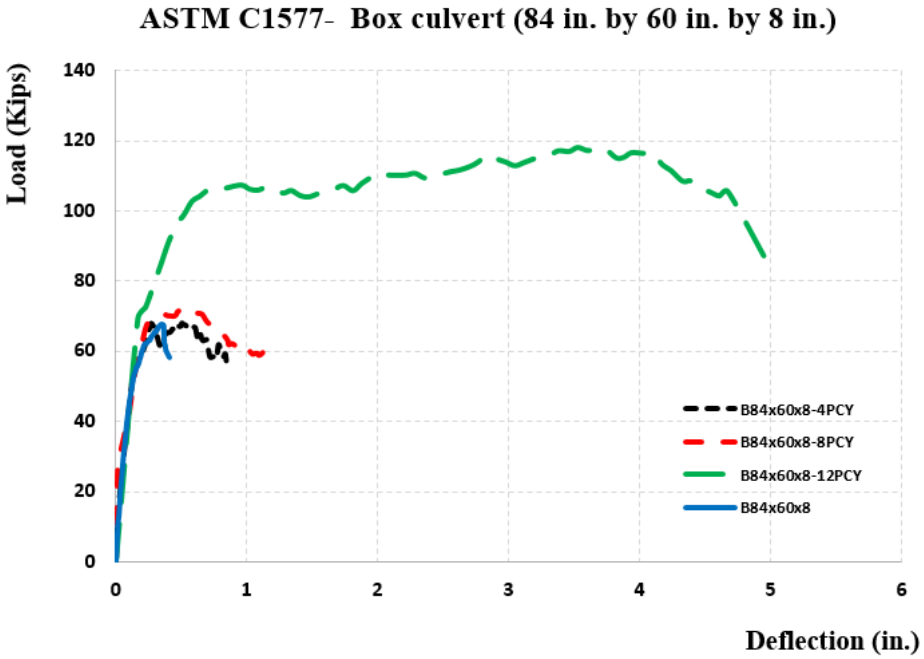

Figure E-18 Load-deflection plot for box culvert 7 ft by 5 ft by 8 in.

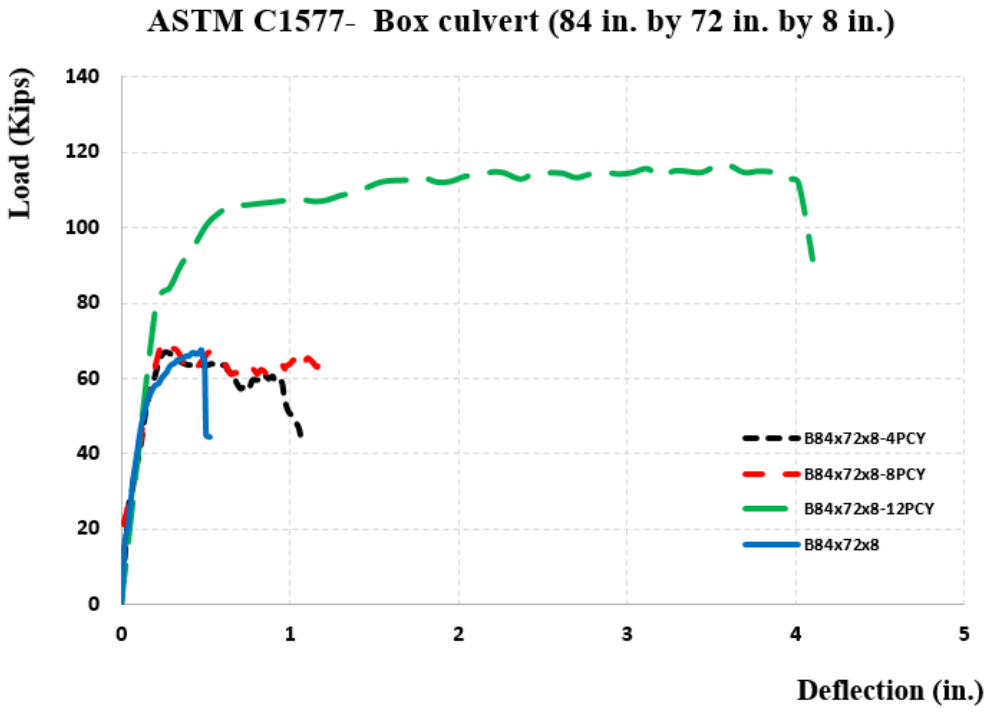

Figure E-19 Load-deflection plot for box culvert 7 ft by 6 ft by 8 in.

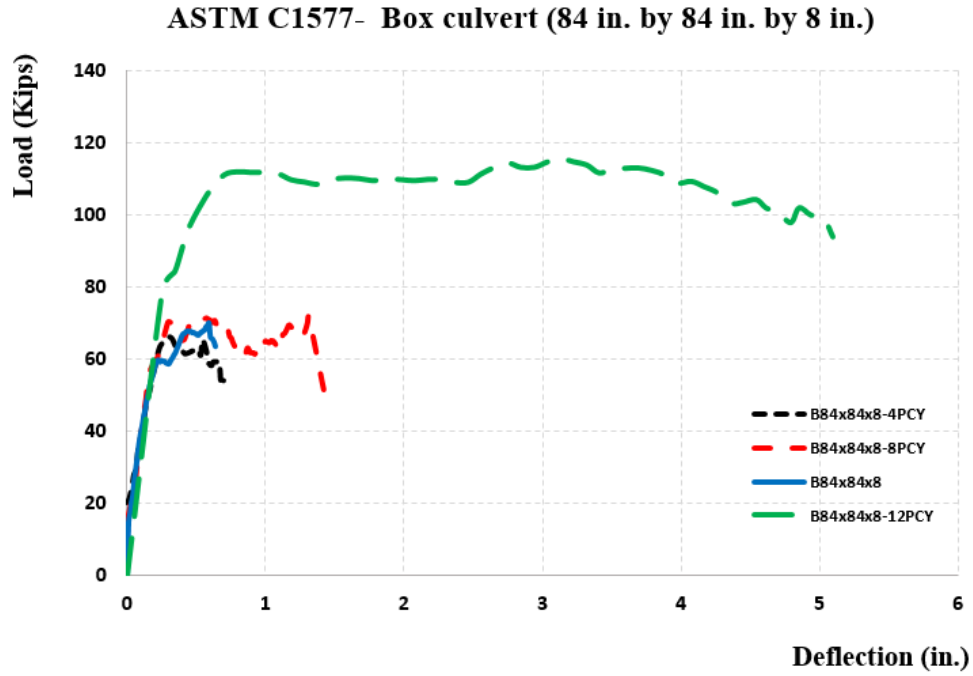

Figure E-20 Load-deflection plot for box culvert 7 ft by 7 ft by 8 in.

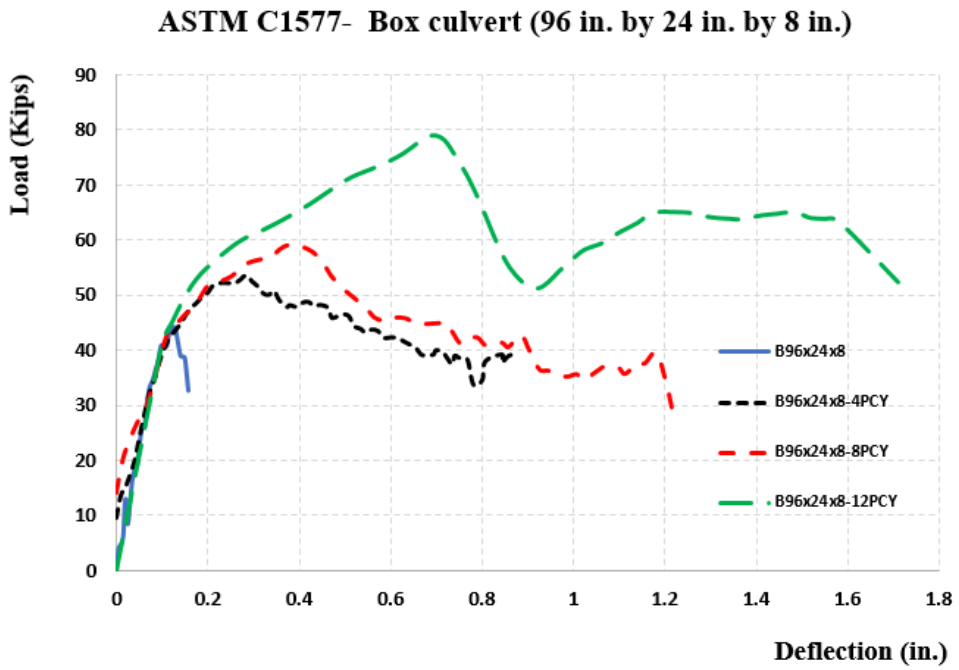

Figure E-21 Load-deflection plot for box culvert 8 ft by 2 ft by 8 in.

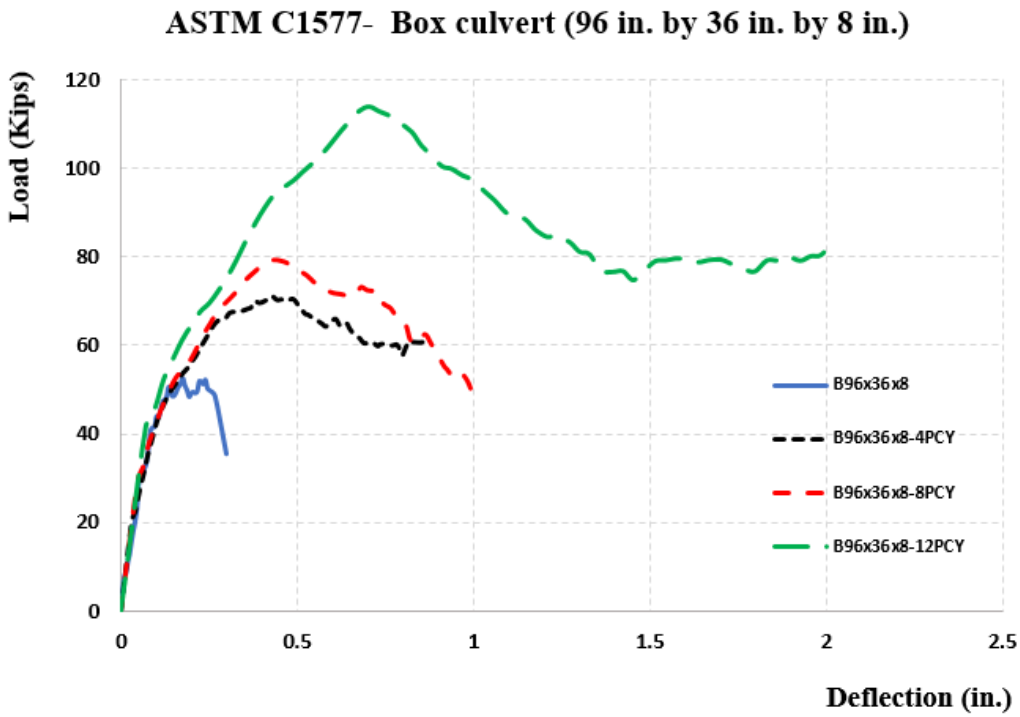

Figure E-22 Load-deflection plot for box culvert 8 ft by 3 ft by 8 in.

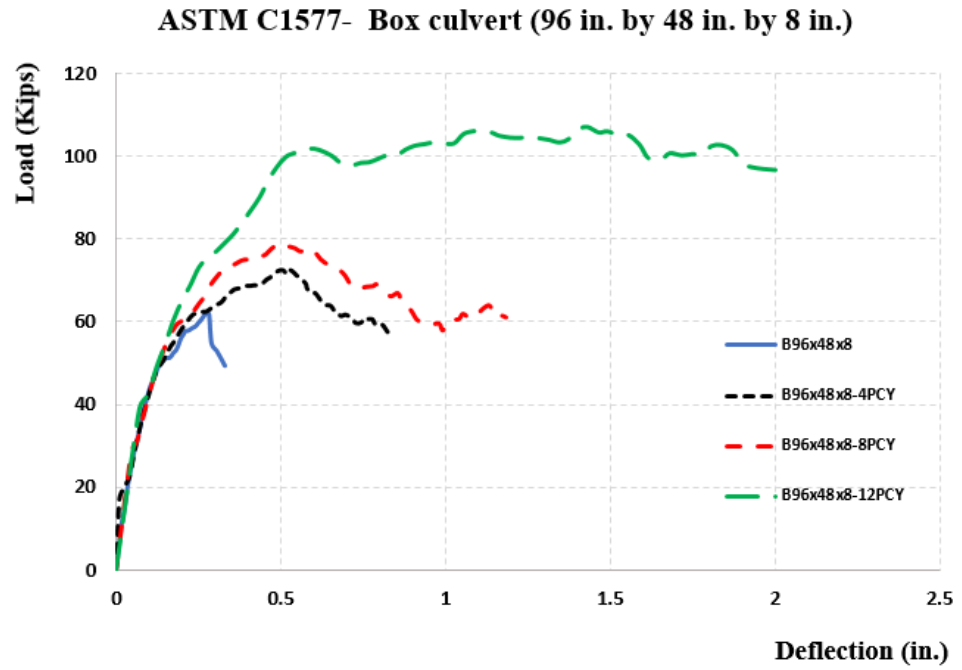

Figure E-23 Load-deflection plot for box culvert 8 ft by 4 ft by 8 in.

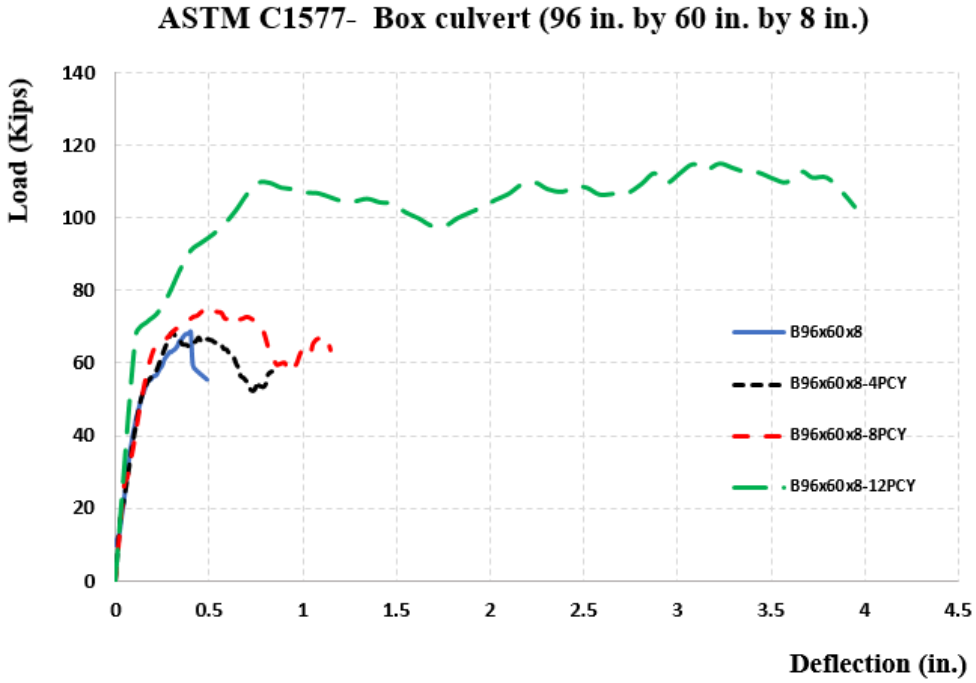

Figure E-24 Load-deflection plot for box culvert 8 ft by 5 ft by 8 in.

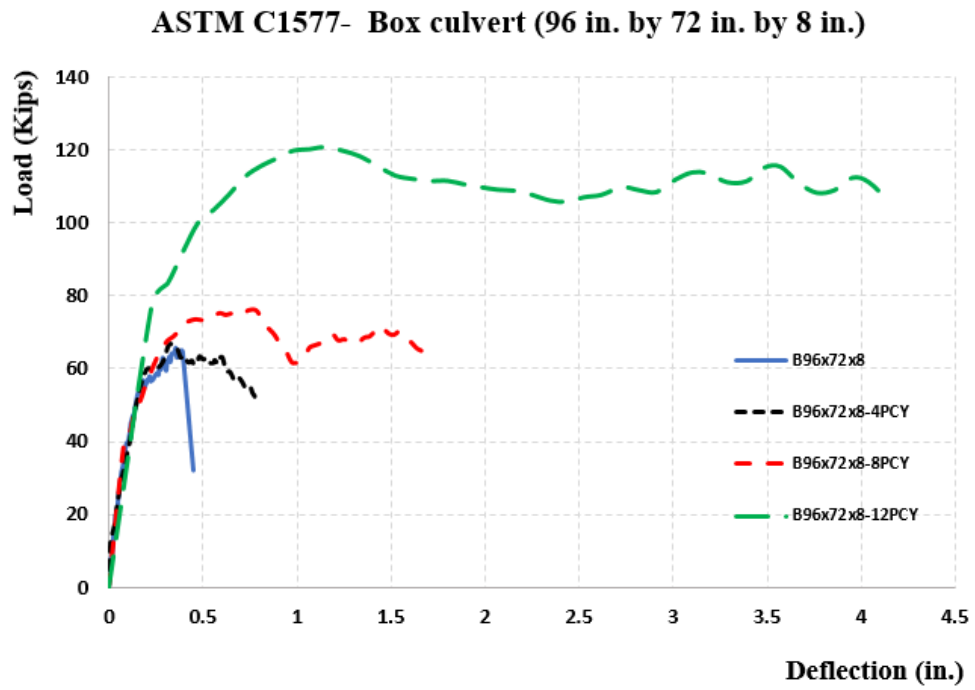

Figure E-25 Load-deflection plot for box culvert 8 ft by 6 ft by 8 in.

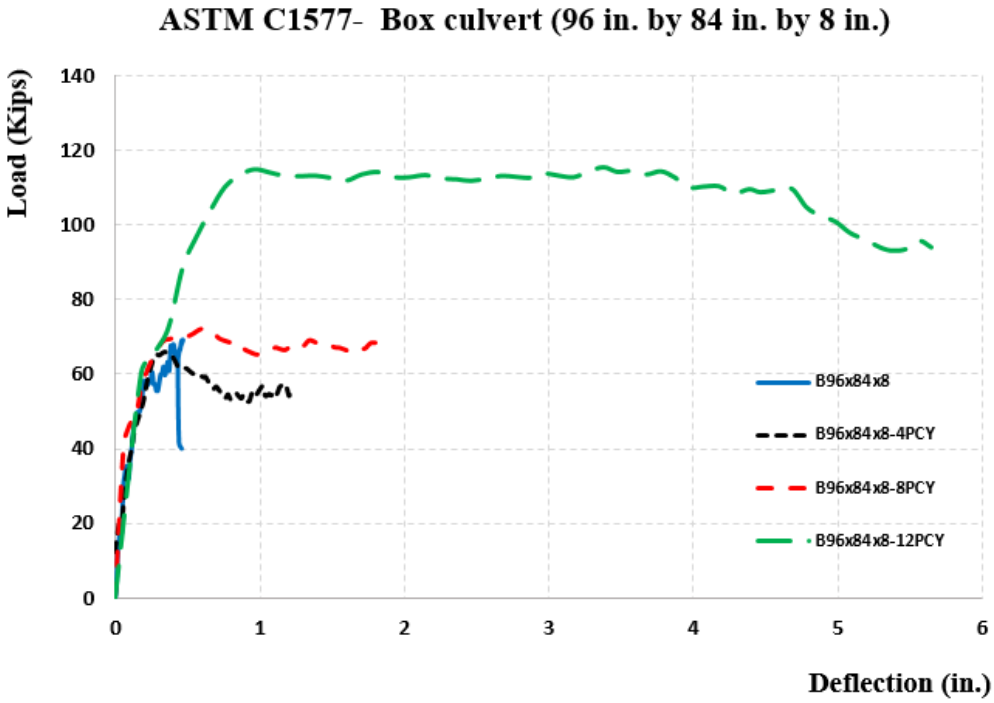

Figure E-26 Load-deflection plot for box culvert 8 ft by 7 ft by 8 in.

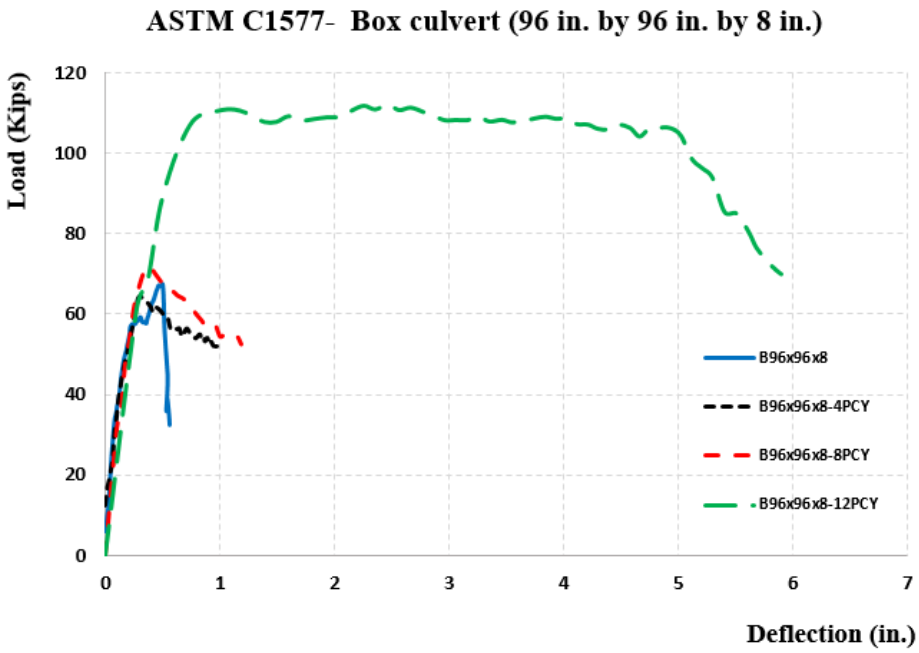

Figure E-27 Load-deflection plot for box culvert 8 ft by 8 ft by 8 in.

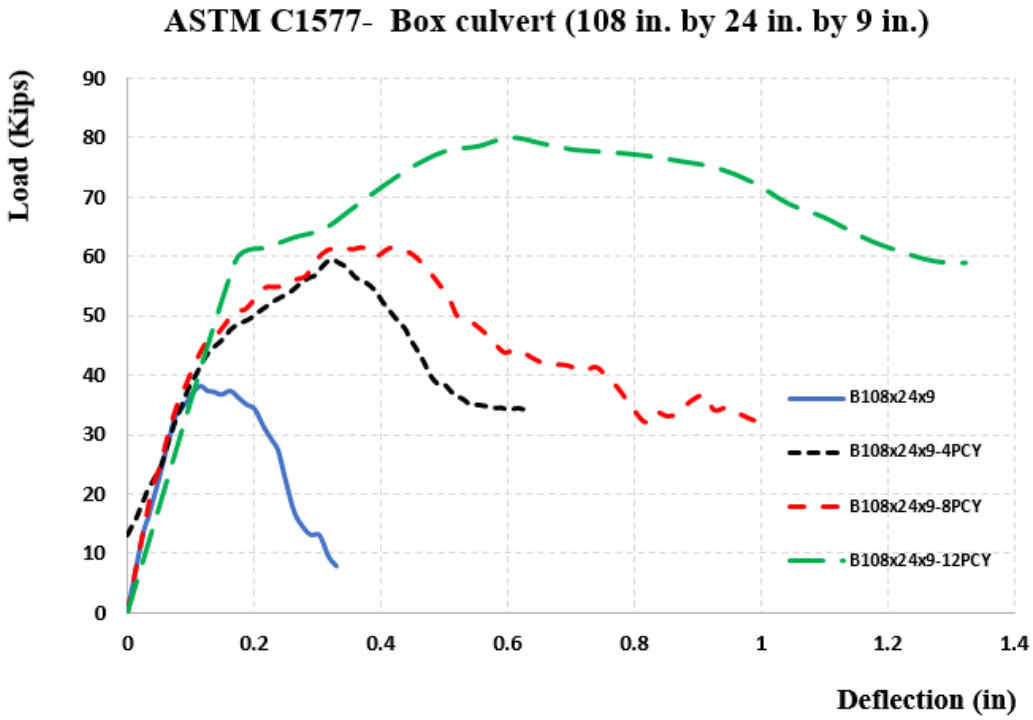

Figure E-28 Load-deflection plot for box culvert 9 ft by 2 ft by 9 in.

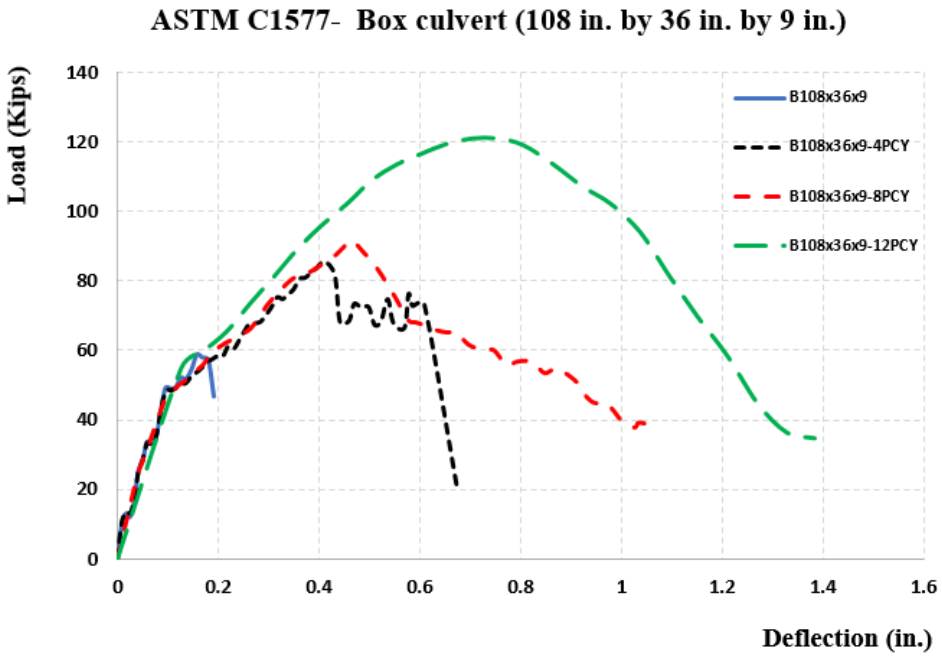

Figure E-29 Load-deflection plot for box culvert 9 ft by 3 ft by 9 in.

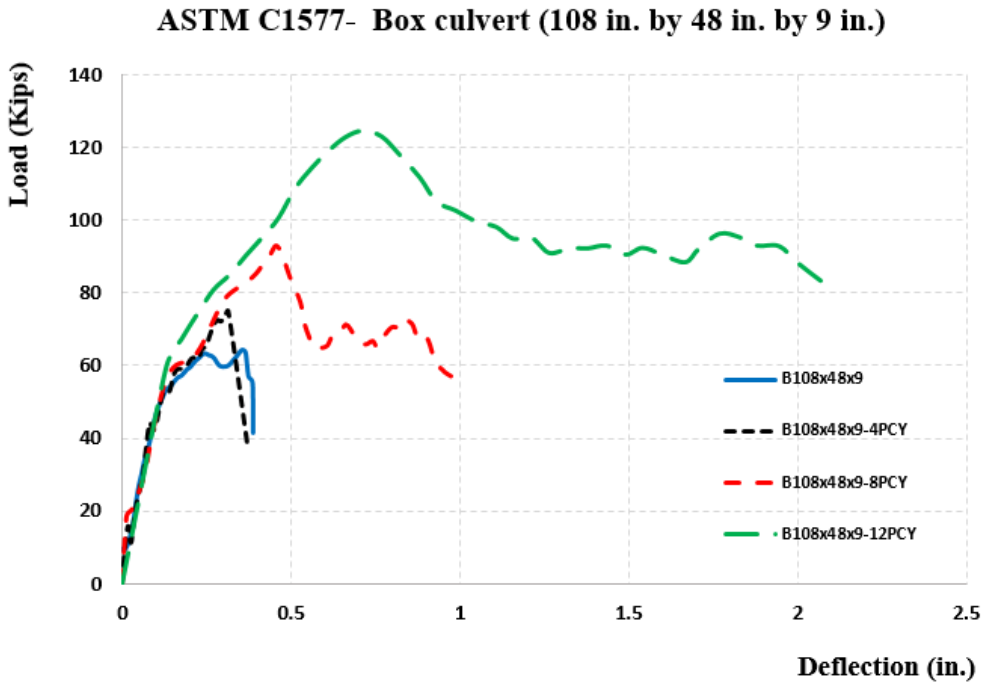

Figure E-30 Load-deflection plot for box culvert 9 ft by 4 ft by 9 in.

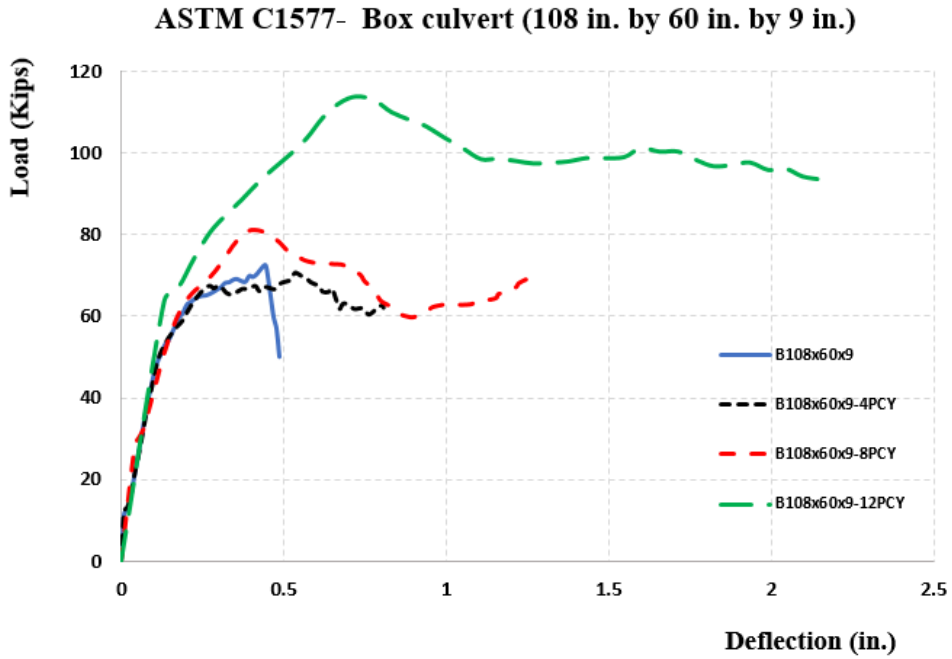

Figure E-31 Load-deflection plot for box culvert 9 ft by 5 ft by 9 in.

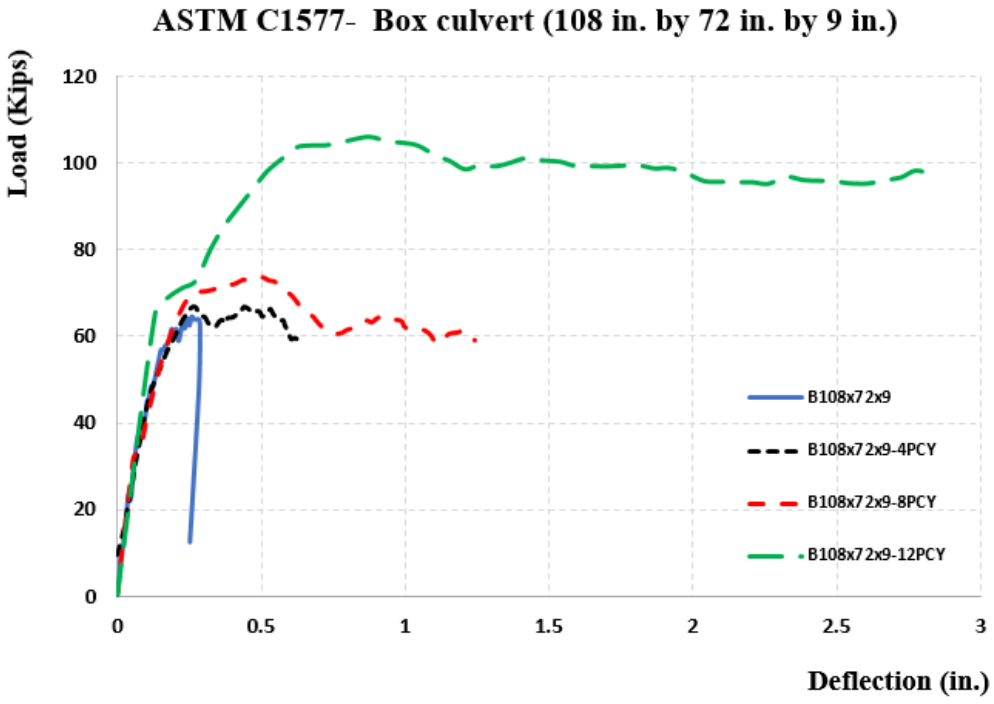

Figure E-32 Load-deflection plot for box culvert 9 ft by 6 ft by 9 in.

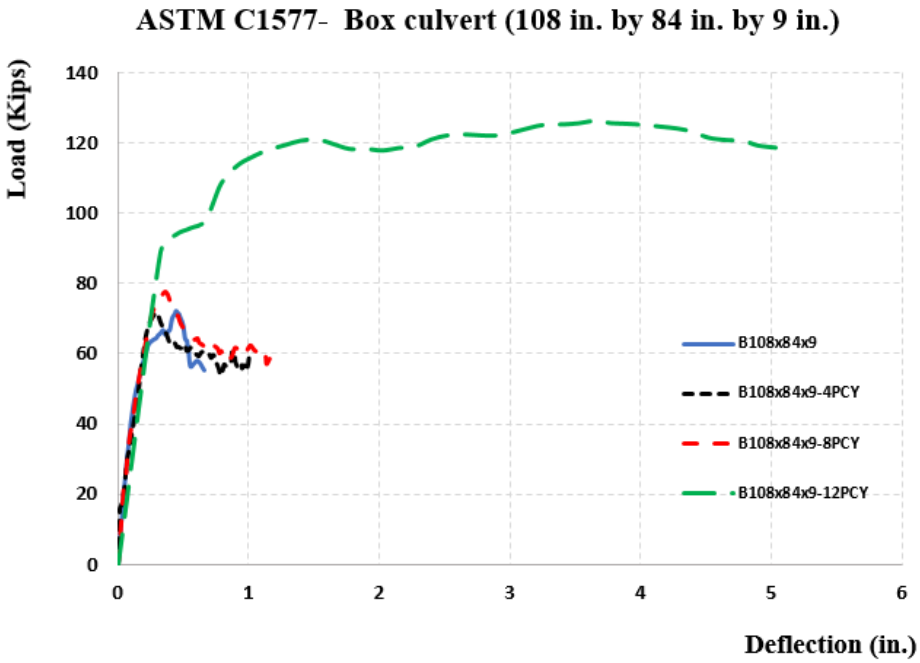

Figure E-33 Load-deflection plot for box culvert 9 ft by 7 ft by 9 in.

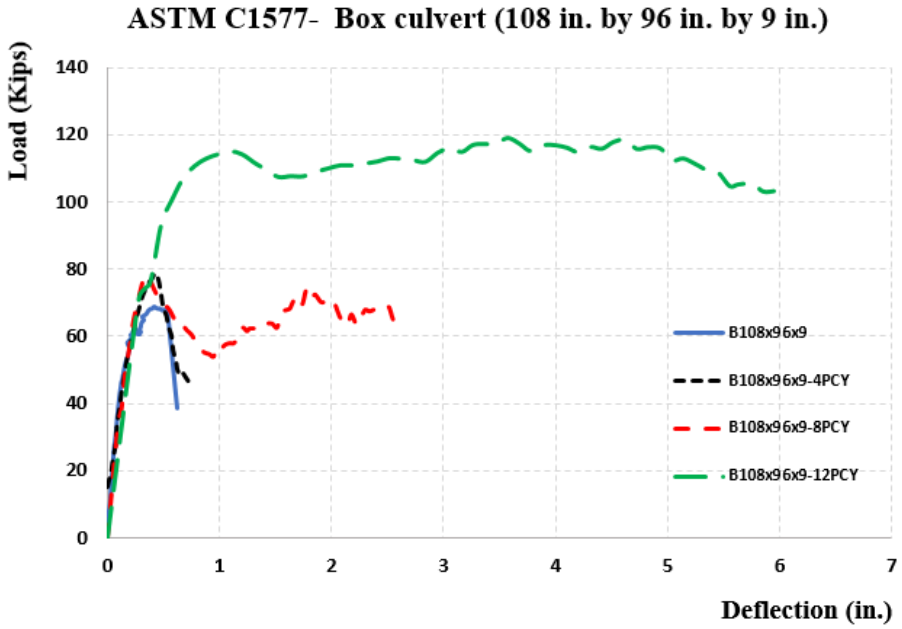

Figure E-34 Load-deflection plot for box culvert 9 ft by 8 ft by 9 in.

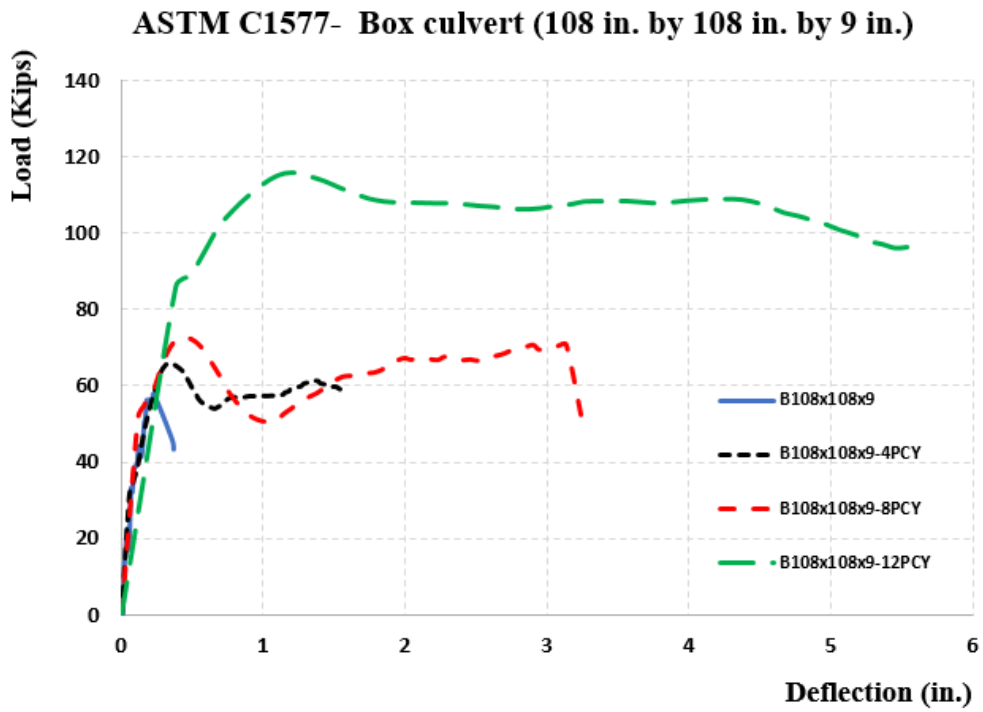

Figure E-35 Load-deflection plot for box culvert 9 ft by 9 ft by 9 in.

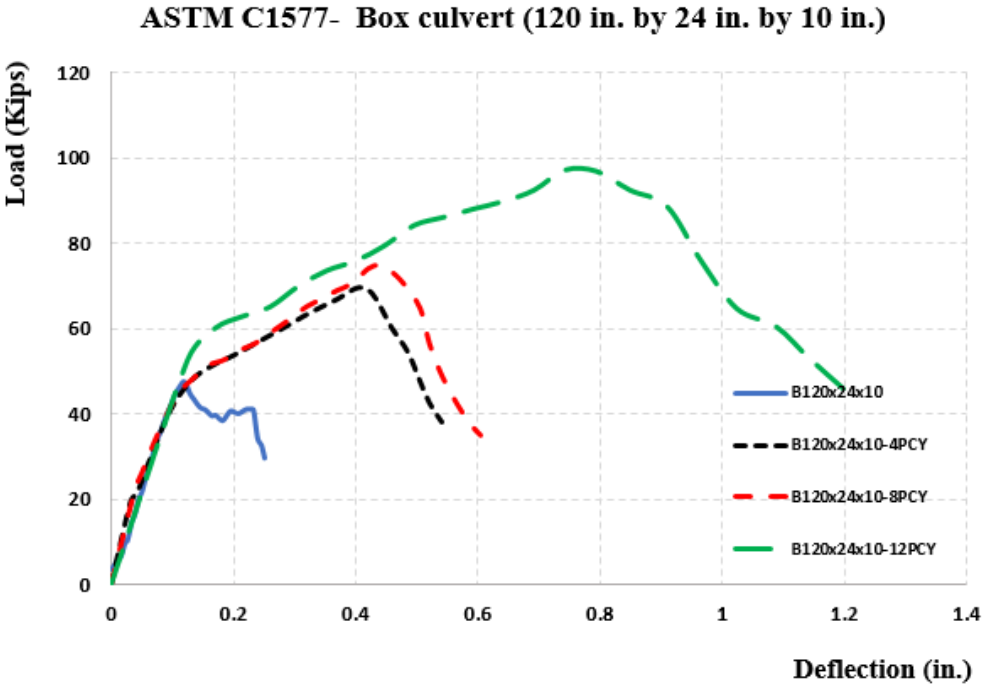

Figure E-36 Load-deflection plot for box culvert 10 ft by 2 ft by 10 in.

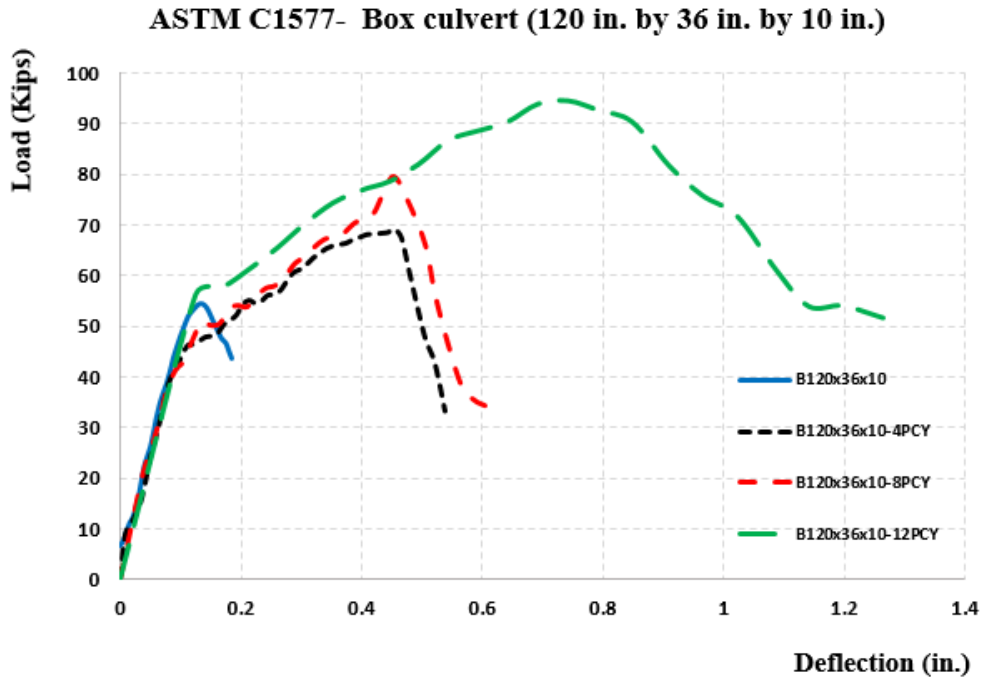

Figure E-37 Load-deflection plot for box culvert 10 ft by 3 ft by 10 in.

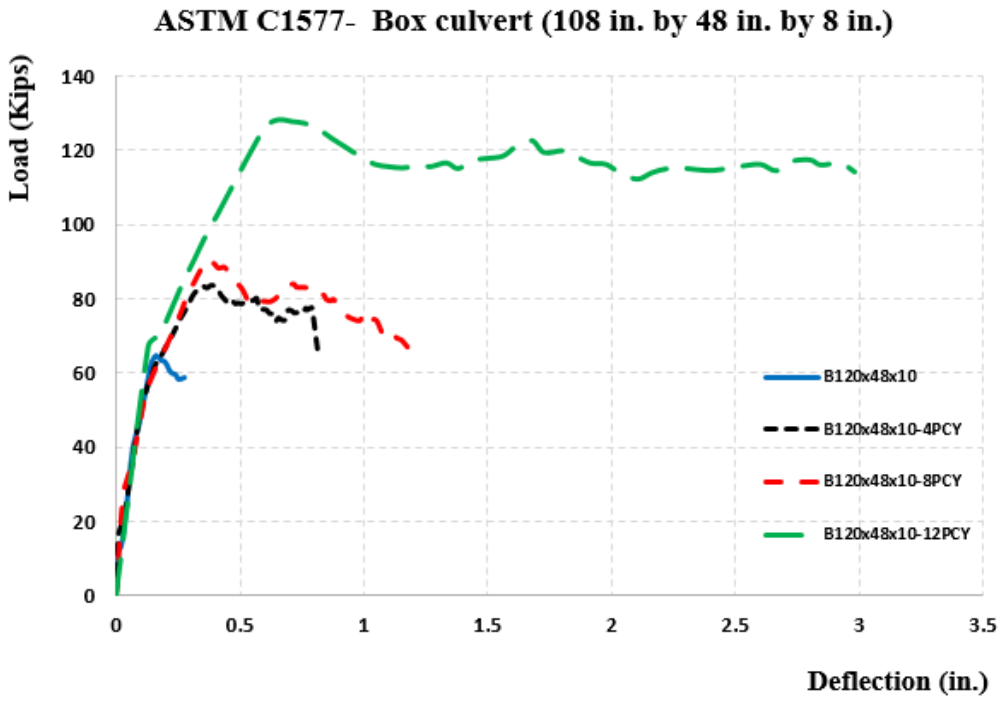

Figure E-38 Load-deflection plot for box culvert 10 ft by 4 ft by 10 in.

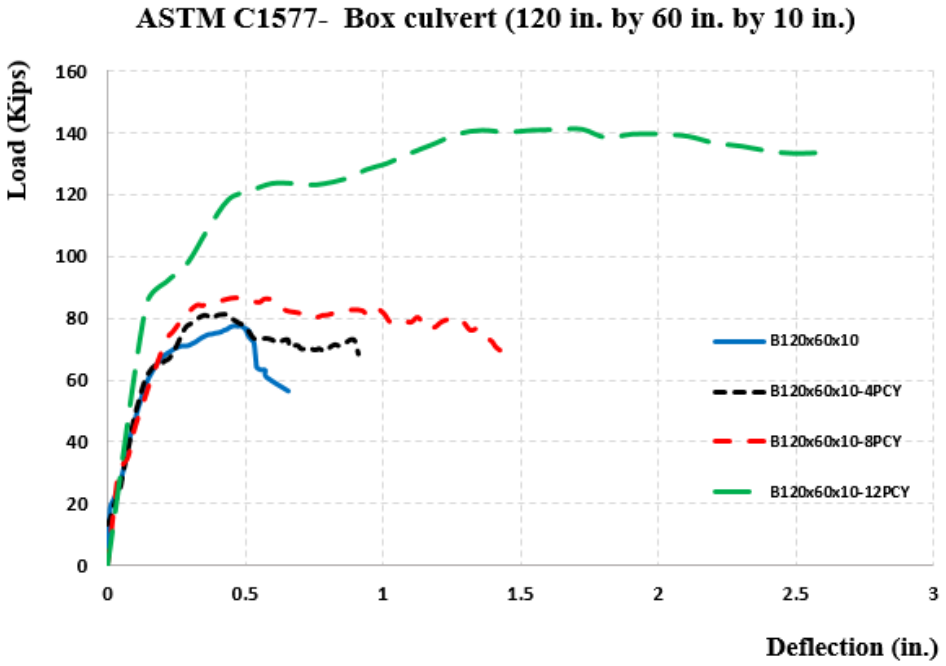

Figure E-39 Load-deflection plot for box culvert 10 ft by 5 ft by 10 in.

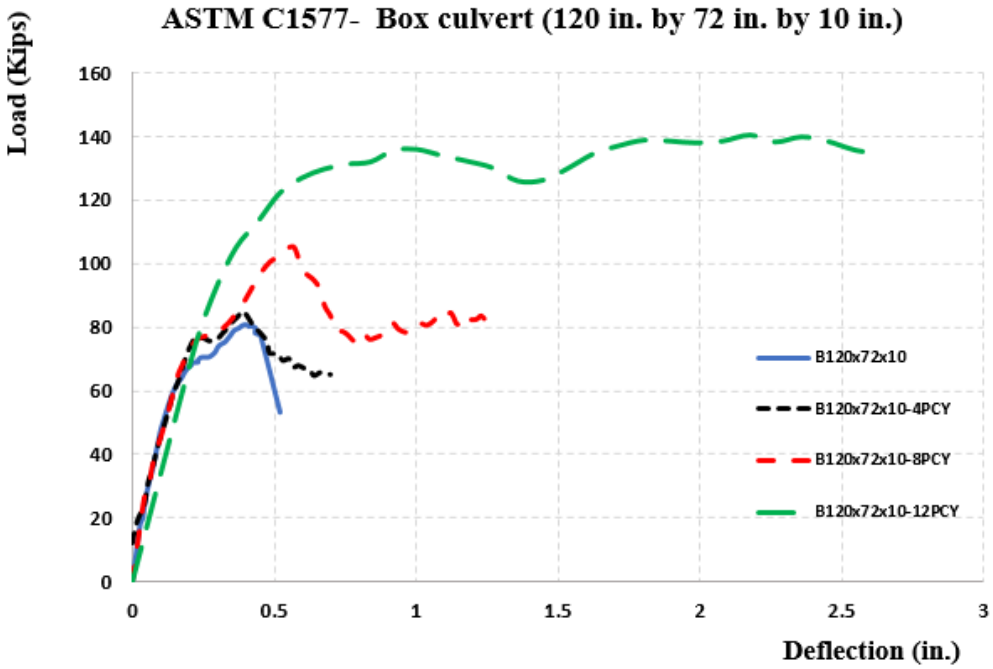

Figure E-40 Load-deflection plot for box culvert 10 ft by 6 ft by 10 in.

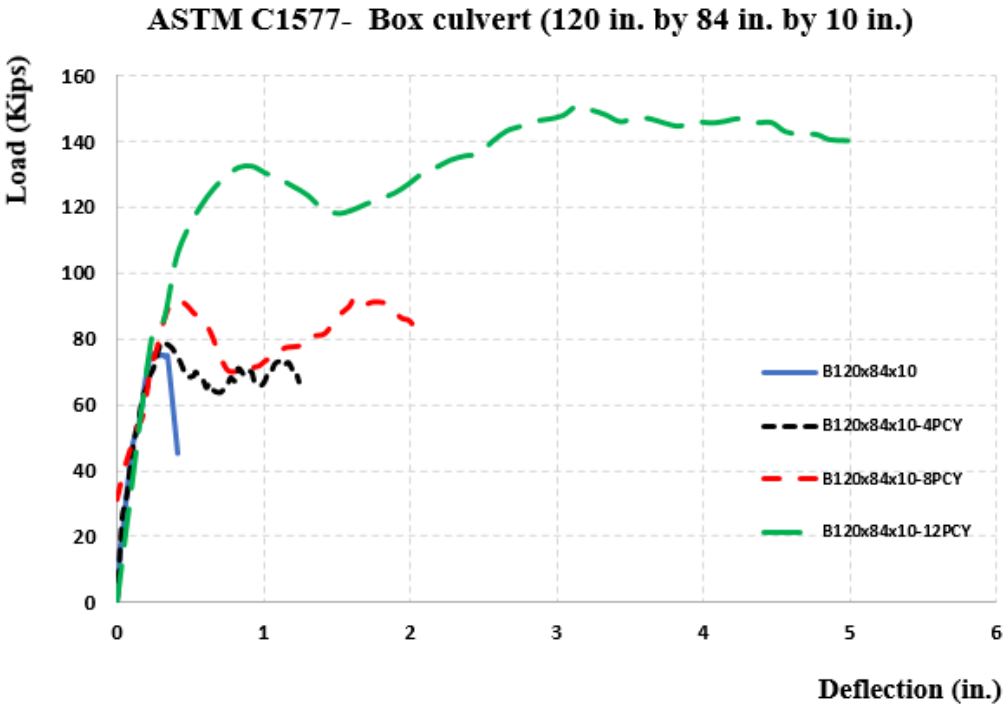

Figure E-41 Load-deflection plot for box culvert 10 ft by 7 ft by 10 in.

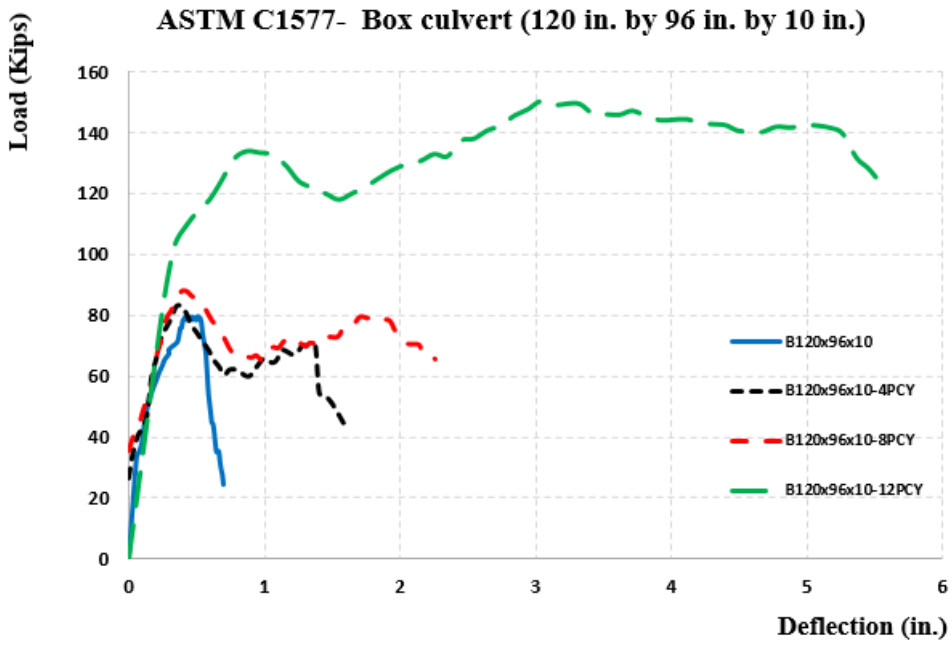

Figure E-42 Load-deflection plot for box culvert 10 ft by 8 ft by 10 in.

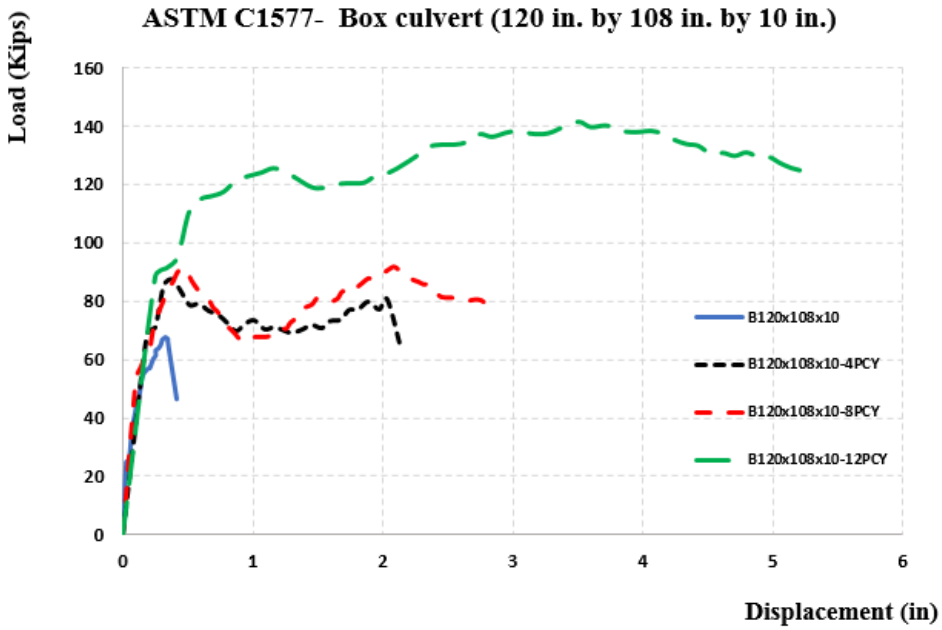

Figure E-43 Load-deflection plot for box culvert 10 ft by 9 ft by 10 in.

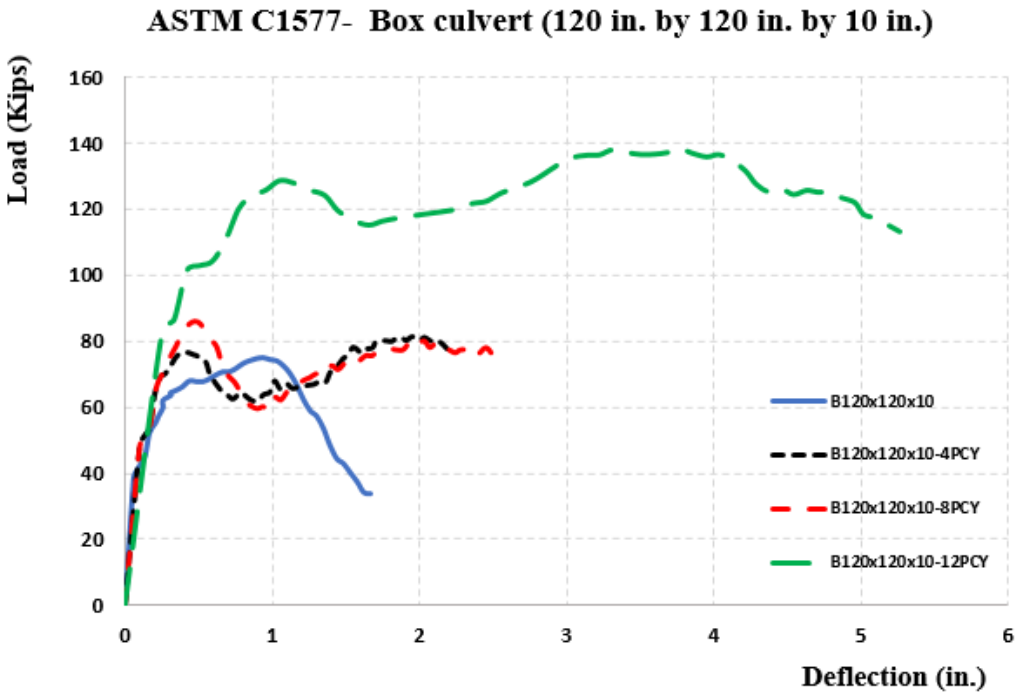

Figure E-44 Load-deflection plot for box culvert 10 ft by 10 ft by 10 in.

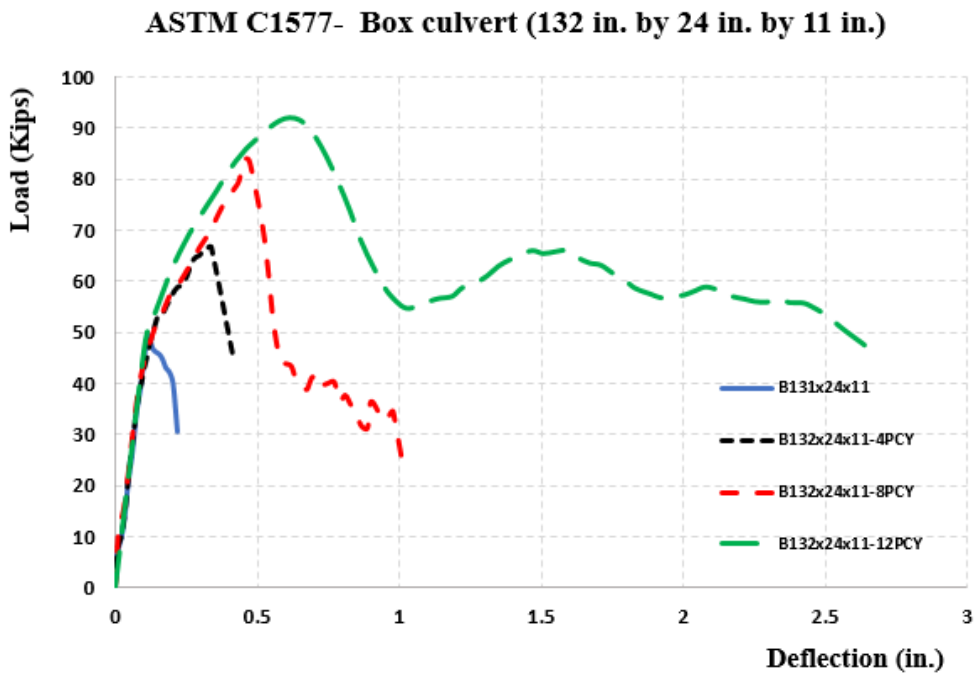

Figure E-45 Load-deflection plot for box culvert 11 ft by 2 ft by 11 in.

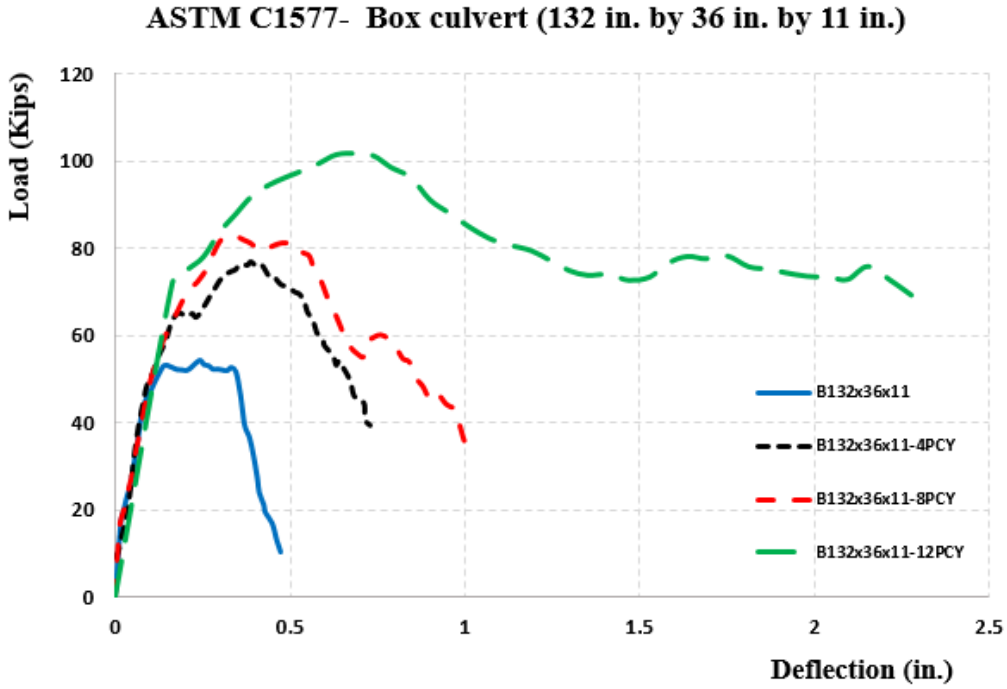

Figure E-46 Load-deflection plot for box culvert 11 ft by 3 ft by 11 in.

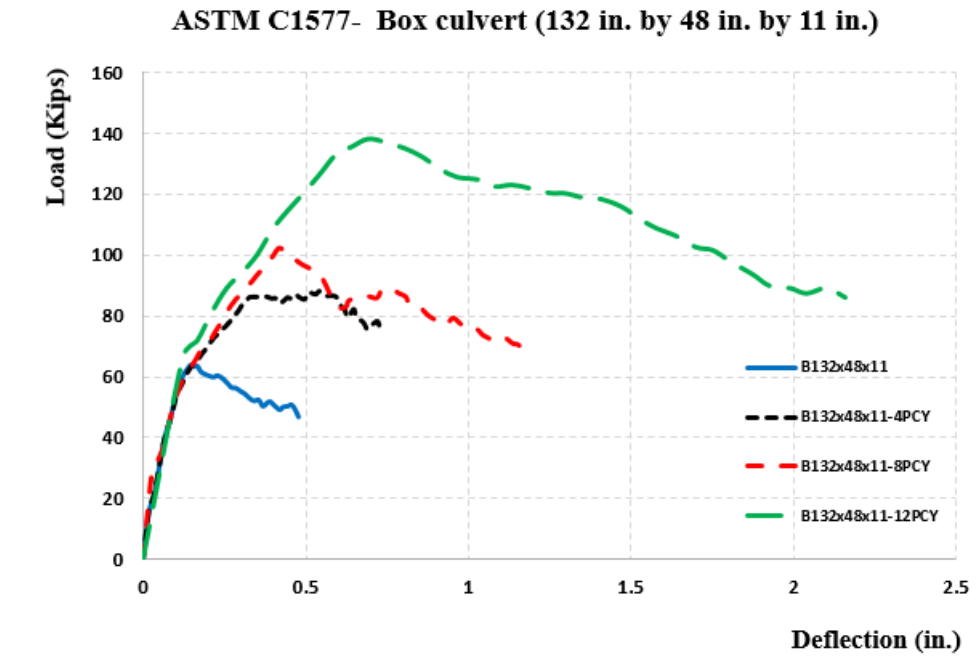

Figure E-47 Load-deflection plot for box culvert 11 ft by 4 ft by 11 in.

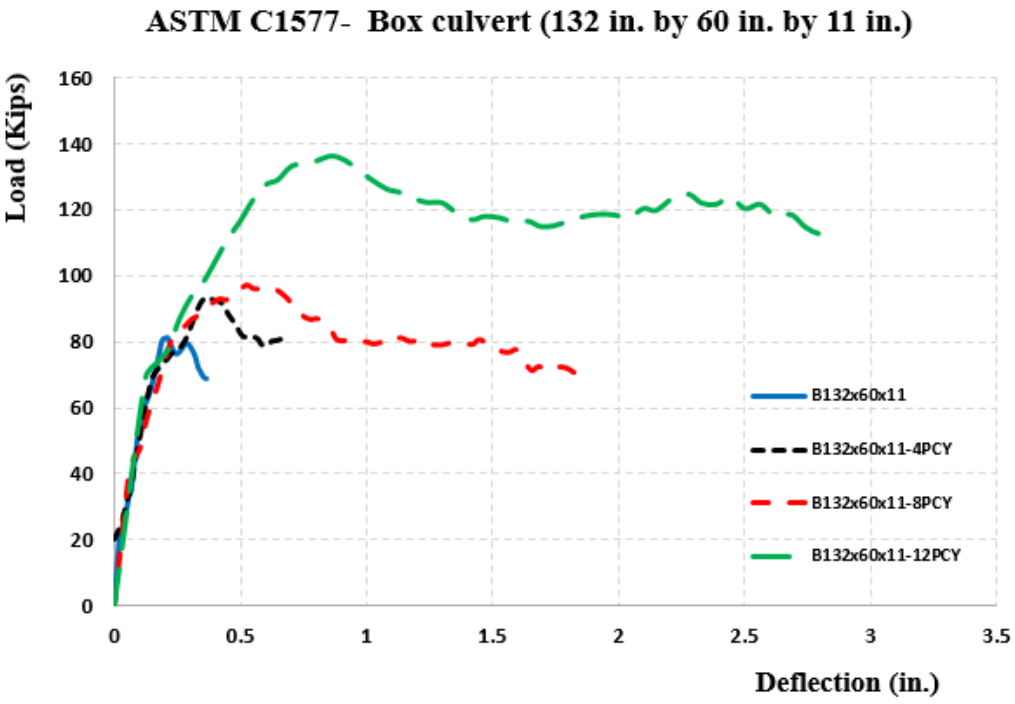

Figure E-48 Load-deflection plot for box culvert 11 ft by 5 ft by 11 in.

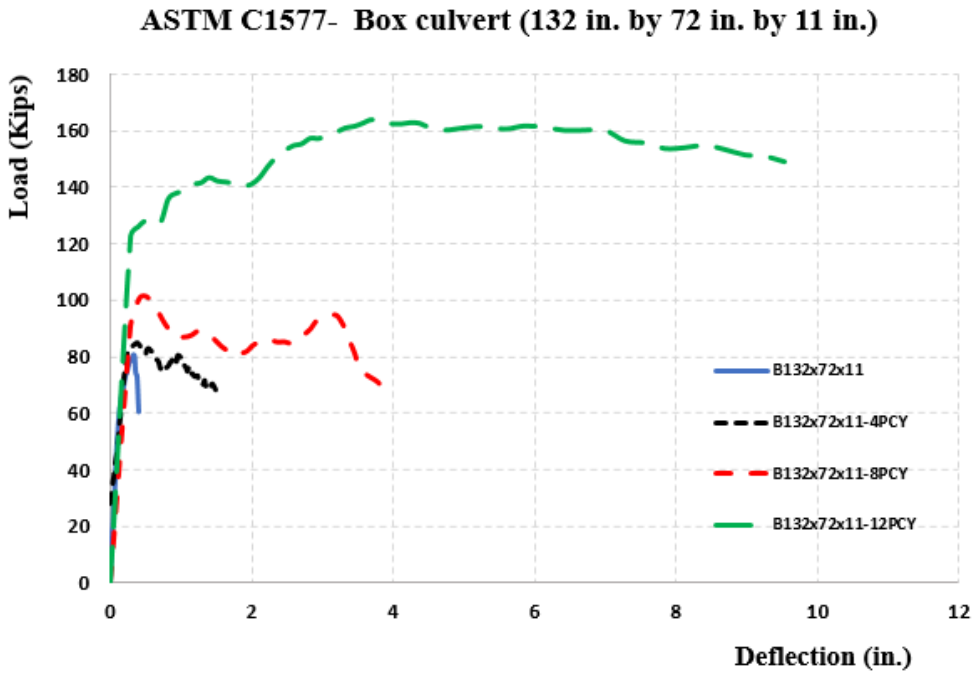

Figure E-49 Load-deflection plot for box culvert 11 ft by 6 ft by 11 in.

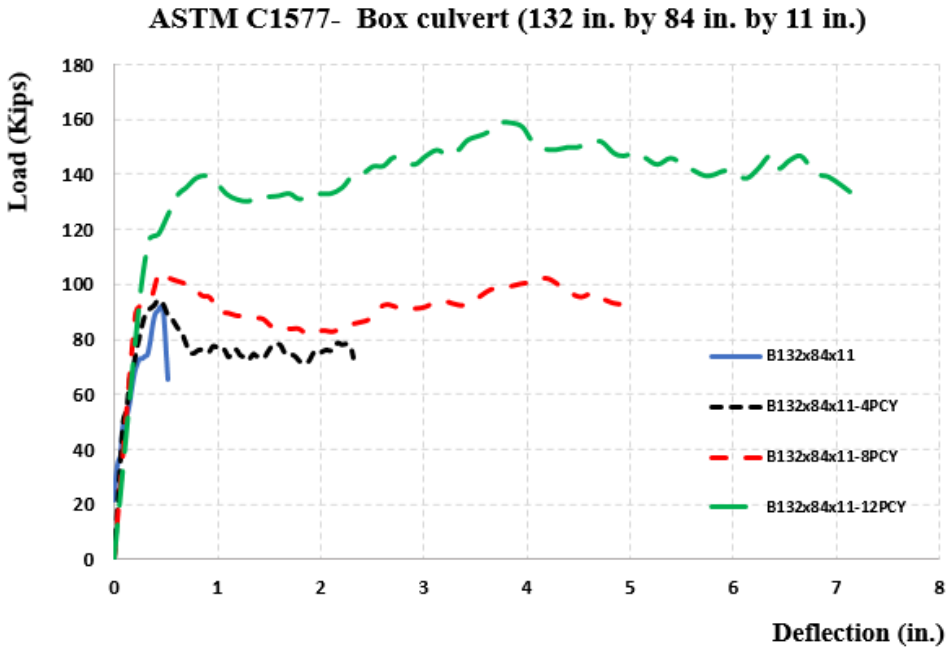

Figure E-50 Load-deflection plot for box culvert 11 ft by 7 ft by 11 in.

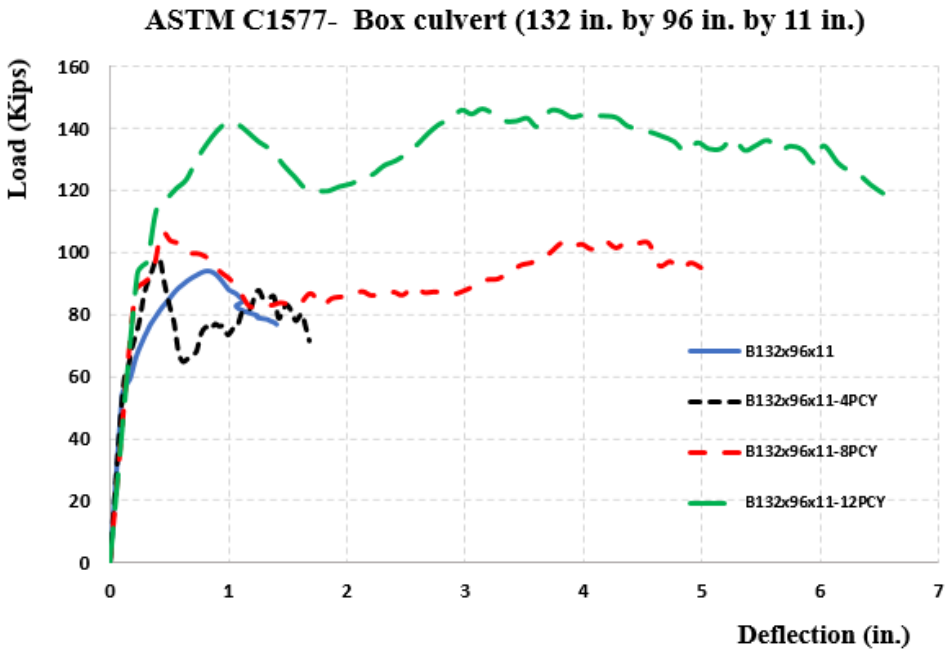

Figure E-51 Load-deflection plot for box culvert 11 ft by 8 ft by 11 in.

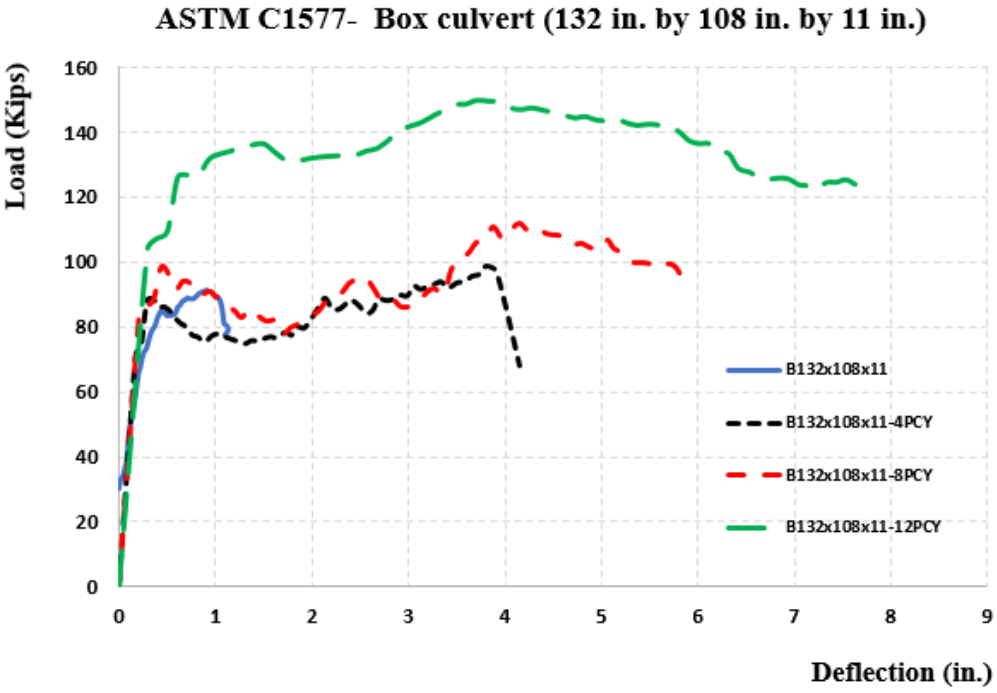

Figure E-52 Load-deflection plot for box culvert 11 ft by 9 ft by 11 in.

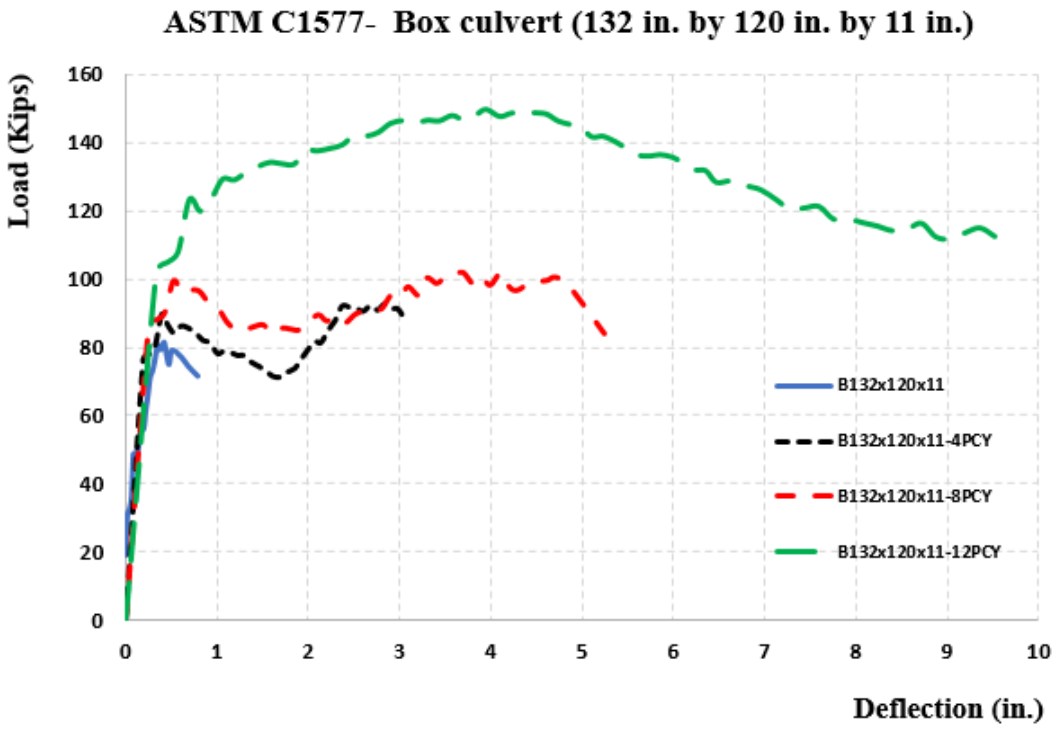

Figure E-53 Load-deflection plot for box culvert 11 ft by 10 ft by 11 in.

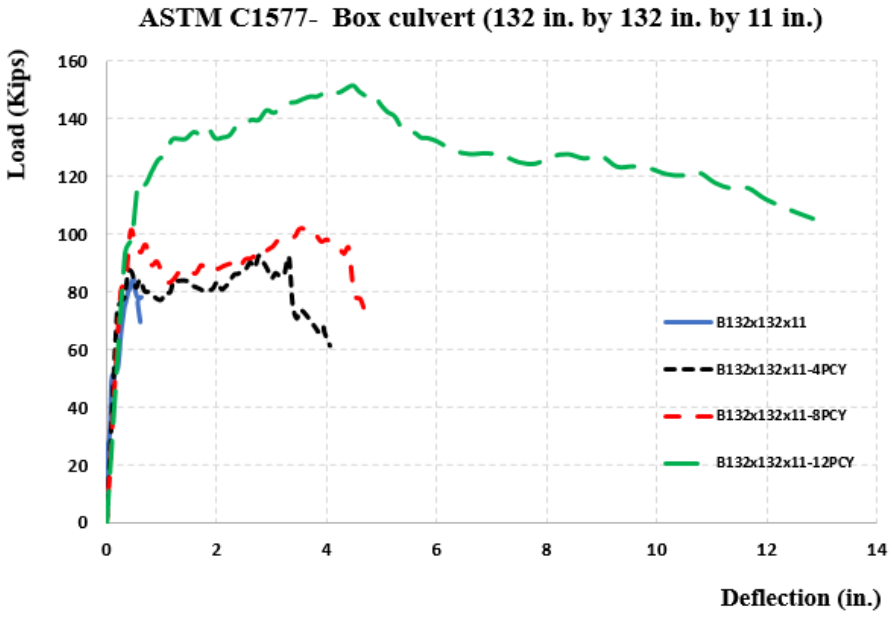

Figure E-54 Load-deflection plot for box culvert 11 ft by 11 ft by 11 in.

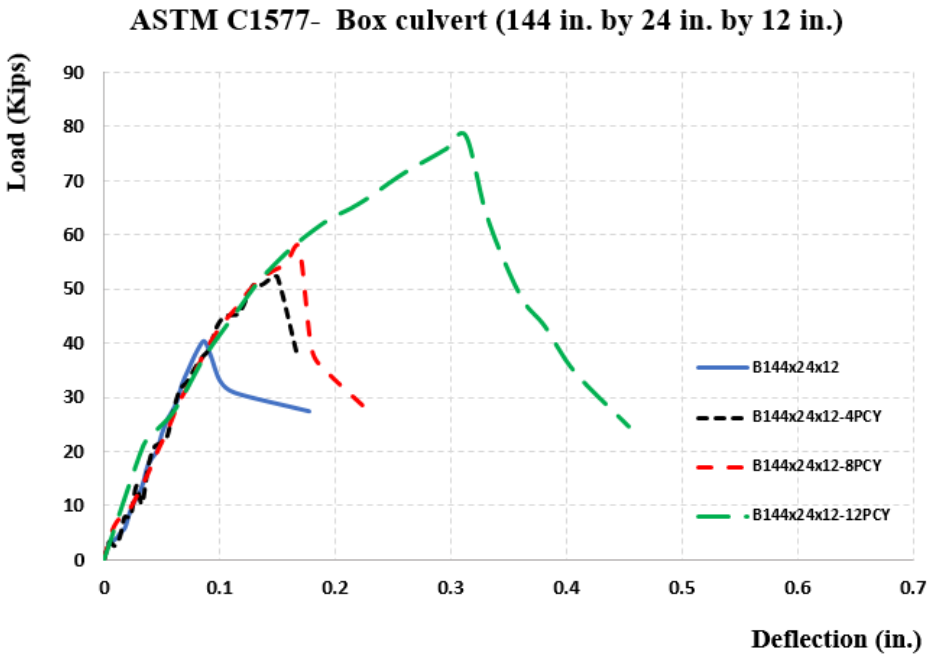

Figure E-55 Load-deflection plot for box culvert 12 ft by 2 ft by 12 in.

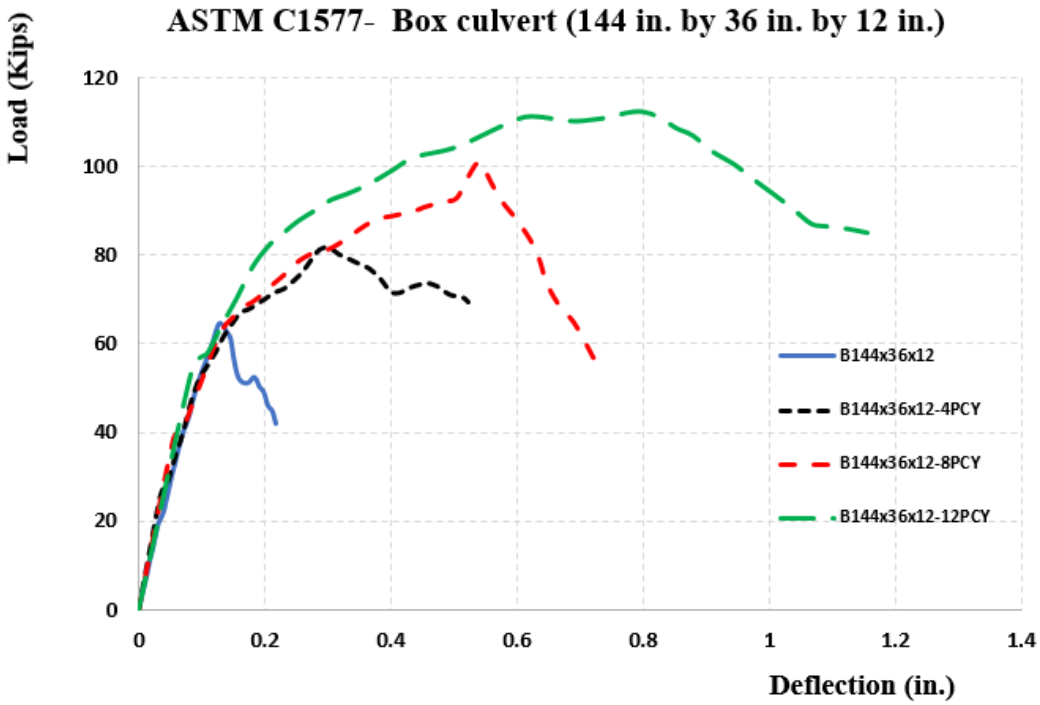

Figure E-56 Load-deflection plot for box culvert 12 ft by 3 ft by 12 in.

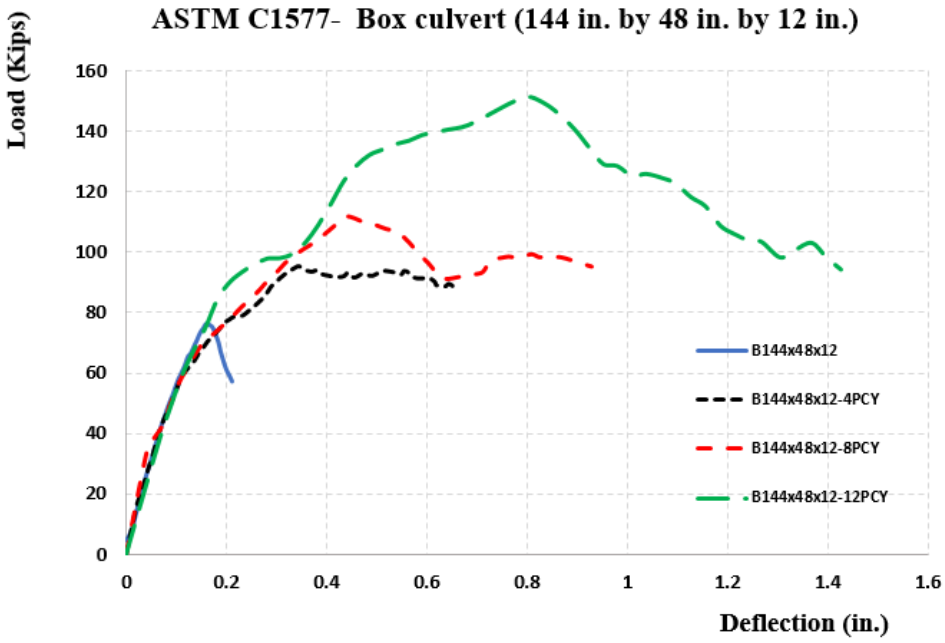

Figure E-57 Load-deflection plot for box culvert 12 ft by 4 ft by 12 in.

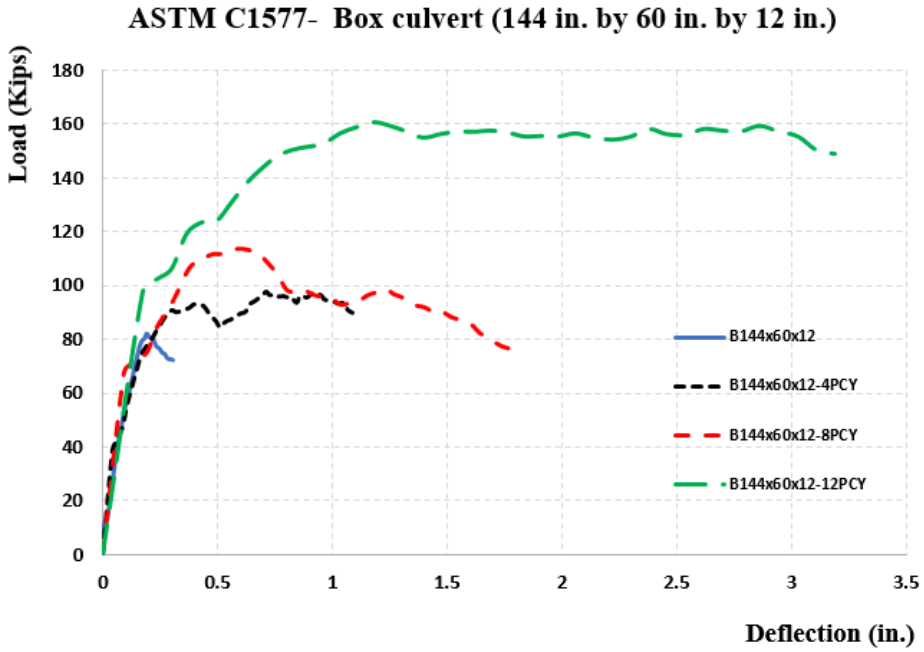

Figure E-58 Load-deflection plot for box culvert 12 ft by 5 ft by 12 in.

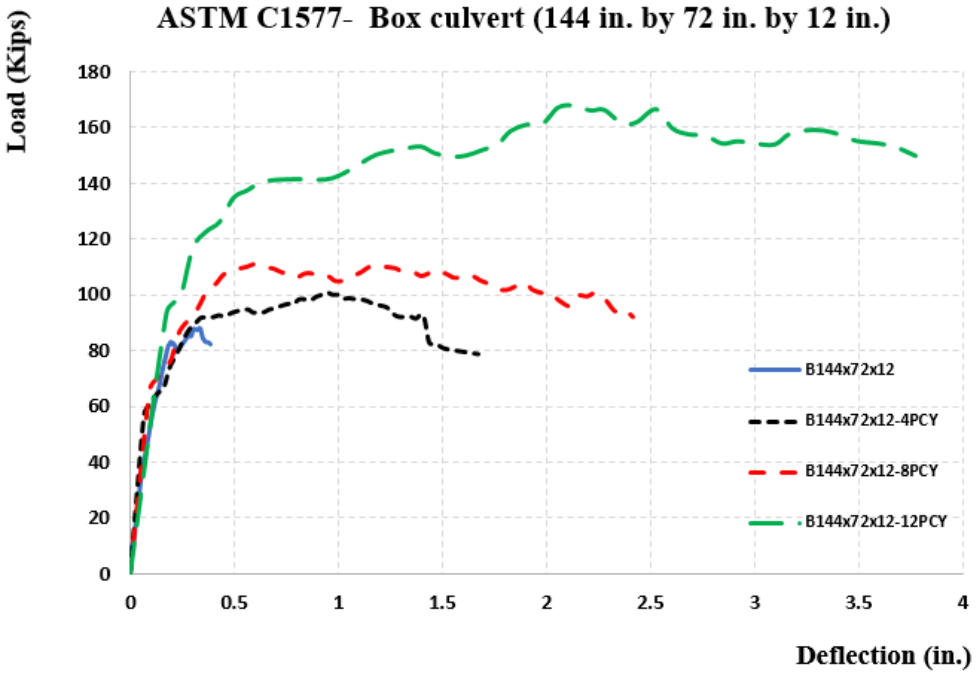

Figure E-59 Load-deflection plot for box culvert 12 ft by 6 ft by 12 in.

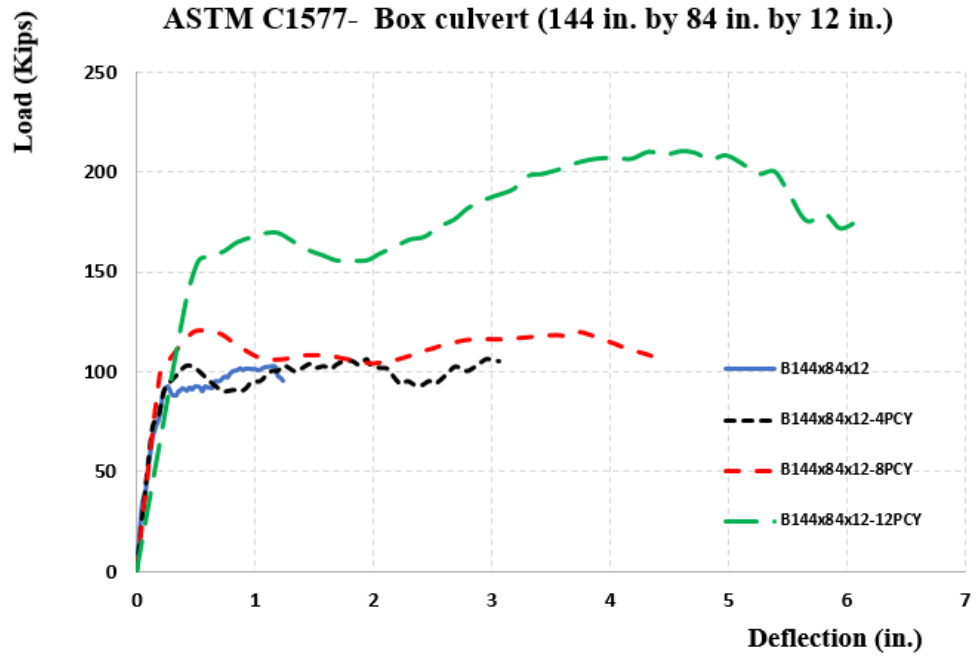

Figure E-60 Load-deflection plot for box culvert 12 ft by 7 ft by 12 in.

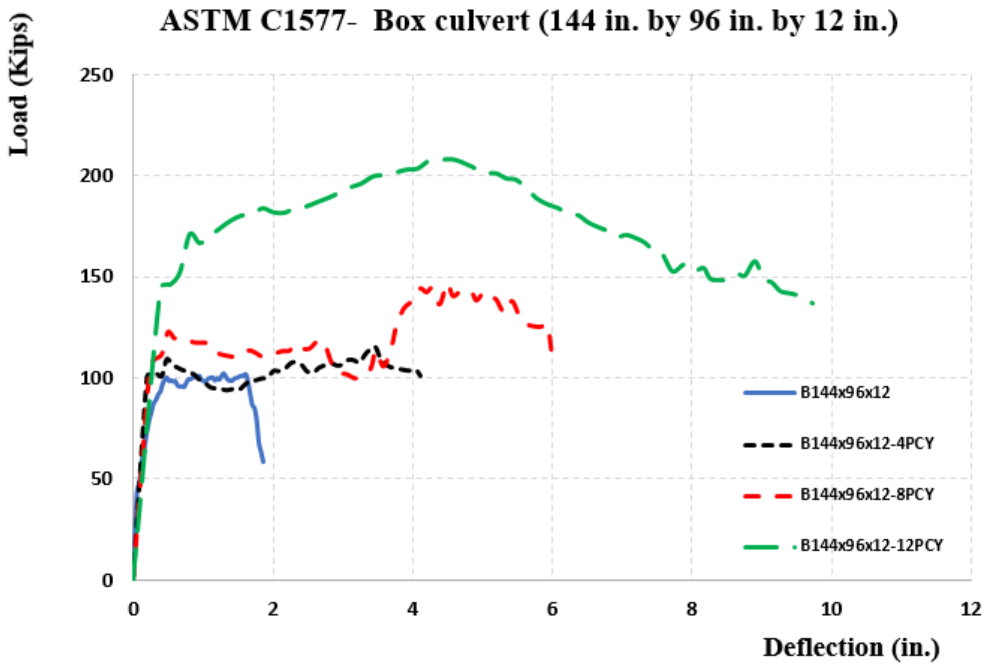

Figure E-61 Load-deflection plot for box culvert 12 ft by 8 ft by 12 in.

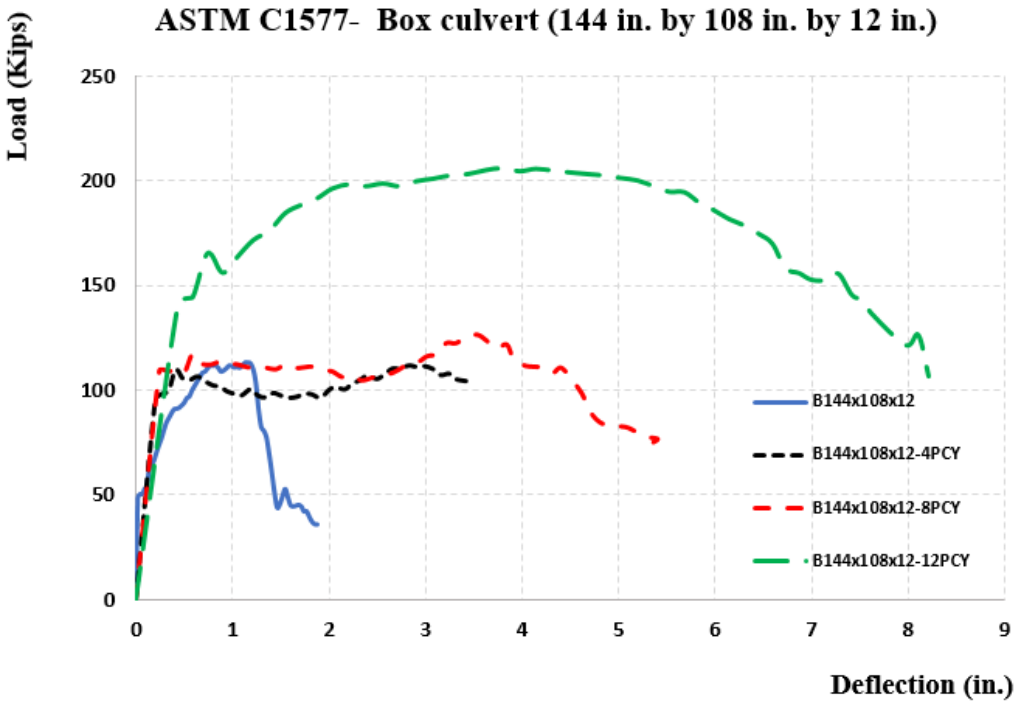

Figure E-62 Load-deflection plot for box culvert 12 ft by 9 ft by 12 in.

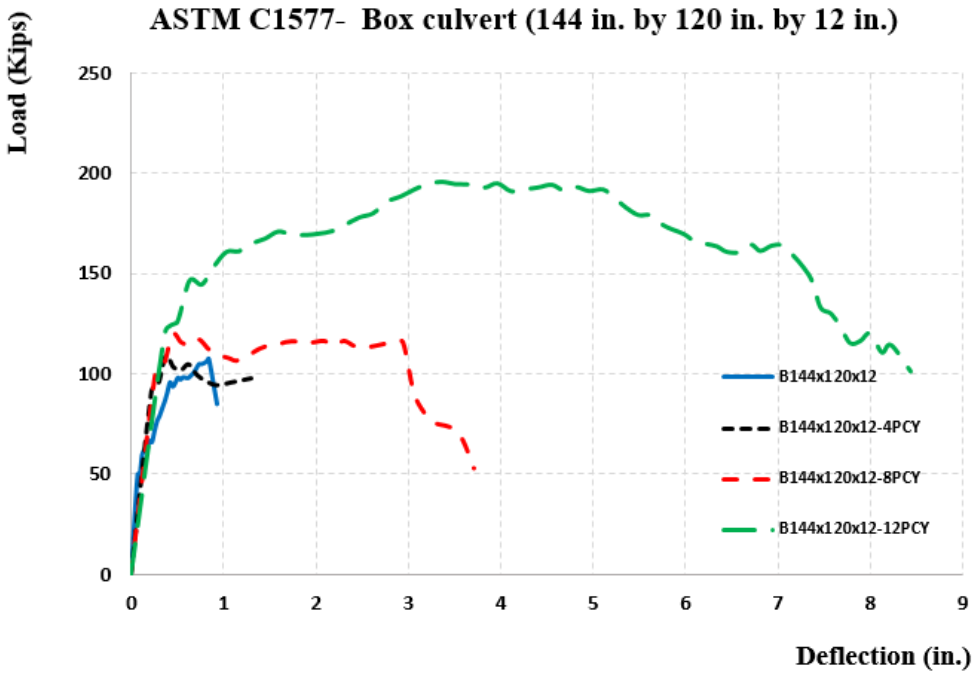

Figure E-63 Load-deflection plot for box culvert 12 ft by 10 ft by 12 in.

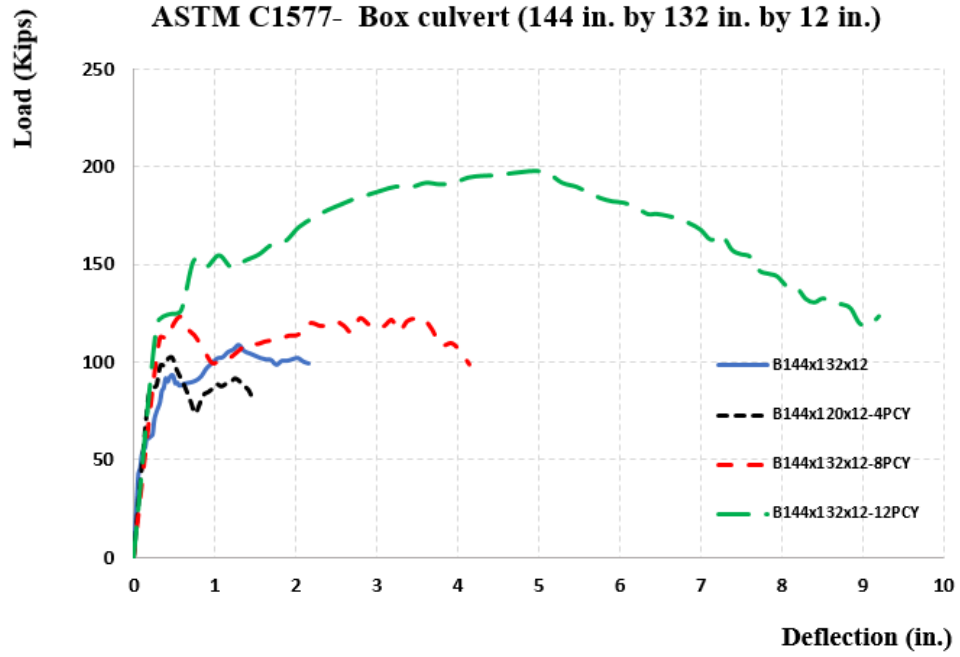

Figure E-64 Load-deflection plot for box culvert 12 ft by 11 ft by 12 in.

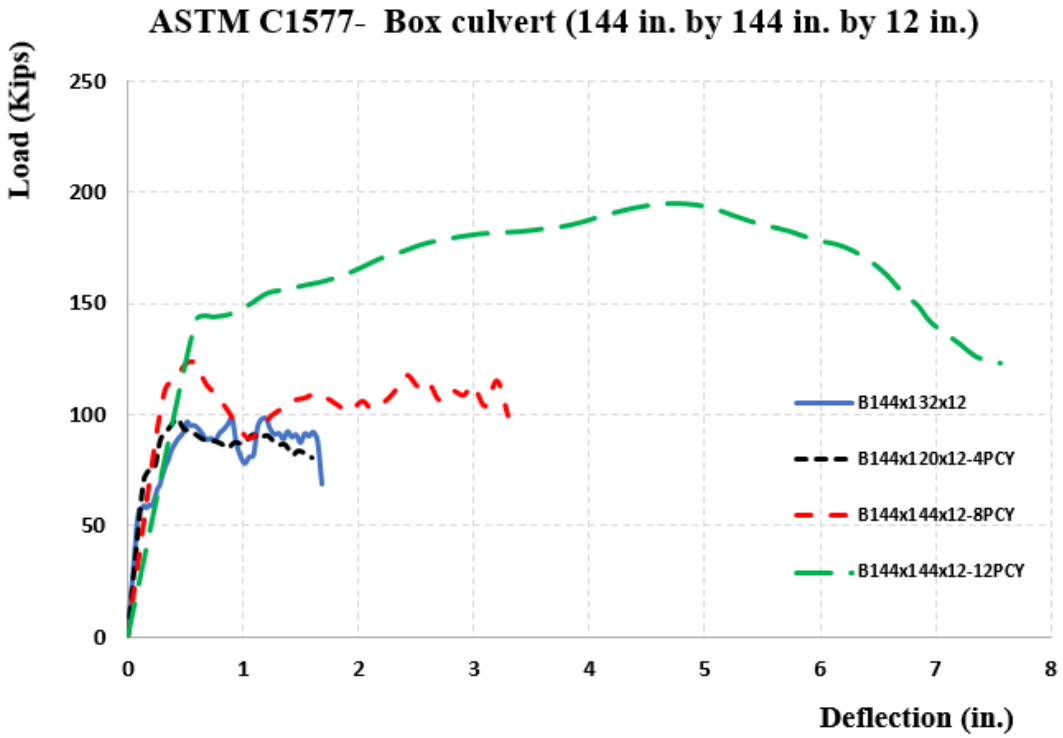

Figure E-65 Load-deflection plot for box culvert 12 ft by 12 ft by 12 in.

References

[1] M. C. Nataraja, "Fiber Reinforced Concrete- Behaviour Properties and Application," Sri Jayachamarajendra College of engineering, Mysore.

[2] 4. ACI Committee, "Fracture Mechanics of Concrete," American Concrete Institute, 1999.

[3] C. L. Guenther, "Evaluation of Shear and Diagonal Tension in Plain Concrete," 2007.

[4] Z. P. Bazant and P. A. Pfeiffer, "Shear fracture test of concretes," *Materiaux et Constructions* , pp. 111-121, 1986.

[5] A. R. Ingraffea and M. J. Panthaki, "Shear Fracture Tests of Concrete Beams," *Finite Element Analysis of Reinforced Concrete Structures,* pp. 151-173, 1985.

[6] S. E. Swartz and N. M. Taha, "Preliminary Investigation of the Suitability of the Ioslpescu Test SpecImen for Determining Mixed Mode Fracture Properties of Concret," Engineering Experiment Station, Kansas State Univ., Manhattan, 1987.

[7] A. Khanlou, G. A. MacRae, A. N. Scott, S. J. Hicks and G. C. Clifton, "SHEAR PERFORMANCE OF STEEL FIBRE-REINFORCED CONCRETE," in *Steel Innovations* , Christchurch, New Zealand, 2013.

[8] A. A. Mirsayah and N. Banthia, "Shear Strength of Steel Fiber-Reinforced Concrete," *Materials Journal,* vol. 99, no. 5, pp. 473-479, 2002.

[9] F. Majdzadeh, S. M. Soleimani and N. Banthia, "Shear strength of reinforced concrete beams with a fiber concrete matrix," *Canadian Journal of Civil Engineering,* pp. 726-734, 2006.

[10] "JSCE," 1999. [Online]. Available: http://www.jsce.or.jp/committee/concrete/e/newsletter/newsletter01/recommendation/FRP-bar/t-20.pdf.

[11] F. F. Wafa, "Properties and Applications of Fiber Reinforced Concrete," *JKAU: Eng. Sci.,* vol. 2, pp. 49-63, 1990.

[12] P. Songa, S. Hwang and B. Sheu, "Strength properties of nylon- and polypropylene-fiber-reinforced concretes," *Cement and Concrete Research 35,* p. 1546 – 1550, 2005.

[13] A. Wilson and A. Abolmaali, "Comparison of Material Behavior of Steel and Synthetic fibers in Dry-Cast Application," *Journal of the Transportation Research Board,* vol. 2332, pp. 23-28, 2013.

[14] B. Boulekbache, M. Hamrat, M. Chemrouk and S. Amziane, "Influence of yield stress and compressive strength on direct shear behaviour of steel fibre-reinforced concrete," *Construction and Building Materials,* vol. 27, pp. 6-14, 2012.

[15] A. Wilson and A. Abolmaali, "Performance of Synthetic Fiber-Reinforced Concrete Pipes," *Journal of Pipeline Systems Engineering and Practice,* vol. 5, no. 3, pp. 1949-1204, 2014.

[16] A. Peyvandi, P. Soroushian and S. Jahangirnejad, "Enhancement of the structural efficiency and performance of concrete pipes through fiber reinforcement," *Construction and Building Materials,* vol. 45, p. 36–44, 2013.

[17] K. Gustafsson and k. Noghabai, "Steel Fibres as Shear Reinforcement in High Strength Concrete Beams," Lulea University of technology, Division of Structural Engineering, 1999.

[18] J. Cho, J. Lundy and S. Chao, "Shear Strength of Steel Fiber Reinforced Prestressed Concrete," *ASCE,* pp. 1058-1066, 2009.

[19] F. Minelli and G. Plizzari, "On the effectivness of Steel fiber as shear reinforcement," *ACI,* vol. 110(3), pp. 379-390, 2013.

[20] R. W. James, "Behavior of ASTM C 850 Concrete Box Culverts Without Shear Connectors," in *Transportation Research Board, National Research council,* Washington D.C., 1984.

[21] A. M. AbdeI-Karim, M. K. Tadros and J. V. Benak, "STRUCTURAL RESeONSE OF FULL-SCALE CONCRETE Box CULVERT," *Journal of Structural Engineering, ASCE,* pp. 3238-3254, 1993.

[22] G. Federick, C. Ardis, K. Tarhini and B. Koo, "Investigation of the Structural Adequacy Of C 850 Box Culverts," Transportation Research Record 1191, Transportation Research Board, National Research council, Washington D.C.,, 1988.

[23] A. Abolmaali and A. K. Garg, "Effect of Wheel Live Load on Shear Behavior of Precast Reinforced Concrete Box Culverts," *JOURNAL OF BRIDGE ENGINEERING, ASCE,* pp. 93-99, 2008.

[24] A. K. Garg, A. Abolmaali and R. Fernandez, "Experimental Investigation of Shear Capacity of Precast Reinforced Concrete Box Culverts," *Journal of Bridge Engineering, ASCE,* pp. 511-517, 2007.

[25] ASTM C1116, "Standard Specification for Fiber-Reinforced Concrete," Annual Book of ASTM Standards, ASTM International, West Conshohocken, PA, 2015.

[26] BASF, "Master Fiber MAC Matrix," BASF The Chemical Company, 2012. [Online]. Available: http://assets.master-builders-solutions.basf.com/Shared%20Documents/EB%20Construction%20Chemcials%20-%20US/Admixture%20Systems/Data%20Sheets/MasterFiber/basf-masterfiber-mac-matrix-tds.pdf.

[27] ASTM C1609, "Standard Test Method for Flexural Performance of Fiber-Reinforced Concrete (Using Beam With Third-Point Loading)," Annual Book of ASTM Standards, ASTM International, West Conshohocken, PA, 2011.

[28] ASTM C617, "Standard Practice for Capping Cylindrical Concrete Specimens," Annual Book of ASTM Standards, ASTM International, West Conshohocken, PA, 2015.

[29] ASTM C39, "Standard Test Method for Compressive Strength of Cylindrical Concrete Specimens," Annual Book of ASTM Standards, ASTM International, West Conshohocken, PA, 2015.

[30] ABAQUS, "Abaqus/CAE User's Guide," 2016.

[31] T. Lok and J. Xiao, "FLEXURAL STRENGTH ASSESSMENT OF STEEL FIBER-REINFORCED CONCRETE," *Journal of Materials in Civil Engineering, ASCE*, pp. 188-196, 1999.

Biographical Information

Mahnaz Mostafazadeh received her B.S. Degree in Civil Engineering from Yazd University, Yazd, Iran, in September 2007 and M.Sc. Degree in Earthquake Engineering from University of Tehran, Tehran, Iran, in January 2010. She completed her Ph.D. Degree in Civil Engineering/Structures at the University of Texas at Arlington in October 2017. Her research interests include nonlinear finite element analysis, behavior of steel and concrete structures including box culverts, nonlinear analysis of structures, and structural stability.

While pursuing her degree, Ms. Mostafazadeh worked as a teaching assistant for different courses such as Mechanics of Materials, Dynamics, Finite Element Analysis and etc. She was also an instructor for Statics, Dynamics, and Mechanics of Materials. She presented her research at international conferences and meeting, including 12th International Conference on Durability of Composite Systems and 2nd Annual Combination of American Concrete Pipe Association’s Pipe School, Pipe Show, and B2B Exchange. Additionally, Ms. Mostafazadeh has published some part of her Ph.D. research at Advances in Civil Engineering Materials, ASTM Journal and she is currently working on two more papers to submit them to the Journal of Bridge Engineering, ASCE.